universität wien

DISSERTATION

Titel der Dissertation

ROLE OF MAP1B AND NO IN AXON GUIDANCE

angestrebter akademischer Grad

Doktorin der Naturwissenschaften (Dr. rer.nat.)

Verfasserin:	Mag. Ewa Krupa
Matrikel-Nummer:	0549595
Dissertationsgebiet:	A 091 490, Molekulare Biologie
Betreuer:	Univ.-Prof. Dr. Friedrich Propst

Wien, August 2009

For my husband and son

ACKNOWLEDGEMENTS

This work was funded by the FWF, Wings of Life, the University of Vienna and the Medical University of Vienna.

I especially thank Univ. Prof. Dr. Friedrich Propst for an opportunity to work in his group, his supervision, continuous support and insightful discussions during these four years.

I would like to thank the members of my PhD committee Univ. Prof. Dipl. Ing. Dr. Johannes Nimpf and Univ. Prof. Dr. John Victor Small, for their helpful comments and suggestions.

I am grateful to Dr. Fatiha Nothias, Michèle Ravaille-Veron and Mag. Ulla Milbretta for an opportunity to realize some of experiments in their laboratory and for their great help.

A lot of thanks go to all present and former colleagues and friends from Department of Biochemistry and Cell Biology, especially to Ilse, Alžbeta, Waltraud, Luise, Rocio, Marianne, Karin, Nevena and Irmi (in order of appearance) for great working atmosphere and invaluable help in scientific and non-scientific fields.

Many thanks go to all my friends for their support and friendship that I needed, especially Mag. Olga Kulak, Mag. Michał Podmagórski and Małgorzata Abdel-Razek.

Special thanks go to my parents Anna and Krzysztof, and my sister Elżbieta for encouraging and reminding me the gold rule "do not give up".

Finally, I would like to thank my husband Marcin and my son Marek, for their constant support, for their understanding, for giving the opportunity to realize dreams and mostly for their unconditional love during my good and bad times.

TABLE OF CONTENTS

SUMMARY **11**

ZUSAMMENFASSUNG **14**

INTRODUCTION **17**

THE NERVOUS SYSTEM **17**
The central nervous system 18
The peripheral nervous system 19
AXON GUIDANCE **19**
Netrins 20
Semaphorins 21
Slits 22
Ephrins 23
Ca^{2+} effectors in controlling and steering growth cone 23
Downstream effectors of Ca^{2+} signals 25
Ca^{2+}/calmodulin-dependent protein kinase II (CaMKII) 25
Calpains 27
Calcineurin 29
Protein kinase C 31
Lysophosphatidic acid 32
THE GROWTH CONE **34**
THE CYTOSKELETON **36**
MYOSIN **39**
RHO GTPASES **41**
NO AS A SIGNALING MOLECULE **43**
Production of NO 44
Mechanism of action 46
Binding to metal centres 46
Protein S-nitrosylation 47
Protein nitrotyrosination 49
Physiological effects of NO 49
Vascular effects 49
Immunological functions 50
Pro- and anti-apoptotic effects of NO 50
NO in the nervous system 51
NO and neurodegenerative diseases 53
MICROTUBULE ASSOCIATED PROTEINS **55**
MAP1s 56
MAP1B 57
Phosphorylation of MAP1B 58
S-nitrosylation of MAP1B 61
Role of MAP1B 62

PART I - PHYSIOLOGICAL RELEVANCE OF NO-INDUCED AXON RETRACTION **66**

RESULTS **67**

Role of NO and MAP1B in axon retraction induced by LPA 67
LPA-induced axon retraction is MAP1B-dependent and involves ROCK and myosin 67
LPA-induced axon retraction does not require nNOS activation.....74
Role of NO and MAP1B in inhibition of neurite outgrowth induced by CSPG..76
Lack of evidence for an involvement of NOS in CSPG-induced inhibition of axon growth.....76
CSPG-induced inhibition of axon regrowth is not MAP1B-dependent.....79
Role of NO and MAP1B in inhibition of neurite outgrowth induced by myelin.81
Lack of evidence for an involvement of NOS in myelin-induced inhibition of axon growth 81

DISCUSSION 83

PART II - MECHANISM OF NO-INDUCED AXON RETRACTION 90

RESULTS.....91
Involvement of other calcium effectors in calcimycin-induced axon retraction .91
CaMKII is not involved in calcimycin–induced axon retraction.....92
Calcineurin is not involved in calcimycin–induced axon retraction.....93
PKC is not involved in calcimycin-induced axon retraction.....95
Calpain is not involved in calcimycin-induced axon retraction 96
Involvement of acto-myosin contractility in axon retraction induced by calcimycin and NO 97
ROCK is necessary for calcimycin- and NO-induced axon retraction 98
Myosin inhibition prevents axon retraction induced by NO 101
Increased levels of cAMP partially attenuate axon retraction induced by calcimycin and SNAP.....107
NO-induced axon retraction does not involve microtubule depolymerization..110
LPA-induced axon retraction does not involve microtubule depolymerization 112
Mechanism of taxol-induced axon retraction 114
Taxol-induced axon retraction is acto-myosin independent 114
Taxol-induced retraction does not involve NOS activation 117
SNAP and LPA induce increased microtubule binding by full length MAP1B 118
Increased microtubule dynamic in MAP1B -/- DRG neurons 120

DISCUSSION 138

PART III - ROLE OF MAP1B AND CDK5 IN LAMININ SIGNALLING PATHWAY 154

RESULTS.....155
Laminin induces different morphology of wild-type and MAP1B-/- DRG neurons 155
Axon retraction induced by roscovitine is MAP1B-dependent.....157
Axon retraction induced by roscovitine involves ROCK and myosin.....161
Axon retraction induced by roscovitine does not involve nNOS activation.....164
Axon retraction induced by roscovitine involves GSK3β.....166
Axon retraction induced by roscovitine does not involve depolymerization of microtubules 167

Roscovitine and LPA induce retraction only in the presence of laminin 168
Roscovitine induces increased microtubule binding by full length MAP1B 170
Expression of cdk5 and p35 is not altered in MAP1B-/- mice 171

DISCUSSION 173

MATERIALS AND METHODS 182

DNA METHODS 182
DNA preparation, restriction digest and ligation 182
Agarose gel 182
Transformation of E. coli 183
Preparation of competent cells 183
Transormation of cells 183
Cloning 184
PROTEIN METHODS 185
Preparation of cell extracts 185
Preparation of brain and DRG homogenates 186
Deteremination of protein concentration (Bradford Method) 186
Immunoblot analysis 186
MAMMALIAN CELL CULTURE METHODS 189
Maintenance of the cell lines 189
Cultivation of dissociated adult DRG neurons 190
Coating of coverslips for N2a cells and DRG neurons 191
Transfection of mammalian cells using Fugene6 191
Transfection of DRG neurons with Amaxa 192
Treatment DRG neurons, N2a cells and Ptk2 192
Treatment of DRG neurons, N2a cells and transfected PtK2 cells with LPA 192
Inhibition of cdk5 in DRG neurons, N2a cells and transfected Ptk2 cells 193
Inhibition of cdk5/GSK3β in DRG neurons 193
Treatment of DRG neurons, N2a cells and transfected PtK2 cells with LPA 193
Inhibition of ROCK (Rho-associated kinase) and myosin in DRG neurons and N2a cells 193
Inhibition of CaMKII, calcineurin, calpain, PKC in DRG neurons 194
S-nitrosylation of MAP1B in DRG neurons and transfected PtK2 cells 194
Inhibition and activation of nNOS in DRG neurons 194
Stabilization of microtubules with taxol in DRG neurons and N2a cells 195
Stimulation of cAMP in DRG neurons 195
Treatment with DMSO –a solvent control 195
MICROSCOPY STUDIES OF CELLS 195
Immunofluorescence microscopy of the cells 195
Time-lapse video microscopy studies of DRG neurons 196
PREPARATION OF AGGRECAN-LAMININ SPOT GRADIENT COVERSLIPS 197
PREPARATION OF MYELIN SPOTTED COVERSLIPS 197
Isolation of myelin from mouse brain 197
Preparation of coverslips 198
ANTIBODIES 198
INHIBITIORS 200

REFERENCES **201**

LIST OF FIGURES AND TABLES **228**

CURRICULUM VITAE **231**

SUMMARY

Microtubule associated protein 1B (MAP1B) is expressed at the highest level during early stages of embryogenesis and is downregulated after birth. It is synthesized as polyprotein that is cleaved into heavy chain (HC) and light chain (LC1). Due to microtubule and actin binding properties MAP1B is proposed to be a crosslinker between cytoskeletal components. MAP1B-/- mice are characterized by the lack of corpus callosum, a prominent axon tract connecting the two cerebral hemispheres, suggesting a role of MAP1B in axon guidance. In addition, in the peripheral nervous system reduced diameters of axons, decreased thickness of the myelin sheaths and reduction in conduction velocity were observed (Meixner et al., 2000).

Nitric oxide (NO) is a messenger molecule, synthesized by nitric oxide synthases (NOSs), which plays a role as neurotransmitter and neuromodulator. At low concentrations NO contributes to physiological processes, whereas at high concentration NO was found to be toxic for cells of the nervous system. NO was found to play an important role in retinotectal pruning during development of chick visual system (Wu et al., 2004) and to induce axon retraction in cultured embryonic chicken DRG neurons (He et al., 2002). Axon retraction induced by NO was impaired in MAP1B-/- DRG neurons and was shown to involve S-nitrosylation of LC1 on cys2457 as a critical step (Stroissnigg et al., 2007).

In the first part of my thesis I examined the potential involvement of NO in two physiological axon retraction paradigms, repulsive axon guidance by lysophosphatidic acid (LPA) and myelin and Chondroitin Sulfate Proteoglycane (CSPG) inhibition of axon regeneration. I found that LPA-induced axon retraction does not require activation of nNOS, but it involves MAP1B, the Rho-associated kinase (ROCK) and myosin, consistent with previous studies. I also analyzed whether NO and MAP1B are implicated in inhibition of axon growth triggered by myelin and by CSPGs, but inhibition of nNOS and NOSs in general did not overcome inhibitory properties of neither CSPGs or myelin. Growth of both wild-type and MAP1B-/- DRG neurons was affected by myelin and CSPGs.

In the second part of my thesis I investigated the mechanism underlying NO-induced axon retraction. To increase NO levels, neurons were treated with calcimycin, which enhances Ca^{2+} levels resulting in activation of nNOS. An increase of Ca^{2+} can activate

potentially also Ca^{2+} effectors other than nNOS. I found that CaMKII, calcineurin, calpain and protein kinase C (PKC) are not involved in calcimycin-induced axon retraction of DRG neurons, whereas I confirmed involvement of nNOS. Further, I showed that ROCK activity and myosin are essential for NO-induced axon retraction, since inhibition of either ROCK or myosin prevented both calcimycin- and NO donor-induced retraction of neurites in mouse DRG neurons and in neuroblastoma N2a cells. In addition, in N2a cells monophosphorylation of the myosin regulatory light chain (MRLC) upon treatment with NO donor was enhanced, suggesting that NO can increase myosin activity. Stimulation of cAMP partially abolished NO-induced axon retraction. I also showed that NO-, calcimycin- and LPA-induced retractions of axons are not due to depolymerization of microtubules. I found that stabilization of microtubules by taxol leads to axon retraction with hallmarks similar to retraction observed upon treatment with an NO donor, calcimycin or LPA, but it does not involve acto-myosin contractility. Moreover, NO donor and LPA treatment increased binding of MAP1B with microtubules in non-neuronal PtK2 cells. Analysis of the dynamics of microtubule plus ends by *in vivo* labelling with GFP-tagged end-binding protein 1 (EB1-GFP), revealed that in MAP1B-/- DRG neurons the velocity, the distance, the time of EB1-GFP comet life and the number of comets per axon length and per growth cone area were enhanced when compared to wild-type DRG neurons. I propose that in wild-type DRG neurons MAP1B binds to microtubules stabilizing and protecting them from severing proteins. In MAP1B-/- neurons lack of MAP1B results in enhanced accessibility of microtubules for severing proteins that cut long microtubules into short dynamic ones, leading to excessive axon branching. Finally, treatment with LPA reduced the velocity, the time of EB1-GFP comet life and the number of comets per axon length in axons of wild-type DRG neurons. Taken together, these results I suggest that LPA and NO induce conformational changes in MAP1B increasing its microtubule binding activity. In the effect microtubules are overstabilized by MAP1B leading to axon retraction.

In the third part of my thesis, I examined involvement of MAP1B in laminin/integrin signaling. I found that the different morphology of wild-type versus MAP1B-/- DRG neurons can be observed when neurons are cultured on laminin, but not on poly-L-lysine only. Inhibition of cdk5 with roscovitine induced axon retraction in wild-type DRG neurons. In MAP1B-/- DRG neurons the response to roscovitine was altered. Retraction induced by inhibition of cdk5 involved ROCK and myosin, and was observed only when neurons were grown on laminin. Inhibition of GSK3β partially

prevented axon retraction induced by roscovitine, whereas inhibition of nNOS had no influence. In addition, roscovitine increased microtubule binding of MAP1B in PtK2 cells, suggesting a similar mechanism as in case of LPA- and NO-induced axon retraction. Thus, laminin/integrin signalling seems to play role both in promotion of axon growth and axon retraction.

ZUSAMMENFASSUNG

Mikrotubuli assoziiertes Protein 1B (MAP1B) ist während der Embryonalphase am stärksten exprimiert und wird nach der Geburt hinunterreguliert. Es wird als Polyprotein synthetisiert, welches anschließend in eine schwere Kette (HC) und eine leichte Kette (LC) gespalten wird. Aufgrund der Fähigkeit von MAP1B sowohl Aktin als auch Mikrotubuli zu binden, wird es als Quervernetzer der beiden Zytoskelettbestandteile angesehen. MAP1B-/- Mäusen fehlt das Corpus Callosum, ein ausgesprochen wichtiger Nerventrakt, der die zwei Gehirnhälften verbindet. Daher kommt die Vermutung, dass MAP1B essentiell für die korrekte Führung der Nerven während der Entwicklung ist. Außerdem kommt es in MAP1B-/- Mäusen zu einem verringerten Axondurchmesser, einer dünneren Myelinschicht und einer Reduktion der Nervenleitgeschwindigkeit (Meixner et al., 2000).

Stickoxid (NO) ist ein Signalmolekül welches von Stickoxidsynthasen (NOS) synthetisiert wird. Es spielt eine Rolle als Neurotransmitter und Neuromodulator. In geringen Konzentrationen unterstützt NO physiologische Prozesse, doch sobald die Konzentration zu stark ansteigt, kann es toxisch auf Nervenzellen wirken. Es wurde herausgefunden, dass NO wichtig für die Entwicklung des visuellen Systems in Hühnern (Wu et al., 2004) ist und, dass es zu Retraktion von kultivierten embryonalen Hühner DRG Neuronen führt (He et al., 2002). NO-induzierte Axonretraktion findet in MAP1B-/- DRG Neuronen nicht statt da dafür die S-Nitrosylierung der leichten Kette von MAP1B am cys2457 nötig ist (Stroissnigg et al., 2007).

Im ersten Teil meiner Dissertation untersuchte ich die mögliche Mitwirkung von NO in zwei physiologischen Axonretraktionsparadigmen: die repulsive Axonführung durch Lysophosphat-Säure (LPA) und die Inhibierung der Axonregeneration durch Myelin und Chondroitin Sulfat Proteoglykane (CSPG). Ich stellte fest, dass LPA-induzierte Axonretraktion nicht von nNOS abhängig ist, aber sehr wohl MAP1B, Rho-assoziierte Kinase (ROCK) und Myosin benötigt. Diese Ergebnisse stehen im Einklang mit vorherigen Studien. Ich analysierte auch ob NO und MAP1B an der Inhibierung des axonalen Wachstums durch Myelin und CSPGs beteiligt sind. Doch die Inhibierung von NO-Synthasen und nNOS im Speziellen konnte das Wachstum der Axone unter diesen Umständen nicht positiv beeinflussen. Das war sowohl in Wildtyp als auch in MAP1B-/- DRG Neuronen der Fall.

Im zweiten Teil meiner Dissertation wollte ich Näheres über den grundlegenden Mechanismus herausfinden der hinter der NO-induzierten Axonretraktion steht. Um die NO-Konzentration in Neuronen zu erhöhen, verwendete ich Calcimycin welches die Kalziumkonzentration in der Zelle erhöht, was unter anderem zur Aktivierung von nNOS führt. Ich fand heraus, dass CaMKII, Calcineurin, Calpain und Protein Kinase C (PKC) nicht für Calcimycin-induzierte Axonretraktion benötigt werden, doch die Involvierung von nNOS konnte ich bestätigen. Weiters entdeckte ich, dass ROCK Aktivität und Myosin essentiell für die NO-induzierte Axonretraktion sind, da deren Inhibierung sowohl Calcimycin- als auch NO-Donor-induzierte Retraktion in DRG Neuronen und N2a Zellen verhindert. Außerdem wurde die Monophosphorylierung der regulierenden leichten Kette von Myosin (MRLC) durch den Einfluß von NO erhöht, was darauf hindeutet, dass NO die Aktivität von Myosin ankurbelt. Die Stimulierung von cAMP konnte teilweise die NO-induzierte Axonretraktion verhindern. Ich konnte zeigen, dass NO-, Calcimycin- und LPA-induzierte Axonretraktion nicht durch Mikrotubulidepolymerisation zustande kommt. Stabilisierung von Mikrotubuli durch Taxol führt zu Axonretraktion. Diese zeigt dieselben Kennzeichen wie sie auch bei einer Retraktion durch einen NO-Donor, Calcimycin oder LPA zu sehen sind. Was hier allerdings nicht involviert war, ist die Aktin-Myosin-Kontraktion. Die Bindung von MAP1B an Mikrotubuli wird durch die Behandlung mit einem NO-Donor oder LPA in nicht-neuronalen PtK2 Zellen verstärkt. Die Dynamik der Mikrotubuli-Plusenden wurde mit Hilfe einer *in vivo* Markierung mit GFP-markiertem end binding Protein (EB1-GFP) analysiert. In MAP1B-/- DRG Neuronen ist die Geschwindigkeit der Kometen höher, die Distanz welche sie zurücklegen größer, die Lebensdauer länger und deren Anzahl höher. Alle Parameter wurden in Bezug auf die Axonlänge und pro Wachstumskegelfläche gemessen. Daraus schliesse ich, dass in Wildtyp DRG Neuronen MAP1B stabilisierend und schützend auf die Mikrotubuli wirkt. In MAP1B-/- Neuronen haben Mikrotubuliteilende Proteine leichteren Zugang zu denselben und schneiden diese in kleine dynamischere Teile, was wiederum zu vermehrter Axonverzweigung führt. LPA-Behandlung verringerte die Geschwindigkeit der Kometen, deren Lebensdauer und deren Anzahl in Wildtyp DRG Neuronen. In Anbetracht all dieser Ergebnisse kann man zu dem Schluss kommen, dass LPA und NO die Konformation von MAP1B ändern und somit seine Mikrotubulibindungskapazität erhöhen. Dadurch werden Mikrotubuli zu stark stabilisiert und das führt zur Axonretraktion.

Im dritten Teil der Dissertation studierte ich die Rolle von MAP1B in Laminin/Integrin Signaltransduktionswegen. Ich beobachtete eine unterschiedliche Morphologie der DRG Neuronen wenn sie auf Laminin oder Poly-L-Lysin kultiviert wurden. Die Inhibierung der Cdk5 durch Roscovitin induzierte Axonretraktion in Wildtyp DRG Neuronen. MAP1B-/- Neuronen reagierten anders auf diese Behandlung. Retraktion durch Cdk5-Inhibierung benötigt ROCK und Myosin und konnte nur bei Neuronen gesehen werden, die auf Laminin gewachsen waren. Inhibierung von GSK3β konnte teilweise die Axonretraktion durch Roscovitin verhindern, doch nNOS-Inhibierung hatte keinen Einfluss darauf. Außerdem verstärkte Roscovitin die Bindung von MAP1B an Mikrotubuli in PtK2 Zellen was an die Eigenschaften von LPA- und NO-induzierter Axonretraktion erinnert. Somit scheint es als würden Laminin/Integrin Signaltransduktionswege sowohl beim Axonwachstum als auch bei der Axonretraktion eine Rolle spielen.

INTRODUCTION

THE NERVOUS SYSTEM

The function of nervous system is to perceive and respond to external stimuli and to conduct signals within the body. It consists of neurons, which convey impulses, and neuroglia, which take also part in transmitting of impulses, supply nutrients to the neurons and provide insulation for neuronal axons and dendrites. In addition, neuroglia partcipate in the repair of the nervous system after injury by destroying pathogens and removing dead neurons. Neurons usually have a cell body in which their nucleus is located, a number of short, branched dendrites and one long unbranched or branched axon. Signals from other neurons are received through the synapses, spread over the cell body and dendrites, and outgoing information is transmitted via the axon.

There are three main classes of neurons: the motor neurons, the sensory neurons and the interneurons. The motor neurons, known also as efferent or effector neurons, convey signals from the central nervous system (CNS) to muscles and from the motor cortex within the CNS. The cell bodies of the motor neurons are localized in the CNS. They extend many dendrites and one axon, which form a neomuscular junction, known as a motor plate, at the target muscle. The sensory neurons, known also as afferent or receptor neurons, transduce signals from a variety of sensory receptors in the peripheral nervous system (PNS) to the CNS. They terminate at the root ganglia of the CNS and transmit information from the limbs, skin, sensory and internal organs, for example they convey a pain and heat. Interneurons carry signals between neurons within the CNS and the PNS.

There are two types of neuroglia: microglia and macroglia. Microglia comprise of specialized macrophages capable of phagocytosis, which multiply when the nervous system is injured. Macroglia comprise of astrocytes, oligodendrocytes, ependymal cells and radial glia in case of the CNS, and of Schwann cells and satellite cells in case of the PNS. Astrocytes participate in anchoring neurons to their blood supply, removing excess ions and recycling neurotransmitters released during synaptic transmission. Oligodendrocytes form myelin sheat around axons of the CNS. In the PNS the same function is fulfilled by Schwann cells.

The central nervous system

The CNS coordinates functions of all parts of the body. It consists of the brain, located in the cranial cavity, and the spinal cord, located in the spinal cavity. The brain is protected by the blood-brain barrier and by the skull. It receives information from spinal cord and its own nerves, like the optic nerves, and transforms them to a proper and coordinated motor output. The spinal cord consists of 31 pairs of nerves and is protected by the vertebrae. The motor nerves go into the ventral root, whereas the sensory nerves go into the dorsal root ganglion (DRG), and then into the spinal cord. The spinal cord conducts sensory information from the PNS to the brain and motor information from the brain to effectors, for example glands or muscles. The spinal cord also acts as a minor reflex centre.

In contrast to the embryonic nervous system or the PNS, adult CNS fails to regenerate after injury. This is attributed to loss of ability to grow of mature neurons and inhibitory properties of the CNS myelin and proteoglycans produced within astroglial scar (Yiu and He, 2006). After injury the growth cones of lesioned axons adopt the shape of so called dystrophic endballs and their further growth is limited by myelin-associated inhibitors from oligodendrocytes and myelin debris (Yiu and He, 2006). The best known myelin-associated components are Nogo, myelin-associated glycoprotein (MAG), oligodendrocyte myelin glycoprotein (OMgp), the transmembrane semaphorin 4D (Sema4D) and ephrin B3 (Yiu and He, 2006). A second source of inhibition is a glial scar, which is formed by microglia, astrocytes, oligodendrocyte precursors and meningeal cells (Yiu and He, 2006). On one hand, they isolate the lesion site and limit the inflammation area, and some astrocytes can even support axon growth (Yiu and He, 2006). On the other hand, most of the astrocytes are highly reactive and release inhibitory molecules called chondroitin sulphate proteoglycans (CSPGs), which form a gradient with the highest concentration at the centre of lesion (Yiu and He, 2006). Both myelin and CSPG increase the intracellular Ca^{2+} level and activate a RhoA signal transduction pathway that induces rearrangement of the actin cytoskeleton (Yiu and He, 2006). Diminution of these inhibitory influences could promote the regrowth of axons after CNS injury.

The peripheral nervous system

The PNS consists of nerves located outside the CNS, which are not protected by bone or by the blood-brain barrier and connect the CNS to the organs and limbs. The cell bodies of the PNS neurons are organized in ganglia and their neurites extend both into the periphery and to the CNS. The PNS is divided into the somatic nervous system (SNS) and the autonomic nervous system (ANS). The SNS is involved in control of body movement and reception of signals from the surrounding environment. The ANS maintains homeostasis in the body, which is performed without conscious control, for example digestion. It consists of efferent and afferent nerves going to and from the CNS. The ANS can be further divided into the parasympathetic nervous system and the sympathetic nervous system. They usually function in opposition to each other. The sympathetic nervous system works in actions that require immediate reaction (for example "fight or flight"), while parasympathetic system functions in actions that do not need a fast response (relaxation).

AXON GUIDANCE

The formation of the correct neuronal connections during development of the nervous system depends on the ability of axons to locate and recognize their targets. Similarly, rebuilding of the correct network of neurons is important in the adult nervous system during regeneration after injury. Targets can be very far away from the cell body of a given neuron and neurites extending from the cell body have to be guided by signals from the environment. These signals are called guidance cues and give information where the axon should grow and when it should turn. The tip of the neurite, called the growth cone, is a specialized structure capable of proper reading and responding to guidance signals. Extracellular guidance cues can attract or repel the growth cone.

Studies on the pattern of nerve process outgrowth and connectivity in the developing mammalian brain by spanish histologist Santiago Ramón y Cajal in 1890 were a breakthrough. He proposed that neurites, for example axons, are navigated to the target cells by diffusible molecules secreted by these cells (Ramón y Cajal, 1890). Direct evidence for the guidance theory was obtained later and by the early 1990s several conserved families of long-range and short-range axon guidance molecules were

discovered. Long range signals are diffusible molecules secreted by cells, while short range signals are non-diffusible, cell surface-bound or bound to the extracellular matrix (ECM) molecules. The best known and understood guidance cues are netrins, semaphorins, slits and ephrins.

Netrins

Netrins are secreted proteins guiding migration of neurons and growth cones during development. The best studied member of the family is netrin-1, which like most members of the group is a bifunctional molecule. For some neurons it is an attractive guidance cue that works through the DCC receptor and for others is a repulsive guidance cue that works through the Unc5 receptor (Keino-Masu et al., 1996; Baker et al., 2006; Round and Stein, 2007). Netrin-1 induced chemoattraction was shown to be important for formation of the corpus callosum, other commisures, corticospinal tract, the optic nerve and the internal capsule (Bradford et al., 2009). Both netrin-1 knockout mice and DCC knockout mice are characterized by the absence of the corpus callosum and the hippocampal commisure (Barallobre et al., 2005). Additionally netrin-1 was found to guide migrating pontine cells which express DCC receptors (Yee et al., 1999). Pontine cells form structures that connect the cerebrum with the cerebellum and in both, netrin-1 and DCC knockout mice, pontine cells are not guided to the midline and the pontine nuclei are missing (Bradford et al., 2009). Netrin-1 also guides interneuron precursors to the maturing olfactory bulb (Murase and Horwitz, 2002). On the other hand, it is a chemorepulsive cue in guiding cerebellar interneurons which migrate from the internal granule layer to the external germinal layer and afterwards take a position in the molecular layer (Guijarro et al., 2006). Unc5 receptors on the migrating neurons detect netrin-1 as a stop signal. Similarly, netrin-1 present at the optic disc prevents entering of oligodendrocytes to the retina (Barallobre et al., 2005).

Netrin-1 can act at short-range within 10-20µm of its source or at long-range through a gradient established within the extracellular milieu (Bradford et al., 2009). Both short- and long-range chemoattraction are maintained through DDC receptors, whereas short-range chemorepulsion requires Unc5 and long-range chemorepulsion involves both Unc5 and DCC receptors (Wen and Zheng, 2006). Interaction between netrin-1 and the DCC receptor induces homodimerization of the receptor (Round and Stein, 2007) which

leads to tyrosine phosphorylation of the kinases FAK, Src and Fyn. This step is believed to activate Rac1 and Cdc42 and in turn promotes extension of the lamellipodium and filopodium. In addition, netrin-1-dependent guidance is regulated by Ca^{2+} influx and Ca^{2+}–dependent pathways (Bradford et al., 2009). Binding of netrin-1 to the DCC receptor leads to Ca^{2+} influx through voltage-gated Ca^{2+} channels and transient receptor potential (TRP) channels mediating attraction also by activation of Rac1 and Cdc42. Chemorepulsive guidance mediated by Unc5 results in low intracellular Ca^{2+} levels and RhoA-dependent growth cone collapse or repulsion (Wen and Zheng, 2006).

Semaphorins

Semaphorins are a family of cell-surface transmembrane and secreted glycoproteins that associate with the cell surface and influence axon guidance (Kolodkin et al., 1993; Lallier, 2004). There are eight subclasses of semaphorins: subclasses 1, 2 and 5 are expressed in invertebrate species and 3-7 were found in vertebrate species. They act as chemorepellents in axon guidance and are involved in axonal steering, axonal fasciculation, neuronal polarity, zonal segregation of axon populations and neuronal cell migration (Takegahara et al., 2005). Additionally, semaphorins were shown to play an important role in regulation of blood vessel pattering, leukocyte movements, organogenesis and angiogenesis (Kitsukawa et al., 1995; Behar, 1996; Sekido et al., 1996; Taniguchi et al., 1997).

Sema3A, known also as collapsin 1, repulses axons of sensory and sympathetic neurons (Luo et al., 1993; Chedotal et al., 1998; Steup et al., 1999). It is highly expressed in E11-E14 mouse embryos and its expression was shown to correlate with the growth of DRG axons toward their central and peripheral targets (Giger et al., 1996). Growth cone collapse of embryonic chicken DRGs induced by Sema3A involves protein kinase G (PKG) and ROCK kinase activity (Dontchev and Letourneau, 2002). Sema4D/CD100 is a transmembrane protein and its mRNA is expressed in human in the embryonic and adult brain, heart, spleen, kidney and lungs (Hall et al., 1996) and in mice throughout embryonic neuronal tissue with highest expression in DRG and cortical plate (Kumanogoh and Kikutani, 2004). Sema4D induces growth cone collapse in hippocampal neurons and retraction of neurites and cell rounding in PC12 cells, which can be blocked by inhibition of the ROCK kinase (Perrot et al., 2002). In addition

upregulation of Sema4D expression in oligodendrocytes was observed 8 days after spinal cord lesion (Moreau-Fauvarque et al., 2003). It was shown that CA1, CA2 and dentate gyrus axons are strongly repelled by both Sema3 and Sema4, whereas entorhinal axons are repelled only by Sema3A (Chedotal et al., 1998). Sema5B induces growth cone collapse in chicken DRGs via influx of Ca^{2+}. First a low-amplitude Ca^{2+} influx is induced which leads to activation of calcineurin. This is followed by a high-amplitude Ca^{2+} influx that activates calpain. Sema5B also induces cleavage of calcineurin by calpain (To et al., 2007).

Two families of receptors for semaphorins were identified – neuropilins (NP1 and NP2) and plexins (Takegahara et al., 2005). Neuropilins show high affinity for subclass 3, for example neuropilin 1 for Sema3A and neuropilin 2 for Sema3F (Chen et al., 1997; Kolodkin, 1997; Nakamura et al., 1998), while plexin-B1 is a receptor for Sema4D. In addition, two molecules unrelated to plexins and neuropilins, were found to interact with semaphorins – CD72 and Tim-2 (Kumanogoh et al., 2000; Kumanogoh et al., 2002).

Slits

Slits are large secreted proteins acting via transmembrane receptors of the Roundabout (Robo) family (Dickson, 2002). In mammals, three homologs of Slits (Slit1, Slit2, Slit3) and four homologs of Robo receptors (robo1, robo2, robo3 and rig-1) were described (Kidd et al., 1998; Webber and Raz, 2006). Slits also bind to other factors involved in axon navigation such as netrin or laminin (Brose et al., 1999). The Slits are midline repellents conserved in vertebrates (Kidd et al., 1998; Brose et al., 1999), but also can stimulate axon branching and elongation, for example in DRG neurons (Wang et al., 1999; Brose and Tessier-Lavigne, 2000). Repulsion is mediated often through growth cone collapse, for example in case of the spinal cord, retinal ganglion neurons, mitral cells of the olfactory bulb, cortical neurons projecting into the corpus callosum, thalamic axons projecting into the cortex, and neurons projecting from the dentate gyrus (Nguyen Ba-Charvet et al., 1999; de Castro, 2003). Double knockout mice for slit1 and slit2 show a second optic chiasm formed at a more anterior location with many axons projecting into the opposite optic field instead of crossing at the normal chiasm (Plump

et al., 2002). In humans who have a mutation of Robo3 the major sensory and motor projections do not cross between the brain and the spinal cord (Jen et al., 2004).

Ephrins

Ephrins are membrane-associated ligands binding to members of the Eph receptor family, which is the largest subfamily of receptor tyrosine kinases (TRK). There are two classes of ephrins and their receptors: ephrins of class A are anchored to the plasma membrane by a glycosylphosphatidylinositol (GPI) linkage and bind EphA receptors; and ephrins of class B which have a transmembrane domain and cytoplasmic tail lacking endogenous catalytic activity, and bind EphB receptors (Dickson, 2002; Egea and Klein, 2007; Klein, 2009). Ephrin-A and its EphA receptor work as repellent guidance cues in topographic mapping of retinal axons along the anterior-posterior axis (Wilkinson, 2001). The ephrin-A gradient establishes the topographic order of retinal axons (Dickson, 2002). In contrast, ephrin-B and EphB receptors mediate attractive signals in mapping along the dorsal-ventral retinal axis (Mann et al., 2002). Ephrin-B was shown to repel forebrain commissural axons from EphB-expressing cells and to attract them to EphA4-expressing cells (Henkemeyer et al., 1996; Kullander et al., 2001). In EphB lacking mouse embryos, the contralateral inner ear efferent growth cones select inappropriate pathways at the midline (Cowan et al., 2000).
The action of the Eph-ephrin system is limited to cell-to-cell communication and functional Eph-ephrin signalling requires higher-order receptor clusters than dimers (Egea and Klein, 2007). Ephrin binding to its receptor stimulates signalling cascades within the Eph-bearing cell, which is called the forward signalling, and within the ephrin-bearing cell, called the reverse signalling. Eph receptors recruit phosphotyrosine-binding adaptor proteins to activate Rho GTPases and remodel the actin cytoskeleton (Song and Poo, 1999; Noren and Pasquale, 2004).

Ca^{2+} effectors in controlling and steering growth cone

Cytoplasmic Ca^{2+} is an important second messenger that was shown to participate in transducing many extracellular signals, which regulate and guide growth cones (Song

and Poo, 1999). The growth of neurites was shown to be regulated by the concentration of intracellular Ca^{2+} ($[Ca^{2+}]_i$) (Henley and Poo, 2004a). Normal growth cone motility depends on an optimal range of $[Ca^{2+}]_i$, which is approximately 100nM. When $[Ca^{2+}]$i levels are above or below this optimal range neurites stop their extension. Thus, moderate increase in $[Ca^{2+}]_i$ level can promote neurite extension, whereas high or low changes of $[Ca^{2+}]_i$ level can inhibit growth cone motility (Connor, 1986; Silver et al., 1989; Zheng, 2000). The resting level of $[Ca^{2+}]_i$ is regulated by three mechanisms: a) Ca^{2+}/ATPase-dependent uptake into internal stores, for example into mitochondria and the endoplasmic reticulum (ER); b) transfer of Ca^{2+} outside the cell by plasma membrane calcium ATPases (Garcia and Strehler, 1999) and c) the Na^{+}/Ca^{2+} exchange (Zheng and Poo, 2007). Changes in $[Ca^{2+}]_i$ are triggered by Ca^{2+} release from intracellular stores through ryanodine- and IP_3-sensitive channels or from Ca^{2+}-influx through plasma membrane Ca^{2+} channels, mainly through voltage-dependent Ca^{2+} channels (VDCCs) and ligand-gated ion channels (Zheng and Poo, 2007). There is considerable evidence showing the importance of Ca^{+2} channels in regulation of growth cone motility. For example, blocking plasma membrane Ca^{2+} channels can inhibit growth cone motility and neurite extension (Mattson and Kater, 1987) and abolish steering of the growth cone by netrin-1 (Hong et al., 2000). Blocking the function of IP_3 receptors in the endoplasmatic reticulum also inhibits neurite growth (Takei et al., 1998). Additionally, intracellular proteins that bind Ca^{2+} can regulate Ca^{2+} changes by buffering, for example calretinin or parvalbumin. Other proteins, for example calpain or calmodulin, can directly regulate the activity of downstream effectors (Henley and Poo, 2004a).

Global increases in growth cone $[Ca^{2+}]_i$ level can regulate axon growth, whereas local increases in $[Ca^{2+}]_i$ can steer growth cones. For example, extracellular application of neurotransmitters, which strongly increases global level of $[Ca^{2+}]_i$ inhibits neurite growth (McCobb et al., 1988), while an extracellular gradient of glutamate (Zheng et al., 1996) or acetylcholine (Zheng et al., 1994) can induce an attractive turning response of the growth cone.

Attractive and repulsive turning responses of the growth cone depend on local changes of Ca^{2+} levels (Song and Poo, 1999; Hong et al., 2000), but how different turning responses are generated by distinct Ca^{2+} signals is still unknown. It is assumed that different local Ca^{2+} signals depends on the baseline level of $[Ca^{2+}]_i$ and activate distinct pathways to transduce attraction or repulsion signals. At the normal resting level of

$[Ca^{2+}]_i$ (~130nM for cultured neurons) a small local increase in Ca^{2+} levels mediates repulsion, while a large local increase in Ca^{2+} levels mediates attraction. When the resting level of $[Ca^{2+}]_i$ is below the optimal range (~60nM for cultured neurons) both small and large increases induce retractive responses of the growth cone (Wen et al., 2004). The Ca^{2+}-dependent response of the growth cone can be additionally modulated by the cAMP pathway. It was shown that elevation of cAMP can switch repulsion to attraction, and vice versa (Song and Poo, 1999; Wen et al., 2004), and that the cAMP/cGMP ratio could affect L-type Ca^{2+} channels to alter intracellular Ca^{2+} signals induced by netrin-1, placing cAMP/cGMP upstream of Ca^{2+} (Nishiyama et al., 2003).

Downstream effectors of Ca^{2+} signals

Ca^{2+}/calmodulin-dependent protein kinase II (CaMKII)

CaMKII is highly expressed in the nervous system and comprises 1-2% of all proteins in the brain (Kolodziej et al., 2000; Griffith, 2004). There exist 28 isoforms which are derived from 4 genes (α, β, γ and δ) and each of these isozymes has a multiples splice variants. In the brain subunits α and β are predominantly expresse (Hudmon and Schulman, 2002a). Monomers of different isozymes are able to coassemble leading to a large number of possible holoenzyme compositions(Griffith, 2004).

The most interesting subunit seems to be CaMKIIβ, since it is expressed early during development and regulates axon extension (Fink et al., 2003). It requires for activation a several fold lower concentration of Ca^{2+}/calmodulin than CaMKIIα and transduces Ca^{2+}signals of low amplitude (Zheng et al., 1994; Wen et al., 2004). CaMKIIα is expressed in mature neurons and regulates axonal branching induced by Ca^{2+} signals of high amplitude (Tang and Kalil, 2005).

CaMKII is activated by Ca^{2+} entering through NMDA receptors, which in turn increases the number and conductivity of AMPA receptors within postsynaptic membranes (Derkach et al., 1999; Shi et al., 1999). CaMKII activity is regulated by Ca^{2+}/calmodulin binding to each subunit and by autophosphorylation at its regulatory domain that can render each subunit partially autonomous from Ca^{2+}/calmodulin binding (Meyer et al., 1992; Hudmon and Schulman, 2002a, 2002b). It was also found that there are CaMKII

binding proteins that can maintain the active state of the kinase in the absence of Ca^{2+}/calmodulin, and one binding partner was shown to inactivate the kinase by inducing inhibitory autophosphorylation (Griffith, 2004). In the rat CaMKIIα phosphorylation of theronine 286 (Thr 286) was shown to enable the kinase to remain active even after dissociation of its activator Ca^{2+}/calmodulin (Fig. 1; Miller et al., 1988). Once the enzyme is Ca^{2+}-independent and Ca^{2+}/calmodulin dissociates, additional autophosphorylation sites within the calmodulin-binding domain become accessible. When these sites are autophosphorylated, Ca^{2+}/calmodulin can not bind again. CaMKII autophosphorylation reactions have been studied quite extensively and are critical for regulation of the kinase by both Ca^{2+}/calmodulin and other protein regulators (Griffith, 2004).

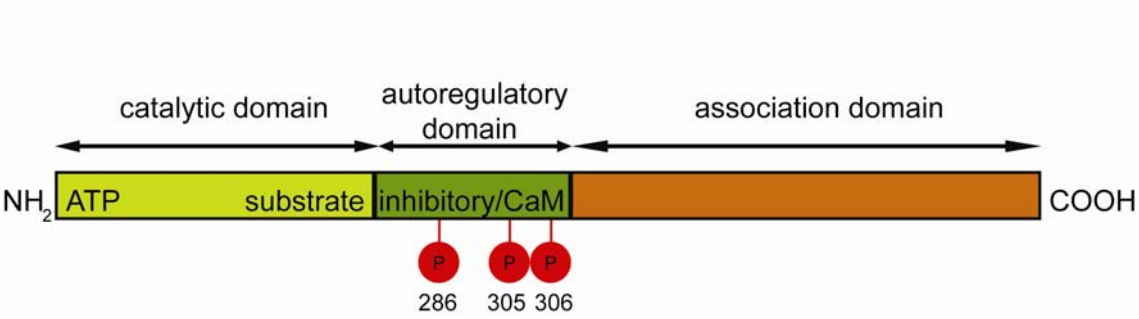

Fig. 1. The domain structure of CaMKII. The catalytic domain is autoinhibited by a pseudosubstrate autoregulatory domain. Binding of Ca^{2+}/calmodulin activates CaMKII. The association domain is instrumental in formation of the multimeric holoenzyme, which composes of 12 subunits. Conserved sites of autophosphorylation in the autoregulatory region are indicated (adapted from Hudmon and Schulman, 2002b).

There is much evidences indicating that increased CaMKII activity mediates long-term potentation (LTP), which underlies some forms of learning and memory (Malenka et al., 1989; Malinow et al., 1989). It was shown that CaMKII activity is necessary for LTP. Increases in CaMKII activity can generate potentate transmission mimicking LTP and LTP can activate CaMKII. Defects in LTP often accompany disturbances in spatial learning, and animals that lack the CaMKIIα do not learn normally in such tasks (Silva et al., 1992). Stimuli which induces LTP increase autophosphorylation of Thr 286 (Fukunaga et al., 1995) and mutation of Thr 286 blocks LTP in CA1 region of hippocampus and learning in the Morris water maze (Giese et al., 1998).

Calpains

Calpains are Ca^{2+}-sensitive cytoplasmic cysteine proteases which cleave many intracellular signalling and structural proteins, like kinases, actin (Potter et al., 1998), neurofilaments (Ishizaki et al., 1983), spectrin (Ishizaki et al., 1983; Johnson et al., 1991) or microtubule-associated proteins, such as tau (Johnson et al., 1989), MAP1 (Fischer et al., 1991), and MAP2 (Fischer et al., 1991; Johnson et al., 1991). The best characterized isoforms of calpain are *μ*-calpain (Capn1, calpain I) and *m*-calpain (Capn 2, calpain II), which require micromolar or milimolar Ca^{2+} for activation, respectively (Li and Banik, 1995). Both forms are present in cells as inactive precursor isoforms, which are activated by calcium induced autoproteolytic cleavage of the N-terminal sequence. Calpains exist as heterodimers consisting of a common small regulatory subunit (Capn4; 30kDa) and large catalytic subunit (80kDa), which associate through an EF-hand motif (Perrin and Huttenlocher, 2002; Goll et al., 2003). Typical calpains, like *μ*-calpain and *m*-calpain, possess C-terminal Ca^{2+}-binding domains, called domain IV which includes an EF-hand motif. Atypical calpains lack EF-hand motifs and contain additional domains. The large subunits of calpain I and calpain II contain 4 domains (Fig. 2). Domain I is a NH_2-terminal region of a catalytic subunit, which interacts with domain VI of the regulatoryl subunit, and probably is important for stability. Domain II is responsible for catalytic activity of enzyme, containing all residues of the catalytic triad – cysteine 105 (Cys 105), histidine 262 (His 262) and asparagine 286 (Asn 286). Domain III binds Ca^{2+} and phospholipids and has a configuration similar to the C2 domain of protein kinase C (PKC) or phospholipase C (PLC). The small subunit contains domain V, the N-terminal hydrophobic region rich in glycine, which probably work as a membrane anchor, and domain VI which binds to Ca^{2+} and to the large subunit (Fig. 2; Wu et al., 2007).

m-calpain has at least four Ca^{2+}-binding domains: the two EF-hands, the cysteine catalytic region and the acidic loop in domain III. In the absence of Ca^{2+} calpains are in an inactive state. Binding of Ca^{2+} leads to conformational changes and their activation (Reverter et al., 2001; Wu et al., 2007). At first when Ca^{2+} binds to the EF-hand regions and domain III, the N-terminal link between large and small domains is eliminated due to autocleavage of domain I (Reverter et al., 2001; Wu et al., 2007). This induces rearrangements within domain II and formation of an active site. Subsequently Ca^{2+} binds directly to Cys 105 in domain II and induces conformational changes positioning

the catalytic site for hydrolysis (Reverter et al., 2001). Calpains lacking EF-hand motifs are activated directly by binding of Ca^{2+} to domain II (Fig. 2).

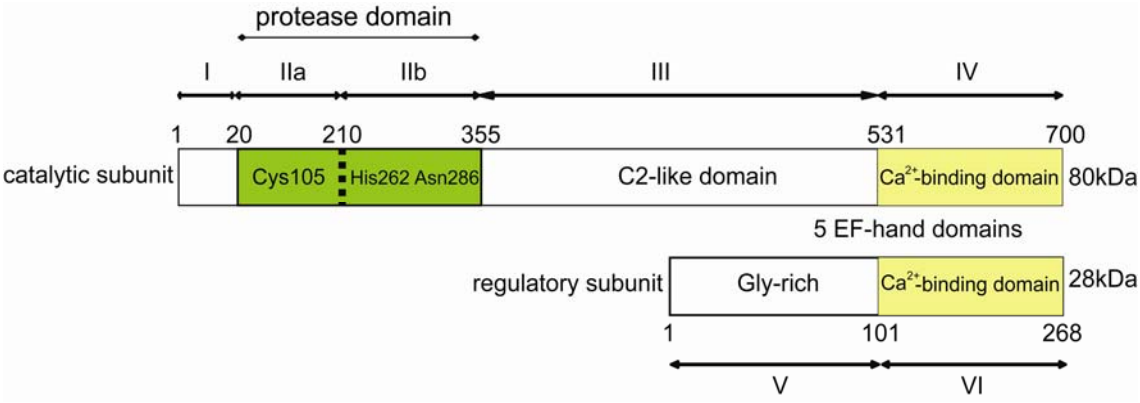

Fig. 2. Schematic of calpain structure. Calpain is a heterodimer consisting of a catalytic subunit and a regulatory subunit. The catalytic subunit consists of four domains (I-IV). Domain I (19 amino acids, white) interacts with domain VI of the regulatory subunit. Domain II (residues 20-355, green) is divided into 2 subdomains (IIa and IIb). It holds catalytic triad (Cys105, His262 and Asn286). Domain III (residues 356-531, white) binds Ca^{2+} and phospholipids, and has a configuration similar to the C2 domain of PKC. Domain IV (residues 532-700, yellow) possesses 5 EF-hand domains and binds Ca^{2+}. The regulatory subunit contains domain V (residues 1-100, white), a hydrophobic glycine rich region that can work as a membrane anchor, and domain VI (residues 102-268, yellow), which binds Ca^{2+} (adapted from Wu et al., 2007).

Calpains catalyze the proteolysis of proteins involved in cell migration, cell differentiation, cell-cycle regulation, signal transduction, cytoskeleton remodelling, embryonic development, apoptosis and nerosis (Wu et al., 2007). To avoid uncontrolled cleavage of proteins, calpain activity is controlled by many mechanisms, for example by the specific inhibitor calpastatin, which binds reversibly to calpain in a Ca^{2+}-dependent manner (Wu et al., 2007). The Ca^{2+} concentration necessary for calpstatin binding is lower than the concentration required for the half-maximal activity of calpains (Wu et al., 2007). Another mechanism controlling calpain activity is phosphorylation. Protein kinase A was shown to inhibit calpain activity by phosphorylation at Ser369 and Thr370 (Shiraha et al., 2002).

Overactivation of calpains, mainly by alterations in Ca^{2+} homeostasis, can lead to abnormal degradation of many proteins and subsequent cell death. This overactivation is linked to many diseases, for example cardiac and cerebral ischemia (Yamashima, 2000), traumatic brain injury (Kampfl et al., 1997), muscular dystrophy or neurodegenerative diseases (Yoon et al., 2006). It is proposed that overactivation of calpain observed in Alzheimer's disease (AD) can play a role in neurodegeneration and

cytoskeletal pathogenesis (Shimohama et al., 1991; Tsuji et al., 1998; Yoon et al., 2006). In okaidic acid-induced neurodegeneration two major synapse constituents – spectrin and synapsin-1 were cleaved by calpain (Yoon et al., 2006). It was also shown that motuporamine C (motC) – an inhibitor of axon outgrowth – induces a strong increase in the level of intracellular Ca^{2+} in embryonic chicken DRG neurons, resulting in the activation of calpain (To et al., 2008). Calpain was shown to be necessary for growth cone collapse, but inhibition of calpain only partially attenuates growth cone collapse induced by motopuramine C (To et al., 2008).

Calcineurin

Calcineurin is a heterodimer that consists of a catalytic subunit, called calcineurin A, and a regulatory Ca^{2+}-binding subunit, called calcineurin B (Klee et al., 1988; Wu et al., 2007). In mammals there are three isoforms of calcineurin A – α, β and γ, known also as α1, α2 and α3, respectively, and two isoforms of calcineurin B – B1 and B2. This serine/threonine protein phosphatase is highly expressed in brain with the highest level in the hippocampus and caudate putamen (Klee et al., 1988; Steiner et al., 1992; Morioka et al., 1997). Calcineurin A was shown to be present in cell bodies, axons, dendrites, postsynaptic densities, and spines (Wu et al., 2007). Approximately 50% of the calcineurin molecules are associated with the plasma membrane and the other 50% are localized in the cytosol (Klee et al., 1988). Calcineurin A comprises of a phosphatase domain, a calcineurin B-binding region, a calmodulin-binding domain, and an autoinhibitory loop, while calcineurin B contains a myristoylated-binding domain, two Ca^{2+}-binding regions that contain two Ca^{2+}-binding EF-hand motifs each and a calcineurin A-binding domain(Wu et al., 2007).

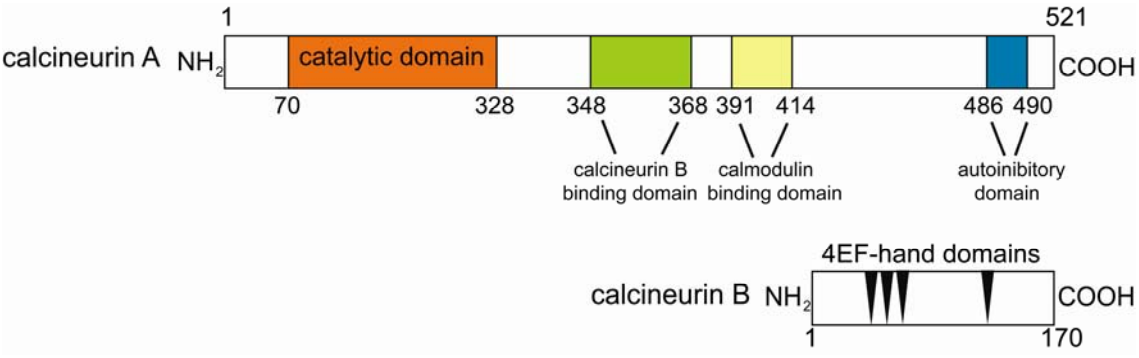

Fig. 3. Schematic of calcineurin structure. Calcineurin is a heterodimer that consists of two subunits – calcineurin A and calcineurins B. Calcineurin A (521 amino acids) is the catalytic

subunit and consists of the catalytic domain (residues 70-328, orange), the calcineurin B-binding domain (residues 348-368, green), the calmodulin binding domain (residues 391-414, light yellow) and the autoinhibitory domain (residues 486-490, blue). Calcineurin B (170 amino acids) is the regulatory subunit and possesses two Ca^{2+}-binding regions that contain two Ca^{2+}-binding EF-hand motifs each (black inverted triangles), and the calcineurin A-binding domain (not shown) (adapted from Wu et al., 2007).

Calcineurin is activated upon binding of Ca^{2+} to calcineurin B and Ca^{2+}-dependent binding of calmodulin to calcineurin A. This induces conformational changes and releases an autoinhibitory domain from the catalytic active site (Klee et al., 1988; Stemmer and Klee, 1991). It was shown in cultured embryonic *Xenopus* spinal neurons that at the normal resting level of $[Ca^{2+}]_i$ small local Ca^{2+}signals activate calcineurin and high local Ca^{2+} signals activate CaMKII, inducing repulsion and attraction, respectively, while at low resting levels of $[Ca^{2+}]_i$ both small and high local Ca^{2+}signals activate calcineurin (Wen et al., 2004). cAMP can switch repulsion mediated by calcineurin into attraction. CaMKII and calcineurin control netrin-1 guidance (Wen et al., 2004). Moreover, Sema5B-induced growth cone colapes in embryonic chicken DRG neurons involved low-amplitude increase in the Ca^{2+} level associated with calcineurin activation followed by high-amplitude increase in the Ca^{2+} level associated with activation of calpain (To et al., 2007). Additionally calcineurin can be activated irreversibly by proteases such as calpain, trypsin and chymotrypsin (Wang et al., 1989; Wu et al., 2004). It was shown *in vitro* that proteases can cleave the C-terminal part of calcineurin A, which contains the calmodulin-binding domain and the autoinhibitory domain, while the N-terminal part, containing the phosphatase catalytic domain and the calcineurin B-binding domain, is resistant to proteolysis (Hubbard and Klee, 1989). Proteolytic truncation converts calcineurin into an active state, which does not require Ca^{2+} and calmodulin for activity (Hubbard and Klee, 1989). In cultured neurons and in mouse hippocampus calcineurin A was shown to be a substrate of calpain (Wu et al., 2004). Calpain was also shown to cleave cain/cabin 1, which is an endogenous inhibitor of calcineurin. For example, in Jurkat cells this cleavage is necessary for calcineurin-mediated cell death (Kim et al., 2002).

As it was mentioned above calcineurin activity can be inhibited by its autoinhibitory domain, which interacts with the catalytic domain of the subunit A (Wu et al., 2007). It can be inhibited also by immunosuppressant cyclosporine A (CsA) and FK506, which prior to inhibition of calcineurin bind to their intracellular immunophilins: cyclophilin A and FKBP12, respectively (Liu, 1991; Wu et al., 2007). They can bind to the N-

terminus of the calcineurin B binding helix, the calcineurin subunit B and the catalytic domain of calcineurin (Liu et al., 1991). In addition, calcineurin was shown to be inhibited by cain/cabin 1, calcipressin, calcineurin homology protein (CHP) and protein kinase A anchoring protein (AKAP79) (Coghlan et al., 1995; Kashishian et al., 1998; Lai et al., 1998; Lin et al., 1999; Kingsbury and Cunningham, 2000).

Due to its impact on the phosphorylation state of proteins calcineurin participates in many cellular processes, for example, in neuronal and muscle development (Antoni et al., 1998; Schiaffino and Serrano, 2002) and Na^+ /K^+ ion transport in the nephron (Tumlin, 1997). Calcineurin was shown also to play a role in Ca^{2+}-dependent disorders, such as in cardiac hypertrophy (Bueno et al., 2002) and AD, where increased calpain I-mediated truncation and activation of calcineurin was observed to correlate with the number of neurofibrillary tangles (NFTs) (Liu et al., 2005).

Protein kinase C

PKCs constitute a family of serine/threonine kinases highly expressed in brain tissue and implicated in signal transduction during neurite growth in the CNS. These enzymes play a role in regulation of short-time events, like neurotransmitters release, mid-term events, like receptor regulation, and long-term events, like synaptic remodelling (Battaini and Pascale, 2005). In mammals at least 12 isoforms of PKC were characterized and each isoform can play an unique role due to specific activation-dependent subcellular localization and substrate phosphorylation (Dempsey et al., 2000). The C-terminal catalytic domain is conserved among the different isoforms, while the N-terminal regulatory domain, which is responsible for binding to activators, shows diversity. Interaction of the pseudosubstrate sequence localized in the regulatory sequence with the substrate binding site in the catalytic domain inhibits the enzyme (Parekh et al., 2000). Binding of Ca^{2+}, diacylglycerol (DAG), phosphatidylserine (PtdSer) or other lipids to the regulatory sequence leads to activation of PKC, which is associated with the translocation of the catalytically inactive enzyme from one compartment to another, where specific activators are available (Battaini and Pascale, 2005). Depending on sensitivity to calcium and diacylglycerol PKCs are divided into three groups: the conventional calcium-dependent PKCs, calcium-independent PKCs, and atypical isozymes (Newton, 2003). The calcium-dependent PKCs (cPKCs): α, βI,

βII and γ require the membrane lipid PtDSer, free calcium, and DAG for the activation. The calcium independent PKCs (nPKCs): δ, ε, η, and θ are activated by DAG and atypical PKCs (aPKCs) ζ and λ/ι are Ca^{2+}- and DAG-independent (Newton, 2003; Battaini and Pascale, 2005).

PKC function and subcellular localization are regulated by downstream and upstream events. Downstream events are maintained by interaction between enzyme and its activator, while upstream events are maintained by phosphorylation at the catalytic region of the newly synthesized PKCs (Newton, 2003). The nascent kinase is first phosphorylated by phosphoinositide-dependent kinase-1 (PDK-1) which allows for the further autophosphorylation of two other residues at the catalytic domain. This leads to maturation of PKCs which adopt an inactive form able to interact with activators (Parekh et al., 2000; Battaini and Pascale, 2005).

PKC activation can be regulated by protein-lipid interaction or protein-protein interaction. In the first case activation of PLC induces the hydrolysis of phosphatydidylinositol-4,5-biphosphate (PIP2) generating inositol-1,4,5-triphosphate (IP3) and DAG. IP3 releases Ca^{2+} from internal stores. Protein-protein interaction also plays an important role in activation of PKCs by changing their localization (Parekh et al., 2000; Newton, 2003). Scaffolding/adaptor proteins RACKs (receptors for activated C kinases) bind with isozyme selectivity to PKCs when they are activated, increase substrate phosphorylation and direct them close to the specific substrates (Mochly-Rosen, 1995). Localization of inactive PKCs can be influenced by other scaffolding proteins RICKs (receptors for inactive C kinases) (Mochly-Rosen and Gordon, 1998).

The role of PKCs in the brain is still largely unknown, but there are some hints from experiments using knockout mice and specific inhibitors. In PKCγ-/- mice spatial memory and LTP are impaired, and neuroprotection by estrogens after ischemia is reduced (Abeliovich et al., 1993; Hayashi et al., 2005). In PKCα-/- mice long-term synaptic depression is not inducible in the cerebellum (Leitges et al., 2004).

Lysophosphatidic acid

Lysophosphatidic acid (LPA) is a component of cell membranes and also is a bioactive, cellular signalling molecule. It has varied effects on different processes, for example, it can influence stimulation of cell proliferation, inhibition of cell survival, increase of

intracellular Ca^{2+} level, focal adhesion and actin stress fiber formation, and activation of many signalling pathways (Fukushima et al., 2002a; Fukushima et al., 2002b). LPA mediates signals by binding to seven-transmembrane domain receptors of the endothelial differentiating gene (EDG) family, which associate with heterotrimeric G-coupled proteins (Sayas et al., 2002b). LPA was shown to signal through three different EDG receptors – EDG-2 (LPA1), EDG-4 (LPA2) and EDG-7 (LPA) (Contos et al., 2000). The mechanism of signal transduction by these receptors is still unclear. Until now it was shown that binding of LPA to EDG-2 and EGD-4 leads to activation of G_i, $G\alpha_q$ and $G\alpha_{12/13}$, while coupling with EDG-7 activates G_i and $G\alpha_q$ (Ishii et al., 2000). Interaction of EDG receptors with G_i promotes inhibition of adenylate cyclase and activation of the Ras-MAPK pathway; binding to $G\alpha_q$ activates PLC and increases the intracellular Ca^{2+} level, while coupling with $G\alpha_{12/13}$ induces activation of RhoA and reorganization of the actin cytoskeleton (Moolenaar et al., 1997).

The first indication that LPA plays a role as a signalling molecule in the nervous system came from studies done on neuronal cell lines. LPA was shown to induce neurite retraction and cell rounding by alteration of the actin cytoskeleton in neuroblastoma N1E-115, SH-SY5Y, and N2a cells (Jalink et al., 1993; Sayas et al., 2002b), and in neuroglioma NG-108 and PC12 cells (Tigyi and Miledi, 1992; Sayas et al., 2002b). In cultured primary neurons LPA has been shown to induce growth cone collapse by influencing the neuronal cytoskeleton (Saito, 1997; Fukushima et al., 2002a; Sayas et al., 2002a). Growth cone collapse and neurite retraction induced by LPA involve Rho and Rho-kinase (ROCK) activation and reorganization of the actomyosin cytoskeleton. Either inhibition of RhoA with C3 transferase or inhibition of ROCK with Y27632 prevents LPA-induced retraction (Jalink et al., 1994; Hirose et al., 1998). Inhibitors of the myosin light chain kinase (MLCK) or cytochalasin D, an agent that blocks actin polymerization, can also abolish axon retraction induced by LPA (Jalink et al., 1993). Additionally, LPA influences dynamics and organization of microtubules. It decreases the level of detyrosinated-tubulin and increases the level of tyrosinated-tubulin in neuroblastoma SH-SY5Y cells, suggesting that lysophospatidic acid signalling destabilizes microtubules (Sayas et al., 2002b). Contrary to this expectation it was shown that in 3T3 fibroblasts LPA stabilizes microtubules (Cook et al., 1998).

In addition, it was found by Sayas et al. that LPA induces hyperphosphorylation of tau and MAP1B with maximum levels at 1h (Sayas et al., 2002b). These authors could also show that GSK3β is involved in tau phosphorylation. Its activity increased after addition

of LPA and inhibition of this kinase with lithium chloride (LiCl) prevented LPA-induced phosphorylation of tau and partially blocked neurite retraction in cerebellar neurons and neuroblastoma SH-SY5Y (Sayas et al., 2002b).

THE GROWTH CONE

The growth cone is a specialized, motile structure at the tip of growing axons, which guides them to their targets during development or regeneration. It reads extracellular signals using several surface receptors and processes them, eventually resulting in the rearrangement of the cytoskeleton and elongation, retraction or turning of neurites (Henley et al., 2004b). Growth cones navigate axon by protrusion or retraction of lamellipodia or filopodia. Lamellipodia are flattened veil-like extensions at the periphery of the growth cone, in which actin filaments form meshwork, which are implicated in neurite extension and cellular movement by membrane extension (Fig. 4; Matthews, 2001; Dent and Gertler, 2003). Filopodia are narrow cylindrical extensions containing bundles of actin filaments, which are able to extend tens of microns from the periphery of the growth cone and play a sensory role in growth cone steering (Kozma et al., 1997; Dent and Gertler, 2003; Gallo, 2006). Phase contrast studies showed that there is correlation between the rate of advance and the shape of the growth cone (Argiro et al., 1984). Also quantitative analysis of filopodia from DRG neurons showed that there is a direct link between filopodial movement and growth cone advance (Bray and Chapman, 1985).

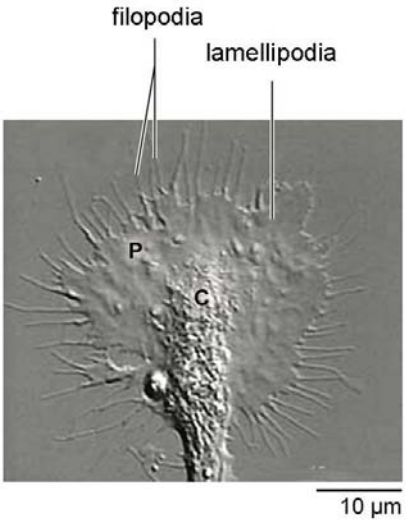

Fig. 4. The morphology of the growth cone. A differential intereference contrast (DIC) image of *Xenopus* growth cone. In general growth cones contain a peripheral (P) domain, consisting of filopodia and lamellipodia, and the central (C) (Zheng and Poo, 2007).

In general growth cones contain a peripheral (P) domain, mostly encompassing filopodia and lamellipodia, the central (C) domain composed of thicker regions rich in organelles and vesicles, and a transitional (T) domain localized between the P domain and C domain (Fig. 4; Dent and Gertler, 2003).

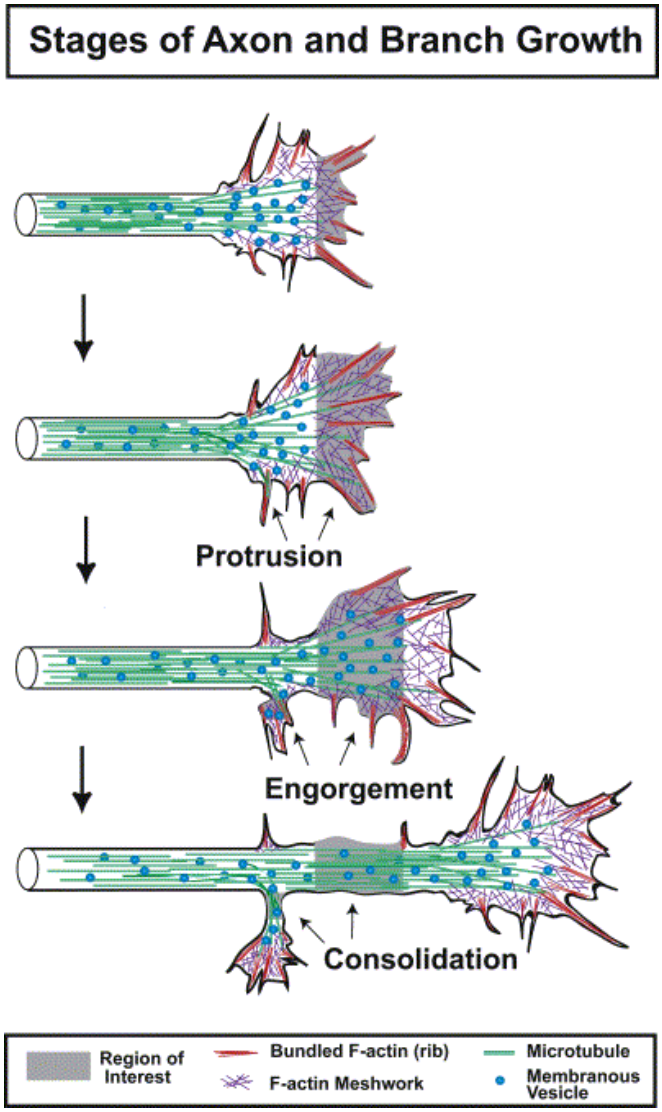

Fig. 5. Stages of axon growth. Elongation of axons consists of three stages termed protrusion, engorgement, and consolidation (Goldberg and Burmeister, 1986). Protrusion occurs when filopodia and lamellipodia extend rapidly through the polymerization of actin filaments. Engorgement occurs when microtubules enter protrusions importing membranous vesicles and organelles. During consolidation the proximal part of the growth cone adopts a cylindrical shape due to depolymerization of F-actin in the neck of the growth cone leading to addition of a new segment of the axon (Dent and Gertler, 2003).

The growth cone exhibits retrograde flow of material from the peripheral to the central region and into the axon shaft itself, and undergoes a repetitive sequence of morphological changes during elongation of the axon, which consists of three stages:

protrusion, engorgement, and consolidation (Goldberg and Burmeister, 1986). Protrusion occurs when filopodia and lamellipodia extend through the polymerization of actin filaments. During engorgement microtubules, enter the protrusions bringing with them vesicles and organelles (mitochondria, endoplasmic reticulum (ER)) (Dent and Gertler, 2003). The last stage is consolidation, which occurs when the proximal part of the growth cone adopts a cylindrical shape due to depolymerization of F-actin in the neck of the growth cone leading to addition of a new segment of the axon (Fig. 5; Dent and Gertler 2003).

THE CYTOSKELETON

The cytoskeleton is a system of filaments that establishes the proper shape of cells and provides mechanical lability, but also allows cells to move in response to signals from the surrounding environment (Alberts et al., 2008). Reorganization of the cytoskeleton is necessary for elongation, retraction or turning of neurites. There are three main types of filaments – microtubules, actin filaments and intermediate filaments, which have different mechanical properties, dynamics and biological roles (Alberts et al., 2008). Differences in properties appear as a result of differences in the structure of the filament subunits and the manner of their self-assembly. All cytoskeletal filaments are constantly remodelled in living cells by the assembly and disassembly of their subunits. Actin filaments and microtubules add and lose subunits only at their ends and one of the ends, called the plus-end, always grows faster than the other (Li and Gundersen, 2008).

Intermediate filaments (IFs) are rope-like fibers made of intermediate filament proteins, with a diameter of 10nm (Alberts et al., 2008). There are five types of subunits found in neuronal IFs - light molecular weight NF (NF-L; 68kDa), medium molecular weight NF (NF-M; 150kDa), high molecular weight NF (NF-H; 200kDa), α-internexin (66kDa), and peripherin (57kDa) (Julien and Mushynski, 1998). IFs form twisted rope-like filaments that help neurons to extend long axons. In difference to microtubules and microfilaments they are nonpolar and are not involved in the generation of cell polarity (Goldman et al., 2008). NFs are made by heteropolymerization of NF-L, NF-M or NF-H (Lee et al., 1993). Peripherin can self-assemble into homopolymers (Ho et al., 1995) or interact with one of the three neurofilament subunits (Parysek et al., 1991). NFs are expressed in differentiated neurons with large diameter axons, while α-internexin

expression is restricted to neurons with smaller axons (Pachter and Liem, 1985; Fliegner et al., 1994), for example, cerebellar granule cells. Peripherin is found predominantly in the PNS; in CNS neurons with projections to the periphery, and in interneurons in the cortex and hippocampus (Brody et al., 1989; Escurat et al., 1990).

Microtubules are long, straight and hollow tubes with an outer diameter of 25nm, composed of tubulin heterodimers assembled from one α-tubulin and one β-tubulin subunit (Luduena, 1998; Alberts et al., 2008; Li and Gundersen, 2008). They are polarized structures with plus and minus ends. In neuronal axons microtubules are very long and oriented with their plus end away from the cell body, whereas in dendrites they are shorter and their polarity is mixed, some have their plus end pointing away from the cell body while others have their plus ends toward the cell body (Alberts et al., 2008). However, in the distal segments of dendrites, microtubules were found to be oriented with their plus end away from the cell body, like in axons (Baas et al., 1988).

Functions of microtubules are modified by their posttranslational modification, such as acetylation, phosphorylation or tyrosination/detyrosination (Luduena, 1998). The central region of the growth cone is rich in stable acetylated and detyrosinated microtubules, whereas in the peripheral region dynamic tyrosinated microtubules are mostly found (Fig. 6). These unstable and dynamic microtubules grow along filopodial actin filaments (Tanaka and Sabry, 1995; lSchaefer et al., 2002). A critical event in growth cone turning may be the stabilization of microtubules in a specific filopodium.

Actin filaments, also called microfilaments and F-actin, are two-stranded helical polymers, with diameters of 5-9nm, formed by globular actin monomers (G-actin) (Alberts et al., 2008). They are organised into linear bundles, two-dimensional networks, or three-dimensional gels. Actin filaments are distributed throughout the cell, but their highest concentration is found in the cell cortex, under the plasma membrane. They provide mechanical support for cell shape and surface projections, like lamellipodia and filopodia, which are used by cells in locomotion (Alberts et al., 2008). Neurons contain almost equal amounts of nonmuscle isotypes of α-actin, β-actin and γ-actin (Choo and Bray, 1978). The highest content of F-actin is in the P and T regions of the growth cone with lower and varying levels of the F-actin in the C region (Fig. 6). Actin polymerization at the so called ”barbed edge”, the plus end, is thought to drive protrusion of lamellipodia and filopodia (Tilney et al., 1981). After polymerization F-actin interacts with a motor protein, myosin, and is retrogradely transported into the growth cone centre where it depolymerises (Lin et al., 1996). In the growth cone F-actin

is dynamic and undergoes turnover (Okabe and Hirokawa, 1990). The balance between the polymerization of actin at the leading edge and retrograde transport of entire filaments determines, for example, whether a filopodium extends or retracts (Dickson, 2002).

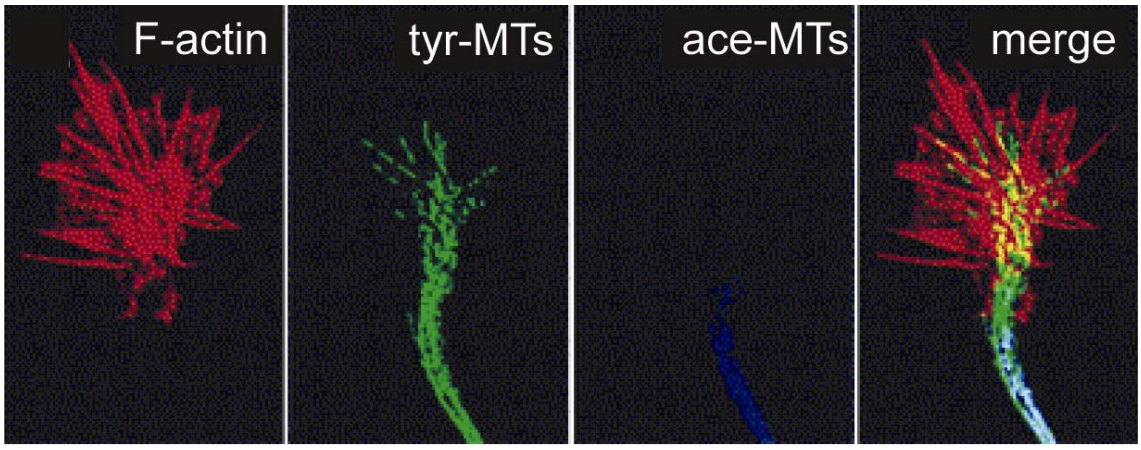

Fig. 6. The cytoskeleton of the growth cone. Representative micrograph of a rapidly extending growth cone of a hippocampal neuron. F-actin (stained with phalloidin, red) is concentrated in the P and T regions of the growth cone. Tyrosinated MTs (tyr-MTs, green) extend from the C region into the actin-rich region. Acetylated MTs (ace-MTs, blue) are restricted to the C region and the axonal shaft, and do not colocalize with F-actin (Dent and Gertler, 2003).

Interaction between microfilaments and microtubules underlies many processes like migration or division of cells, neurite elongation, retraction or response to guidance cues. Reaction to guidance cues requires rearrangement of microtubules and microfilaments and a crosstalk between them. It was observed that in response to a repulsive guidance signal actin bundles are locally lost in the growth cone region next to the source of the signal. Subsequently, in the same region dynamic microtubules are also lost, resulting in the growth cone turning away from the signal. Elongation of axons and dendrites requires active transport of cytoskeletal components, microtubule-actin interactions, and the generation of contractile forces by growth cone to induce tension, which is based on actomyosin contractility (Lamoureux et al., 1997). In addition, myosin-based contractility is essential for axon retraction induced by many guidance cues. Myosin activity is in part regulated by the GTPase RhoA and its downstream effector ROCK (Kozma et al., 1997; Katoh et al., 1998; Wahl et al., 2000).

MYOSIN

Myosins are motor proteins that move along F-actin (Ramamurthy et al., 2004). They are usually composed of a head, tail, and neck domain. The head domain, universal for all myosins, binds to actin filaments and uses ATP hydrolysis to generate force and move along filaments towards the plus end (an exception is myosin VI which moves towards the minus end) (Tan et al., 1992). The neck domain is a linker and lever for transferring force generated by motor protein. The tail domain has specific properties for each type of myosin, for example it can mediate interaction with cargo molecules and other myosin subunits (Ramamurthy et al., 2004).

There are two classes of myosins. Members from the myosin I class consist of a single heavy chain with a molecular weight between 110 and 190 kDa, and at least one light chain with a molecular weight ranging from 14 to 27 kDa (Tan et al., 1992). The function of myosin I is unknown, but it is suggested to play a role in vesicle transport. Myosin II isoforms are expressed in almost all eukaryotic cell types. Specific isoforms of muscle myosin are expressed in muscle, while nonmuscle myosin isoforms are expressed in many cell types. Myosin IIB represents approximately 70% of entire myosin II expressed in the CNS. All myosins II are hexameric molecules consisting of up to two heavy chains with a molecular weight around 200 kDa and one or two sets of light chain with molecular weight between 16 and 20 kDa (Tan et al., 1992) bound to the neck domain of the heavy chain. The N-terminal motor domain of the heavy chain, containing the actin and nucleotide binding sites, is responsible for ATPase activity (Tan et al., 1992). One of the light chains regulates the activity of the head domain and is called the regulatory light chain or phosphorylatable light chain (MRLC), due to the fact that activity of myosin is regulated by phosphorylation of the light chain (Tan et al., 1992). The second light chain is called an essential light chain and is not phosphorylated. It was shown that the head domain is not sufficient for a proper function of myosin II, despite the fact that it contains all elements necessary for force generation (De Lozanne and Spudich, 1987; Wessels et al., 1988). Throughout the entire tail domain there are many repeated motifs which are essential for formation of an α-helical coiled-coil structure. The smallest repeating motif consists of seven amino acids with small hydrophobic amino acids located in the first and fourth position (Tan et al., 1992). Repeating patterns of four seven-residue motifs form positive and negative

charges on the surface of the coiled-coil which interact with a charged region of other myosin hexamers to form filaments.

As mentioned above, phosphorylation of the MRLC increases ATPase activity of myosin II (Tan et al., 1992). It was found that the light chain can be phosphorylated by MLCKs, Ca^{2+}-activated phospholipid-dependent protein kinase (Endo et al., 1982), PKC and *in vitro* by some other kinases, such as CaMKII, the cell cycle-dependent protein kinase $pp34^{cdc2}$ and the reticulocyte protease-activated protein kinase I (Tan, 1992). Two sites in MRLC were found to be phosphorylated by MLCK *in vitro* – serine 19 (Ser 19) (Pearson et al., 1984) and threonine 18 (Thr18) (Ikebe et al., 1986). Phosphorylations at Ser 19 and Thr 18 occurs with ratio 1000:1 (Ikebe et al., 1986). Phosphorylation of the MRLC induces changes in myosin conformation. The unphosphorylated molecule favours the folded state called 10S, which releases products of ATP hydrolysis at a very slow rate, binds to actin weaker in comparison to the extended form 6S, and under physiological conditions is unable to form filaments. Phosphorylation at Ser 19 is sufficient to induce conformational changes into the 6S form and additional phosphorylation at Thr 18 further stabilizes this form (Tan et al., 1992).

Phosphorylation of myosin by PKC occurs on three major sites - at threonine 9 (Thr 9), serine 1 (Ser 1) and serine 2 (Ser 2). PKC phosphorylation seems to have no effect on ATPase activity if the MRLC has not previously been phosphorylated by MLCK and it has different effects in different systems (Tan et al., 1992). On one hand it was shown that in smooth muscle PKC phosphorylation can decrease affinity for actin (Ikebe et al., 1986), but on the other hand it was shown for unique embryonic smooth muscle myosin isoforms that it can increase the actin-activated ATPase (de Lanerolle and Nishikawa, 1988). Phosphorylation by PKC does not induce conformational changes of myosin – it remains predominantly in the 10S form, and it can inhibit phosphorylation by MLCK, and vice versa (Tan, 1992; Tan et al., 1992).

Phosphorylation of the MRLC by CaMKII and protease-activated protein kinase I appears at Ser 19 and is not observed after phosphorylation by MLCK. It seems to be important during a phase following the intracellular Ca^{+2} increase and enhances actin-activated ATPase activity. Phosphorylation by $pp34^{cdc2}$ appears at Ser 1 and Ser 2, but the effects have not been determined. Dephosphorylation of the MRLC is carried out by protein phosphatase type 1M (PP1M) (Tan et al., 1992).

In most nonmuscle cells and in muscle as well the heavy chain of myosin can also be phosphorylated. The phosphorylation sites are located within the tail domain and usually in close proximity to the carboxyl terminus (Tan et al., 1992). Phosphorylation by Myosin Heavy Chain Kinases (MHCKs) was shown to decrease or inhibit the actin-activated ATPase activity (Collins and Korn, 1980; Cote et al., 1981). The heavy chain can be phosphorylated also by PKC, casein kinase II (CK II) and CaMK. The mechanism by which phosphorylation of the heavy chain regulates activity of myosin is unknown.

As it was mentioned above axon retraction is mediated by myosin II which interacts with F-actin to generate contractile forces. It was shown that myosin II activity is required for axon retraction induced by semaphorin 3A and that myosin II acts downstream of RhoA-ROCK (Gallo, 2006).

RHO GTPASES

Rho family GTPases cycle between an inactive GDP-bound state and an active GTP-bound state (Luo, 2000). They are turned on by guanine nucleotide exchange factors (GEFs), which exchange GDP to GTP (Fig. 7). Most GEFs contain a Dbl-homology (DH) domain by which they bind and stabilize Rho GTPases in a nucleotide-free state (Moon and Zheng, 2003). GTPases are switched off by Rho GTPase activating proteins (GAPs), which stimulate hydrolysis of GTP to GDP (Fig. 7). Additionally, Rho GTPases are controlled by GDP dissociation inhibitors (GDIs), which bind inactive GDP-bound proteins and stabilize Rho GTPases in an inactive state (DerMardirossian and Bokoch, 2005).

The members of the Rho family GTPases are Rho (Ras homologous), Rac (Ras-related C3 botulinum toxin substrate) and Cdc42 (cell division cycle 42) subfamilies. There are three isoforms of Rho: RhoA, RhoB and RhoC. In neurons RhoA is expressed at higher level than the other isoforms (Lehmann et al., 1999). Rho GTPases were shown to regulate cytoskeleton function. For example, Rho is involved in the formation of actin fibers (Hall, 1994), Rac participates in the regulation of lamellipodia and membrane ruffling (Ridley et al., 1992) and Cdc42 ioregulates the formation of filopodia (Tapon and Hall, 1997). The three GTPases can regulate each other's activity. For example, in Swiss 3T3 cells the effects of over-active Rho, Rac and Cdc42 mutants on the actin

cytoskeleton suggest that Cdc42 activates Rac, which in turn activates Rho (Nobes and Hall, 1995). On the other hand there are many studies showing that Rho and Rac can inhibit each other, what results in their opposing effects on cell migration and growth cone extension (Xu et al., 2003; Seasholtz et al., 2004).

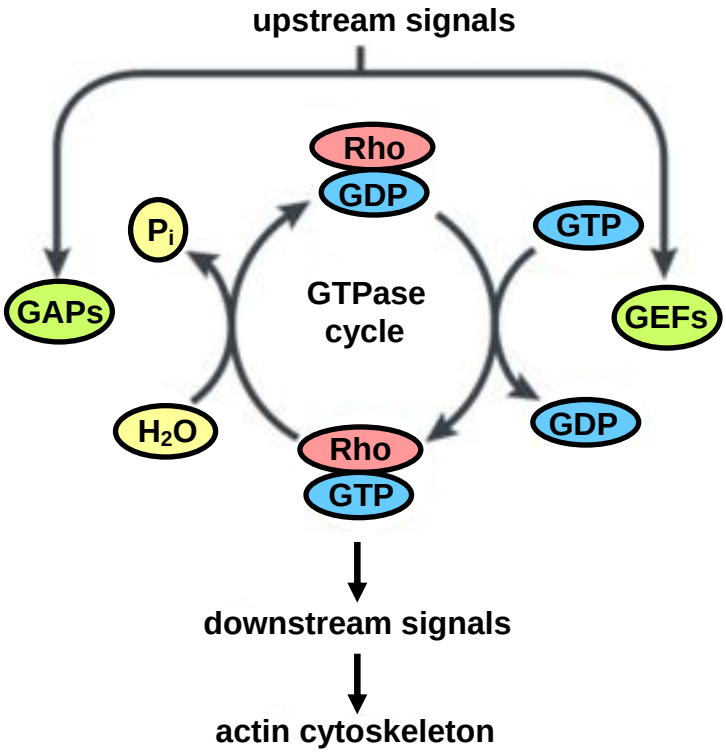

Fig. 7. Schematic of Rho GTPase activation. In response to upstream signals Rho GTPases (Rho) are activated by guanine nucleotide exchange factors (GEFs) that exchange GDP to GTP. Rho GTPase activating proteins (GAPs) inactivate RhoGTPases by stimulating the hydrolysis of GTP to GDP by Rho. Active Rho GTPases stimulate their downstream effectors, such as ROCK, resulting in rearrangement of actin cytoskeleton (Luo, 2000).

Rho GTPases play an important role in many neuronal processes, for example in the generation of neurons by regulating cytokinesis (Lee et al., 2000), in neuronal migration (Zipkin et al., 1997), in establishing neuronal polarity (Bradke and Dotti, 1999), and in synapse development (Weston et al., 2000). Studies *in vivo* and in many neuronal-like cell lines and primary neurons show that axon extension is regulated positively by Rac and Cdc42 (Jalink et al., 1994; Luo et al., 1994; Kozma et al., 1997; Lamoureux et al., 1997; Kalman et al., 1999; Luo, 2000) and negatively by Rho (Jin and Strittmatter, 1997; Kozma et al., 1997; Kalman et al., 1999). Axonal initiation and elongation in *Drosophila melanogaster* embryonic sensory neurons is affected by expression of constitutively active or dominant negative Rac and Cdc42 (Luo et al., 1994). Rho activation leads to growth cone collapse and inhibition of neurite extension in many cell

lines and primary neurons, which can be prevented by inactivation of Rho with C3 transferase from *Clostridium botulinum* (Jalink et al., 1994; Jin and Strittmatter, 1997; Kozma et al., 1997; Lehmann et al., 1999). It specifically ADP-ribosylates Rho at asparagine 41 (Asn 41) and inactivates the G-protein (Ren et al., 1999). For example, C3 transferase can promote DRG neurons outgrowth on myelin, MAG and Nogo-66 substrates (Fournier et al., 2003) and attenuates LPA-induced neurite retraction (Jalink et al., 1994). Up- and downregulation of the Rho/ROCK pathway in cultured cerebellar granule neurons affects axon numbers and growth cone sizes – a dominant active form of RhoA reduces numbers of neurites and expression of C3 in these cells increases the number of neurites (Bito et al., 2000).

Rho subfamily members are activated by chemorepulsive molecules and transduce signals to actin filaments through many downstream effector proteins which bind the active form of Rho GTPases (Jin and Strittmatter, 1997). Among these proteins are protein kinase N (PKN), phosphatidylinositol 4-phosphate 5-kinase (Ren et al., 1999), the Rho-associated kinase p160ROCK (ROCK I) and the ROCK-related kinase (ROCK II). Activated ROCK I or ROCK II can directly phosphorylate the MRLC or indirectly increase the MRLC phosphorylation by inactivation of the regulatory myosin light chain phosphatase (MLCP) (Amano et al., 1996; Redowicz, 1999). ROCK I and ROCK II activity can be inhibited by the pyridine derivative Y27632 (Uehata et al., 1997). ROCK inhibition by Y27632 promotes DRG neurons outgrowth on myelin, MAG and Nogo-66 substrates (Fournier et al., 2003) and initiates formation of axons, promotes axonal maturation during the very early stages of axonogenesis and enhance axon elongation in mouse cerebellar granule cells (Bito et al., 2000). Ephrin A5 induced growth cone collapse in retinal ganglion cells could be reduced by treatment wit Y27632 (Wahl et al., 2000).

NO AS A SIGNALING MOLECULE

Nitric oxide (NO) is a short lived free radical molecule that can be detected in all tissues. It functions as a vasorelaxant, as a neurotransmitter and as an effector in the immunoresponse. NO is also an important modulator of synaptic plasticity during brain development, sensory and visual processing, and memory formation. In addition, it can also regulate gene expression, protein functions and the response of cells to redox

perturbations due to the ability to modify free radicals like the superoxide anion, key redox regulators such as glutathione, and macromolecules like proteins (Martinez-Ruiz and Lamas, 2004). On the other hand NO plays a role in many pathological events, like neurodegenerative diseases, ischemia, and epilepsy, and is responsible for neuroinflammatory cell damage and exicitotoxic cell death (Zhang and Snyder, 1995).

NO was described for the first time as a neuronal messenger molecule in 1988 by Garthwaite and colleagues. They observed that cerebellar granule neurons upon exposure to glutamate agonists release an endothelium-derived relaxing factor-like substance (Garthwaite et al., 1988).

NO is an atypical messenger molecule. It is synthesized only when required instead of being stored in synaptic vesicles and released by exocytosis. It also does not bind to any membrane-associated receptor proteins, but can diffuse from one cell to another and interact directly with targets (Schuman and Madison, 1994; Bicker, 2005). The activity of NO is terminated by reaction with a substrate and not by enzymatic degradation or reuptake mechanisms.

Production of NO

NO is produced mainly by a family of enzymes called nitric oxide synthases (NOS) that convert L-arginine and oxygen into NO and L-citrulline. Three members of the NOS family exist - neuronal NOS (nNOS, NOS I), endothelial NOS (eNOS, NOS III) and inducible NOS (iNOS, NOS II). All isozymes share 50-60% sequence homology (Guix et al., 2005). nNOS and eNOS are constitutively expressed and are Ca^{2+}/calmodulin-dependent enzymes that produce small amounts of NO that acts for a few minutes, while iNOS is Ca^{2+} -independent and produces high amounts of NO acts for hours or even days (Iadecola et al., 1997; Ebadi and Sharma, 2003).

eNOS is expressed preferentially in endothelial cells, but also in other cell types such as neurons, iNOS in glial and immune cells such as macrophages (Guix et al., 2005), while nNOS is found predominantly in developing (Bredt and Snyder, 1994) and mature neurons (Cork et al., 1998). There are four major isoforms of nNOS: cytoplasmic nNOSγ and nNOSβ, and isoforms anchored to subcellular structures via the PDZ domain, nNOSα and nNOSμ (Fig. 8; Guix et al., 2005; Alderton et al., 2001).

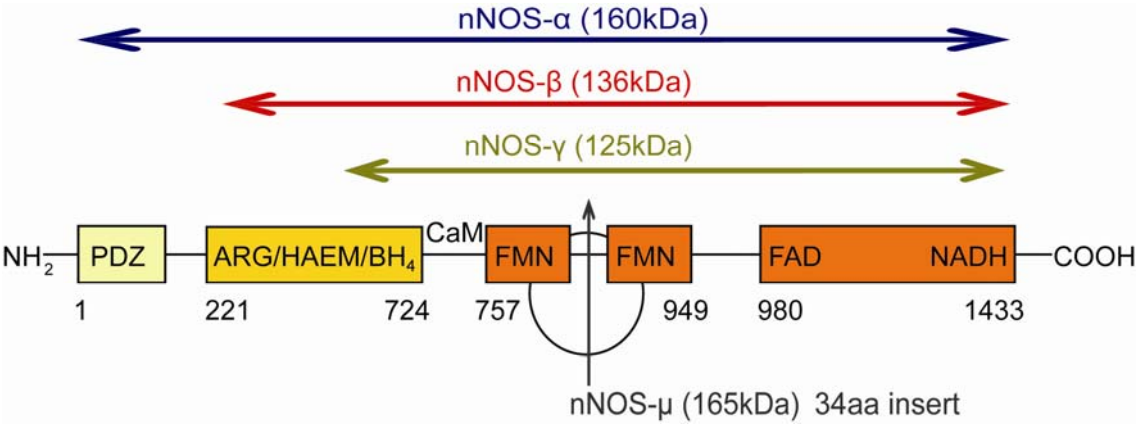

Fig. 8. Splice variants of nNOS. Four different protein products of detected human nNOS splice variants are predicted. The schematic representation shows nNOSα, described as full length nNOS (residues 1-1433); two cytoplasmic variants: nNOSβ (residues 236-1433) and nNOSγ (residues 336-1433), which lack the PDZ domain; and nNOSμ that has an additional 34 amino acids between the CaM and FAD/FMN binding sites. The PDZ domain mediates associatation of nNOS with membrane (adapted from Alderton et al., 2001).

All the NOSs have two domains that work independently. The COOH-terminal domain has a reductase activity and consists of sites binding Ca^{2+}/calmodulin, flavine adenine dinucleotide (FAD), flavine adenine mononucleotide (FMN) and reduced nicotinamide adenine dinucleotide phosphate (NADPH) (Fig. 9). The NH_2-terminal domain shows oxygenase activity and contains binding sites for tetrahydrobiopterin (BH4), heme and L-arginine (Fig. 9; Stuehr, 1999). Heme and BH4 are necessary for the conversion of L-arginine to NO and citrulline (Mayer et al., 1991). Coupling of Ca^{2+}/calmodulin to NOS activates the enzyme enabling electron influx into the active centre of NOS (Abu-Soud and Stuehr, 1993). Calmodulin promotes interaction between the oxygenase and reductase domains and is necessary for the electron flow from NADPH to the flavins and from flavins onto heme (Abu-Soud and Stuehr, 1993; Irikura et al., 1995).

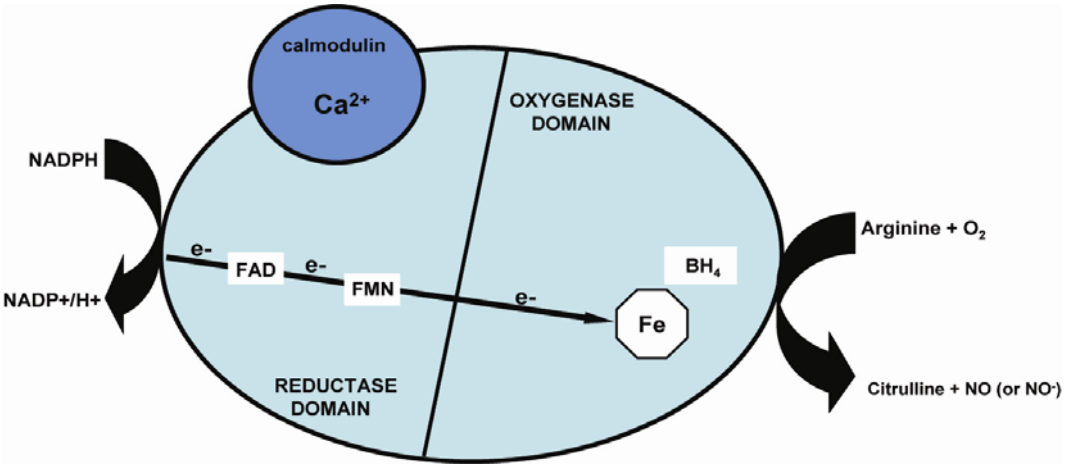

Fig. 9. Schematic structure of NOS. nNOS is a dimeric enzyme comprised of two identical monomers that are bridged by a zinc tetrathiolate (Zn-S4) cluster. NOS consists of two domains:

a reductase domain and an oxygenase domain, which work independently. Electrons (e−) are derived from NADPH to the reductase domain and carried via FAD and FMN to heme (Fe), located at the oxygenase domain. Interactions of electrons with heme and BH4 catalyse the reaction of oxygen with L-arginine, generating citrulline and NO (under some conditions NO^- can be produced instead of NO). Ca^{2+}/CaM is necessary for the electron flow from NADPH to the flavins and from flavins onto heme (adapted from Alderton et al., 2001).

NO production is regulated mainly by phosphorylation of NOS. Phosphorylation of nNOS by CaMK, cAMP-dependent protein kinase (PKA), cGMP-dependent protein kinase (PKG) and PKC decreases its catalytic activity (Nakane et al., 1991; Dawson and Dawson, 1996; Komeima et al., 2000), while dephosphorylation by calcineurin increases its activity. Contrary, it was also shown that phosphorylation of nNOS by PKC increased its activity (Nakane et al., 1991) and by PKA had no influence on its activity (Brune and Lapetina, 1991).

In addition NO can be also produced by the reduction of nitrites in acids, by the xanthine oxidase pathway or by the reaction of H_2O_2 with L-arginine in a non-enzymatic way (Maiese and Boccone, 1995; Nagase et al., 1997).

Mechanism of action

Binding to metal centres

NO can directly interact with the metal ion within heme groups of proteins. The main cellular target for NO is the soluble guanylate cyclase (sGC) (Ignarro, 1991). NO reacts with Fe^{2+} located in the centre of the heme group of sGC, resulting in pulling Fe^{2+} out of the plane of the porphyrin ring and a conformational change that increases conversion of guanosine-5'-triphosphate (GTP) to cyclic guanosine-3',5'-monophosphate (cGMP) (Guix et al., 2005). cGMP is a second messenger that activates protein kinases, for example PKGI, which controls $[Ca^{2+}]_i$ levels, and PKGII regulating the flux of anions, such as chloride (French et al., 1995; Lau et al., 2003). cGMP-dependent phosphorylation stimulates release of neurotransmitters by inducing phosphorylation of synaptic vesicle proteins. cGMP also modulates functions of some phosphdiesterases of cyclic nucleotides (PDE), for example, it induces inhibition of PDEIII resulting in increase of intracellular cAMP levels and activation of cAMP-dependent pathways (Ono and Trautwein, 1991).

NO binds to heme at the copper-heme centre of the reduced form of cytochrome c oxidase as a competitive inhibitor of oxygen. But when the enzyme is oxidized, NO can interact with copper instead of heme, generating nitrate with the bound oxygen, leading to enzyme inactivation (Yoshikawa, 2000; Cooper, 2002). Other examples are the interactions of NO with the heme groups of cytochrome P450 and haemoglobin (Martinez-Ruiz and Lamas, 2004). The interaction of NO with the heme group of cyclooxygenase (COX) is proposed to be mechanism leading to its activation and increased production of prostaglandin (Salvemini et al., 1993).

Protein S-nitrosylation

S-nitrosylation is a covalent posttranslational modification of proteins. As other modifications it is evoked by a stimulus, precisely targeted, spatio-temporally restricted (accurately regulated in time and space) and is involved in the cell's flexibility in response to changes in an extracellular environment (Hess et al., 2005; Hao et al., 2006). In contrast to other posttranslational modifications such as acetylation or phosphorylation, S-nitrosylation is a non-enzymatical reaction. It can be achieved by NO, by nitrosating species like N_2O_3, or by transferring a nitrosyl group from metal-NO complexes or from already existing nitrosothiols. The latter is called transnitrosylation (Paige et al., 2008). An example of transnitrosylation is the transfer of the NO moiety from S-nitroso-glutathione (GSNO) to thiol group of a cysteine residue in a protein (Hess et al., 2005). A number of enzymes were found to promote S-nitrosylation. For example, Cu, Zn superoxide dismutase (SOD) promotes S-nitrosylation of haemoglobin (Hess et al., 2005). The molecular mechanism of S-nitrosylation is poorly understood. It occurs at free thiol groups of cysteine of target proteins. In a sequence motif favourable for S-nitrosylation the cystein residue can be flanked by aspartic acid (Asp), glutamic acid (Glu), and basis arginine (Arg), histidine (His), and lysine (Lys). Deprotonation of the thiol is suppressed and enhanced by neighbouring acidic and basic groups, respectively (Hess et al., 2005). On the other hand, also cysteins located in hydrophobic environments can be S-nitrosylated. The extend of S-nitrosylation is determined by the concentrations of the nitrosylating agent and the target, which depends on production of NO by NOSs, subcellular localization of NOSs and their targets, and stability of the bond (Martinez-Ruiz and Lamas, 2004). It should be noted that the NOSs can produce

other reactive nitrogen species (RNS) that can work as nitrosylating agents. Some of the proteins to be S-nitrosylated are physically associated with eNOS and nNOS, indicating that subcellular compartmentalization can play an important role for modification. An example is the colocalization of nNOS and the NMDA receptor (NMDAR). nNOS binds through its PDZ domain to the postsynaptic scaffolding protein PSD93/95 which also binds to the NMDAR and thus brings it to close proximity of nNOS. S-nitrosylation is also determined by the stability of the S-nitrosothiol. In general, the modification is very labile and can be reversed without need for an enzyme, especially in the highly reducing cytosolic environment (Martinez-Ruiz and Lamas, 2004). Moreover, the addition and removal of the NO group can influenced by conformational changes of the protein.

Recently it was shown that S-nitrosothiols differ in their stability (Paige et al., 2008). Most of the nitrosothiols are labile when exposed to physiological concentrations of glutathione (GSH). Their generation is increased when the cellular level of NO is enhanced, suggesting that their role in signalling is only temporary and associated directly with the time of NO production. The stable nitrosothiols appear to result from conformational changes induced by S-nitrosylation that reduce their accessibility to the reducing cytosolic environment (Paige et al., 2008). For example, S-nitrosylation of cysteine β93 in haemoglobin induces a conformational change so that the nitrosothiol is hidden in a hydrophobic pocket making it inaccessible for the environment. This conformational change can be reversed by deoxygenation (Singel and Stamler, 2005). S-nitrosylation was shown to modulate activity of many ion channels, enzymes, growth factors, G-proteins and transcription factors (Stamler et al., 1997a; Stamler et al., 1997b). S-nitrosylation of the NMDARs (Lipton, 1999), protein tyrosine phosphatase (PTPase), capases, dimethylarginine dimethylaminohydrolases (DDAHs) and JNKs results in downregulation of their activity. Matrix metalloproteinase 9 (MMP-9) was shown to be directly activated by S-nitrosylation (Gu et al., 2002). Also the type 1 ryanodine receptor/ Ca^{2+} ionophore of skeletal muscle (RyR1) and cyclic-nucleotide-gated Ca^{2+} permeable channels (CNGs) are activated by S-nitrosylation. In addition, S-nitrosylation of haemoglobin influences blood flow (Stamler et al., 1997a) and platelet aggregation (Pawloski et al., 1998).

Protein nitrotyrosination

Nitrotyrosination is a posttranslational modification of proteins that works by addition of a nitro (-NO_2) group to one carbon atom of the aromatic ring of tyrosine. By preventing phosphorylation of proteins or inducing conformational changes nitration results in loss of their function. For example, loss of function was observed in case of nitration of actin (Aslan et al., 2003) and mitochondrial superoxide dismutase (MnSOD) (Ischiropoulos et al., 1992). In case of cytochrome c (Cassina et al., 2000), PKC (Hink et al., 2003) or JNKs (Go et al., 1999) nitration results in activation of these proteins.

Physiological effects of NO

NO can play both protective and toxic role, what depends mainly on its intracellular concentration, the NOS isoform generating NO, the availability of the substrate, type of cell and the extra- and intracellular milieu in which NO is produced. Since the level of NO can not be regulated by its storage, production of NO by NOS seems to be the main step regulating NO level. At the low concentration NO plays a physiological role in modulation of the vascular tone, during immunoresponse and inflammation, and in neurotransmission.

Vascular effects

NO was shown to stimulate vessel relaxation and it affects mainly the vascular smooth muscle cells (VSMCs) inducing hyperpolarization of the membrane by direct activation Ca^{2+}-dependent K^+-channels or by triggering the synthesis of cGMP and PKG-dependent opening or closing of ion channels, such as Ca^{2+}-dependent K^+-channels (Guix et al., 2005). Contraction of VSMCs is induced by phosphorylation of MLC by Ca^{2+}/calmodulin-dependent MLCK and can be reverted by the MLCP. ROCK can phosphorylate and inhibit the latter, favouring contraction. NO activates cGMP-dependent protein kinase cGKIα that inhibits ROCK, thus, resulting in reversion of contraction. In addition, contraction of VSMCs can be triggered by PLCβ, which activates PKC and mobilizes intracellular Ca^{2+} (Guix et al., 2005). Increased Ca^{2+} levels

activate the MLCK, inducing contraction (Guix et al., 2005). NO activates cGMP-dependent kinases that inhibit PLCβ2 and PLCβ3 (Xia et al., 2001) and thus also leads to relaxation of VSMCs.

Immunological functions

Upon immunological or inflammatory stimulation iNOS produces large amounts of NO that can react with reactive oxygen species (ROS), resulting in the formation $ONOO^-$, which is an anti-tumor and anti-microbial agent (Xie and Nathan, 1994). On the other hand, high levels of NO can be toxic, inactivating enzymes of the respiratory chain and inducing apoptosis (Guix et al., 2005). Additionally, NO is also known as a regulator of leukocyte adhesion in blood vessels (Kubes et al., 1991).

Pro- and anti-apoptotic effects of NO

NO was shown to be both anti- and pro-apoptotic, depending on its concentration, flux, co-existence of other noxious agents and cell type (Guix et al., 2005). The action of NO is mostly determined by the redox state of the cells. It seems that NO produced by NOSs in the cell plays role as anti-apoptotic molecule, while NO delivered by chemical donors is associated with apoptosis. The anti-apoptotic role of NO is mainly associated with S-nitrosylation of caspases 1, 3 and 9 resulting in their inhibition (Kim et al., 1997; Mannick et al., 1999; Thippeswamy et al., 2001). In addition, NO inhibits the mitochondrial permeability transition pore (MPTP) and cytochrome c release, and induces the expression of cytoprotective genes, such as HSP70 (Hao et al., 1999; Brookes et al., 2000). On the other hand, NO was shown to be a pro-apoptotic molecule as it binds to cytochrome c oxidase and induces $O_2^{\bullet -}$ formation in mitochondria, resulting in mitochondrial swelling, transient permeability, cytochrome c and calcium release, damages of the mitochondrial complexes I, II, IV and V, aconitase, creatine kinase, the mitochondrial membrane, mitochondrial DNA and mitochondrial SOD (Brown, 1999). Moreover, NO-induced apoptosis is also concomitant with an increase in the ratio of Bax/Bcl-xL, which results in release of cytochrome c and activation of caspases (Kolb, 2000).

NO in the nervous system

NO is a well-known neurotransmitter and neuromodulator in both the CNS and the PNS, where it works through cGMP activation (Trabace and Kendrick, 2000; Guix et al., 2005). In the CNS it plays a role in pain perception (Yamamoto et al., 1993), control of sleep (Monti and Jantos, 2004), thermoregulation, appetite, neural development (Cheng et al., 2003) and synaptic plasticity (Dinerman et al., 1994).

Activation of the brain's NMDARs results in NO synthesis (Garthwaite et al., 1988). Under physiological conditions NMDARs control several processes in neuronal development, synaptic plasticity and memory, but excessive activation leads to neuronal cell death. This indicates that proper regulation of NMDAR activity is crucial for neuronal survival. As it was mentioned before the NMDAR is anchored to the plasma membrane and nNOS is brought to close proximity of NMDAR through the interaction with the scaffolding protein PSD93/95. It was observed that in many regions of the brain, such as hippocampus, striatum and hypothalamus NMDAR increases influx of Ca^{2+} which activates nNOS (Guix et al., 2005). Activated nNOS produces NO which oxidizes the free sulfhydryl groups on the NMDA channel complex to form S-nitrosothiols resulting in inhibition of NMDAR (Lei et al., 1992a). This suggests that NO works as a negative feedback modulator which reduces NMDA activity (Lipton, 1999) and consequently attenuates NMDA-mediated neurotoxicity (Meffert et al., 1994). In contrast, NO was shown to play a role in glutamate- and NMDA-induced death of cultured cortical neurons, while inhibition of NO production prevents the NMDA-mediated cell killing (Dawson et al., 1991). These contradictory results can be due to a two-phase action of nNOS upon activation by NMDAR. As I mentioned, increased levels of Ca^{2+} induced by NDMAR activate nNOS, which produces NO. High levels of NO can mediate toxicity of NMDAR, for example by S-nitrosylation or nitration of glutamine synthase, which has a role in ammonia detoxification in brain. Inhibition of nNOS during this initial phase of its activation can prevent neurotoxicity. During the subsequent phase NMDAR is S-nitrosylated by NO, which prevents the accumulation of toxic levels of Ca^{2+} through unrestrained NMDAR activity. Inhibition of nNOS at this step could prevent protective effects of NO. Consistent with this model, simultaneous treatment of cortical neurons with NMDA and nNOS inhibitors resulted in inhibition of NMDA toxicity (Dawson et al., 1991) and the activity of NMDAR was found to be decreased upon S-nitrosylation (Lipton, 1999).

As I mentioned, the main target of NO is sGC. Once nNOS is activated, for example by NMDAR-mediated Ca^{2+} influx, it produces high levels of NO, which reacts with the metal centre of sGC, leading to its activation and increased conversion of GTP to cGMP. cGMP as a second messenger activates many protein kinases, for example PKG. Activated PKG can phosphorylate nNOS, resulting in inhibition of nNOS activity. Inhibition of nNOS activity by PKG represents a negative feedback regulation of nNOS. In addition, it was found that CaMKII can be S-nitrosylated at Cys6, resulting in its inactivation, what can contribute to NO-induced neurotoxicity in the brain (Song, 2008). Paradoxically, it was observed that CaMKII can phosphorylate nNOS at Ser847, resulting in decrease of nNOS activity, possibly by blocking the binding of Ca^{2+}/calmodulin (Nakane et al., 1991; Komeima et al., 2000; Rameau et al., 2004).

In vivo and *in vitro* studies show that NO enhances glutamate release (Prast et al., 1998), which is suggested to be an important mechanism in memory formation. LTP has been proposed as the main mechanism underlying memory and learning, which occurs when excitatory synapses are stimulated by the depolarization of postsynaptic neurons accompanied by release of neurotransmitter from presynaptic cells (Guix et al., 2005). This mechanism requires sending of a signal from the postsynaptic cell to the presynaptic neuron. NO is proposed to be this retrograde messenger, which activates release of glutamate through a cGMP-dependent pathway (Fig. 10; Nowicky and Bindman, 1993). When the level of NO is low, glutamate release is decreasing although the cGMP level is elevated, but NO-induced increase of cGMP level reverses the inhibitory effect on glutamate release. The critical seems to be not the level of NO and cGMP, but rather increase in cGMP levels stimulated by increase in cGMP levels (Guix et al., 2005). Application of NOS inhibitors to the postsynaptic neurons prevents LTP, what can be reversed by L-arginine addition (Kitto et al., 1992; Zorumski and Izumi, 1993). Another support for a role of NO in LTP is the finding that LTP is also blocked by hemoglobin which intercepts NO in the synaptic cleft as it passes from the postsynaptic to the presynaptic cell (Dawson and Dawson, 1996). nNOS knockout mice and eNOS knockout mice showed only slightly reduced LTP, while double knockout mice for nNOS and eNOS (nNOS-/- and eNOS-/- mice) showed a strong decrease in LTP indicating that nNOS and eNOS can compensate loss for each other in the postsynaptic synthesis of NO (Son et al., 1996).

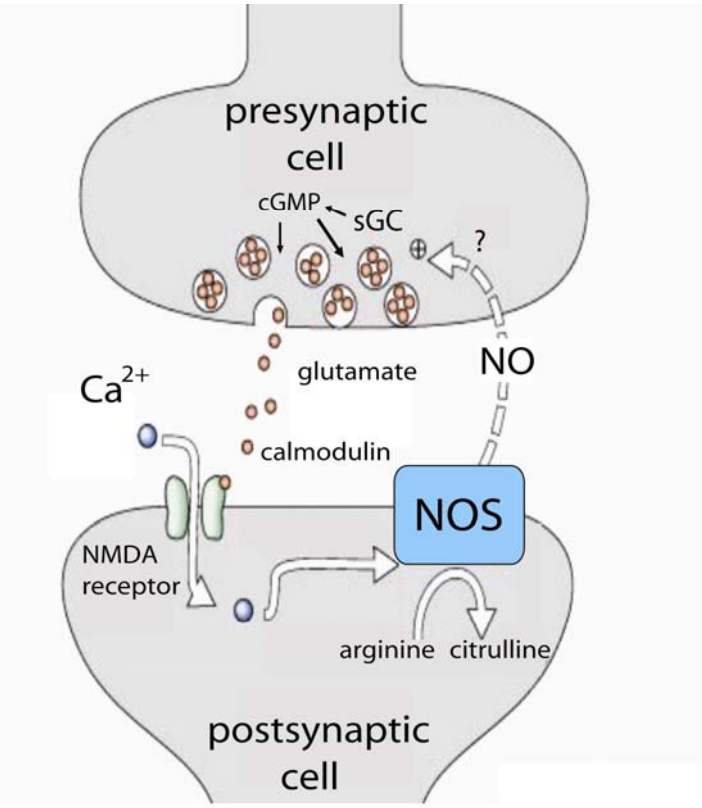

Fig. 10. **NO plays a role as a transcellular secondary messenger in LTP.** NMDAR-mediated Ca^{2+} influx activates NOS, which converts arginine to NO and citrulline. NO diffuses through the cell membranes from the postsynaptic neuron to the presynaptic neuron, where it activates release of glutamate through a cGMP-dependent pathway (Huang, 1999).

Nitric oxide was also shown to directly or indirectly regulate the release of neurotransmitters. For example, effect of NO on GABA and serotonin (5-HT) production is biphasic depending on its concentration. The basal level of NO decreases GABA and serotonin (5-HT) release, while high concentrations of NO increase their release (Kaehler et al., 1999). NO and NMDA receptors stimulate production of noradrenalin (NE). Treatment with NO donors increases release of NE in the hippocampus both *in vivo* and *in vitro* and NOS inhibitors decrease NE release (Feldman and Weidenfeld, 2004). On the other hand, NO and $ONOO^-$ deactivate NE by direct reaction with it (Kolo et al., 2004).

NO and neurodegenerative diseases

nNOS activation following continuous stimulation of excitatory amino acid receptors that mediate glutamate toxicity or iNOS activation by cytokines or endotoxin can lead

to production of high amounts of NO, which were found to be toxic for cells of the nervous system (Guix et al., 2005). All neurodegenerative processes like Huntington's disease (HD), Alzheimer's disease, Parkinson's disease (PD), amyotrophic lateral sclerosis (ALS), multiple sclerosis (MS), and ischemia involve oxidative stress, suggesting involvement of NO.

AD is associated with accumulation of the neurotoxic β-amyloid peptide (Aβ) that induces formation of neuritic plaques and intracellular neurofibrillary tangles caused by hyperphosphorylation of tau (Selkoe, 2001). Aβ triggers formation of ROS which can react with NO to form $ONOO^-$, resulting in nitrotyrosination of proteins (Miranda et al., 2000; Tran et al., 2003). The hippocampus cerebral cortex of AD patients shows higher tyrosine nitration levels in comparison to those from healthy people (Hensley et al., 1998). In the brains from patients with the AD NOS positive neurons are interspersed in the tissue and can NO diffuse to NOS negative neurons (Hyman et al., 1992). An increased expression of NOS was found in neurons with neurofibrillary tangles in the entorhinal cortex and hippocampus of AD patients (Thorns et al., 1998). In addition, in brains of patients with AD nNOS-positive astroscytes were also found in proximity of amyloid plaques - in the subiculum and the CA1 region of the hippocampus, and in the areas were lost of neurons was observed – in the II layer of the entorhinal cortex and in the CA4 region of the hippocampus (Thorns et al., 1998; Guix et al., 2005).

The high levels of NO after ischemia and stroke are mainly due to iNOS activation which increases from 12h to 7 days after injury (Iadecola et al., 1995). Additionally, increased levels of intracellular Ca^{2+}-induced by ischemia activate eNOS and nNOS in the feedback mechanism aimed at improving blood supply (Eliasson et al., 1999; Guix et al., 2005). Both iNOS knockout mice (Iadecola et al., 1997) and nNOS knockout mice (Eliasson et al., 1999) show a reduction in neuronal death after cerebral ischemia, while eNOS knockouts show an increase in neuronal death after stroke (Huang, 1999).

In patients with MS an elevated expression of iNOS in macrophages, astrocytes and peripheral mononuclear cells was found at sites of inflammation (Guix et al., 2005). When inflammation was reduced, iNOS expression decreases in demyelinated plaques in MS patients (Liu et al., 2001; Guix et al., 2005). In the cerebrospinal fluid (CSF), urine, and serum from patients with MS increased levels of NO metabolites - nitrite and nitrate were found (Giovannoni et al., 1997; Yamashita et al., 1997; Giovannoni et al., 1999).

MICROTUBULE ASSOCIATED PROTEINS

Microtubule associated proteins (MAPs) are a family of heterogeneous proteins regulating microtubule assembly and crosstalk between cytoskeletal filaments (Vecino and Avila, 2001). According to molecular weight MAPs have been classified into three classes. The low molecular mass (LMM) MAPs are kinesin-type proteins, dynamin, MAP2c and tau. MAP1S and MAP4 make up intermediate molecular mass (IMM) MAPs. MAP1A, MAP1B, MAP2 and cytoplasmic dynein belong to the high molecular mass (HMM) MAPs. Taking into account structural and functional aspects, MAPs are classified as fibrous (MAP1, MAP2, MAP4, tau), molecular motors (dynein, kinesin, dynamin) and assembly regulating proteins (STOPs and chartins). The fibrous MAPs are believed to regulate cellular differentiation and the shape and the size of the cell. Some of the fibrous MAPs, for example MAP1B and MAP2, regulate the activity of motor proteins responsible for intracellular transport (Jimenez-Mateos et al., 2005; Jimenez-Mateos et al., 2006).

One of the best known MAPs is tau. It is found predominantly in axons as a soluble phosphorylated protein. It promotes polymerization of microtubules and stabilizes them, an activity that is probably regulated by phosphorylation at sites located within its microtubule-binding domain (Hanger et al., 2009). Both phosphorylation and splicing of tau are developmentally regulated. The highest phosphorylation is observed at embryonic and early developmental stages, suggesting involvement of tau in embryogenesis and early development (Hanger et al., 2009).

MAP2 is expressed mainly in dendrites and plays an important role in dendritic differentiation (Farah and Leclerc, 2008). Suppression of MAP2 in cultured primary neurons inhibits the differentiation of neurites into dendrites and overexpression of MAP2 in non-neuronal cells induces formation of processes similar to dendrites (Edson et al., 1993; LeClerc et al., 1993; Belanger et al., 2002). MAP2-dependent dendritic differentiation seems to involve stabilization of microtubules. Interaction between MAP2 and microtubules is supposed to play an important role in defining dendritic identity via binding membranous organelles and signalling molecules to microtubules (Farah and Leclerc, 2008). MAP2 knockout mice show a reduction of dendritic length in hippocampal neurons (Harada et al., 2002).

MAP1s

MAP1 proteins are a family of thermolabile MAPs that stabilize microtubules. There are three members of the group: MAP1A, MAP1B and MAP1S. MAP1A is found mainly in adult axons, where it is localized in dendrites, whereas MAP1B is highly expressed during development predominantly in axons (Bloom et al., 1984; Halpain and Dehmelt, 2006). The expression of MAP1S increases during the postnatal period, but in contrast to MAP1A its level is already high after birth (Orban-Nemeth et al., 2005). The highest levels of MAP1S are found in brain and testis (Orban-Nemeth et al., 2005). All three MAP1s are synthesized as the polyprotein precursors that are cleaved into a heavy chain (HC) and a light chain (LC1 for MAP1B, LC2 for MAP1A and LCS for MAP1S) (Fig. 11; Tögel et al., 1999).

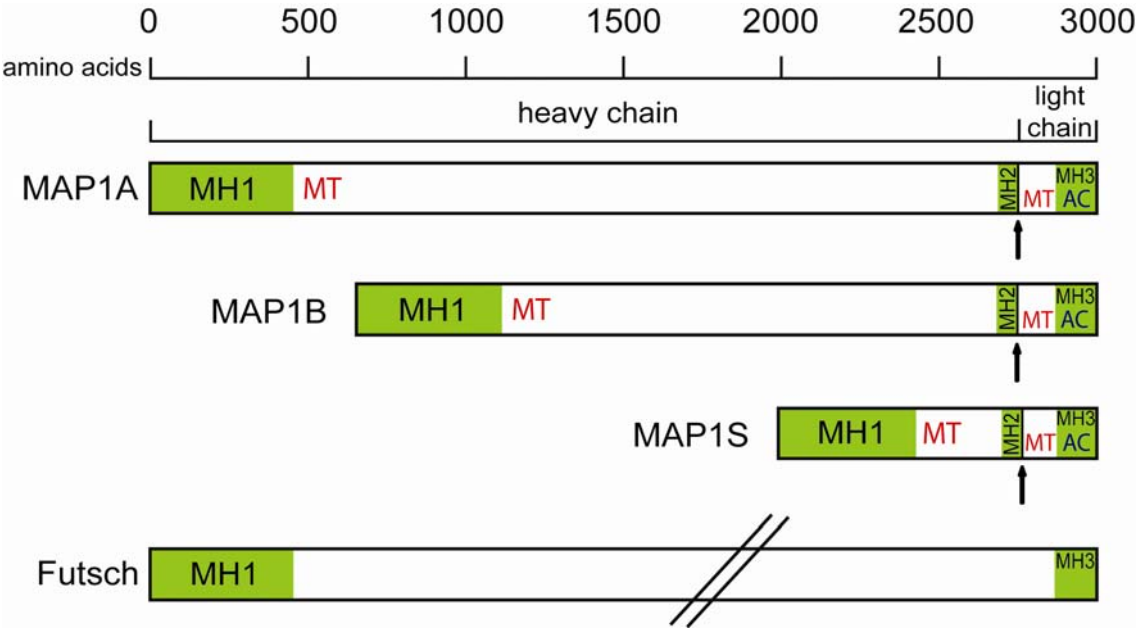

Fig. 11. Schematic representation of the MAP1 family. All MAP1 proteins are synthesized as polyprotein precursors which are posttranslationally cleaved into heavy and light chains (cleavage site indicated by black arrow). MAP1B, MAP1A and MAP1S share three homology domains (MH1, MH2, MH3, indicated by green boxes). MAP1A, MAP1B and MAP1S contain microtubule binding domains on the HCs, and microtubule and actin binding domains on the LCs. The actin binding domain is located in MH3 (green box). The Drosophila homologue Futsch shares only two homlogy domains (MH1 and MH3) with the mammalian members of the MAP1 family.

MAP1B, MAP1A and MAP1S show three regions of high homology, which are called MAP1 homology domains: MH1, MH2 and MH3. The MH1 domain is located at the NH_2 terminus of the heavy chain with approximately 500 amino acids in size. The MH2

domain is located at the COOH terminus of the heavy chain with 133 amino acids in size and MH3 is located at the COOH terminus of the light chain with approximately 125 amino acids in size (Fig. 11; Langkopf et al., 1992). In addition to microtubule-binding activity (Schoenfeld, 1994; Orban-Nemeth et al., 2005), all three MAP1s can bind also to microfilaments (Pedrotti et al., 1994; Pedrotti et al., 1996a; Pedrotti and Islam, 1996b; Tögel et al., 1998; Noiges et al., 2002; Orban-Nemeth et al., 2005).

MAP1B

As mentioned above MAP1B is one of the earliest MAPs expressed in the nervous system, with the highest level during embryonic development. It is downregulated during early postnatal development (Soares et al., 1998; Gordon-Weeks and Fischer, 2000; Meixner et al., 2000). The regions of the nervous system that show neuronal plasticity and regenerative properties, for example the olfactory bulb and epithelium, the hippocampus, and the retinal photoreceptors, maintain high levels of MAP1B also in the adult (Gordon-Weeks and Fischer, 2000).

The mature MAP1B complex consists of the heavy chain (300kDa) and one or more light chains, the LC1 (32kDa), LC2 (30kDa), and/or LC3 (18kDa) that is the product of separate gene (Langkopf et al., 1992; Gordon-Weeks and Fischer, 2000; Meixner et al., 2000; Orban-Nemeth et al., 2005; Halpain and Dehmelt, 2006). The interaction between the heavy and light chains is mediated by the MH1 in the heavy chain and the MH3 domains in the LC1 and LC2 (Tögel et al., 1998). LC1 and LC2 can interact with both MAP1B and MAP1A HCs (Schoenfeld et al., 1989; Noiges et al., 2002). There are two microtubule binding domains, one is a 120kDa fragment located within N-terminus of heavy chain and the second is located at the N-terminus of LC1 (Fig. 12; Zauner et al., 1992; Tögel et al., 1998). The microtubule-stabilizing activity of full length MAP1B is weaker than that of MAP2. It was found that the heavy chain of MAP1B can suppress the binding of the light chain to microtubules. When the LC1 is overexpressed in Ptk2 cells, which express low levels of endogenous MAP1B, it binds to microtubules inducing the formation of wavy microtubule bundles (Tögel et al., 1998). Co-expression of the heavy chain inhibits this effect. The C-terminal domain of light chain contains the heavy chain binding site, the microfilament binding site and the light chain

polymerization site (Tögel et al., 1998; Noiges et al., 2002; Halpain and Dehmelt, 2006).

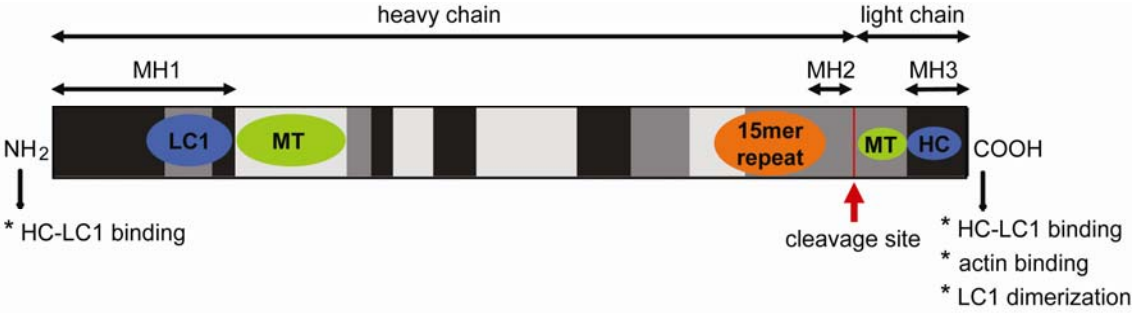

Fig. 12. Schematic representation of MAP1B. MAP1B, similar to other MAP1s, is synthesized as polyprotein precursor, which is cleaved into a heavy and a light chain at the indicated cleavage site. The microtubule binding domains on both light and heavy chains (MT, green), three MAP1 homology domains (MH1, MH2, MH3) and the twelve 15mer repeats (orange) are indicated (Zauner et al., 1992; Tögel et al., 1998). LC1 bundles and stabilzes microtubules, while HC might have a regulatory function. The interaction between the heavy and light chains is mediated by the NH_2 terminus of the heavy chain and the COOH terminus of the LC1. In addtition, on the COOH-terminus of LC1 an actin binding domain and a dimerization domain are located, as indicated. The degree of conserved amino acid sequence between human, rat and mouse MAP1B are presented by black and grey boxes. The highest degree of conservation is indicated by black boxes (adapted from Trančíková, PhD thesis, 2007).

The MAP1B precursor is encoded by one gene consisting of seven exons, which can be transcribed in several alternative ways – the regular transcript type 1 containing all seven axons (≥90% of transcripts), and the type 2 transcript encoding an NH_2-terminally truncated precursor and containing noncoding exons upstream of exon 3 (≤10% of transcripts) (Kutschera et al., 1998; Meixner et al., 2000).

Phosphorylation of MAP1B

Phosphorylation of MAPs can modulate their function, since it can affect their binding to microtubules. Several studies demonstrated that MAP1B phosphorylation increases its association with microtubules *in vivo* and *in vitro* (Pedrotti et al., 1996a) and correlates with axonogenesis and neurite outgrowth (Fischer and Romano-Clarke, 1990; Gordon-Weeks et al., 1993; Vecino and Avila, 2001).

Analysis of the primary sequence of MAP1B reveals multiple potential sites for phosphorylation. Indeed, more than 33 phosphorylation sites have been identified (Collins et al., 2005), but only for a few the consequences of phosphorylation for

MAP1B function are known (Gordon-Weeks et al., 1995; Goold et al., 1999). Nevertheless, some features of MAP1B phosphorylation have been elucitated using monoclonal antibodies specific for certain, as yet unidentified phosphoepitops. There are at least two modes of MAP1B phosphorylation: mode I sites, that are generated by proline directed serine/theronine kinases (PDPKs) and result in a decreased migration of MAP1B in SDS-PAGE, and mode II sites, that are generated by CKII and do not change the electrophoretic behaviour of the protein (Ulloa et al., 1993a; Ulloa et al., 1993b). There is evidence that MAP1B is phosphorylated at mode I sites by cycline dependent kinase 5 (cdk5α) (Pigino et al., 1997), glycogen synthase kinase 3β (GSK3β) (Lucas et al., 1998), MAP1B kinase (M1BK) (Hoshi et al., 1990) and c-Jun N-terminal kinase (JNK) *in vivo* (Kawauchi et al., 2003). *In vitro* experiments show that MAP1B can be dephosphorylated by protein phosphatase 2B (PP2B) and protein phosphatase 2A (PP2A) (Ulloa et al., 1993c; Ulloa et al., 1994a; Gong et al., 2000). Mode II phosphorylated sites were shown to be dephosphorylated *in vitro* by protein phosphatase I (PP1) (Ulloa et al., 1993c). Mode I phosphorylated isoforms are expressed only during development and are distributed in a gradient along in growing or regenerating axons with the highest concentration at the growth cone (Black et al., 1994; Boyne et al., 1995; Gordon-Weeks and Fischer, 2000). Mode II phosphorylated isoforms are also found in adulthood and similar to unphosphorylated MAP1B are distributed uniformly in the cell body, axons, and dendrites (Gordon-Weeks et al., 1993; Ulloa et al., 1994a; Tonge et al., 1996; Ramon-Cueto and Avila, 1997; Ma et al., 1999; Ramon-Cueto and Avila, 1999; Gordon-Weeks and Fischer, 2000; Ma et al., 2000).

Generally, in the CNS the expression level of total MAP1B significantly decreases after maturation of the nervous system, but phosphorylated MAP1B (MAP1B-P) remained at high levels in regenerating neurons and brain areas with high morphological and synaptic plasticity (Nothias et al., 1996; Ramon-Cueto and Avila, 1997). In primary hippocampal and sympathetic neurons and in neuronal cell lines (PC12, SY5Y) total MAP1B and MAP1B-P are abundant in actively growing axons with the highest expression at the growth cone (Aletta et al., 1988; Diaz-Nido et al., 1988; Ulloa et al., 1993b; Black et al., 1994; Ulloa et al., 1994a; Boyne et al., 1995; Gordon-Weeks and Fischer, 2000; Haque et al., 2004). In the PNS, unphosphorylated and phosphorylated MAP1B remain at high levels in adulthood. Expression of MAP1B-P was observed in ganglion cell somata and growing axons within fish optic nerve and in regenerating axons after optic nerve crush, suggesting that MAP1B-P plays a role not only during

development, but also in regeneration (Vecino and Avila, 2001). It was also shown that sciatic nerve transsection was rapidly followed by increased expression of MAP1B-P in lamina II of the corresponding segment of the spinal cord, indicating plasticity of myelinated fibers (Soares et al., 2002). Undifferentiated PC12 cells expressed predominately unphosphorylated isoforms of MAP1B, which are present mostly in the cytoplasm, while during neuritogenesis the expression of MAP1B-P and its binding to microtubules increase (Aletta et al., 1988; Diaz-Nido et al., 1988). Downregulation of CKII by antisense oligonucleotides prevented neurite extension and decreases association of MAP1B with microtubules, suggesting that mode II phosphorylation may play a role in microtubule stabilization by MAP1B and in axon extension (Ulloa et al., 1993b). On the other hand, it was shown *in vitro* that dephosphorylation at PDPK within MAP1B increased its binding to microtubules, suggesting that phosphorylation of MAP1B by the PDPKs can decreased its affinity for microtubules (Pedrotti et al., 1996a; Pedrotti and Islam, 1996b). Additionally, hyperphosphorylation of MAP1B induced by inhibition of protein phosphatase 2A (PP2A) and protein phosphatase 2B reduced its binding to microtubules in rat brain slices (Gong et al., 2000). All these contradictory results can be due to several potential phosphorylation site of MAP1B (33 sites (Collins et al., 2005)) and use of monoclonal antibodies specific for certain, but so far unidentified phosphoepitops, since general antibodies for mode I or mode II phosphorylated MAP1B do not exist. It is most likely that consequences of phosphorylation at different sites were analyzed, but results were generalized for modes. Inhibition of GSK3β by WNT7a or lithium chloride induced axonal spreading and increased growth cone area of cerebellar neurons, associated with the loss of unstable microtubules and MAP1B-P (Lucas et al., 1998; Goold et al., 1999). High levels of MAP1B-P were associated with the loss of detyrosinated microtubules in COS cells transfected with both MAP1B and GSK3β, suggesting that MAP1B phosphorylated by GSK3β regulates microtubule dynamic instability in extending axons (Goold et al., 1999). Transfection with MAP1B prevents nocodazole mediated microtubule depolymerization, but this protection was reduced by MAP1B phosphorylation. Binding of MAP1B to tyrosinated microtubules could inhibit tubulin detyrosination and generation of stable microtubules from unstable ones. It is possible that in the growing axons MAP1B-P maintains the unstable state of microtubules (Goold et al., 1999). Inhibition of GSK3β in DRGs increased the level of stable microtubules in growth cones (Goold et al., 1999). In PC12 cells NGF induced expression of a new isoform of

GSK3β and GSK3β phosphorylation of MAP1B which is associated with neurite formation and extension. Neurite extension is sensitive to inhibition of GSK3β and this correlates with a decrease of MAP1B phosphorylation (Goold and Gordon-Weeks, 2001).

Another kinase implicated in MAP1B phosphorylation is cdk5α. Antisense oligonucleotides for cdk5α or p35 in cultured cerebellar macroneurons decreased the level of mode I phosphorylated MAP1B and its binding to microtubules (Pigino et al., 1997; Paglini et al., 1998). On the other hand, it was shown that inhibition of cdk5α by roscovitine did not suppress mode I phosphorylation of MAP1B in culture of mouse embryonic cortical neurons, while a JNK inhibitor – SP600125 did (Kawauchi et al., 2005).

In addition, phosphorylation of MAP1B was shown to influence also its binding to microfilaments. *In vitro* experiments showed that dephosphorylation of the PDPK sites by alkaline phosphatase increased its binding to F-actin (Pedrotti and Islam, 1996b).

Several extracellular factors are known to induce phosphorylation of MAP1B. For example, reelin (Gonzalez-Billault et al., 2005), laminin (DiTella et al., 1996), netrin-1 (Del Rio et al., 2004) and LPA can induce MAP1B phosphorylation through the activation of cdk5 and GSK3β in the Rho-dependent and the Rho-independent ways.

S-nitrosylation of MAP1B

Recently it was shown that LC1 can be S-nitrosylated in mouse brain and N2a cells (Stroissnigg et al., 2007). By creating specific mutants it was shown that cys2457 at the COOH terminus of LC1 is S-nitrosylated. This cystein is conserved among all three MAP1 LCs and is located at the very COOH terminus end of the LCs. However, the sequence flanking this cystein do not correspond to a consensus sequence, which has been postulated to be important for S-nitrosylation (Stroissnigg et al., 2007).

The specificity of S-nitrosylation requires close proximity of nNOS and its target proteins. Using yeast 2-hybrid β-galactosidase assays it was shown that the COOH-terminal domain of the LC1 interacted with the NH_2-terminal fragment of nNOS via the PDZ domain of nNOS (Stroissnigg et al., 2007). Co-immunoprecipitation studies using brain lysates showed that approximately 30% of LC1 co–precipitated with nNOS (Stroissnigg et al., 2007). Additionally, colocalization of LC1 and nNOSα was observed

in PtK2 cells co-transfected with constructs encoding LC1 and full length nNOSα. Both proteins were associated with microtubules. Interaction sites other than the PDZ domain might be present in nNOS, since in co-transfection experiments with LC1 and full length nNOS-β, which lacks the PDZ domain, colocalization of LC1 and nNOS-β was also observed. In the absence of LC1 both nNOSα and nNOSβ were found in the cytoplasm (Trančíková, 2007).

Full length MAP1B overexpressed in PtK2 cells is found predominantly in cytoplasm, but when cells were additionally treated with SNAP, a nitrosylating agent, its microtubule binding increased (Stroissnigg et al., 2007). Interaction between LC1 and HC1 was not affected by S-nitrosylation of LC1. A similar increase in microtubule binding was observed with LC1 after treatment with SNAP, but not when cys2457 was mutated to serine (Stroissnigg et al., 2007). Theses results excluded the possibility that the increase of MAP1B binding to microtubules is due to nitrosylation of tubulin.

Moreover, in N2a neuroblastoma cells activation of nNOS by the calcium ionophore calcimycin (A23187) resulted in an increase of NO levels and retraction of neurites. This correlated with enhanced S-nitrosylation of LC1. In comparison untreated N2a cells differentiated well and showed low levels of S-nitrosylated LC1in the presence of a basal level of NO (Stroissnigg et al., 2007).

Likewise, studies in adut mouse DRG neurons brought strong evidences that NO-induced axon retraction is MAP1B-dependent. DRG neurons are primary sensory neurons that convey sensory information, for example about pain and temperature, to the CNS. They are pseudo-unipolar neurons having one axon with two branches and each of them works as a single axon. In addition, they express high levels of MAP1B and display a high level of plasticity and a strong regenerative response upon nerve injury (Newton, 2003; Bouquet et al., 2004). Activation of nNOS by calcimycin or treatment with SNAP lead to axon retraction and growth cone collapse in wild-type DRG neurons. In MAP1B -/- neurons axon retraction was much reduced indicating an important role of MAP1B in NO-induced axon retraction (Stroissnigg et al., 2007).

Role of MAP1B

The developmental regulation of MAP1B and its high expression in growing and regenerating neurons indicate its importance for neurogenesis and neurite outgrowth.

Both expression of MAP1B and its phosphorylation increase during neurite outgrowth *in vitro*, for example during differentiation of human neuroblastoma SY5Y cells (Haque et al., 2004). Neurite extension induced by nerve growth factor (NGF) in PC12 cells is also associated with an increase in MAP1B levels (Aletta et al., 1988). Depletion of MAP1B with antisense oligodeoxynucleotides inhibits initiation of neurite outgrowth in PC12 cells and cerebellar macroneurons (Brugg et al., 1993; DiTella et al., 1996; Pedrotti et al., 1996a). In primary cultures of sympathetic and hippocampal neurons total and phosphorylated isoforms of MAP1B are localized mainly in growing axons and their level decreases after a few days in culture, suggesting that MAP1B plays a role during initiation and elongation of neurites (Boyne et al., 1995). Neurites of DRG explants from MAP1B-/- mice showed a twofold higher terminal and collateral branching and the turning response of their growth cones is impaired in comparison to neurites from wild-type DRG explants, suggesting a role for MAP1B in the growth cone guidnace and collateral branching (Bouquet et al., 2004). Cultured CNS and PNS neurons from a MAP1B hypomorphus mutant mouse line generate shorter axons than those from wild-type mice, and also axonogenesis seems to be inhibited (Gonzalez-Billault et al., 2005). In large DRG neurons that give rise to myelinated fibers, high MAP1B-mRNA levels are observed indicating a potential role of MAP1B in plasticity of myelinated fibers. In addition MAP1B expression increases before maturation of oligodendrocytes suggesting a role in formation of myelin-forming processes (Vouyiouklis and Brophy, 1993).

Many observations indicate that phosphorylated MAP1B plays a role during neuronal regeneration. MAP1B is expressed during regeneration of mouse retinal explants (Bates et al., 1993) and mode I phosphorylated MAP1B levels increase during regeneration of cat trochlear motoneurons (Book et al., 1996) and retinal ganglion cells (Vecino and Avila, 2001). After sciatic nerve lesion within several days total and mode I phosphorylated MAP1B isoforms are present in growth cones of regenerating axons (Fawcett et al., 1994; Bush et al., 1996; Ramon-Cueto and Avila, 1999). A high level of mode II phosphorylated MAP1B is found in the somata of DRG neurons, in the somata and dendrites of spinal motor neurons, and in Schwann cells and oligodendroglia associated with the regenerating axons (Ramon-Cueto and Avila, 1999). It was shown that sciatic nerve transsections induce increased MAP1B expression in lamina II of the spinal cord with highest levels between 8 and 15 days after the injury, both in mice and rats (Soares et al., 2002). Moreover after sciatic nerve transsection relatively high levels

of MAP1B and its mRNA are observed in DRGs (Ma et al., 2000). There is no increase in the level of MAP1B-P, suggesting a difference between regeneration and neuronal development, where MAP1B-P is expressed at high levels. After spinal cord injury MAP1B-P is expressed in the grey matter in both dorsal and ventral horns and around the central canal. In white matter, high levels of MAP1B are found on terminal enlargements in the proximity of the injury and in pre-apoptotic somata of neurons axotomized by the lesion (Soares et al., 2007). These results suggest a role of MAP1B in axon extension and retraction, but also in neuronal degeneration.

Four MAP1B mutant alleles were generated in mice. In the mice generated by Edelman at al. the MAP1B coding region was interrupted by insertion of STOP codon at codon 571. Mice homozygous for this allele die in utero before day 10 of gestation and heterozygotes show neurological disorders, such as ataxia (Edelmann et al., 1996). This can be due to expression of the N-terminal fragment of the MAP1B heavy chain (the first 571 amino acids) with potential dominant-negative activity (Tögel et al., 1998; Meixner et al., 2000). In contrast, in MAP1B knockout obtained by Takei at al., homozygotes survive and show only a delay in development of the nervous system (Takei et al., 1997). In these mice an NH_2-terminally truncated MAP1B protein is synthesized, which probably is sufficient to fulfil many functions of MAP1B (Kutschera et al., 1998; Meixner et al., 2000). The third MAP1B knockout mice were generated by insertion of a gene-trapping vector between exons 2 and 3 of the MAP1B gene resulting in premature termination of MAP1B translation. Homozygotes die shortly after birth and show serious neuronal abnormalities in all laminated structures, for example in the hippocampus, the cerebral cortex and the cerebellum (Gonzalez-Billault et al., 2005). All these knockout mice are not full knockouts, in that they express truncated isoforms of MAP1B or trace amounts of the full-length protein (Edelmann et al., 1996; Takei et al., 1997; Kutschera et al., 1998; Gonzalez-Billault et al., 2005). The homozygotes of the fourth knockout do not express MAP1B and show many neural defects, for example absence of the corpus callosum and formation misguided cortical axon bundles, and a reduction in the number of large myelinated axons and decreased nerve conduction velocity in the adult sciatic nerve (Meixner et al., 2000).

Over the past years evidence has been accumulating that MAP1B, in addition to its role in neuronal development and regeneration, can play a role in pathological processes. It was found that in patients with Alzheimer disease MAP1B is hyperphosphorylated and colocalizes with neurofibrillary tangles (Ulloa et al., 1994b). The light chain of MAP1B

interacts with gigaxonin – a protein responsible for giant axonal neuropathy (GAN). Two different mutations found in GAN patients led to loss of interaction between MAP1B and gigaxonin and an increased level of MAP1B of MAP1B as a consequence (Ding et al., 2002). MAP1B is also implicated in fragile X syndrome by its Drosophila homologue Futsch. Fragile X syndrome is characterized by the absence of the fragile X mental-retardation protein (FMRP), which was found to be an mRNA-binding protein playing an important role in the regulation of dendritic mRNA localization and/or synaptic protein synthesis (Antar et al., 2005). It was observed that FMRP granules colocalize with ribosomes, ribosomal RNA and MAP1B mRNA in dendrites and spines of cultured hippocampal neurons (Antar et al., 2005). It is possible that the absence of FMRP results in impairment of MAP1B mRNA translation, leading to alteration in local regulation of dynamics of cytoskeletal components that are involved in development and morphology of synapses. MAP1B is also linked to spinocerebellar ataxia type 1 (SCA1), which is caused by toxicity of ataxin1. It is postulated that the leucine-rich acidic nuclear protein (LANP) binds to ataxin1 and mediates toxicity. In undifferentiated N2a cells LANP is predominantly a nuclear protein, during neuritogenesis LANP Tran locates from the nucleus to the cytoplasm, where it interacts with LC1, and modulates the effects of MAP1B on neurite extension (Opal et al., 2003). Binding of mutant ataxin-1 to LANP in the nucleus, can reduce the microtubule-stabilizing interactions of LANP and MAP1B, resulting in alteration of cytoskeletal arrangements or abnormalities in subcellular trafficking (Opal et al., 2003).

PART I - PHYSIOLOGICAL RELEVANCE OF NO-INDUCED AXON RETRACTION

RESULTS

Role of NO and MAP1B in axon retraction induced by LPA

LPA-induced axon retraction is MAP1B-dependent and involves ROCK and myosin

It was shown recently in our lab that treatment of adult DRG neurons from wild-type mice with 10μM calcium ionophore calcimycin (A23187) for 15min induces axon retraction. Calcimycin increases calcium influx and thus activates Ca^{2+}–dependent nNOS, resulting in growth cone collapse and retraction of neurites with reconfiguration of the microtubules into sinusoidal bundles, retraction bulb and trailing remnant (retracted phenotype; Fig. 13) in 43% of the cells. 17% of cells displayed a collapsed morphology characterized by bead-like swellings of the axon with depletion of microtubules (collapsed phenotype; Fig. 13) and about 40% of the neurons remained unchanged in comparison to untreated cells (unchanged phenotype; Fig. 13; Stroissnigg et al., 2007). In case of MAP1B-/- DRG neurons the same number of cells with collapsed pheonotype was observed (15%), indicating that MAP1B has no influence on this effect. In contrast, only 27% of the MAP1B-/- neurons retracted in response to calcimycin treatment, whereas 60% of the cells remained unchanged. These results suggest involvement of MAP1B in axon retraction induced by NO (Stroissnigg et al., 2007). In addition, treatment of cultured wild-type DRG neurons with the NO donor SNAP also induces axon retraction characterized by reconfiguration of the microtubules into sinusoidal bundles (Stroissnigg et al., 2007). Approximately 45% of cells displayed a retracted phenotype compared to 8% when cells were left untreated. Response of MAP1B-/- DRG neurons to SNAP treatment was impaired (only 13% of neurons retracted compared to 6% in case of untreated neurons). These results indicate that MAP1B is necessary for NO-induced axon retraction and growth cone collapse (Stroissnigg et al., 2007).

Axons retracting in response to calcimycin or SNAP treatment show similar hallmarks to axons retracting in response to physiological cues, for example LPA. Thus it is

interesting if nNOS, NO, and nitrosylation of MAP1B are involved in axon guidance by physiological guidance cues.

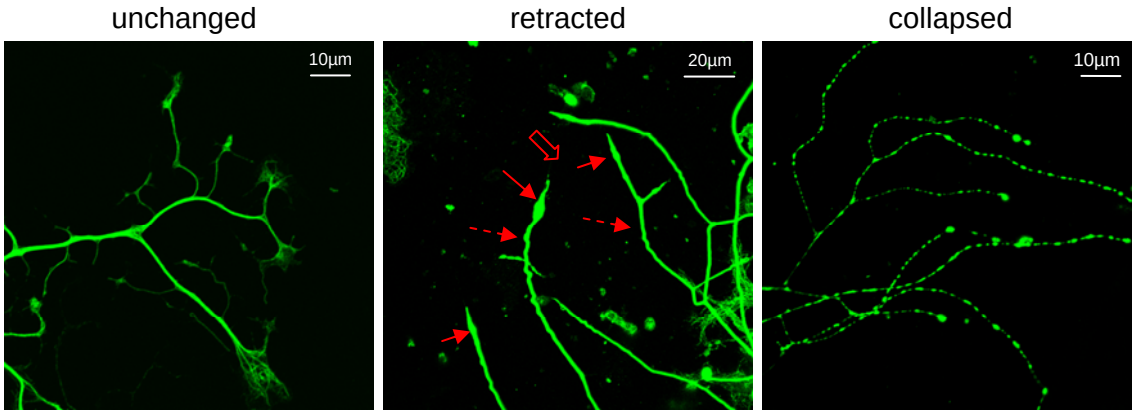

Fig. 13. Response of wild-type neurons to activation of nNOS by calcimycin. Adult wild-type DRG neurons were grown on coverslips coated with poly-L-lysine and laminin, treated with 10µM calcimycin for 15min, fixed with 4% PFA, stained for tubulin and analyzed by confocal microscopy. Microtubule configuration in response to calcimycin was classified as unchanged (compared to untreated cells), or retracted (sinusoidal microtubules (interrupted arrow), retraction bulb (filled arrows), trailing remnant (open arrow)) or collapsed (bead-like swelling of the axon - interrupted microtubule staining).

LPA is a well-known physiological guidance cue that induces axon retraction involving activation of the Rho and myosin pathway (Jalink et al., 1994). To determine the role of MAP1B and NO in retraction induced by LPA, wild-type and MAP1B-/- DRG neurons were grown on poly-L-lysine and laminin coated coverslips, treated with 10µM LPA for 30min or left untreated, fixed and stained for tubulin and MAP1B HC as a control. I observed that 47% of wild-type DRG neurons showed retracted phenotype when treated with LPA, while the response of MAP1B-/- DRG neurons was impaired and only 8% of cells showed retraction hallmarks (Fig. 14). Additionally, I also compared the behaviour of wild type and MAP1B-/- DRG neurons upon LPA treatment using time-lapse microscopy. Cells were cultured for 20-24h and then were monitored for 20min before addition of LPA (Fig. 15). Without any stimulation, axons from both types of neurons elongated at the same rate. Addition of 10µM LPA (time point 0' on graphs) induced growth cone collapse within 5-10min followed by retraction with formation of sinusoidal bends, reminiscent of the sinusoidal microtubules bundles revealed by immunofluorescences After addition of LPA to MAP1B-/- DRG neurons, I did not even observe growth cone collapse and neurites continued elongation at the same rate as before treatment (Fig. 15).

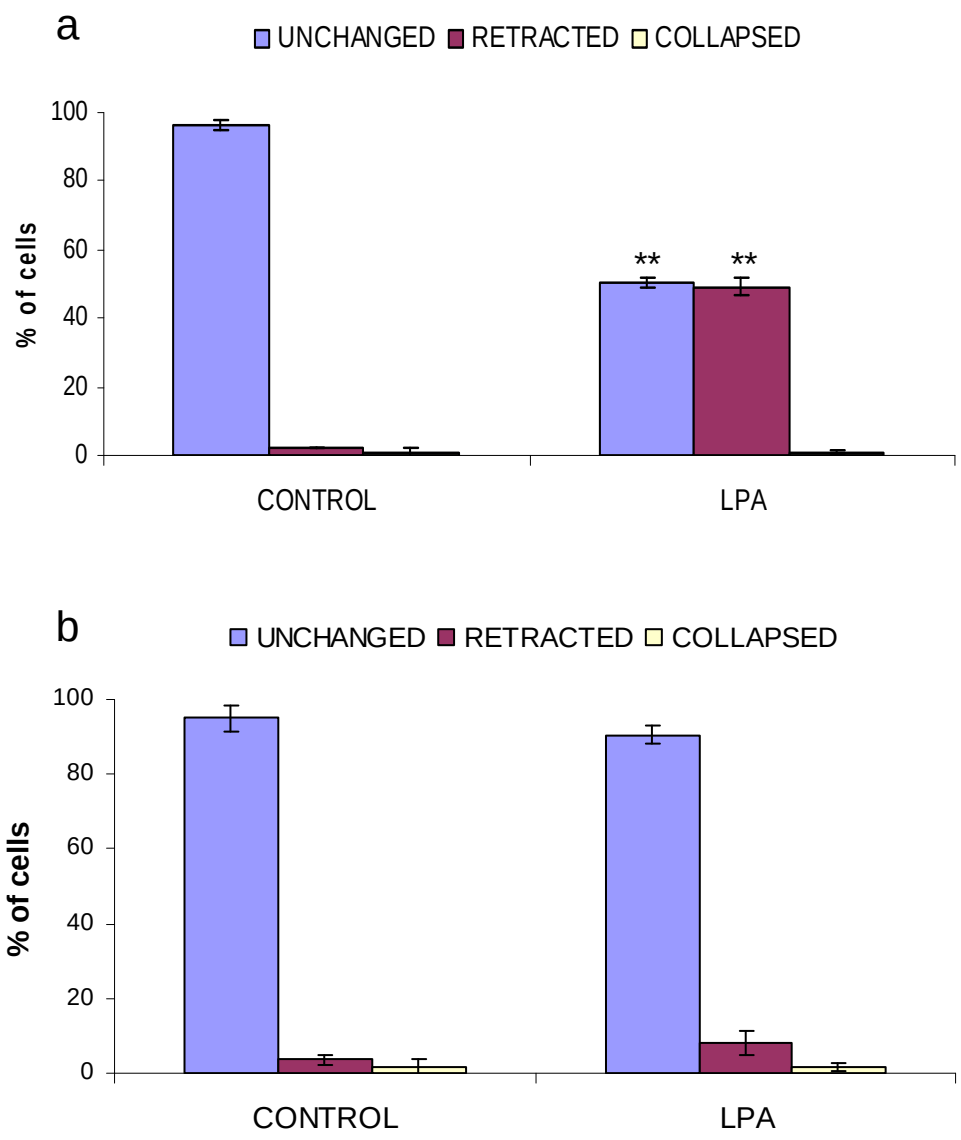

Fig. 14. LPA-induced axon retraction is impaired in MAP1B-/- DRG neurons. DRG neurons from wild-type (a) and MAP1B-/- (b) mice were grown on coverslips coated with poly-L-lysine and laminin, were left untreated or were treated with 10µM LPA for 30min, as indicated, fixed with 4% PFA, stained for tubulin and analyzed by confocal microscopy.For quantitative analysis, approximately 100 cells in each of 3 independent experiments were assessed for microtubule configuration. Error bars represent standard deviations. Asterisks indicate that the values for cells treated with LPA were significantly different from corresponding values of untreated neurons (**, $p<0.001$).

It was shown that inhibition of ROCK with the pyridine derivative Y27632, which inhibits ROCK by competing with ATP for the ATP-binding site on the catalytic domain, prevented axon retraction induced by LPA in B103 rat neuroblastoma cells (Ishizaki et al., 2000). I could reproduce these results. Treatment of wild-type DRG neurons with 10µM Y27632 for 1h prior to treatment with LPA abolished axon retraction (13% of neurons retracted in comparison to 45% when cells were treated with LPA only; Fig. 16).

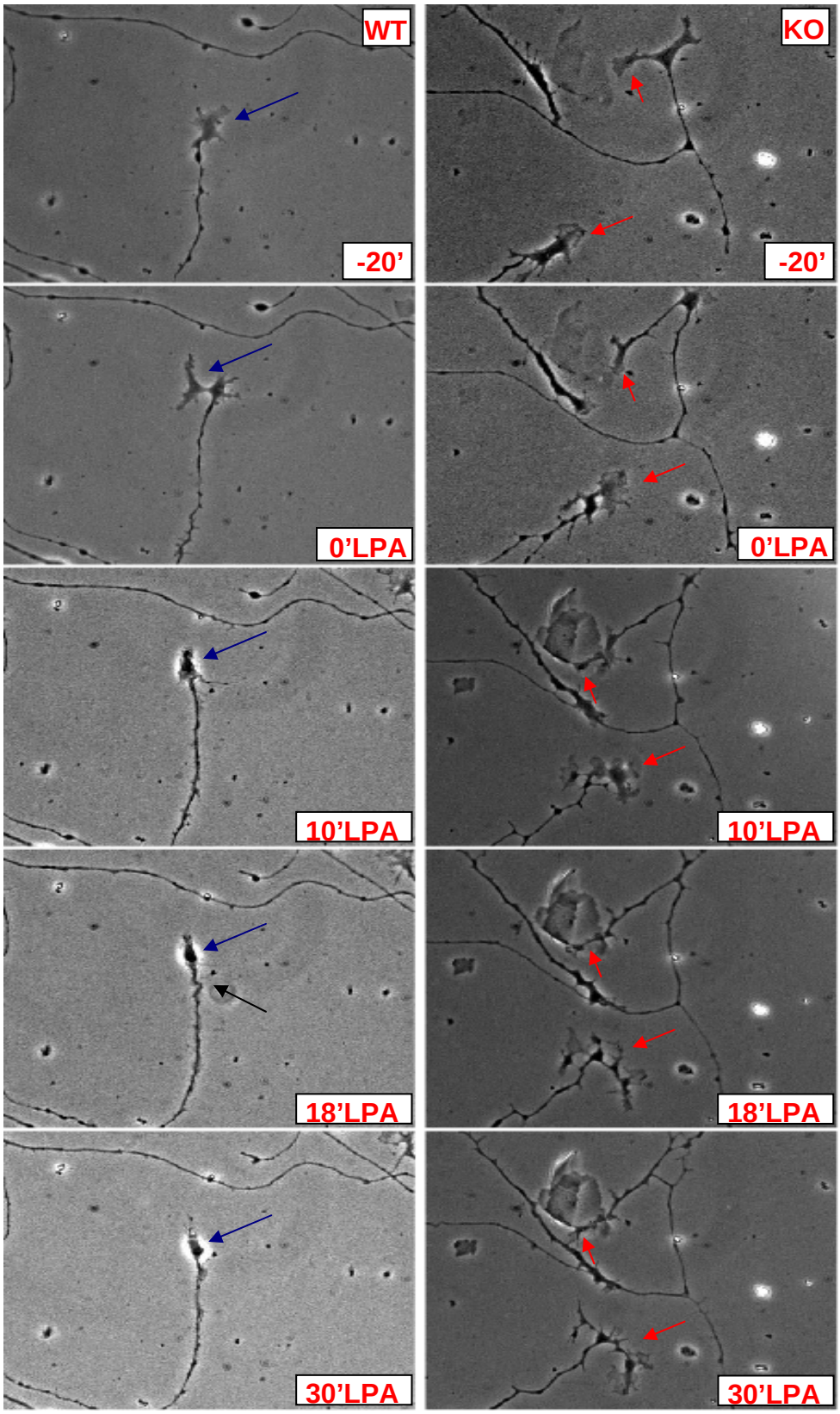

Fig. 15. Response of wild-type and MAP1B-/- neurons to LPA treatment. Adult wild-type (WT) and MAP1B-/- (KO) DRG neurons were grown on coverslips coated with poly-L-lysine and laminin for 20-24h. Images were recorded for 20min, then 10µM LPA was added and recording was continued for 30min with 1min intervals between images. Application of LPA induced growth cone collapse (blue arrows) and axon retraction with sinusoidal bundles (black

arrow) in wild-type neurons. Axons of MAP1B-/- neurons did not retract and continued growth (protrusion of filopodia by axons is indicated by red arrows).

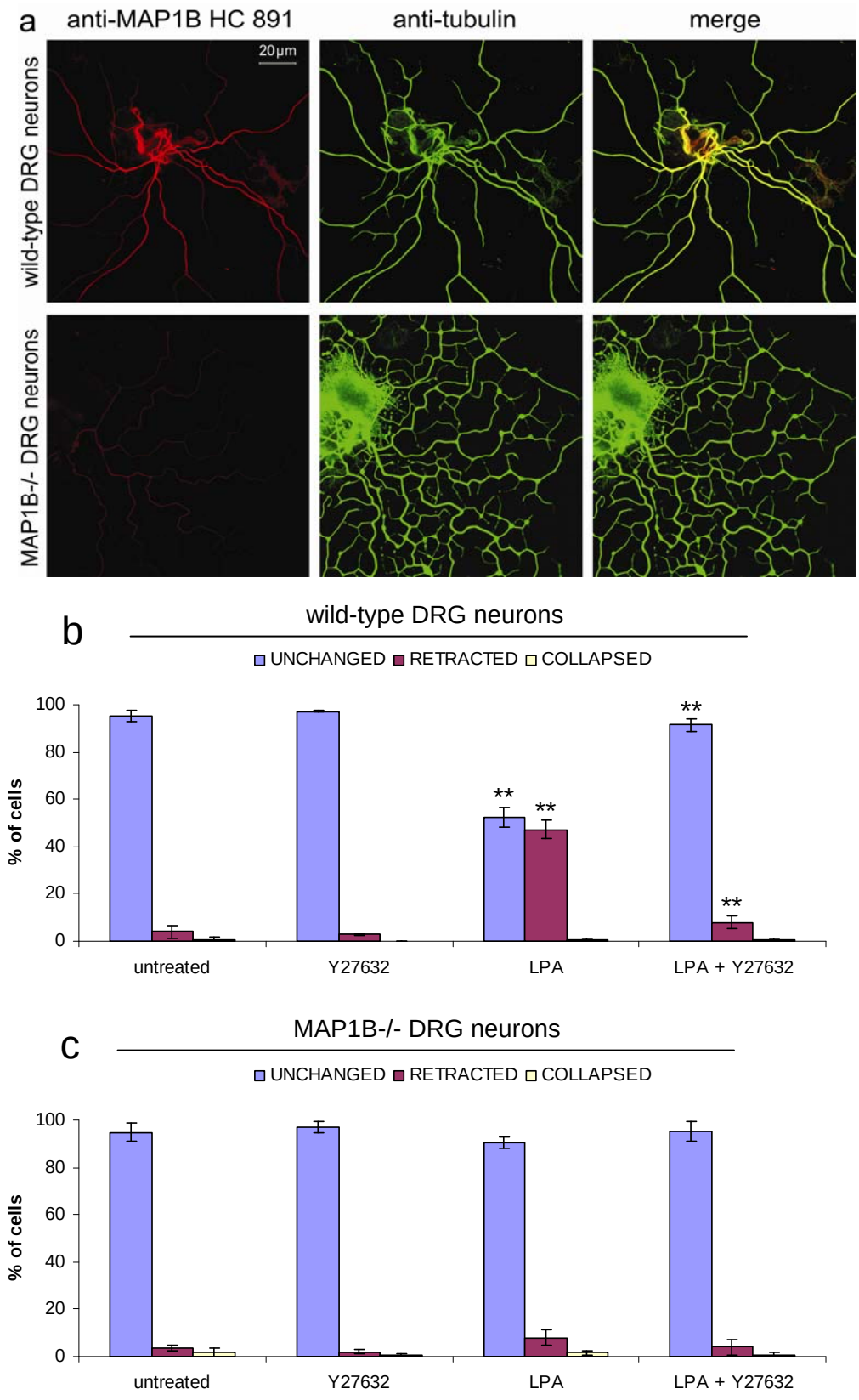

Fig. 16. Inhibition of ROCK prevents LPA-induced axon retraction. DRG neurons from wild-type (b) and MAP1B-/- (c) mice were grown on coverslips coated with poly-L-lysine and

laminin, were left untreated, or were treated with 10µM Y27632 for 1h, with 10µM LPA for 30min, or with 10µM Y27632 for 1h followed by 10µM LPA for 30min, as indicated, fixed with 4% PFA, stained for tubulin and analyzed by confocal microscopy. (a), representative micrographs of wild-type and MAP1B -/- DRG neurons stained for tubulin and MAP1B HC. (b, c), for quantitative analysis, approximately 100 cells in each of 3 independent experiments were assessed for microtubule configuration. Inhibition of ROCK by Y27632 prevented axon retraction induced by LPA. Error bars represent standard deviations. Asterisks indicate that the values for cells treated with LPA were significantly different from corresponding values of untreated neurons and the values for cells treated with Y27632 followed by LPA were significantly different from corresponding values of neurons treated with LPA only (**, $p<0.001$).

To further determine the role of acto-myosin contractility in LPA-induced axon retraction I inhibited myosin with blebbistatin. Binding of blebbistatin to myosin results in stabilization of the metastable state of myosin and inhibition of its transition to the force-producing state, thus inhibiting myosin activity (Allingham et al., 2005). Wild-type DRG neurons were cultured as described and 10µM blebbistatin was applied for 15min prior treatment with LPA (Fig. 17). Only 13% of neurons showed retraction hallmarks in response to LPA when myosin was inhibited (compared to 33% in case of cells treated with LPA only; Fig. 17).

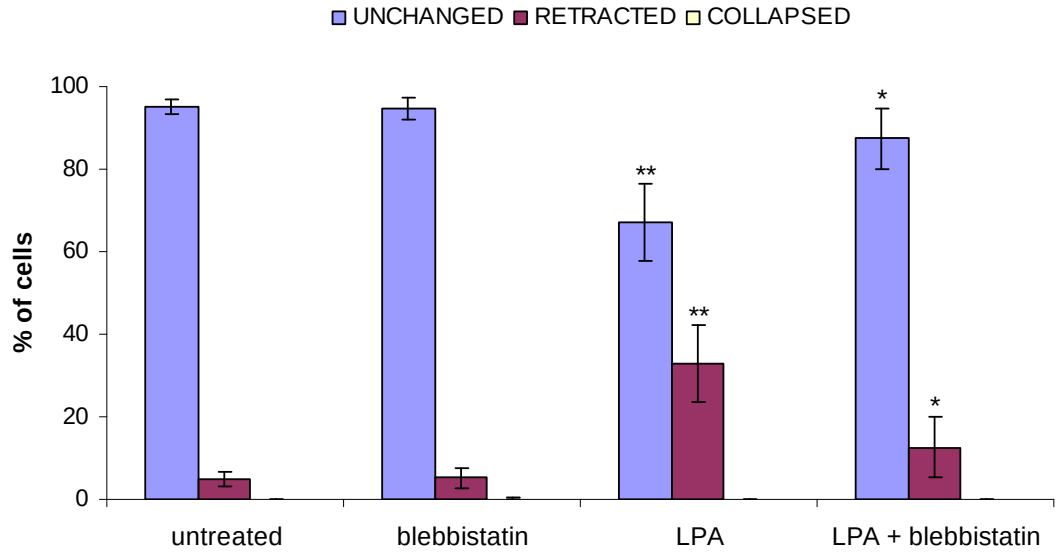

Fig. 17. Inhibition of myosin prevents axon retraction induced by LPA in wild-type DRG neurons. DRG neurons from wild-type mice were grown on coverslips coated with poly-L-lysine and laminin, were left untreated, or were treated with 100µM blebbistatin for 15min, with 10µM LPA for 30min, or with 100µM blebbistatin for 15min followed by 10µM LPA for 30min, as indicated, fixed with 4% PFA, stained for tubulin and analyzed by confocal microscopy. For quantitative analysis, approximately 100 cells in each of 3 independent experiments were assessed for microtubule configuration, which was classified as unchanged, retracted or collapsed. Inhibition of myosin by blebbistatin prevented axon retraction induced by LPA. Error bars represent standard deviations. Asterisks indicate that the values for cells treated with LPA were significantly different from corresponding values of untreated neurons and the

values for cells treated with blebbistatin followed by LPA were significantly different from corresponding values of neurons treated with LPA only (*, $p<0.05$, and *, $p<0.01$).

LPA was also shown to induce retraction of neurites in N2a neuroblastoma cells. These cells express MAP1B and can be induced to differentiate in culture by cultivation on laminin, by removal of serum, or by stimulating the cAMP pathway. To determine if LPA-induced retraction of neurites in N2a cells also involves the Rho/ROCK pathway, cells were grown on poly-L-lysine and laminin pre-coated glass coverslips for 20-24h, treated with 10µM LPA for 30min, with 10µM Y27632 for 1h before application of 10µM LPA for 30min, with 10µM Y27632 for 1h or left untreated. Cells with neurites exceeding one cell diameter in length were classified as unchanged and cells with neurites shorter than one cell diameter in length or without neurites were classified as retracted.

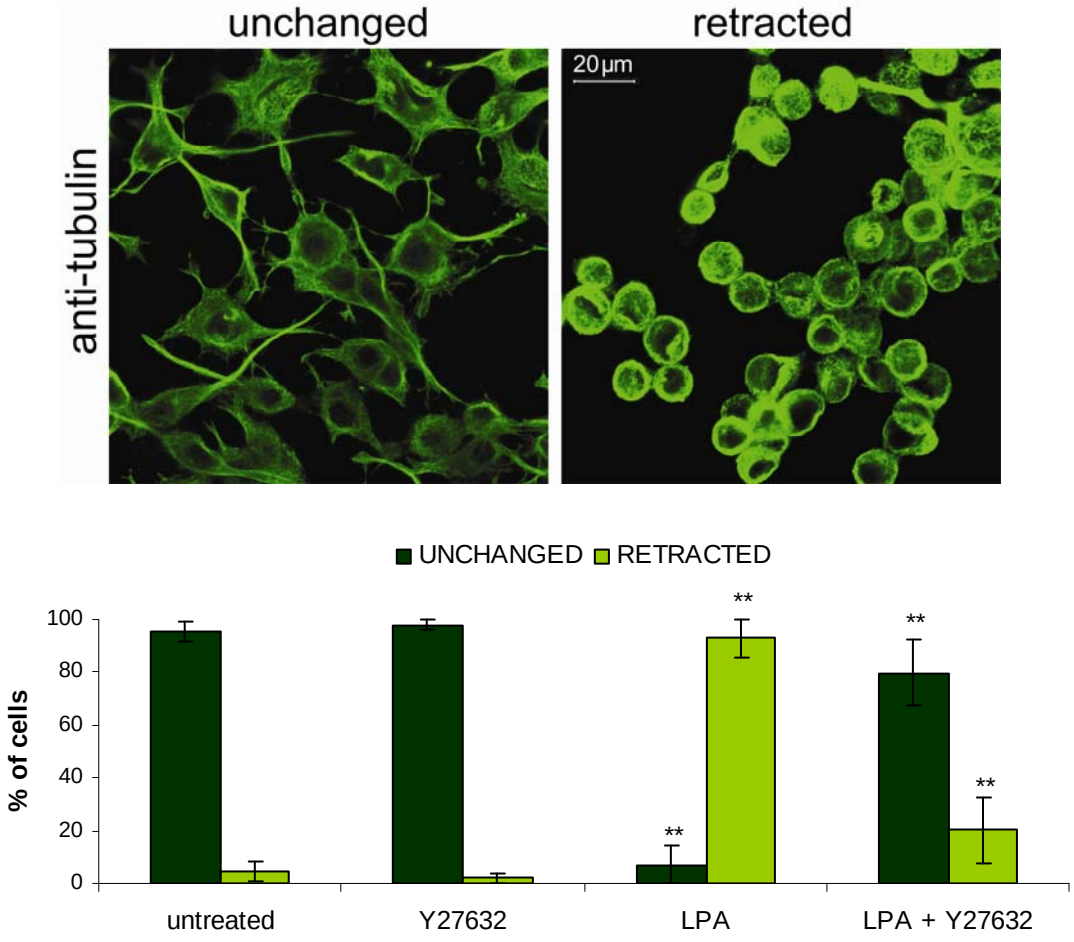

Fig. 18. Inhibition of ROCK abolishes neurite retraction of N2a neuroblastoma cells induced by LPA. N2a neuroblastoma cells grown on coverslips coated with poly-L-lysine and laminin, were left untreated or were treated with 10µM Y27632 for 1h, 10µM LPA for 30min, or with 10µM Y27632 for 1h followed by 10µM LPA for 30min, as indicated, fixed, and stained for tubulin. The upper panel shows representative micrographs of unchanged and retracted N2a cells after treatment. The morphology of cells was quantified by counting cells with neurites

exceeding one cell diameter in length. Inhibition of myosin abolished LPA-induced neurite retraction. For quantitative analysis, 200 cells in each of 4 independent experiments were scored. Error bars represent standard deviations. Asterisks indicate that the values for cells treated with LPA were significantly different from corresponding values of untreated cells and the values for cells treated with Y27632 followed by LPA were significantly different from corresponding values of neurons treated with LPA only (**, $p<0.001$).

Analogous to studies in DRG neurons I examined involvement of myosin in LPA-induced retraction of neurites in N2a neuroblastoma cells. N2a cells were grown as described on poly-L-lysine and laminin to induce differentiation, treated with 100µM blebbistatin for 15min following treatment with 10µM LPA for 30min. Inhibition of myosin impaired LPA-induced neurite retraction in N2a cells and only 24% of cells showed retraction compared to 62% when cells where treated with LPA only (Fig. 19).

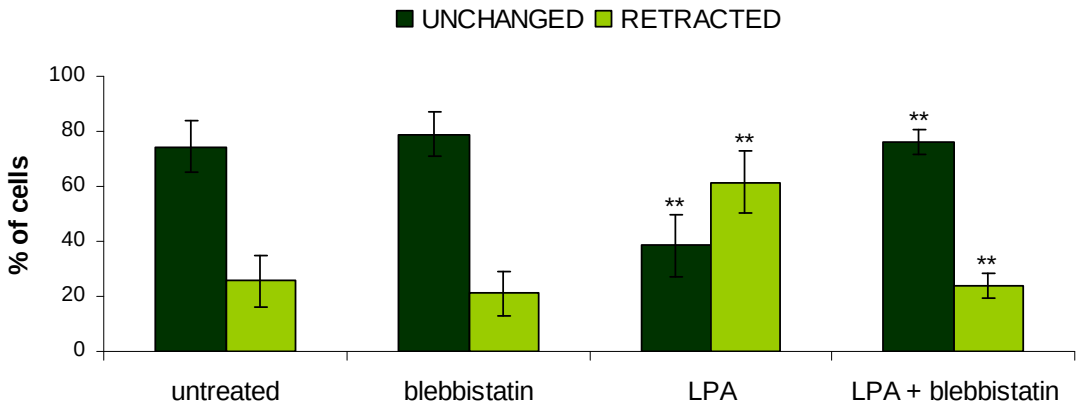

Fig. 19. Inhibition of myosin abolishes LPA-induced neurite retraction of N2a neuroblastoma cells. N2a neuroblastoma cells were grown on coverslips coated with poly-L-lysine and laminin, were left untreated or were treated with 100µM blebbistatin for 15min, 10µM LPA for 30min, or with 100µM blebbistatin for 15min followed by 10µM LPA for 30min, as indicated, fixed, and stained for tubulin. The morphology of cells was quantified by counting cells with neurites exceeding one cell diameter in length. Inhibition of myosin abolished LPA-induced neurite retraction. Inhibition of myosin partially abolished LPA-induced neurite retraction. For quantitative analysis, 200 cells in each of 6 independent experiments were scored. Error bars represent standard deviations. Asterisks indicate that the values for cells treated with LPA were significantly different from corresponding values of untreated cells and the values for cells treated with blebbistatin followed by LPA were significantly different from corresponding values of neurons treated with LPA only (**, $p<0.005$).

LPA-induced axon retraction does not require nNOS activation

As LPA-induced axon retraction shows the same hallmarks as calcimycin- and SNAP-induced retraction and is also MAP1B-dependent, it was interesting to examine if NO

and nNOS are involved in LPA-induced retraction. To determine if LPA induces nNOS activation, wild-type DRG neurons were pre-treated with 300µM NPA for 1h. NPA is a specific nNOS inhibitor. Cells were then treated with 10µM LPA for 30min. Inhibition of nNOS did not abolish retraction induced by LPA and approximately 39,9% of cells showed retraction hallmarks compared to 46% in case of untreated cells (Fig. 20).

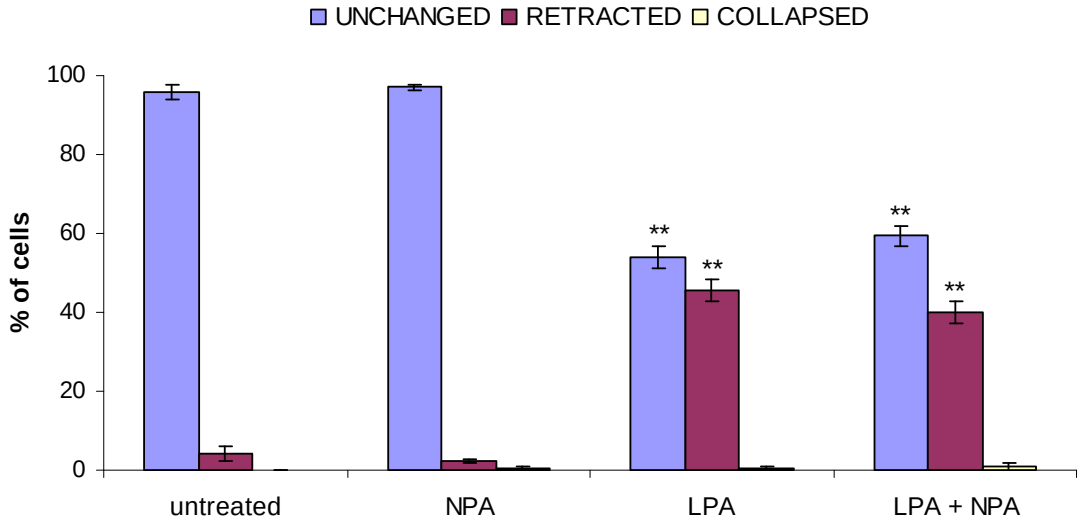

Fig. 20. Inhibition of nNOS does not prevent axon retraction induced by LPA in wild-type DRG neurons. DRG neurons from wild-type mice were grown on coverslips coated with poly-L-lysine and laminin, were left untreated, or were treated with 300µM NPA for 1h, with 10µM LPA for 30min, or with 300µM NPA for 1h followed by 10µM LPA for 30min, fixed with 4% PFA, stained for tubulin and analyzed by confocal microscopy. For quantitative analysis, approximately 100 cells in each of 3 independent experiments were assessed for microtubule configuration, which was classified as unchanged, or retracted or collapsed. Inhibition of nNOS by NPA did not prevent axon retraction induced by LPA. Error bars represent standard deviations. Asterisks indicate that the values for cells treated with NPA followed by LPA and for values from cell treated with LPA only were significantly different from corresponding values of untreated neurons (*, $p<0.001$).

Similarly, in N2a cells pre-treatment with NPA did not abolished retraction of neurites in response to LPA. Approximately 93% of cells retracted in case of cells treated with NPA followed by LPA or in case of cells treated with LPA only. Due to the fact that NPA inhibits specifically nNOS, we can not exclude involvement of other NOS in LPA-induced neurites retraction. Thus, I repeated this experiment with the broad range NOS inhibitor L-NAME. As in case of NPA pretreatment, L-NAME did not prevent retraction if neurites (about 98% of cells retracted compared to 93% when cells were treated with LPA only; Fig. 21).

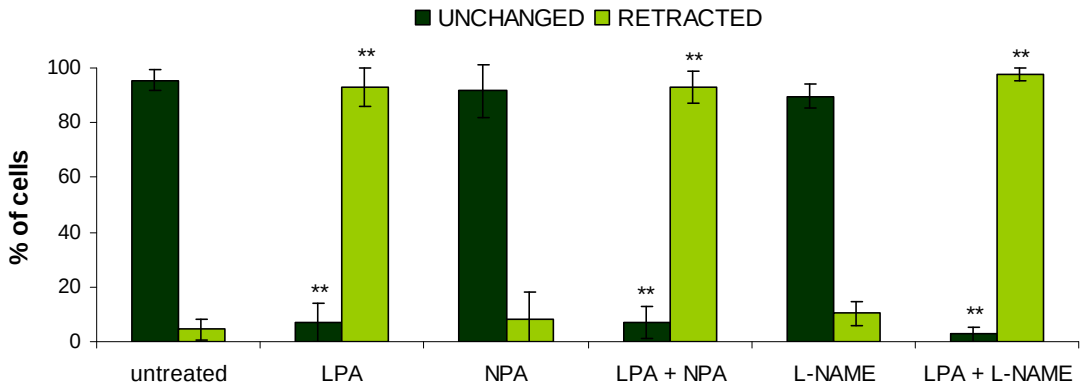

Fig. 21. Inhibition of NOSs does not abolish LPA-induced neurite retraction of N2a neuroblastoma cells. N2a neuroblastoma cells were grown on coverslips coated with poly-L-lysine and laminin, were left untreated or were treated with 300µM NPA for 1h, with 300µM L-NAME for 1h, with 10µM LPA for 30min, with 300µM NPA for 1h followed by 10µM LPA for 30min, or with 300µM L-NAME for 1h followed by 10µM LPA for 30min, as indicated, fixed, and stained for tubulin. The morphology of cells was quantified by counting cells with neurites exceeding one cell diameter in length. Inhibition of myosin abolished LPA-induced neurite retraction. Inhibition of nNOS as well all NOSs did not partially abolish LPA-induced neurite retraction. For quantitative analysis, 200 cells in each of 4 independent experiments were scored. Error bars represent standard deviations. Asterisks indicate that the values for cells treated with LPA only, with NPA followed by LPA, or with L-NAME followed by LPA were significantly different from corresponding values of untreated cells (**, $p<0.001$).

In summary, LPA-induced neurite retraction seems to be MAP1B-dependent, since MAP1B-/- DRG neurons failed to response to LPA, but does not involve nNOS activation. NPA and L-NAME had no influence on amount of retracted neurites. As shown before in other system, in adult DRG neurons and in N2a neuroblastoma cells LPA-induced neurite retraction involves ROCK and myosin.

Role of NO and MAP1B in inhibition of neurite outgrowth induced by CSPG

Lack of evidence for an involvement of NOS in CSPG-induced inhibition of axon growth

Adult CNS neurons fail to regenerate after injury, mainly due to decreased ability to grow, because of inhibitory and repulsive components of the surrounding environment.

In the region of the glial scar formed after lesion, several growth inhibitory molecules, such as myelin-associated components or CSPGs, are released.

CSPGs, produced after injury by astrocytes, are organized in a gradient pattern with the highest concentrations in the centre of the lesion. They inhibit neurite growth *in vivo* (Davies et al., 1999) and *in vitro* (Zhou et al., 2006). It was shown that delivery of chondroitinase ABC (ChABC), which degradates CSPGs, to the lesioned dorsal columns of adult rats promoted regeneration (Bradbury et al., 2002; Barritt et al., 2006).

The signalling pathways activated by CSPG are unknown. It was observed, that inhibition of RhoA with C3-transferase or ROCK with Y27632 promotes axon growth on CSPG (Dergham et al., 2002; Borisoff et al., 2003). Interestingly CSPGs elevate calcium levels in the growth cone and this could trigger activation of nNOS. Thus, I decided to investigate a role of nNOS and NO in CSPG-induced inhibition of axon growth.

I used an *in vitro* model that imitates the glial scar observed *in vivo* after spinal cord injury (Tom et al., 2004). In this system, aggrecan (a major component of CSPG) and laminin formed a gradient pattern similar to this observed at the lesion site and axons from adult DRG neurons which reached an area of aggrecan formed bulbous growth cones similar to dystrophic growth cones observed *in vivo* (Tom et al., 2004). According to this protocol coverslips were coated with 10µg/ml poly-L-lysine, and then were spotted with 2µl of a solution of aggrecan (0.7mg/ml), which is a main component of CSPG, and laminin (5µg/ml). After the spots dried coverslips were covered with laminin (10µg/ml). The CSPG concentration was highest in the rim and lowest in the centre of the spot, whereas the laminin concentration was greatest in the centre of the spot and lowest at the periphery. This can be visualized by staining (Fig. 22). Axons from DRG neurons growing on laminin in the surrounding area were not able to enter into the spot and axons from neurons growing within the centre of the spot did not grow out of the spot. In both cases, axons usually grow along the rim, or sometimes stop growth at the rim forming dystrophic endings.

To determine if CSPG-induced inhibition of axon growth involves nNOS or NOS generally, 300µM NPA or 300µM L-NAME, respectively, were added 6h or 12h after plating of the neurons. No changes in axon behaviour were observed and neurons could not cross the rim of aggrecan, similar as under control conditions in the absence of NOS inhibitor (Fig. 22). Surprisingly, application of Y27632 or blebbistatin also did not overcome inhibitory properties of aggrecan and neurites could not enter into the spot

and could not grow out of the spot (Fig. 22). This is contrary to previous results showing that inhibition of Rho or ROCK abolished CSPG-induced inhibition of axon regrowth.

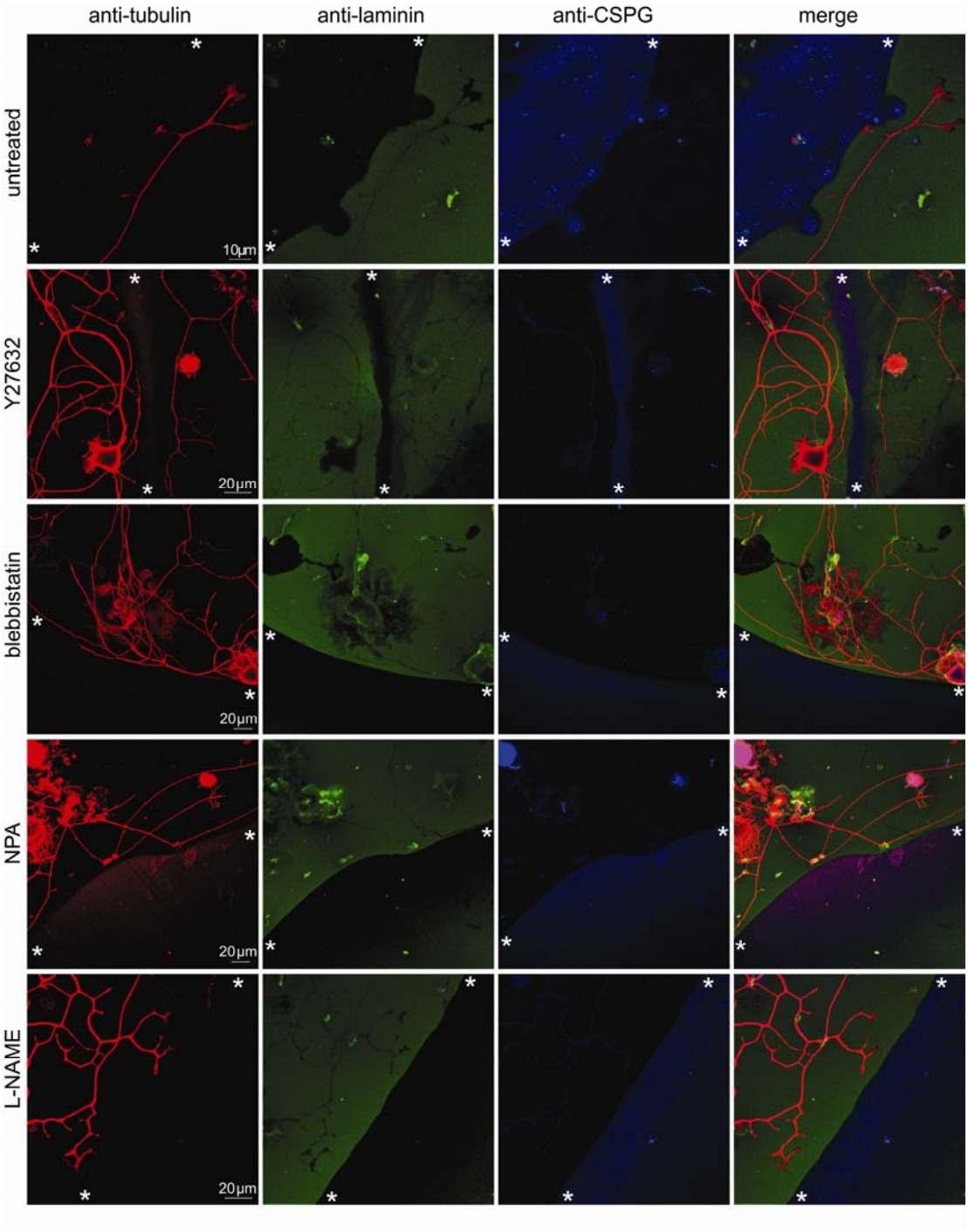

Fig. 22. Inhibition of ROCK, myosin and NOS does not overcome inhibition of axon outgrowth induced by aggrecan in wild-type DRG neurons. Glass coverslips were coated with poly-L-lysine and were spotted with 2µl of a solution of aggrecan (0.7mg/ml) and laminin (5µg/ml). After the spots were allowed to air dry, the coverslips were covered with laminin (10µg/ml). DRG neurons from wild-type mice were grown for 6h or 12h, and subsequently were treated for 12-18h with 10µM Y27632, with 100µM blebbistatin, with 300µM NPA, or with 300µM L-NAME, or were left untreated, as indicated, fixed with 4% PFA. Samples were

stained for tubulin (red), laminin (green) and aggrecan (anti-CSPG, blue) neurites were not able to cross the rims of aggrecan (* asterisks), even if ROCK or myosin were inhibited.

CSPG-induced inhibition of axon regrowth is not MAP1B-dependent

In order to examine a potential role of MAP1B in aggrecan-induced inhibition of neurite growth, MAP1B-/- DRG neurons were grown on coverslips prepared as described above.

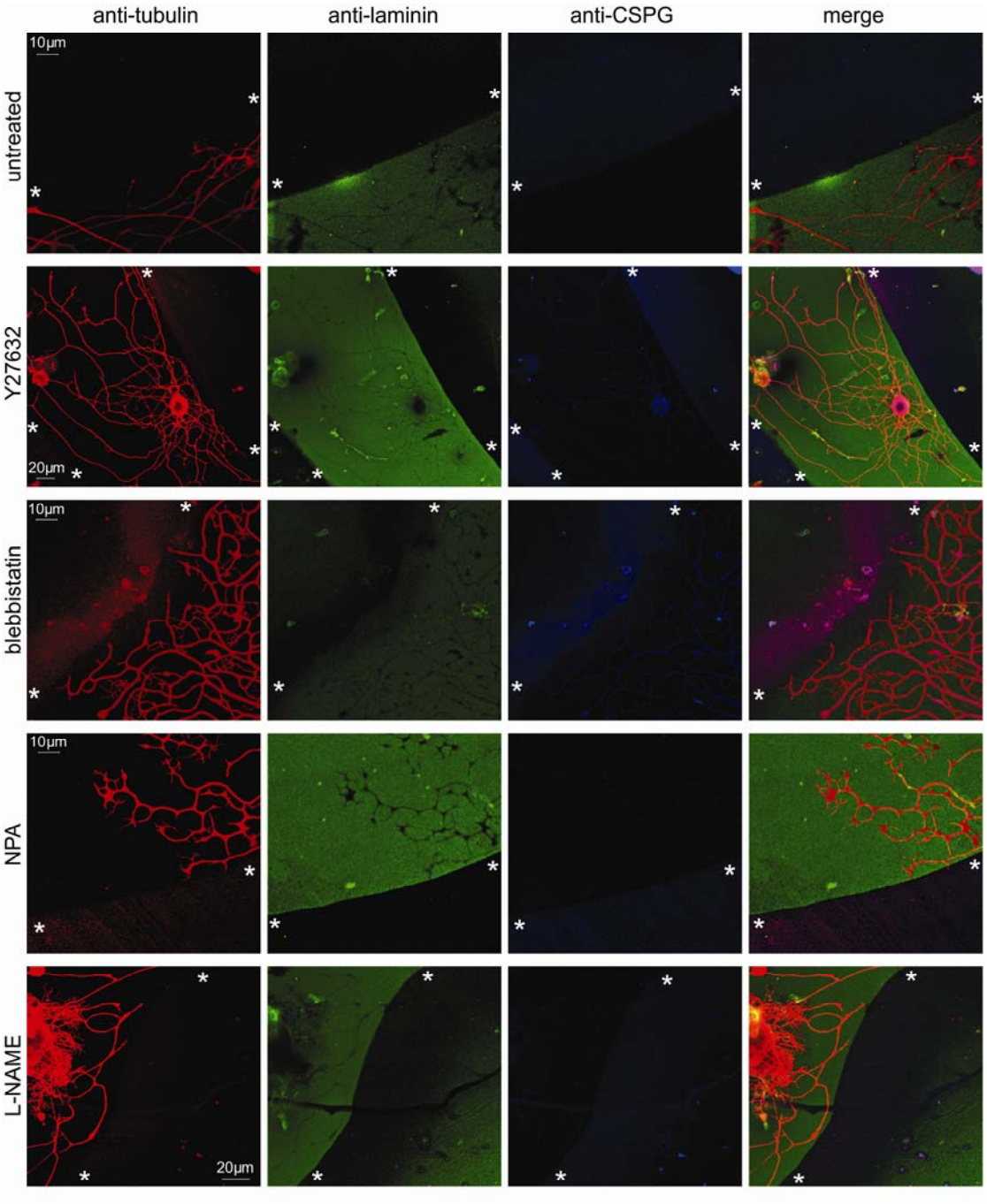

Fig. 23. Inhibition of ROCK, myosin and NOS does not overcome inhibition of axon outgrowth induced by aggrecan in MAP1B-/- DRG neurons. Glass coverslips were coated with poly-L-lysine and were spotted with 2µl of a solution of aggrecan (0.7mg/ml) and laminin

(5µg/ml). After the spots were allowed to air dry, the coverslips were covered with laminin (10µg/ml). DRG neurons from wild-type mice were grown for 6h or 12h, and subsequently were treated for 12-18h with 10µM Y27632, with 100µM blebbistatin, with 300µM NPA, or with 300µM L-NAME, or were left untreated, as indicated, fixed with 4% PFA. Samples were stained for tubulin (red), laminin (green) and aggrecan (anti-CSPG, blue). Neurites were not able to cross the rims of aggrecan (* asterisks), even if ROCK or myosin were inhibited.

Similar to wild-type neurons, axons of MAP1B-/- DRG neurons could not cross an aggrecan barrier in either direction. Bath application of NPA, L-NAME, Y27632 or blebbistatin also did not abolish inhibitory properties of aggrecan, suggesting that MAP1B does not play a role in mediation of CSPG-signalling and in both wild-type and MAP1B-/- DRG neurons aggrecan signalling involves by the same mechanism (Fig. 23).

Laminin is an attractive and permissive substrate and it is possible that neurons growing on such a favourable substrate will not attempt to cross aggrecan rims. Thus, I tried another type of coating. Coverslips were plated with less favourable poly-L-lysine and 2µl spots of a mixture of aggrecan (0.7mg/ml) and laminin (5µg/ml) were applied, left to dry prior to plating of DRG neurons. I thought that neurons growing on a less permissive substrate would be attracted by laminin and would grow through the rim of aggrecan. However, even under these conditions axons from both wild-type and MAP1B-/- DRG neurons did not enter aggrecan spots. Inhibition of ROCK (Fig. 24) and blebbistatin (not shown) did not enable them to enter the aggrecan area either and NPA and L-NAME also had no influence on axon behaviour (not shown).

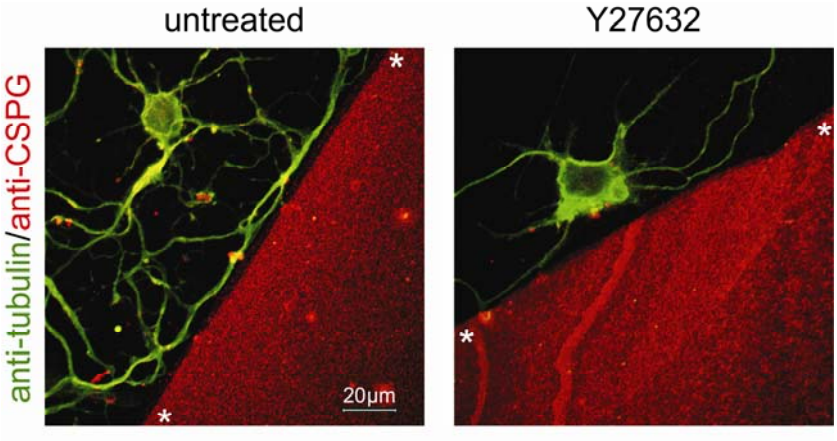

Fig. 24. Aggrecan inhibits growth of axons. Glass coverslips were coated with poly-L-lysine and were spotted with 2µl of aggrecan (0.7mg/ml). Spots were allowed to air dry and wild-type DRG neurons were plated and grown for 6h or 12h, treated with 10µM Y27632 or left untreated, and fixed with 4% PFA. Samples were stained for tubulin (green), and aggrecan (anti-CSPG, red). Micrographs show merge of stainings for tubulin and CSPG. Neurites were not able to cross the rims of aggrecan (* asterisks).

Role of NO and MAP1B in inhibition of neurite outgrowth induced by myelin

CNS myelin is the main source of neurite growth inhibitory factors, such as Nogo and myelin-associated glycoprotein (MAG), after injury. Axons outgrowth in a variety of neurons was inhibited when they were grown on CNS myelin proteins (Schwab and Caroni, 1988) and inhibitory properties of myelin were abolished by anti-myelin antibodies (Schnell and Schwab, 1990). Similar to CSPG, the mechanism by which myelin molecules inhibit axon growth is not well understood. There are several lines of evidence suggesting that myelin inhibition is mediated by the Rho/ROCK pathway. For example, activation of RhoA was observed after treatment of cerebellar granule neurons with the Nogo peptide or when these neurons were grown on myelin components. RhoA was also shown to be activated after spinal cord injury (Niederost et al., 2002; Dubreuil et al., 2003; Madura et al., 2004). Moreover, inhibition of RhoA with C3-transferase or with RhoA antagonists, or inhibition of ROCK with Y27632 promotes axon growth on myelin and promotes regeneration after spinal cord injury (Lehmann et al., 1999; Dergham et al., 2002; Niederost et al., 2002; Dubreuil et al., 2003; Fournier et al., 2003). Interestingly, myelin similar to CSPG, also induces local elevations of Ca^{2+} in the growth cone (Wong et al., 2002). Thus, I decided to study potential involvement of nNOS in myelin-induced inhibition of axon growth.

Lack of evidence for an involvement of NOS in myelin-induced inhibition of axon growth

To determine the potential role of MAP1B and NO in myelin-induced inhibition of axon growth wild-type and MAP1B-/- DRG neurons were grown on coverslips coated with poly-L-lysine, on which 2µl drops of myelin isolated from mouse brain were dried. Axons from both types of neurons could not enter the myelin areas, even when they were treated with blebbistatin (Fig. 25), with Y27632, or with NPA (not shown). Instead, when they reached the myelin border most of them extended along side of it, only when cells were treated with Y27632 some of the axons could enter myelin area, but it was seldom (Fig. 25).

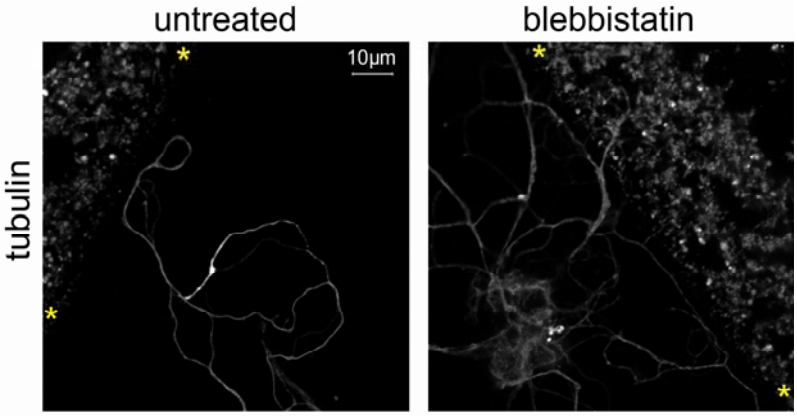

Fig. 25. Myelin inhibits growth of axons. Glass coverslips were coated with poly-L-lysine and were spotted with 2µl of CNS myelin. After the spots were allowed to air dry wild-type DRG neurons were plated, grown for 6h or 12h, treated for 12-18h with 100µM blebbistatin, or were left untreated, and fixed with 4% PFA. Samples were stained for tubulin. Neurites were not able to cross into the areas coated with myelin (* asterisks).

DISCUSSION

NO was shown to induce axon retraction in chicken and mouse DRG neurons (He, 2002; Stroissnigg et al., 2007). The levels of intracellular NO were increased by application of the calcium ionophore calcimycin, or the NO donors NOC7 and SNAP. Calcimycin increases Ca^{2+} levels leading to activation of nNOS and enhanced production of NO. As I mentioned, Ca^{2+} plays an important role in regulation of neurite growth and axonal guidance. Many guidance cues, such as netrin-1, MAG, and NGF increase Ca^{2+} levels, resulting in attraction, repulsion or collapse of the growth cone. Different guidance cues induce various changes in Ca^{2+} levels. For example, netrin-1 stimulates a middle-amplitude increase in Ca^{2+} levels, whereas MAG stimulates a low-amplitude increase in Ca^{2+} levels. Thus, it was interesting to investigate if nNOS, NO, and nitrosylation of MAP1B are involved in axon guidance by physiological guidance cues.

LPA is a well-known physiological guidance cue that is suggested to play a role during migration of neurons and neurite formation. It is present in adult brain and can be produced by postmitotic neurons, such as mouse embryonic cortical neurons (Das and Hajra, 1989; Sugiura et al., 1999; Fukushima et al., 2000). The LPA receptor 1 (LPA1) is expressed at a high level in the ventricular zone of the cerebral cortex, suggesting that LPA might be involved in cortical development (Fukushima et al., 2000; Fukushima et al., 2002b). In many neuronal cell lines (NIE-115, NG108-15, SH-SY5Y, PC12 cells) and cultured primary neurons (cortical neurons, dorsal root ganglia neurons, cerebellar granule neurons) LPA induces growth cone collapse and axon retraction, involving activation of the Rho/ROCK pathway and acto-myosin contractility (Jalink et al., 1993; Jalink et al., 1994; Saito, 1997; Sayas et al., 1999; Fukushima et al., 2000; Sayas et al., 2002a; Fukushima and Morita, 2006; Bouquet et al., 2007). LPA-induced neurite retraction is reversible and after a distinct time length (depending on the cell type) neurites usually regrow, suggesting that LPA-induced retraction is transient and may regulate the time of neurite outgrowth during development (Fukushima et al., 2002a; Bouquet et al., 2004; Fukushima, 2004). It was shown in PC12 cells that depending on the presence of extracellular Ca^{2+} levels LPA induced release of Ca^{2+} from internal stores (Tigyi et al., 1996a). Ca^{2+} influx through the membrane seemed to play an

important role in neurite retraction induced by LPA, since LPA did not induce retraction of neurites when cells were cultured in Ca^{2+} free medium or when Ca^{2+} influx was blocked by divalent cations (Saito, 1997). Likewise, it was found that LPA increased intracellular Ca^{2+} levels also in rat adult DRG neurons (Elmes et al., 2004). Moreover, LPA enhanced NMDA-evoked currents in rat hippocampal neurons (Lu et al., 1999). Thus, by modulating of NMDA currents LPA can activate nNOS resulting in an increased production of NO. In addition, LPA-induced apoptosis of NGF-differentiated PC12 cells involved NO, as it was shown that NOS inhibitors (L-NAME and 7-NI) protected cells against apoptosis stimulated by LPA (Steiner et al., 1992; Holtsberg et al., 1998). We were interested in LPA-induced retraction of neurites rather than in apoptosis of neurons, but the observed stimulation of NO production during LPA-induced apoptosis raised the possibility that during LPA-induced axon retraction NO production might be stimulated as well. This and the observation that morphology of neurons retracting in response to LPA is similar to that induced by calcimycin and SNAP, was the reason to examine potential involvement of NO in axon retraction induced by LPA.

As a first step I treated wild-type and MAP1B-/- DRG neurons with LPA and analyzed response by immunofluorescence microscopy. I found that in MAP1B-/- DRG neurons reaction to LPA was impaired. About 47% of wild-type DRG neurons retracted in response to LPA, whereas in MAP1B-/- DRG neurons only 8% showed retraction morphology. Time-lapse microscopy confirmed these results, since wild-type DRG neurons retracted within 5-10min after application of LPA, but MAP1B-/- DRG neurons continued elongation at the same rate as before treatment. These observations are consistent with previous experiments showing that LPA-induced retraction is MAP1B-dependent . I also reproduced studies showing that LPA involves the Rho/ROCK pathway and acto-myosin contractility (Jalink et al., 1994; Fukushima and Morita, 2006; Bouquet et al., 2007). Treatment of wild-type DRG neurons with Y27632, a ROCK inhibitor, and with blebbistatin, a myosin inhibitor, prior to application of LPA, abolished almost completely axon retraction. In addition, I performed analogous experiments in N2a neuroblastoma cells, which express high levels of MAP1B. Approximately 90% of cells retracted in response to LPA, which was prevented by inhibition of ROCK or myosin.

To analyze potential involvement of NO in axon retraction induced by LPA I inhibited nNOS. nNOS is the major isoform of NOSs in the nervous system and its inhibition was shown to prevent calcimycin-induced axon retraction in mouse adult DRG neurons (Stroissnigg et al., 2007). Treatment of adult wild-type DRG neurons with NPA, which is the nNOS specific inhibitor, prior to application of LPA did not abolish axon retraction. In addition, both NPA and L-NAME (a broad range NOS inhibitor), did not prevent LPA-induced neurite retraction in N2a cells. Thus, I can conclude that LPA-induced neurite retraction does not involve activation of NOSs. but I can not exclude involvement of NO, since. Although I did not measure its level prior and after application of LPA, it seems that LPA does not induce prosuction of NO since there are almost no other sources of NO other than synthesis by NOSs.

I found it interesting that LPA-induced axon retraction was impaired in MAP1B-/- DRG neurons. In the second part of my thesis I tried to clarify how MAP1B mediates LPA-induced axon retraction, but I would like to point out already here that LPA was found to increase activity of GSK3β, which is known to phosphorylate MAP1B. Increased activity of GSK3β was accompanied by enhanced phosphorylation of tau and MAP1B (Sayas et al., 2002b). Thus, GSK3β might be involved in LPA-induced, MAP1B dependent axon retraction.

After injury neurons from the CNS fail to regenerate and their growth cones often become swollen and adapt irregular shapes, forming so called dystrophic endballs, which are similar to the collapsed growth cones observed during retraction of cultured neurons (Yiu and He, 2006). The regrowth of injured axons is limited by several inhibitory and repulsive guidance cues, such as myelin-associated inhibitors, which are produced by oligodendrocytes and myelin debris from the surrounding milieu (Yiu and He, 2006). In addition, reactive astrocytes and many inflammatory cells form a glial scar at the lesion site, which is an additional barrier for regeneration. After injury these reactive astrocytes produce large amounts of CSPGs, which are organized in a gradient pattern. The highest concentration of CSPGs is in the centre of the lesion and the lowest concentration is at the most distal region from the centre of lesion, called penumbra (Yiu and He, 2006). In addition to inhibitory molecules also growth-promoting molecules, such as laminin, are released after injury, but as growth cones reach the area with high concentrations of CSPGs they can not extend further and form dystrophic enballs although permissive molecules are deposited as well (Yiu and He, 2006). The main components of CSPGs are aggrecan, brevican, versican, neurocan, phosphacan

and NG2. They consist of a protein core and long sulphated glycosaminoglycan (GAG) chains, which are responsible for the inhibitory properties of CSPGs (Yiu and He, 2006). It was shown that CSPGs upregulated levels of intracellular Ca^{2+} in the growth cones from chick DRG neurons and the CSPGs-induced Ca^{2+} elevation was abolished by general Ca^{2+} channel blockers. Neurons still omitted the CSPG area, suggesting that avoidance of CSPGs by DRG neurons may not depend on increased levels of Ca^{2+}.(Snow et al., 1994). Nevertheless, it was interesting to examine if enhanced Ca^{2+} levels might stimulate nNOS and cause growth cone collapse and axon retraction through increased production of NO. To examine the potential role of nNOS and MAP1B in CSPGs-induced inhibition of axon growth. I used an *in vitro* model that imitates the glial scar observed *in vivo* after spinal cord injury (Tom et al., 2004). In this system, aggrecan (a major component of CSPG) and laminin formed a gradient pattern similar to this observed at the lesion site and axons from adult DRG neurons which reached an area of aggrecan formed bulbous growth cones similar to dystrophic growth cones observed *in vivo* (Tom et al., 2004). According to this protocol coverslips were coated with poly-L-lysine, and then were spotted with mixture of aggrecan and laminin. After the spots dried coverslips were covered with laminin. The highest concentration of aggrecan was found in the rim and the lowest in the centre of the spot, whereas the laminin concentration was highest in the centre of the spot and lowest at the rim. Axons from adult wild-type DRG neurons growing on laminin in the surrounding area did not enter into the CSPG spot and axons from neurons growing within the centre of the spot were not able to grow out of the spot. In both cases, axons usually grow along the rim, or sometimes stop the growth at the rim forming dystrophic endings, similar to collapsed growth cones that I observed after treatment of DRG neurons with LPA, calcimycin or SNAP. To determine if CSPGs involve nNOS or NOS generally, neurons were treated with NPA or L-NAME, respectively, 6h or 12h after plating. However, I did not observe any changes in axon behaviour. To my surprise, inhibition of ROCK with Y27632 or myosin with blebbistatin also did not overcome inhibitory properties of aggrecan and neurites were not able to cross the rim of aggrecan. This is contrary to previous results showing that inhibition of Rho or ROCK abolished CSPG-induced inhibition of axon growth (Borisoff et al., 2003; Monnier et al., 2003). Inhibition of ROCK with Y27632 was shown to promote axon outgrowth of chick embryonic DRG explants that were grown on aggrecan (Borisoff et al., 2003). CSPGs were found to reduce the number of axons per explant and the mean axon length in chick embryonic

retinal explants grown on mixture of laminin and CSPGs, which was prevented by inhibition of Rho with C3 transferase and ROCK with Y27632 (Monnier et al., 2003). Likewise, inhibition of Rho and ROCK stimulated growth of rat postnatal cerebellar granule neurons (Sivasankaran et al., 2004) and rat embryonic cortical neurons on CSPG (Dergham et al., 2002). The different outcome in my studies could be due to a different type of culture, different species as source of neurons, and the different developmental stage. For example, Borisoff and colleagues used chick embryonic DRG explants, Monnier and colleagues used chick embryonic retinal explants, whereas I used dissociated mouse adult DRG neurons. Moreover, it is important to mention that chick embryonic DRG explants used in the studies of Borisoff and colleagues were cultured in the presence of NGF, BDNF or NT3, while I cultured mouse adult DRG neurons in absence of any growth factor. This can influence the results. I could not grow neurons in presence of NGF since it was shown that NGF inhibits expression of nNOS in adult DRG neurons (Thippeswamy et al., 2005). In addition, Zhou and colleagues observed that inhibition of ROCK with Y27632 was not sufficient to rescue axon growth of naive adult mouse DRG neurons, which were grown in the presence of CSPGs (Zhou et al., 2006). Likewise, when neurons stimulated by a pre-conditioning lesion (PCL) were grown on coverslips coated with laminin and aggrecan inhibition of ROCK did not overcome inhibitory properties of aggrecan. Thus, it seems that although CSPGs work through the Rho/ROCK pathway, its inhibition is not enough to overcome inhibiting properties of CSPGs in some types of neurons. In addition, I can not exclude involvement of the Rho pathway in CSPG-induced inhibition of axon growth, since I only inhibited ROCK, which is a main, but not the only downstream effector of Rho. For example, Rho can activate PKN, citron, citron kinase, mDia1, mDia2, Rhophilin and Rhotekin. Several of theses effectors may also inhibit neurite growth and additional experiment will be needed to clarify the issue. I also decided to examine if MAP1B is involved in aggrecan-induced inhibition of neurite growth. MAP1B-/- DRG neurons were grown on coverslips prepared as described above. Similar to wild-type neurons, axons of MAP1B-/- DRG neurons were not able to cross an aggrecan barrier in either direction. Bath application of NPA, L-NAME, Y27632 or blebbistatin also did not overcome inhibitory properties of aggrecan, suggesting that CSPG-signalling is not dependent on MAP1B.

Laminin is a strongly permissive substrate. Thus, neurons growing on such an attractive substrate potentially might not attempt to cross aggrecan rims. Therefore, I decided to

coat coverslips only with poly-L-lysine, which is much less permissive than laminin. Then I spotted on them a mixture of laminin and aggrecan, without additional coating with laminin. I expected that axons would grow through aggrecan rim, since they grew on less permissive substrate and would be attracted by laminin. Nevertheless, even under these conditions neurons were not able to cross the aggrecan rim and inhibition of ROCK or myosin did not overcome inhibition by aggrecan. Likewise, after inhibition of nNOS and NOSs in general neurons could not enter the aggrecan rim.

As I mentioned, the regrowth of injured axons is limited also by myelin-associated inhibitors, such as Nogo, MAG, Omgp, Sema4D and ephrinB3. It was shown that MAG increased the level of intracellular Ca^{2+} in *Xenopus* neurons and rat postnatal cerebellar neurons (Wong et al., 2002; Hasegawa et al., 2004; Henley et al., 2004b) and MAG-dependent repulsion of axonal growth cones requires Ca^{2+} signalling (Song et al., 1998; Henley et al., 2004b). Likewise, the neurite growth inhibitor NI-35, which is a myelin-associated protein, induced growth cones collapse of rat DRG neurons and chick retinal ganglion cells involving an increase in levels of Ca^{2+} (Bandtlow et al., 1993; Löschinger et al., 1997). Inhibition of Ca^{2+} release from internal stores by dantrolene or depletion of caffeine-sensitive intracellular calcium stores abolished growth cone collapse induced by NI-35 (Bandtlow et al., 1993). Thus, I decided to examine if enhanced levels of Ca^{2+} induced by myelin can trigger activation of nNOS and production of NO. Coverslips were coated with poly-L-lysine and spots of myelin were dried on them. Both, wild-type and MAP1B-/- DRG neurons were not able to enter the myelin area and as they reached the myelin border they continued growth along side of it. Inhibition of ROCK, myosin as well nNOS did not overcome inhibitory properties of myelin. Only in rare cases axons entered the myelin area after inhibition of ROCK. These are somewhat results contradictory to ones already published. For example, Rho inhibition with C3 transferase and ROCK inhibition with Y27632 promoted outgrowth of chick embryonic DRG neurons, rat embryonic cortical neurons and rat postnatal cerebellar granule neurons on myelin, MAG, Nogo-66 or the N-terminal part of Nogo-A (NiG) substrate (Dergham et al., 2002; Niederost et al., 2002; Borisoff et al., 2003; Fournier et al., 2003; Sivasankaran et al., 2004). In addition, after spinal cord injury enhanced activation of Rho was observed and treatment of injured spinal cord from adult mice with C3 or Y27632 promotes long distance regeneration (Madura et al., 2004). As for my results with CSPGs, the discrepancy between my results and the published results of others

could be due to different species, different stages of development and different types of neurons used in these studies.

Although, it seems that nNOS activation is not involved in retraction induced by LPA and inhibition of axon growth triggered by myelin and CSPGs, there are several hints that it can be involved in retraction induced by other guidance cues, such as netrin-1 or semaphorins. It was shown that Ca^{2+} mediates netrin-1-induced turning of growth cones of *Xenopus* neurons (Hong et al., 2000). The turning response was dependent on Ca^{2+} influx through plasma membrane Ca^{2+} channels and Ca^{2+} release from internal stores (Hong et al., 2000). Likewise, Sema5b was shown to induce growth cone collapse by stimulating Ca^{2+} influx in chick DRG neurons, thus potentially it can involve nNOS activation (To et al., 2007). It will be interesting to examine if increased levels of Ca^{2+} induced by these guidance cues, followed by repulsion or collapse of the growth cone or by retraction of neurites, involves activation of nNOS, increased production of NO and S-nitrosylation.

It was found that inhibition of NOSs with L-NAME in transected peripheral nerves in the mouse is associated with enhanced regeneration of myelinated fibers (Zochodne et al., 1997). Moreover, it was shown in rats that the spinal nerve lesion induced upregulation of nNOS in the spinal cord (Gordh et al., 1998). Intraperitoneally application of L-NAME to rats for 6 weeks before operation significantly reduced NOS upregulation and the structural changes in the spinal cord were less prominent (Gordh et al., 1998). Other examples for a role of nNOS and NO can be found during development of the mammalian nervous system. NO was shown to be involved in pruning of retinotectal synapses during development of the chick visual system. During development the transient retinotectal connections are refined in order to form a proper pattern and inhibition of NO synthesis decreased the loss of connections (Wu et al., 1994). It seems that NO is produced by tectal cells, since they express NOS, and diffuses to retinal cells, playing a role as a messenger between these two types of cells (Wu et al., 1994). Likewise, NO is also involved in the pattering of retinogeniculate connections in ferrets (Cramer et al., 1996). All these results indicate a potential role of NOS in physiological and pathophysiological processes. However, many questions concerning the mechanism of NO signalling – for example through the cGMP pathway or through S-nitrosylation of proteins – remain open.

PART II - MECHANISM OF NO-INDUCED AXON RETRACTION

RESULTS

Involvement of other calcium effectors in calcimycin-induced axon retraction

Calcimycin-induced axon retraction was shown to be dependent on the activation of nNOS. Furthmore, it involves S-nitrosylation of MAP1B as a critical step (Stroissnigg et al., 2007). However, we still do not known much about the exact mechanism leading to retraction. It should be taken into consideration that calcimycin-increased Ca^{2+} level can lead to activation of many signalling pathways. To confirm that axon retraction induced by calcimycin involves activation of nNOS, wild-type DRG neurons were treated with 300µM NPA for 1h and then with 10µM calcimycin for 15min. As has been shown before (Stroissnigg et al., 2007) nNOS inhibition reduced the number of retracted cells (about 5% of wild-type DRG neurons showed retraction compared to 31% when neurons were treated with calcimycin only). About 11% of wild-type DRG neurons displayed collapsed morphology when treated both with NPA and calcimycin in comparison to 6% of neurons after treatment with calcimycin only (Fig. 26). Inhibition of nNOS by NPA (NPA treatment only) did not lead to significant changes in organization of microtubules compared to untreated neurons. These results confirm that calcimycin-induced activation of nNOS can trigger axon retraction.

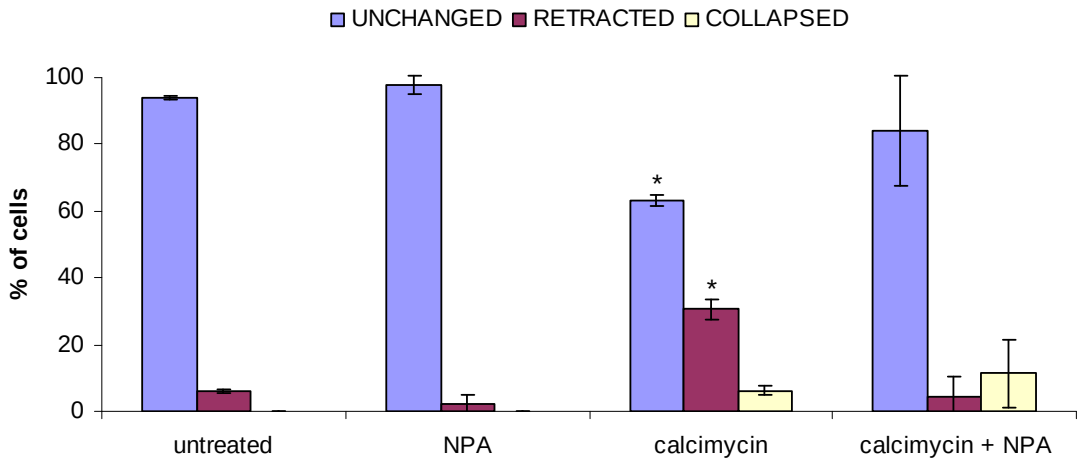

Fig. 26. Calcimycin-induced axon retraction requires the activity of nNOS. Adult wild-type DRG neurons were grown on coverslips coated with poly-L-lysine and laminin, were left untreated, or were treated with 300µM NPA for 1h, with 10µM calcimycin for 15min, or with

300μM NPA for 1h followed by 10μM calcimycin for 15min, as indicated, fixed with 4% PFA, stained for tubulin and analyzed by confocal microscopy. For quantitative analysis, approximately 100 cells in each of 2 independent experiments were assessed for microtubule configuration, which was classified as unchanged, retracted (retraction bulb, trailing remnant, sinusoidal bundles) or collapsed. Calcimycin induced axon retraction and axon collapse. Inhibition of nNOS by NPA decreased the number of cells displaying retraction hallmarks, but it did not influence the number of cells showing axon collapse. Error bars represent standard deviations. Asterisks indicate that the values for cells treated with NPA followed by calcimycin were significantly different from corresponding values of cells treated with calcimycin only and the values from cells treated with calcimycin only were significantly different from corresponding values of untreated neurons (*, $p<0.05$).

It was shown in various cell types that an increase in the intracellular Ca^{2+} leads to activation of calmodulin, which in turn activates various calmodulin-dependent enzymes and signalling pathways. Thus, I examined the potential role of signal transduction pathways other than nNOS in calcimycin induced axon retraction. There are several Ca^{2+}-dependent effectors and I decided to study CaMKII, calcineurin, PKC, and calpain. To determine the role of these effectors wild-type DRG neurons were plated on poly-L-lysine and laminin coated glass coverslips, grown for 24h in the absence of NGF, treated with specific inhibitor followed by treatment with 10μM calcimycin for 15min, fixed and stained for tubulin and MAP1B HC as a control.

CaMKII is not involved in calcimycin-induced axon retraction

As I mentioned before, it was shown in cultured embryonic *Xenopus* spinal neurons that at the normal resting level of $[Ca^{2+}]_i$ small local Ca^{2+}signals activated calcineurin and high local Ca^{2+} signals activated CaMKII, inducing repulsion and attraction, respectively, while at low resting levels of $[Ca^{2+}]_i$ both small and high local Ca^{2+}signals activated calcineurin (Wen et al., 2004). Although, we induce global rather than local increase in Ca^{2+} levels, it can also lead to activation of CaMKII. To determine the role of CaMKII in calcimycin-induced retraction I decided to inhibit CaMKII with autocamtide-2-relate inhibitory peptide (AIP), which is a highly specific, and potent inhibitor of CaMKII.

AIP at 1μM completely inhibits CaMKII, but does not affect PKC, PKA, CaMKIV and other kinases. In my experiments I used N-terminal myristoylated AIP (myrAIP), which is a cell permeable form of AIP. Wild-type DRG neurons were treated with 10μM myrAIP for 30min followed by treatment with 10μM calcimycin for 15min, fixed and

stained for tubulin. About 39% of neurons treated with myrAIP and calcimycin showed retraction hallmarks compared to 44% when neurons were treated with calcimycin only (Fig. 27). This difference as well as other slight differences resulting from the two different treatments was not statistically significant, suggesting that CaMKII is not involved in axon retraction induced by calcimycin (Fig. 27). Inhibition of CaMKII by myrAIP (treatment with myrAIP only) did not induce any significant changes in the phenotype of neurons when compared to neurons that were untreated.

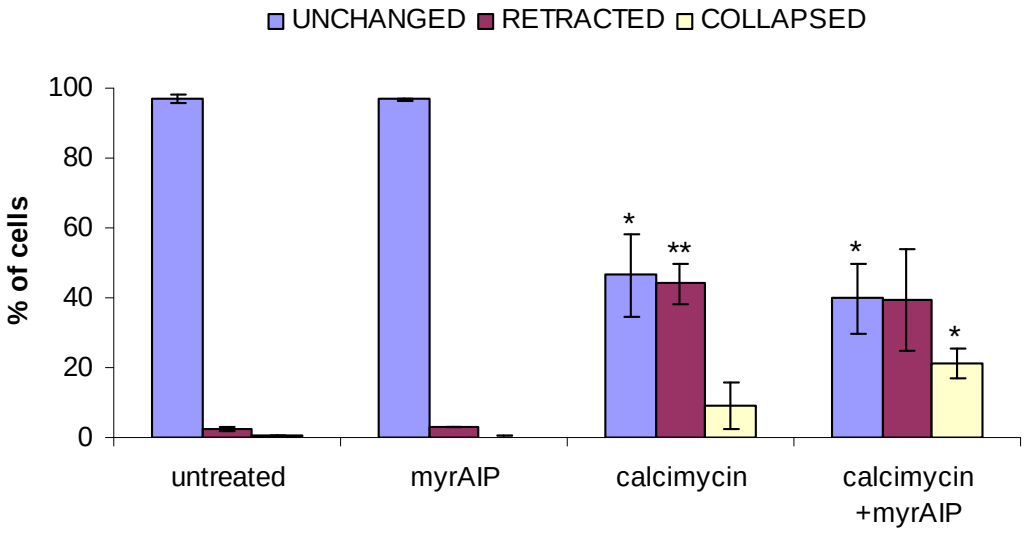

Fig. 27. Inhibition of CaMKII does not prevent axon retraction induced by calcimycin in wild-type DRG neurons. DRG neurons from wild-type mice were grown coverslips coated with poly-L-lysine and laminin, were left untreated, or were treated with 10µM myrAIP for 30min, with 10µM calcimycin for 15min, or with 10µM myrAIP for 30min followed by 10µM calcimycin for 15min, as indicated, fixed with 4% PFA, stained for tubulin and analyzed by confocal microscopy. For quantitative analysis, approximately 100 cells in each of 2 independent experiments were assessed for microtubule configuration, which was classified as unchanged, retracted or collapsed. Calcimycin induced axon retraction and axon collapse. Inhibition of CaMKII by myrAIP did not influence the number of cells showing either retraction hallmarks or axon collapse. Error bars represent standard deviations. Asterisks indicate that the values for cells treated with myrAIP followed by calcimycin and from the values of cells treated with calcimycin only were significantly different from corresponding values of untreated neurons (*, $p<0.05$, and **, $p<0.01$).

Calcineurin is not involved in calcimycin-induced axon retraction

It is known that low-amplitude calcium signals activate calcineurin (Wen et al., 2004) and it was shown that inhibition of calcineurin increased neurite outgrowth in *Xenopus* spinal neurons (Lautermilch and Spitzer, 2000). It was also observed that Sema5B

induced Ca^{2+} influx via Co^{2+}-sensitive Ca^{2+} channels, leading to a two-step increase in Ca^{2+} level and growth cone collapse in chicken embryonic DRG neurons. A low-amplitude rise of Ca^{2+} level induced activation of calcineurin followed by high amplitude rise of Ca^{2+} level and activation of calpain (To et al., 2007). Inhibition of calcineurin partially attenuated growth cone collapse induced by Sema5b (To et al., 2007). In addition, calcineurin was shown to dephosphorylate tau and other MAPs and thus its activation by increased Ca^{2+} levels could possibly have an influence on MAP1B, which has been shown to be involved in axon retraction.

To examine the potential role of calcineurin in axon retraction in our system I used cyclosporine A (CSA), an immunosuppressant that forms a complex with cyclophilin inhibiting the phosphatase activity of calcineurin. Pretreatment of wild-type DRG neurons with 5µM CSA for 20min did not abolish retraction of neurons (37% in comparison to 38% in case of calcimycin treatment only; Fig. 28). This demonstrates that calcineurin is not involved in axon retraction induced by calcimycin. Additionally, inhibition of calcineurin by CSA (treatment with CSA only) did not lead to any significant changes in axonal microtubule organization when compared to untreated neurons.

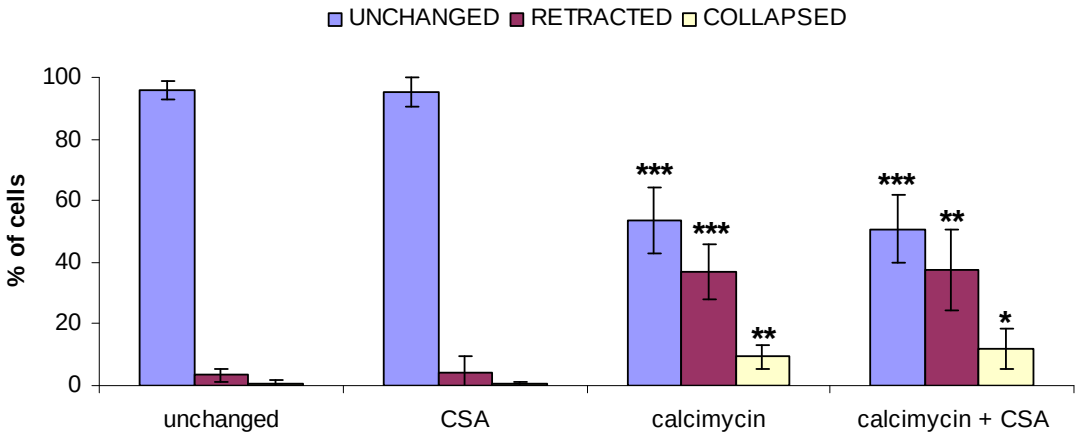

Fig. 28. Inhibition of calcineurin does not prevent axon retraction induced by calcimycin in wild-type DRG neurons. DRG neurons from wild-type mice were grown on coverslips coated with poly-L-lysine and laminin, were left untreated, or were treated with 5µM CSA for 20min, with 10µM calcimycin for 15min, or with 5µM CSA for 20min followed by 10µM calcimycin for 15min, as indicated, fixed with 4% PFA, stained for tubulin and analyzed by confocal microscopy. For quantitative analysis, approximately 100 cells in each of 4 independent experiments were assessed for microtubule configuration, which was classified as unchanged, retracted or collapsed. Calcimycin induced axon retraction and axon collapse. Inhibition of calcineurin by CSA did not influence the number of cells showing either retraction hallmarks or axon collapse. Error bars represent standard deviations. Asterisks indicate that the

values for cells treated with CSA followed by calcimycin and values for cells treated with calcimycin only were significantly different from corresponding values of untreated neurons (*, $p<0.05$, **, $p<0.005$, and ***, $p<0.001$).

PKC is not involved in calcimycin-induced axon retraction

To investigate involvement of PKC in axon retraction induced by calcimycin, prior to application of calcimycin wild-type neurons were pretreated for 1.5h with 50µM GÖ6976, which is a specific inhibitor of PKC α and β1 isozymes. Inhibition of PKC did not change the amount of cells displaying retraction hallmarks (28% in comparison to 32% when cells were treated with calcimycin only; Fig. 29). The level of cells showing collapsed phenotype was reduced to 6% compared to 18% in case of neurons treated with calcimycin only, what is associated with increase number of unchanged neurons (66% compare to 50% when cells were treated with calcimycin only; Fig. 29). However, neither of these differences were not statistically significant. Inhibition of PKC by GÖ6976 (treatment with GÖ6976 only) did not induce any significant changes in neurons in comparison to untreated neurons.

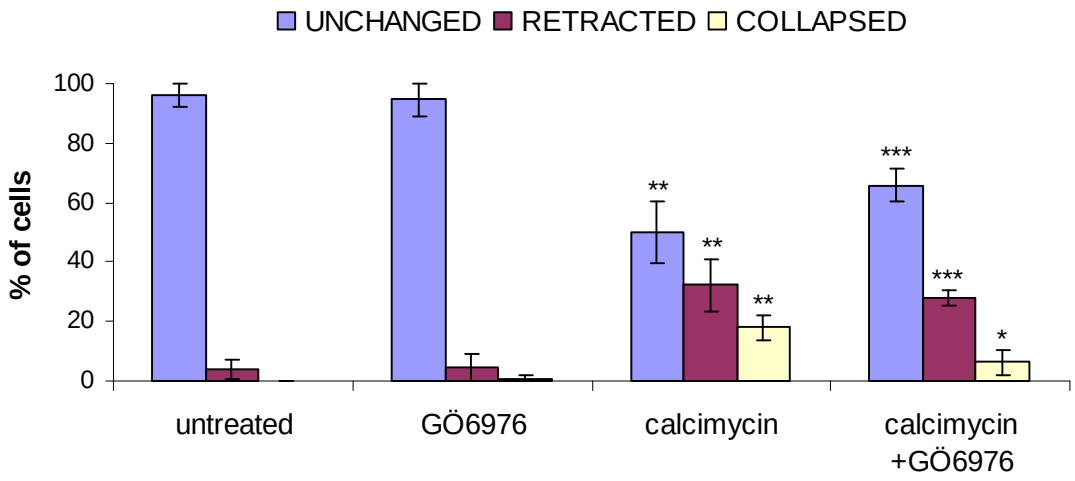

Fig. 29. Inhibition of PKC does not prevent axon retraction induced by calcimycin in wild-type DRG neurons. DRG neurons from wild-type mice were grown on coverslips coated with poly-L-lysine and laminin, were left untreated, or were treated with 50µM GÖ6976P for 1.5h, with 10µM calcimycin for 15min, or with 50µM GÖ6976 for 1.5h followed by 10µM calcimycin for 15min, as indicated, fixed with 4% PFA, stained for tubulin and analyzed by confocal microscopy. For quantitative analysis, approximately 100 cells in each of 4 independent experiments were assessed for microtubule configuration, which was classified as unchanged, or retracted or collapsed. Calcimycin induced axon retraction and axon collapse. Inhibition of calcineurin by GÖ6976 did not influence the number of cells showing retraction hallmarks, but reduced the number of collapsed neurons. Error bars represent standard deviations. Asterisks indicate that the values for cells treated with GÖ6976 followed by calcimycin and the values for cells treated with calcimycin only were significantly different from corresponding values of untreated neurons (*, $p<0.05$, **, $p<0.01$, and ***, $p<0.001$).

Calpain is not involved in calcimycin-induced axon retraction

There is much evidence that increased Ca^{2+} levels can activate calpain resulting in axon retraction, growth cone collapse or neuronal cell death. As mentioned above, Sema5B induced growth cone collapse involved elevation of Ca^{2+} levels and activation of calcineurin and calpain (To et al., 2007). It was also shown that exposure of cultured hippocampal neurons to glutamate, which induced an increase in Ca^{2+} levels, led to activation of calpain above basal levels (Hajieva et al., 2009). Depolarization, which induced neurite retraction, also led to elevation of Ca^{2+} and activation of calpain, and inhibition of calpain abolished retraction induced by depolarization in adult rat spiral ganglion neurites (SGNs) (Roehm et al., 2008). Calpain is also involved in growth cone collapse followed a high-amplitude increase in Ca^{2+} levels stimulated by motuporamine C in chicken embryonic DRG neurons (To et al., 2008).

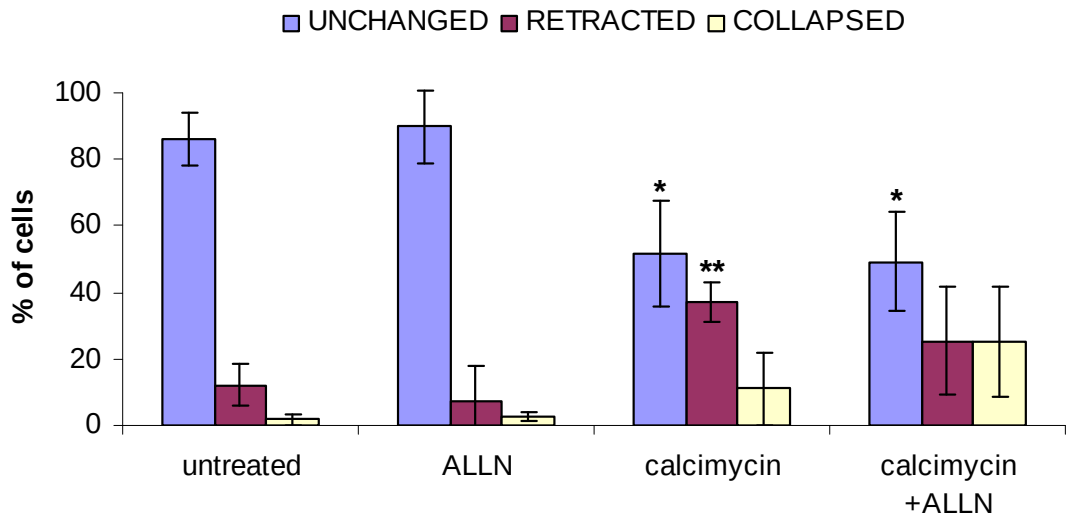

Fig. 30. Inhibition of calpain does not prevent axon retraction induced by calcimycin in wild-type DRG neurons. DRG neurons from wild-type mice were grown on coverslips coated with poly-L-lysine and laminin, were left untreated, or were treated with 200µM ALLN for 1h, with 10µM calcimycin for 15min, or with 200µM ALLN for 1h followed by 10µM calcimycin for 15min, as indicated, fixed with 4% PFA, stained for tubulin and analyzed by confocal microscopy. For quantitative analysis, approximately 100 cells in each of 4 independent experiments were assessed for microtubule configuration, which was classified as unchanged, or retracted or collapsed. Calcimycin induced axon retraction and axon collapse. Error bars represent standard deviations. Asterisks indicate that the values for cells treated with ALLN followed by calcimycin and the values for cells treated with calcimycin only were significantly different from corresponding values of neurons untreated (*, $p<0.01$, and **, $p<0.005$).

To study involvement of calpain in axon retraction induced by calcimycin I used ALLN, which is a cell permeable, peptide aldehyde inhibitor of calpain and other

neutral cysteine proteases. Pretreatment of wild-type DRG neurons with 200µM ALLN for 1h slightly reduced the number of neurons displaying retraction in response to calcimycin treatment (26% compared to 37% in case of calcimycin treatment only; Fig. 30). This reduction is associated with small increase in number of collapsed neurons (25% compared to 11% when cells were treated with calcimycin treatment only). These differences are not significant and it seems that calpain is not involved in axon retraction induced by calcimycin. Inhibition of calpain by ALLN (treatment with ALLN only) did not lead to significant changes in axonal microtubule organization when compared to untreated neurons (Fig. 30).

Involvement of acto-myosin contractility in axon retraction induced by calcimycin and NO

According to a recent model, axon extension and retraction depend on the balance between two opposing forces (Baas and Ahmad, 2001). The extension force is based on microtubules with distally oriented plus ends, and dynein, a minus end-directed motor protein. The retraction force is based on F-actin and myosin. As mentioned above, NO-induced axon retraction in DRG neurons shows the typical retraction hallmarks: sinusoidal microtubule bundles along the axonal shaft, a retraction bulb, and a trailing remnant (Hess et al., 1993; Ernst et al., 2000; He et al., 2002). A similar morphology showed neurons retracting in response to the inhibition of cytoplasmic dynein (Baas and Ahmad, 2001) or activation of the RhoA GTPase (Billuart et al., 2001; Zhang et al., 2003; Bouquet et al., 2007). It was shown in our lab that the COOH terminus of LC1 interacts with its NH_2 terminus, which contains the microtubule binding domain (Stroissnigg et al., 2007). This interaction between COOH- and NH_2-terminal domains of LC1 results in a conformation characterized by a reduced microtubule binding activity. It was proposed that activation of nNOS increases NO levels and leads to S-nitrosylation of cys2457 within LC1, leading to a conformational change with a higher microtubule binding activity (Stroissnigg et al., 2007). Interaction between MAP1B and microtubules might inhibit dynein, resulting in reduction of the extension force and axon retraction (Fig. 31; Stroissnigg et al., 2007). It seems that in MAP1B-/- neurons nNOS activation and high levels of NO do not inhibit dynein action and thus do not induce axon retraction. Our hypothesis that MAP1B inhibits dynein comes from studies

showing that MAP1B affects dynein function, particularly its interaction with LIS1 (lissencephaly-related protein 1) and can block dynein-dependent retrograde transport (Jimenez-Mateos et al., 2005; Jimenez-Mateos et al., 2006; Trančíková, 2007). In addition, the microtubule binding sites in dynein and in MAP1B share sequence homology (Koonce and Tikhonenko, 2000). On the other hand, several physiological guidance cues were shown to induce axon retraction and growth cone collapse through actin rearrangement regulated by activation of RhoA and myosin II (Hirose et al., 1998; van Leeuwen et al., 1999; Billuart et al., 2001; Zhang et al., 2003). Thus, I decided to investigate the potential role the acto-myosin forces in NO-induced axon retraction.

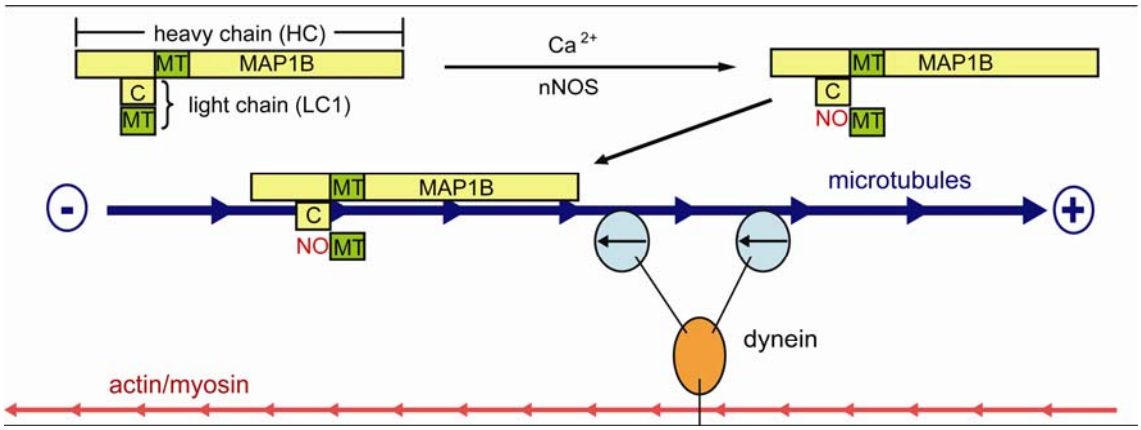

Fig. 31. A model for MAP1B mediated effects of nNOS activation. Axon extension or retraction depends on the balance between two opposing forces. The extension force is based on microtubules (blue) with their plus ends oriented distally, and dynein, a minus end-directed motor (direction showed by black arrows in the light blue domains). The retraction force is based on F-actin and myosin (red). The microtubule binding domain (MT) of heavy chain (HC) and light chain (LC1) of MAP1B are indicated by dark green boxes. It was shown that the COOH terminus of LC1 interacts with its NH_2 terminus, which contains the microtubule binding domain (Stroissnigg et al., 2007). This interaction between COOH- and NH_2-terminal domains of LC1 results in a conformation characterized by a reduced microtubule binding activity (Stroissnigg 2007). It was proposed that activation of nNOS increases NO levels and leads to S-nitrosylation of cys2457 within LC1 (symbolised by C-NO), leading to a conformational change with a higher microtubule binding activity (Stroissnigg et al., 2007). Interaction between MAP1B and microtubules might inhibit dynein, resulting in reduction of the extension force and axon retraction. (adapted from Stroissnigg et al., 2007).

ROCK is necessary for calcimycin- and NO-induced axon retraction

To examine involvement of acto-myosin in axon retraction induced by NO I planned to inhibit the Rho pathway and look if it would influence NO-induced axon retraction. It was shown that RhoA transduces signals via binding to its downstream partners, such as

ROCK I and ROCK II. Thus, I decided to inhibit ROCK with Y27632, which I used in experiments with LPA. Y27632 has a specifity 100-fold higher for ROCK than for PKA, PKC or MLCK and 20-fold higher than for two other RhoA downstream effectors – protein kinase N and citron kinase.

Again wild-type DRG neurons were plated on poly-L-lysine and laminin coated coverslips, grown for 24h in the absence of NGF, pretreated with 10µM Y27632 for 1h and treated with 10µM calcimycin for 15min or were left untreated, fixed and stained for tubulin and MAP1B HC as a control. Pretreatment of neurons with Y27632 prevented axon retraction and collapse induced by calcimycin (7% and 6%, respectively, in comparison to 30% and 19% when cells were treated with calcimycin only, respectively). In addition, inhibition of ROCK by Y27632 did not lead to significant changes in axonal microtubule organization compared to untreated neurons (Fig. 32).

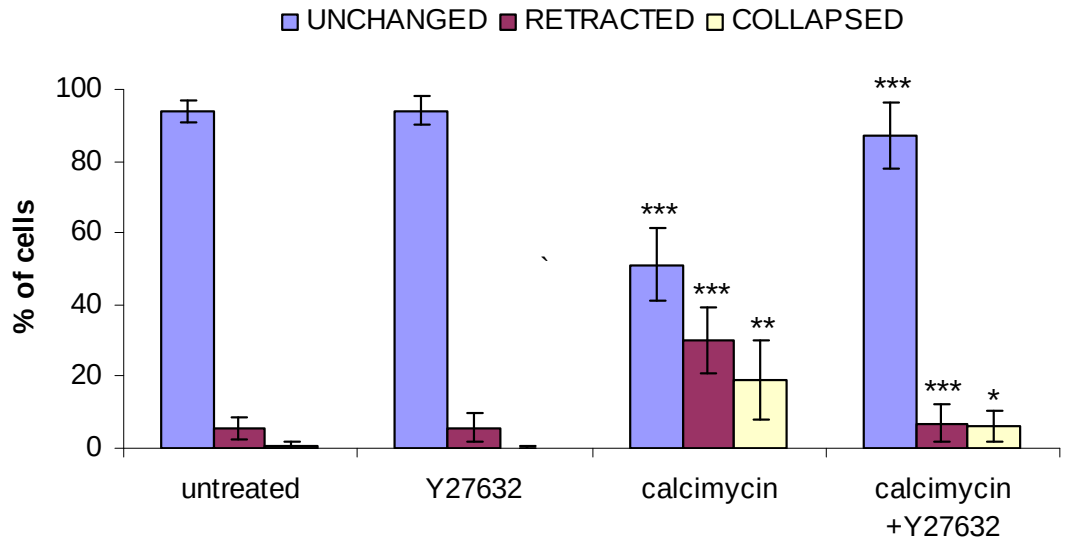

Fig. 32. Inhibition of ROCK prevents axon retraction induced by calcimycin in wild-type DRG neurons. DRG neurons from wild-type mice were grown on coverslips coated with poly-L-lysine and laminin, were left untreated, or were treated with 10µM Y27632 for 1h, with 10µM calcimycin for 15min, or with 10µM Y27632 for 1h followed by 10µM calcimycin for 15min, as indicated, fixed with 4% PFA, stained for tubulin and analyzed by confocal microscopy. For quantitative analysis, approximately 100 cells in each of 4 independent experiments were assessed for microtubule configuration, which was classified as unchanged, or retracted or collapsed. Calcimycin induced axon retraction and axon collapse. Inhibition of ROCK by Y27632 prevented axon retraction induced by calcimycin. Error bars represent standard deviations. Asterisks indicate that the values for cells treated with calcimycin were significantly different from corresponding values of untreated neurons and the values for cells treated with Y27632 followed by calcimycin were significantly different from corresponding values of neurons treated with calcimycin only (*, $p<0.05$, **, $p<0.005$, and ***, $p<0.001$).

I also examined the involvement of ROCK in axon retraction induced by the nitrosylating agent SNAP. Wild-type neurons were cultured as described before and left untreated, or treated with 100µM SNAP for 1h, 10µM Y27632 for 1h, or treated with 10µM Y27632 for 1h followed by treatment with 100µM SNAP for 1h. Inhibition of ROCK with Y27632 abolished retraction induced by SNAP in wild-type DRG neurons (5% neurons showing retraction hallmarks in comparison to 49% in case of cells treated with SNAP only; Fig. 33).

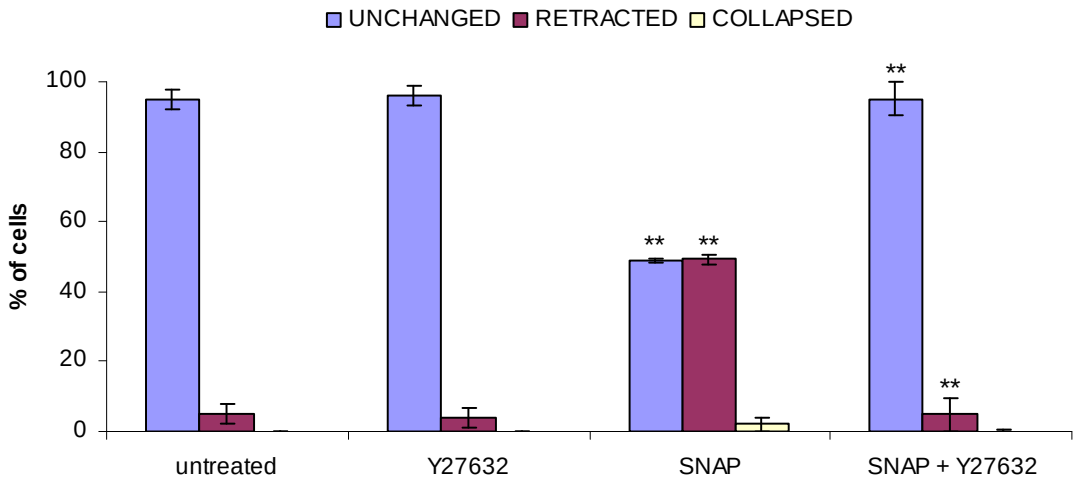

Fig. 33. Inhibition of ROCK prevents axon retraction induced by SNAP in wild-type DRG neurons. DRG neurons from wild-type mice were grown on coverslips coated with poly-L-lysine and laminin, were left untreated, or were treated with 10µM Y27632 for 1h, with 100µM SNAP for 1h, or with 10µM Y27632 for 1h followed by 100µM SNAP for 1h, as indicated, fixed with 4% PFA, stained for tubulin and analyzed by confocal microscopy. For quantitative analysis, approximately 100 cells in each of 3 independent experiments were assessed for microtubule configuration, which was classified as unchanged, or retracted or collapsed. SNAP induced axon retraction. Inhibition of ROCK by Y27632 prevented axon retraction induced by SNAP. Error bars represent standard deviations. Asterisks indicate that the values for cells treated with SNAP were significantly different from corresponding values of untreated neurons and values for cells treated with Y27632 and SNAP were significantly different from corresponding values of neurons treated with SNAP only (**, $p<0.001$).

It was shown in our lab that treatment of N2a neuroblastoma cells with 100µM SNAP for 1h increased nitrosylation of MAP1B LC1 (1.7-fold above the level observed in untreated cells) and inhibited differentiation of N2a cells over-expressing LC1 (Stroissnigg et al., 2007). To investigate involvement of ROCK in SNAP-induced neurite in N2a neuroblastoma cells, cells were grown on poly-L-lysine and laminin pre-coated glass coverslips, pretreated with 10µM Y27632 for 1h and then treated with 100µM SNAP for 1h. Inhibition of ROCK reduced neurite retraction induced by SNAP (14% of cells lacking neurites in comparison to 79% when cells were treated with SNAP only). Y27632 also slightly reduced the level of cells lacking neurites when

compared to untreated cells (4% and 16% of cells, respectively), but this differences was not statistically significant (Fig. 34).

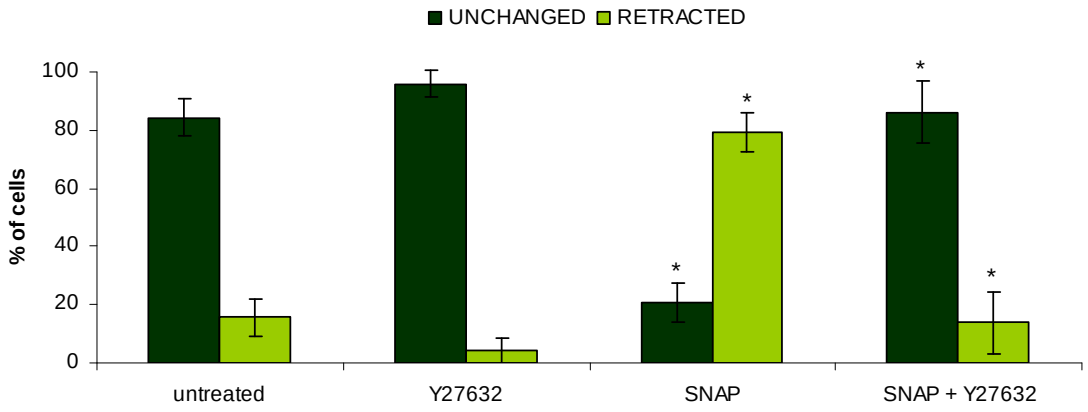

Fig. 34. Inhibition of ROCK abolishes neurite retraction of N2a neuroblastoma cells induced by SNAP. N2a neuroblastoma cells were grown on coverslips coated with poly-L-lysine and laminin, were left untreated, or were treated with 100µM SNAP for 1h, with 10µM Y27632 for 1h, or with 10µM Y27632 for 1h followed by treatment with 100µM SNAP for 1h, as indicated, fixed, and stained for tubulin. The morphology of cells was quantified by counting cells with neurites exceeding one cell diameter in length. SNAP induced neurite retractionFor quantitative analysis, 200 cells in each of 2 independent experiments were scored. Error bars represent standard deviations. Inhibition of ROCK reduced the level of neurite retraction induced by SNAP. Asterisks indicate that the values for cells treated with SNAP were significantly different from corresponding values of untreated and the values from cells treated with Y27632 followed by SNAP were significantly different from corresponding values of cells treated with SNAP only (*, $p<0.05$).

Myosin inhibition prevents axon retraction induced by NO

For further analysis of involvement of acto-myosin contractility in axon retraction induced by NO, I tested the effect of myosin inhibition by blebbistatin. Pretreatment of wild-type DRG neurons with 100µM blebbistatin for 15min reduced the level of neurons retracting in response to calcimycin (5% compared to 29% in case of cells treated with calcimycin only). The amount of cells showing hallmarks of collapse was not affected by addition of blebbistatin prior to calcimycin (Fig. 35).

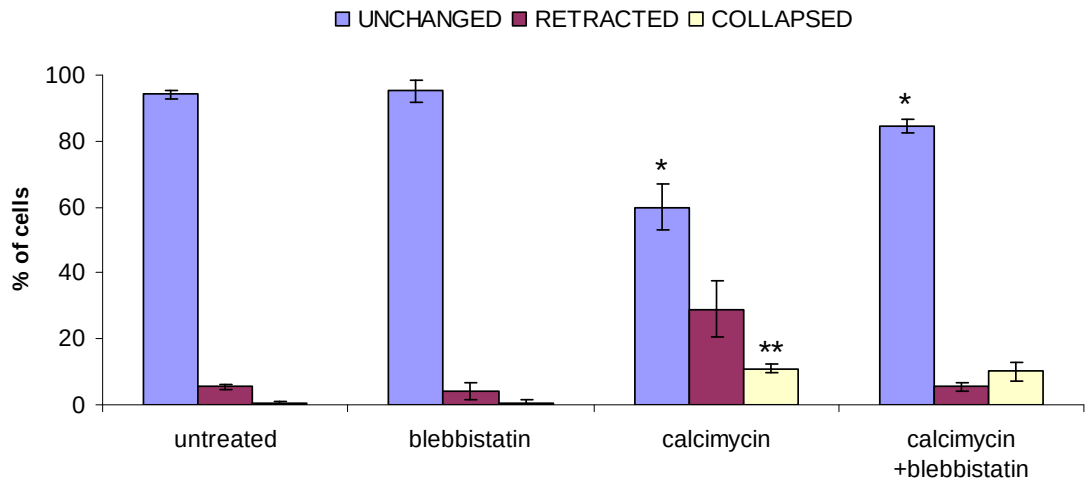

Fig. 35. Inhibition of myosin prevents axon retraction induced by calcimycin in wild-type DRG neurons. DRG neurons from wild-type mice were grown on coverslips coated with poly-L-lysine and laminin, were left untreated, or were treated with 100µM blebbistatin for 15min, with 10µM calcimycin for 15min, or with 100µM blebbistatin for 15min followed by 10µM calcimycin for 15min, as indicated, fixed with 4% PFA, stained for tubulin and analyzed by confocal microscopy. For quantitative analysis, approximately 100 cells in each of 2 independent experiments were assessed for microtubule configuration, which was classified as unchanged, or retracted or collapsed. Calcimycin induced axon retraction and axon collapse. Inhibition of myosin by blebbistatin prevented axon retraction induced by calcimycin. Error bars represent standard deviations. Asterisks indicate that the values for cells treated with blebbistatin followed by calcimycin were significantly different from corresponding values of neurons treated with calcimycin only and the values for cells treated with calcimycin only were significantly different from corresponding values of untreated neurons (*, $p<0.05$, and **, $p<0.01$).

Additional evidence supporting the role of myosin in axon retraction induced by calcimycin was obtained in experiments done in N2a neuroblastoma cells. These cells express a high level of nNOS in addition to MAP1B (Stroissnigg et al., 2007). Activation of nNOS by calcimycin significantly increased the number of cells lacking neurites (Stroissnigg et al., 2007) and resulted in an approximately 2-fold increase in S-nitrosylated LC1 compared to the level from untreated cells (Stroissnigg et al., 2007). Inhibition of nNOS in these cells by NPA resulted in a 2-fold reduction of the level of S-nitrosylated LC1, as compared to untreated cells (Stroissnigg et al., 2007). To investigate the potential role of myosin in calcimycin-induced neurite retraction in N2a cells I cultured them as described before and treated with 100µM blebbistatin for 15min prior to treatment with 10µM calcimycin for 1h, fixed and stained for tubulin. Inhibition of blebbistatin reduced the level of cells lacking neurites to 22% from 50% when cells were treated with calcimycin only (Fig. 36).

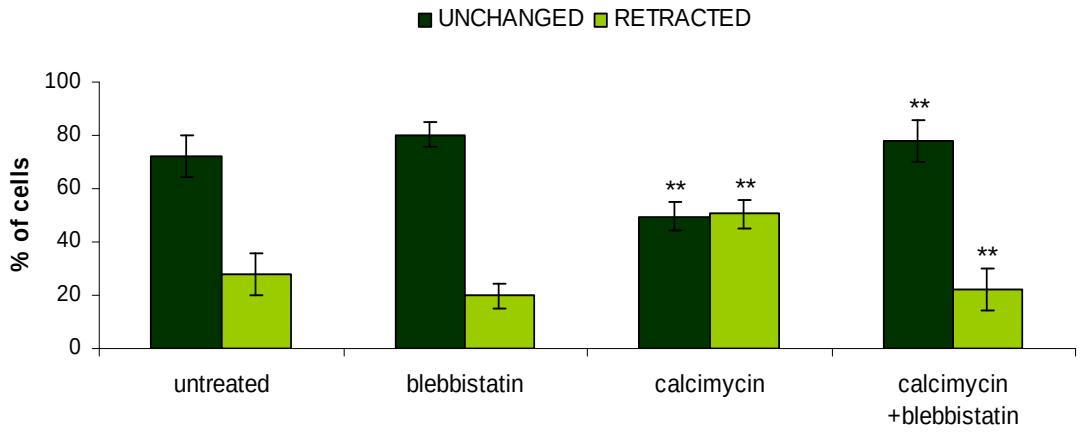

Fig. 36. Inhibition of myosin abolishes neurite retraction of N2a neuroblastoma cells induced by calcimycin. N2a neuroblastoma cells were grown on coverslips coated with poly-L-lysine and laminin, were left untreated, or were treated with 10µM calcimycin for 1h, with 10µM blebbistatin for 1h, or with 10µM blebbistatin for 1h followed by treatment with 10µM calcimycin for 1h, as indicated, fixed with 4% PFA, and stained for tubulin. The morphology of cells was quantified by counting cells with neurites exceeding one cell diameter in length. Inhibition of myosin partially abolished calcimycin-induced neurite retraction. For quantitative analysis, 200 cells in each of 5 independent experiments were scored. Error bars represent standard deviations. Asterisks indicate that the values for cells treated with calcimycin were significantly different from corresponding values of untreated cells and values for cells treated with blebbistatin followed by calcimycin were significantly different from corresponding values of neurons treated with calcimycin only (**, $p<0.001$).

Subsequently, involvement of myosin in axon retraction induced by SNAP was analyzed. In wild-type DRG neurons, inhibition of myosin by addition of 100µM blebbistatin for 15min prior to treatment with 100µM SNAP abolished axon retraction almost completely (6% in comparison to 30% when cells were treated with SNAP only; Fig. 37).

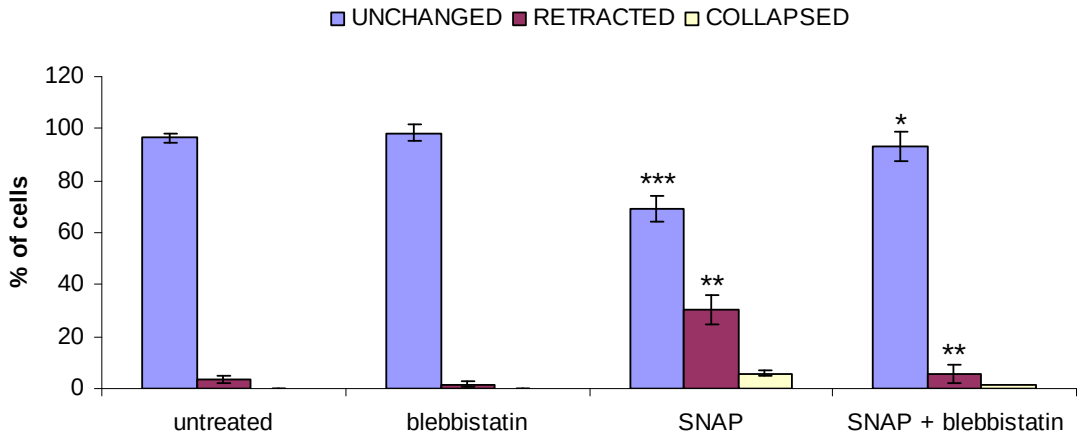

Fig. 37. Inhibition of myosin prevents axon retraction induced by SNAP in wild-type DRG neurons. DRG neurons from wild-type mice were grown on coverslips coated with poly-L-lysine and laminin, were left untreated, or were treated with 100µM blebbistatin for 15min, with

100µM SNAP for 1h, or with 100µM blebbistatin for 15min followed by 100µM SNAP for 1h, as indicated, fixed with 4% PFA, stained for tubulin and analyzed by confocal microscopy. For quantitative analysis, approximately 100 cells in each of 3 independent experiments were assessed for microtubule configuration, which was classified as unchanged, or retracted or collapsed. SNAP-induced axon retraction and inhibition of myosin by blebbistatin prevented axon retraction induced by SNAP. Error bars represent standard deviations. Asterisks indicate that the values for cells treated with SNAP were significantly different from corresponding values of untreated neurons and the values for cells treated with blebbistatin followed SNAP were significantly different from corresponding values of neurons treated with SNAP only (*, $p<0.05$, **, $p<0.005$, and **, $p<0.001$).

Finally, involvement of myosin in SNAP-stimulated neurite retraction of N2a neuroblastoma cells was determined. The number of cells with neurites exceeding one cell diameter in length was increased when blebbistatin was added before SNAP treatment (86% of cells with neurites in contrast to 21% when treated with SNAP only; Fig. 38).

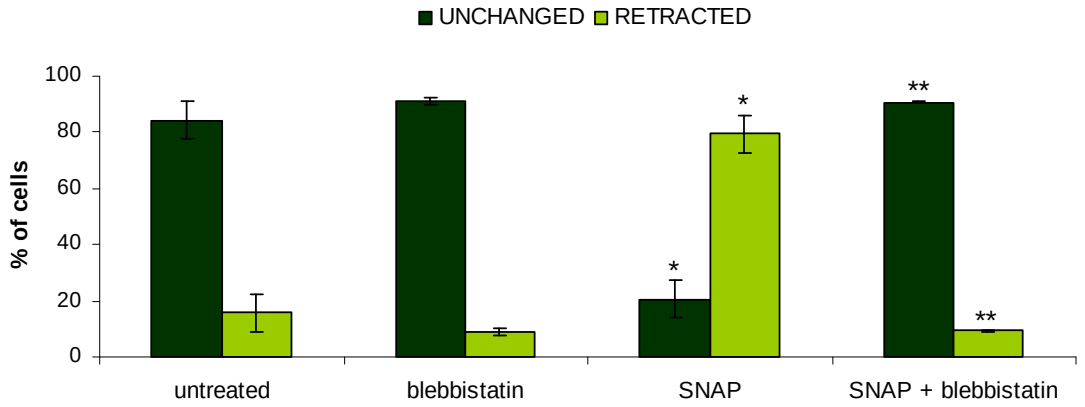

Fig. 38. Inhibition of myosin abolished neurite retraction of N2a neuroblastoma cells induced by SNAP. N2a neuroblastoma were cells grown on coverslips coated with poly-L-lysine and laminin, were left untreated, or were treated with 100µM blebbistatin for 15min, 100µM SNAP for 1h, or with 100µM blebbistatin for 15min followed by 100µM SNAP for 1h, as indicated, fixed with 4% PFA, and stained for tubulin. The morphology of cells was quantified by counting cells with neurites exceeding one cell diameter in length. Inhibition of myosin partially abolished calcimycin-induced neurite retraction. For quantitative analysis, 200 cells in each of 2 independent experiments were scored. Error bars represent standard deviations. Asterisks indicate that the values for cells treated with SNAP were significantly different from corresponding values of untreated cells and the values for cells treated with blebbistatin and SNAP were significantly different from corresponding values of neurons treated with SNAP only (*, $p<0.05$ and **, $p<0.005$).

These results demonstrated that ROCK and myosin are necessary for axon retraction induced by NO, but did not clarify if acto-myosin forces are enhanced in response to NO. It is known that myosin II activity is stimulated by phosphorylation of MRLC at Ser19 and Thr18 (Somlyo and Somlyo, 2003). Monophosphorylation of MRLC at Ser19

(phospho-MRLC) increases its ATPase activity and the stability of myosin II filaments. Phosphorylation both at Ser19 and Thr18 (di-phospho-MRLC) further increases the activity of myosin II and stabilizes its filaments. It was shown that LPA-enhanced intracellular tension involves the Rho/ROCK pathway and the diphosphorylation of MRLC (Mizutani et al., 2006). Thus, I decided to study levels of monophosphorylation and diphosphorylation of MRLC in response to SNAP and LPA treatment in N2a neuroblastoma cells.

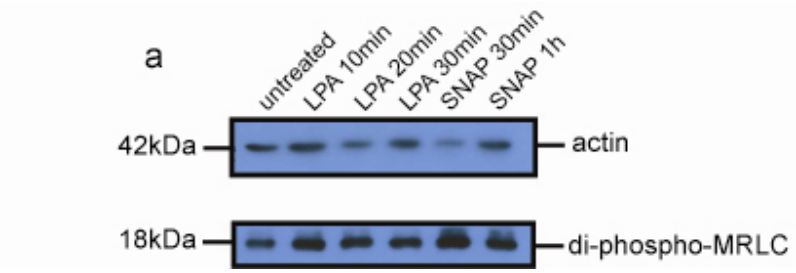

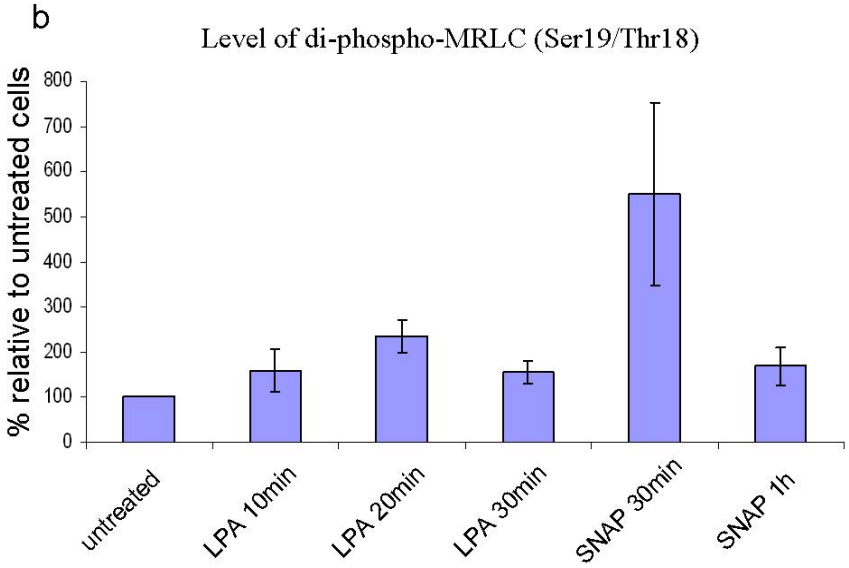

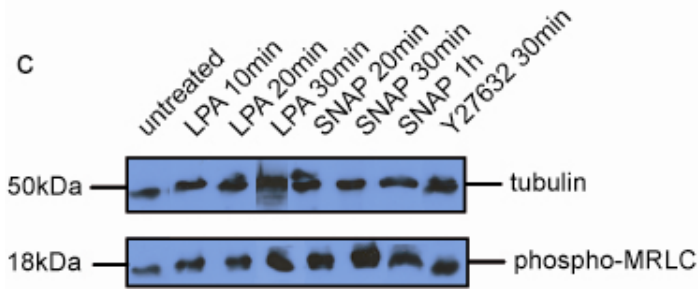

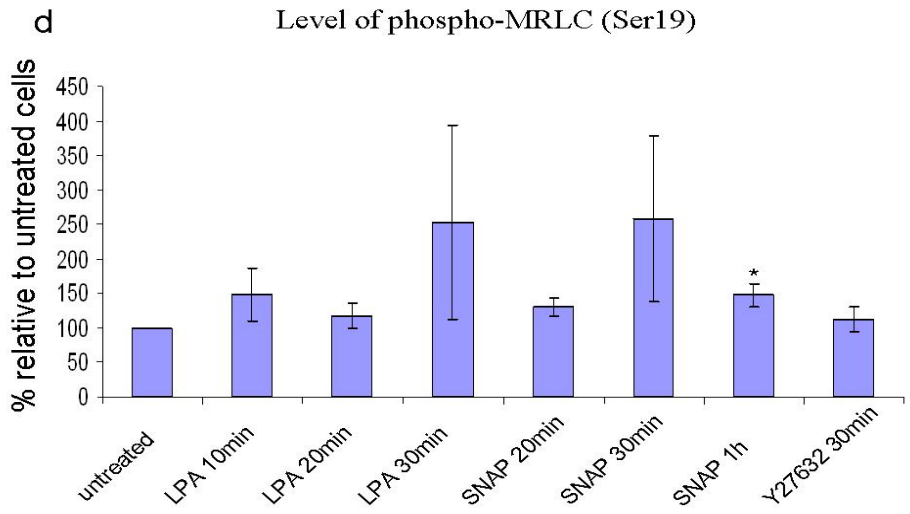

Fig. 39. NO- and LPA-induced axon retraction involves activation of myosin. N2a cells were grown on 6cm plates, and either were left untreated, or treated with 10µM LPA, with 100µM SNAP, or with 10µM Y27632, as indicated. Cell lysates were fractioned by SDS-PAGE and analyzed by immunoblotting using anti-Ser19/Thr18 (di-phospho-MRLC) and anti-Ser19 (phospho-MRLC) antibodies. Bands were quantified using the Quanti Scan 3 software. For quantitative analysis, blots from 2 or 3 independent experiments were scored. In each treatment the values show levels of phosphorylation at Ser 19/Thr18 (a) or at Ser19 (b) normalized to actin (a) or tubulin b) which were used as a loading control. Error bars represent standard deviations. Asterisks indicate that the level of phospho-myosin LC2 from lysates of cells treated with roscovitine was significantly different from corresponding value of untreated cells (*, $p<0.05$).

I observed increased levels of both mono- (Ser19) and diphosphorylation (Ser19/Thr18) of MRLC after treatment with LPA or SNAP. Enhanced diphosphorylation of MRLC was observed after application of LPA for 20min (236% of values from untreated cells) and 100µM SNAP for 30min (550% of values from untreated cells), but differences were not statistically significant. The highest levels of monophosphorylation of MRLC were found after treatment of N2a cells with 10µM LPA for 10min and for 30min (149% and 238% of values from untreated cells, respectively), and after treatment with 100µM SNAP for 30min and for 1h (259% and 153% of values from untreated cells, respectively), but only in case of treatment with 100µM SNAP for 1h increase was statistically significant. Treatment with Y27632 which inhibits ROCK and potentially phosphorylation of MRLC, as a downstream effector of Rho/ROCK pathway, did not reduce level of monophosphorylation of MRLC (119% of values from untreated cells) (Fig. 39).

Increased levels of cAMP partially attenuate axon retraction induced by calcimycin and SNAP

Several experiments *in vivo* and *in vitro* showed that cAMP and cGMP regulate growth cone navigation and axonal outgrowth. For example, the ratio of cAMP/cGMP determines the response of neurons to netrin-1. A high ratio of cAMP/cGMP stimulated increase in the level of intracellular Ca^{2+} and induced an attractive response of the growth cone to netrin-1, whereas a low ratio reduced the level of intracellular Ca^{2+} and lead to a repulsive response of the growth cone to netrin-1 (Nishiyama et al., 2003). Moreover, it was shown in cultured embryonic *Xenopus* spinal neurons that at the normal resting level of $[Ca^{2+}]_i$ small local Ca^{2+}signals activated calcineurin and induced repulsive responses of the growth cone, which could be switched by cAMP elevation to attractive responses (Wen et al., 2004).

To examine if stimulation of cAMP can influence axon retraction induced by NO, prior to treatment with calcimycin and SNAP wild-type DRG neurons were treated with dibutryl-cAMP or forskolin, which stimulates production of cAMP.

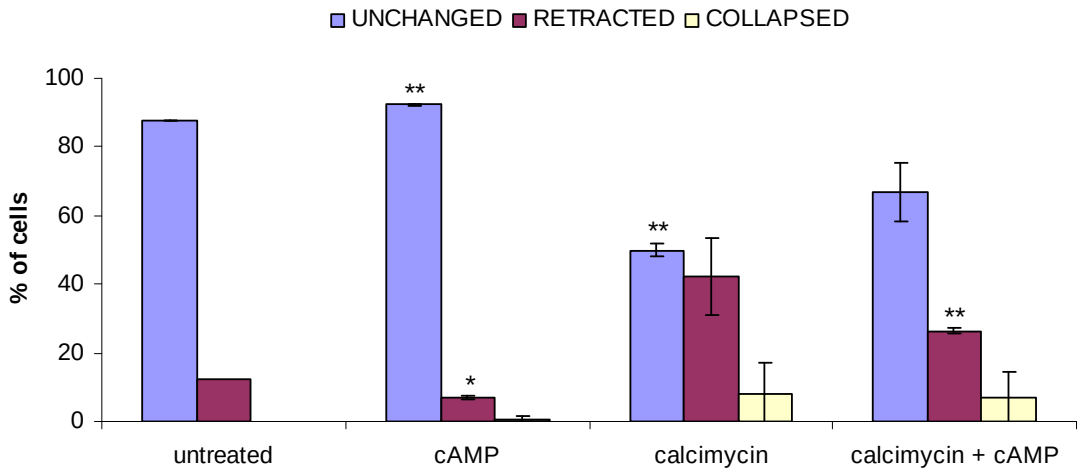

Fig. 40. Addition of cAMP partially abolishes retraction of axons induced by calcimycin in wild-type DRG neurons. DRG neurons from wild-type mice were grown on coverslips coated with poly-L-lysine and laminin, were left untreated, or were treated with 1µM dibutryl-cAMP for 1h, with 1µM calcimycin for 15min, or with 1µM dibutryl-cAMP for 1h followed by 1µM calcimycin for 15min, as indicated, fixed with 4% PFA, stained for tubulin and analyzed by confocal microscopy. For quantitative analysis, approximately 100 cells in each of 2 independent experiments were assessed for microtubule configuration, which was classified as unchanged, retracted, or collapsed. Error bars represent standard deviations. Asterisks indicate that the values for cells treated with calcimycin or with dibutryl-cAMP were significantly different from corresponding values of untreated cells and the values for cells treated with dibutryl-cAMP followed by calcimycin were significantly different from corresponding values of cells treated with calcimycin only (*, $p<0.05$, and **, $p<0.01$).

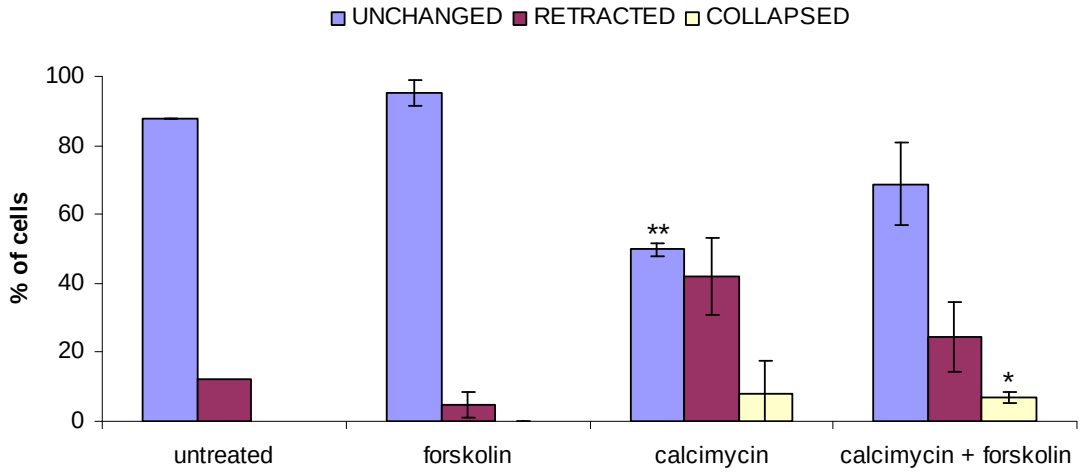

Fig. 41. Addition of forskolin partially abolishes retraction of axons induced by calcimycin in wild-type DRG neurons. DRG neurons from wild-type mice were grown on coverslips coated with poly-L-lysine and laminin, were left untreated, or were treated with 20µM forskolin for 3h, with 1µM calcimycin for 15min, or with 20µM forskolin for 3h followed by 1µM calcimycin for 15min, as indicated, fixed with 4% PFA, stained for tubulin and analyzed by confocal microscopy. For quantitative analysis, approximately 100 cells in each of 2 independent experiments were assessed for microtubule configuration, which was classified as unchanged, retracted or collapsed. Error bars represent standard deviations. Asterisks indicate that the values for cells treated with calcimycin were significantly different from corresponding values of untreated cells and the values for cells treated with forskolin followed by calcimycin were significantly different from corresponding values of neurons treated with calcimycin only (*, $p<0.05$, and **$p<0.005$).

Addition of 1µM dibutryl-cAMP prior treatment with calcimycin reduced the values of neurons showing retraction hallmarks to 26% in comparison to 42% when cells were treated with calcimycin only (Fig. 40). Application of dibutryl-cAMP did not prevent axon collapse when compare to calcimycin treatment only (Fig. 40). Pretreatment of neurons with 20µM forskolin for 3h also partially abolished axon retraction induced by calcimycin (24% in comparison to 42% when cells were treated with calcimycin only) and did not influence axon collapse; Fig. 41).

Similarly, wild-type DRG neurons were treated with 1µM dibutryl-cAMP for 1h prior to application of SNAP, which partially reduced the number of neurons showing retraction hallmarks induced by SNAP (17% compared to 38% in case of treatment with SNAP only; Fig. 42). Finally, 20µM forskolin reduced by a factor of 2 the number of neurons showing retraction hallmarks in wild-type DRG neurons when compared to cells treated with SNAP only (Fig. 43). Forskolin on its own also slightly reduced the number of cells displaying axon retraction in comparison to untreated cells.

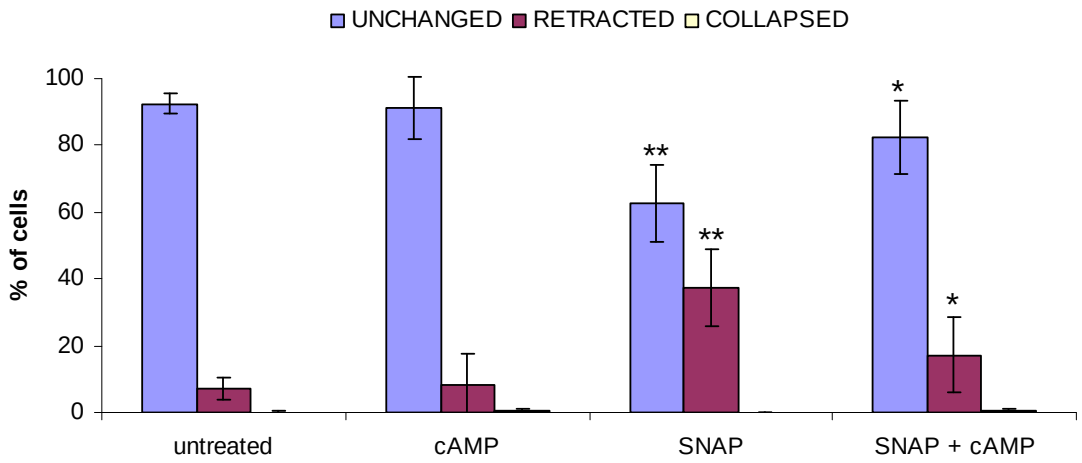

Fig. 42. Addition of cAMP partially abolishes retraction of axons induced by SNAP in wild-type DRG neurons. DRG neurons from wild-type mice were grown on coverslips coated with poly-L-lysine and laminin, were left untreated, or were treated with 1µM dibutryl-cAMP for 1h, with 100µM SNAP for 1h, or with 1µM dibutryl-cAMP for 1h followed by 100µM SNAP for 1h, as indicated, fixed with 4% PFA, stained for tubulin and analyzed by confocal microscopy. For quantitative analysis, approximately 100 cells in each of 4 independent experiments were assessed for microtubule configuration, which was classified as unchanged, retracted or collapsed. Error bars represent standard deviations. Asterisks indicate that the values for cells treated with SNAP were significantly different from corresponding values of untreated neurons and the values for cells treated with dibutryl-cAMP followed by SNAP were significantly different from corresponding values of neurons treated with SNAP only (*, $p<0.05$, and **, $p<0.005$).

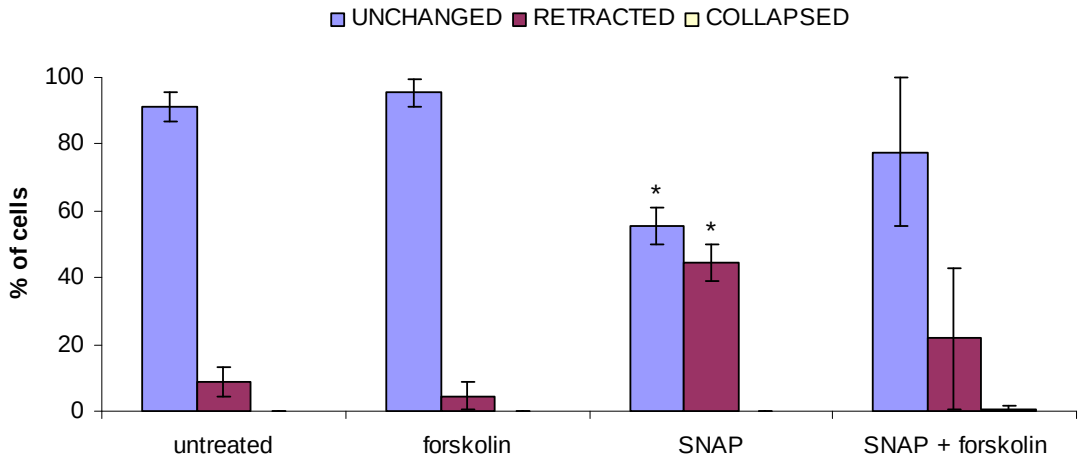

Fig. 43. Addition of forskolin partially abolishes retraction of axons induced by SNAP in wild-type DRG neurons. DRG neurons from wild-type mice were grown on coverslips coated with poly-L-lysine and laminin, were left untreated, or were treated with 20µM forskolin for 3h, with 100µM SNAP for 1h, or with 20µM forskolin for 3h followed by 100µM SNAP for 1h, as indicated, fixed with 4% PFA, stained for tubulin and analyzed by confocal microscopy. For quantitative analysis, approximately 100 cells in each of 2 independent experiments were assessed for microtubule configuration, which was classified as unchanged, retracted or collapsed. Error bars represent standard deviations. Asterisks indicate that the values for cells treated with SNAP were significantly different from corresponding values of untreated neurons (*, $p<0.05$).

NO-induced axon retraction does not involve microtubule depolymerization

It seems that upon SNAP, calcimycin or LPA treatment microtubules retreat backwards to accommodate the shortening of the axon and thus adapt a coiled and bundled configuration, but it can not be excluded that they depolymerise during this reconfiguration. Thus, to examine if depolymerization takes plays during NO-induced axon retraction, wild-type and MAP1B-/- DRG neurons were grown on poly-L-lysine and laminin coated coverslips. After 24h, 3nM or 100nM (not shown) taxol which stabilizes microtubules against disassembly was applied to neurons for 30min prior SNAP treatment, then cells were fixed and stained for tubulin. Pretreatment of neurons with taxol did not abolishe retraction induced by SNAP and axons retracted even more dramatically than axons from cells treated with SNAP only (64% of wild-type DRG neurons retracted in comparison to 37% in case of treatment with SNAP only; Fig. 44). It seems that even such a low concentrations of taxol alters morphology of axons, which retract showing all typical hallmarks as retraction bulb, sinusoidal bundles of microtubules and trailing remnant (approximately 68% of wild-type DRG neurons treated with 3nM retracted; Fig. 44). Interestingly MAP1B-/- DRG neurons also displayed axon retraction in response to taxol, 74% and 80% of cells retracted when treated with taxol only or with SNAP and taxol, respectively (in comparison about 12% of cells treated with SNAP only showed retraction morphology; Fig. 45).

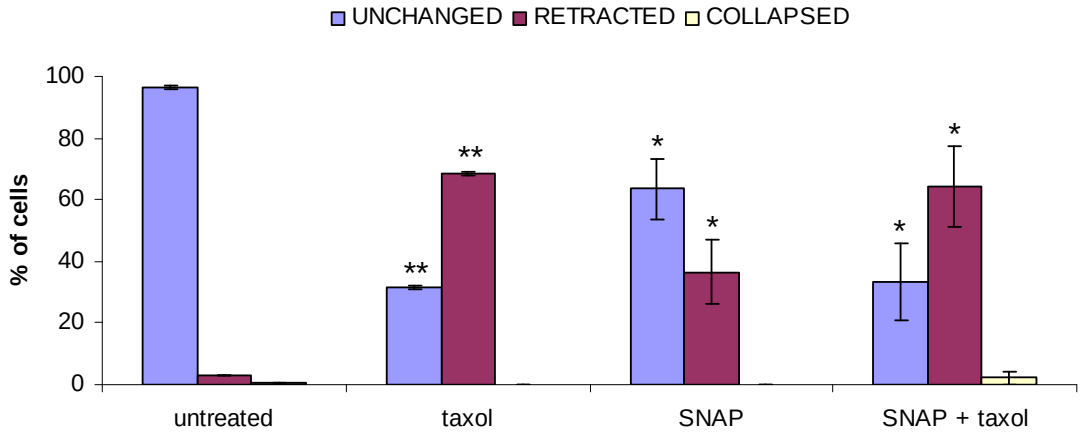

Fig. 44. Treatment with taxol does not abolish SNAP-induced neurite retraction in wild-type neurons and induces axon retraction on its own. DRG neurons from wild-type mice were grown on coverslips coated with poly-L-lysine and laminin, were left untreated, or were treated with 3nM taxol for 30min, with 100µM SNAP for 1h, or with 3nM taxol for 30min followed by 100µM SNAP for 1h, as indicated, fixed with 4% PFA, stained for tubulin and

analyzed by confocal microscopy. For quantitative analysis, approximately 100 cells in each of 3 independent experiments were assessed for microtubule configuration, which was classified as unchanged, retracted or collapsed. Error bars represent standard deviations. Asterisks indicate that the values for cells treated with SNAP, with taxol or with taxol followed by SNAP treatment were significantly different from corresponding values of untreated neurons (*, $p<0.01$, and **, $p<0.001$).

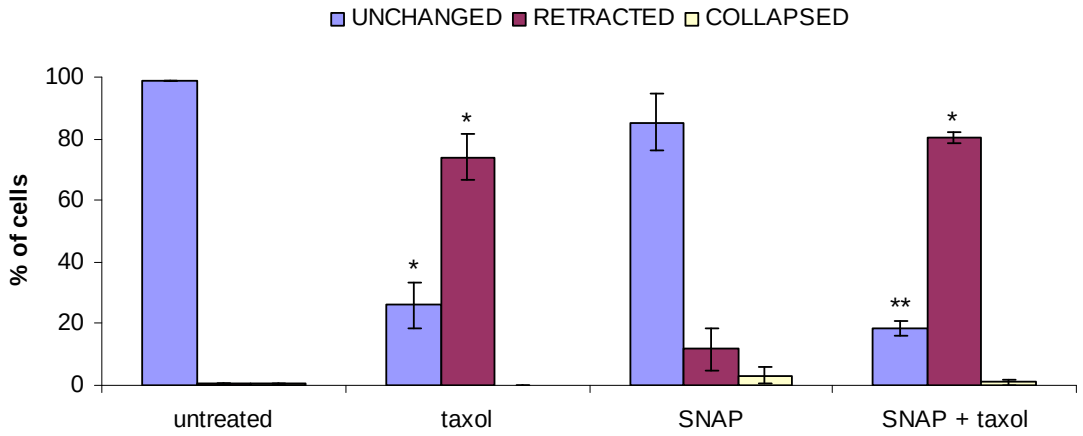

Fig. 45. Taxol induces axon retraction also in MAP1B-/- DRG neurons. DRG neurons from MAP1B-/- mice were grown on coverslips coated with poly-L-lysine and laminin, were left untreated, or were treated with 3nM taxol for 30min, with 100µM SNAP for 1h, or with 3nM taxol for 30min followed by 100µM SNAP for 1h, as indicated, fixed with 4% PFA, stained for tubulin and analyzed by confocal microscopy. For quantitative analysis, close to 100 cells in each of 3 independent experiments were assessed for microtubule configuration, which was classified as unchanged, retracted or collapsed. Error bars represent standard deviations. Asterisks indicate that the values for cells treated with SNAP or with taxol followed by SNAP were significantly different from corresponding values of untreated neurons (*, $p<0.005$, and **, $p<0.001$).

I also examined the influence of microtubule stabilization on calcimycin-induced retraction of neurites in N2a cells. Cells were grown on poly-L-lysine and laminin coated coverslips as described before and then treated with 3nM taxol for 30min, with 10µM calcimycin for 1h, or with 3nM taxol and followed by 10µM calcimycin for 1h, or were left untreated, then fixed and stained for tubulin. As in DRG neurons taxol did not prevent retraction of neurites and combination of calcimycin and taxol increased number of cells lacking long neurites (81% of cells lacking neurites when compared to 43% when treated with calcimycin only). About 52% of N2a cells treated with taxol lacked neurites or had neurites shorter than one cell diameter in length when compared to 27% when cells were left untreated (Fig. 46).

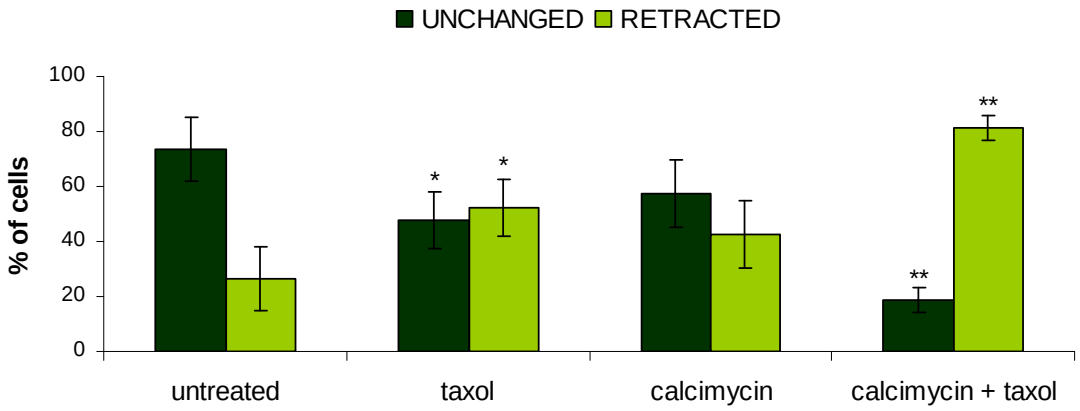

Fig. 46. Treatment with taxol does not abolish calcimycin-induced neurite retraction in N2a cells. N2a neuroblastoma cells grown on coverslips coated with poly-L-lysine and laminin, subsequently cells were left untreated or were treated with 3nM taxol for 30min, with 10µM calcimycin for 15min, or with 3nM taxol for 30min followed by 10µM calcimycin for 15min, as indicated, fixed with 4% PFA, and stained for tubulin. The morphology of cells was quantified by counting cells with neurites exceeding one cell diameter in length. Inhibition of myosin partially abolished calcimycin induced neurite retraction. For quantitative analysis, 200 cells in each of 4 independent experiments were scored. Error bars represent standard deviations. Asterisks indicate that the values for cells treated with calcimycin or with taxol followed by calcimycin treatment were significantly different from corresponding values of untreated cells (*, $p<0.05$, and **, $p<0.001$).

LPA-induced axon retraction does not involve microtubule depolymerization

Axons retracting in response to LPA treatment show a similar phenotype to axons retracting in response to calcimycin or SNAP. Moreover, retraction in response to all three cues is MAP1B-dependent and involves ROCK and myosin. Thus, it was interesting to investigate if LPA-induced retraction, like SNAP-induced retraction, does not involve depolymerization of microtubules.

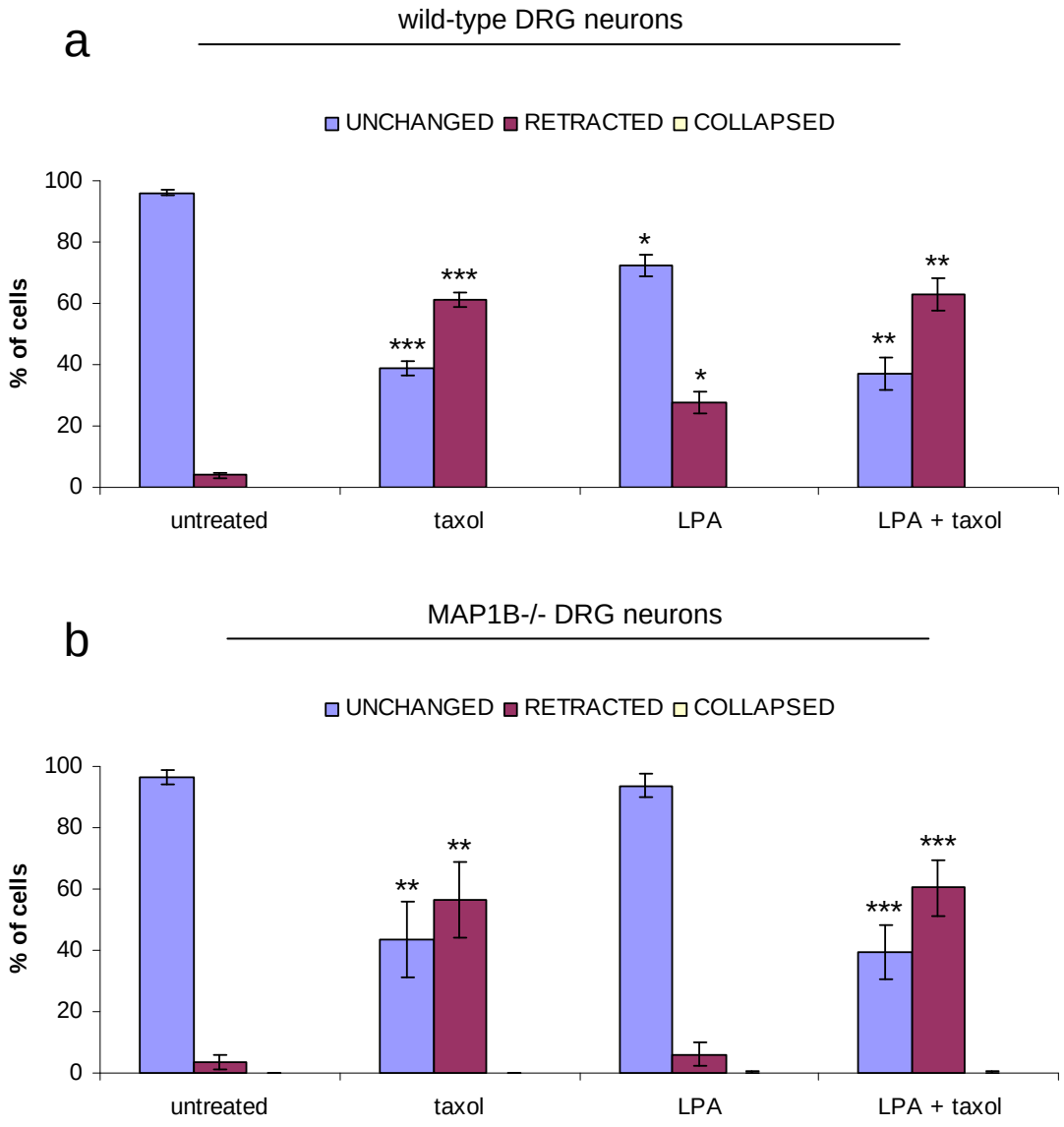

Fig. 47. Treatment with taxol does not prevent LPA-induced neurite retraction of wild-type neurons. DRG neurons from wild-type (a) and MAP1B-/- (b) mice were grown on coverslips coated with poly-L-lysine and laminin, were left untreated, or were treated with 3nM taxol for 30min, with 10µM LPA for 30min, or with 3nM taxol for 30min followed by 10µM LPA for 30min, as indicated, fixed with 4% PFA, stained for tubulin and analyzed by confocal microscopy. (a, b), for quantitative analysis, approximately 100 cells in each of 3 (a) or 4 (b) independent experiments were assessed for microtubule configuration which was classified as unchanged, retracted or collapsed. Error bars represent standard deviations. Asterisks indicate that the values for cells treated with LPA, with taxol or with taxol followed by LPA were significantly different from corresponding values of untreated neurons (*, $p<0.05$, **, $p<0.005$, and ***, $p<0.001$).

Similarly to previous experiments, both wild-type and MAP1B-/- DRG neurons were treated with 3nM taxol for 30min prior to treatment with 10µM LPA for 30min. As expected, stabilization of microtubules by taxol did not prevent retraction induced by LPA (63% of wild-type DRG neurons showed retraction hallmarks when compared to

28% when cells were treated with LPA only). About 60% of cells from MAP1B-/- DRG neurons displayed retraction hallmarks when treated with taxol and LPA, in contrast to 6% when treated with LPA only (Fig. 47).

Likewise, I examined if LPA-induced inhibition of neurites retraction in N2a neuroblastoma cells involves depolymerization of microtubules. Cells were grown as described before, treated with 3nM taxol for 30min prior to application of 10µM LPA for 30min, fixed and stained. Taxol did not prevent retraction induced by LPA in N2a cells, 90% of cells were lacking neurites when compared to 62% when cells were treated with LPA only (Fig. 48).

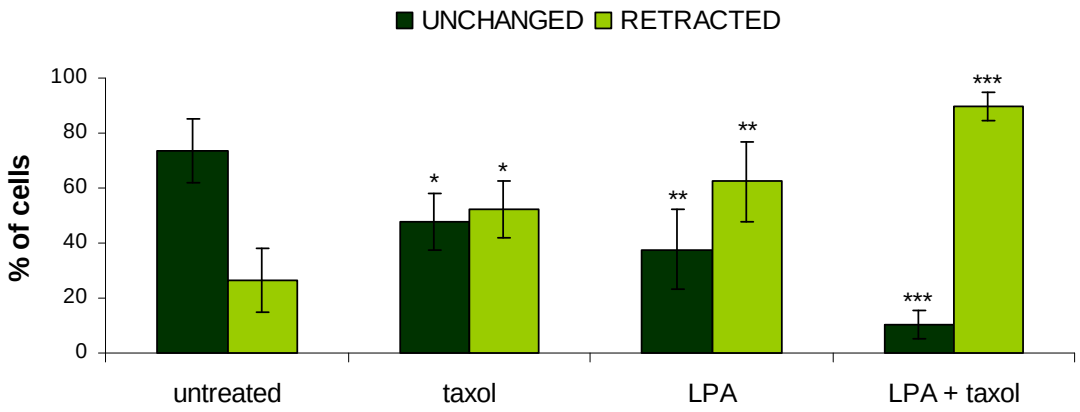

Fig. 48. Treatment with taxol does not abolish LPA-induced neurite retraction in N2a cells. N2a neuroblastoma cells were grown on coverslips coated with poly-L-lysine and lamini, were left untreated or were treated with 3nM taxol for 30min, with 10µM LPA for 30min, or with 3nM taxol for 30min followed by 10µM LPA for 30min, as indicated, fixed with 4%, and stained for tubulin. The morphology of cells was quantified by counting cells with neurites exceeding one cell diameter in length. For quantitative analysis, 200 cells from each of 4 independent experiments were scored. Error bars represent standard deviations. Asterisks indicate that the values for cells treated with LPA, with taxol, or with taxol followed by LPA were significantly different from corresponding values of untreated cells (*, $p<0.05$, **, $p<0.01$, and **, $p<0.001$).

Mechanism of taxol-induced axon retraction

Taxol-induced axon retraction is acto-myosin independent

As retraction induced by taxol shows all hallmarks characteristic for axons retracting in response to SNAP, calcimycin or LPA, it was interesting to investigate if it too is ROCK- and myosin-dependent.

To determine involvement of acto-myosin contractility in taxol-induced retraction, both wild-type and MAP1B-/- DRG neurons were cultured as described before, treated with

Y27632 or blebbistatin prior to application of taxol, fixed, stained and analysed by microscopy.

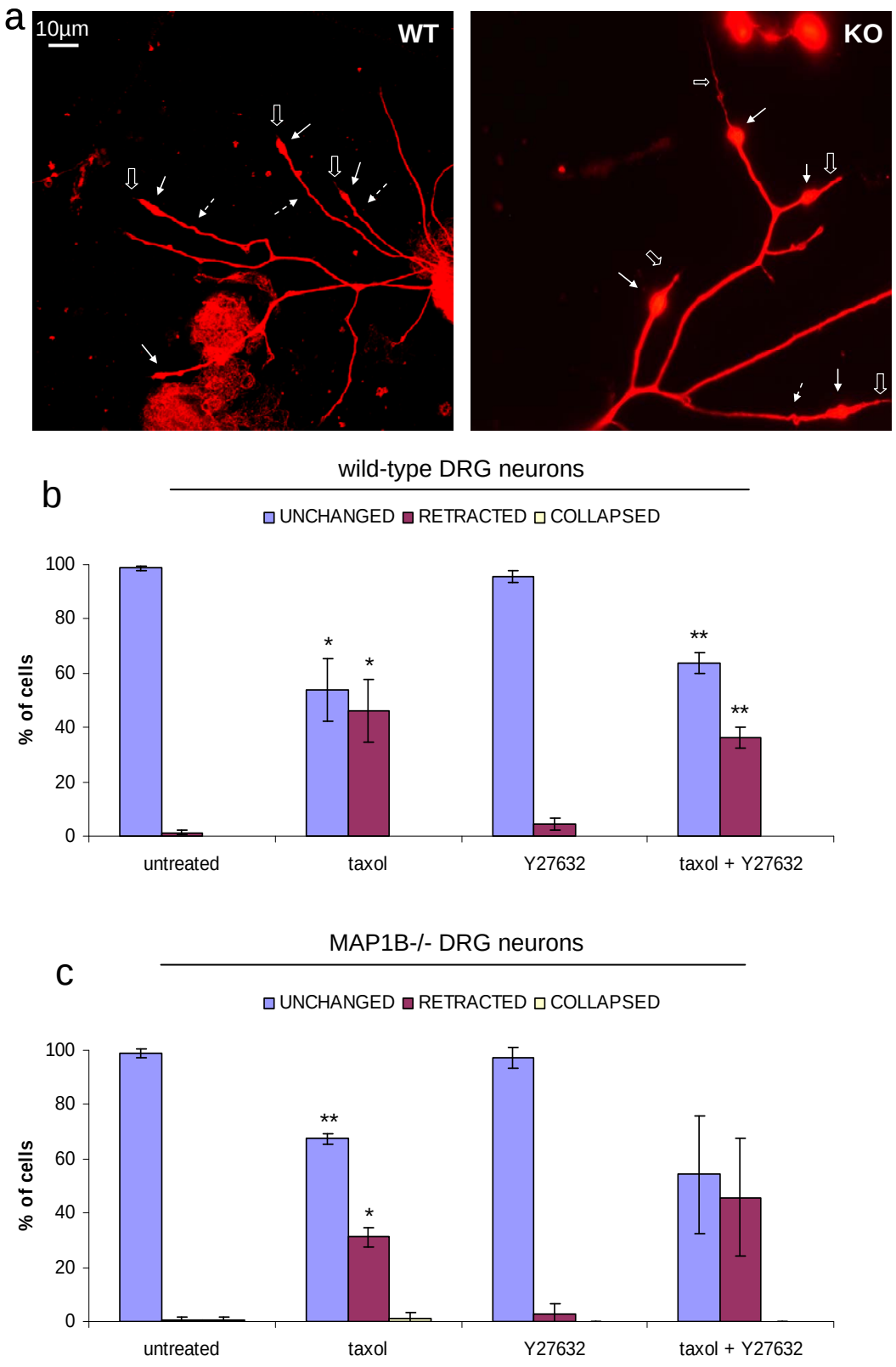

Fig. 49. Inhibition of ROCK does not prevent taxol-induced neurite retraction in wild-type and MAP1B-/- DRG neurons. DRG neurons from wild-type and MAP1B-/- mice were grown

on coverslips coated with poly-L-lysine and laminin, were left untreated, or were treated with 3nM taxol for 30min, with 10µM Y27632 for 1h, or with 10µM Y27632 for 1h followed by 3nM taxol for 30min, fixed with 4% PFA, as indicated, stained for tubulin and analyzed by confocal microscopy. (a), representative micrographs of axon retraction (sinusoidal microtubules (interrupted arrow), retraction bulb (filled arrows), trailing remnant (open arrow) of wild-type (WT) and MAP1B-/- (KO) DRG neurons in response to taxol. (b, c), for quantitative analysis, approximately 100 cells in each of 3 (b) or 2 (c) independent experiments were assessed for microtubule configuration which was classified as unchanged, retracted or collapsed. Error bars represent standard deviations. In case of WT DRG neurons treated with Y27632 followed by taxol standard deviations are high since only two independent experiments were done, which brought two significantly different results. Asterisks indicate that the values for cells treated with taxol or with Y27632 followed by taxol were significantly different from corresponding values of untreated neurons (*, $p<0.01$, and **, $p<0.005$).

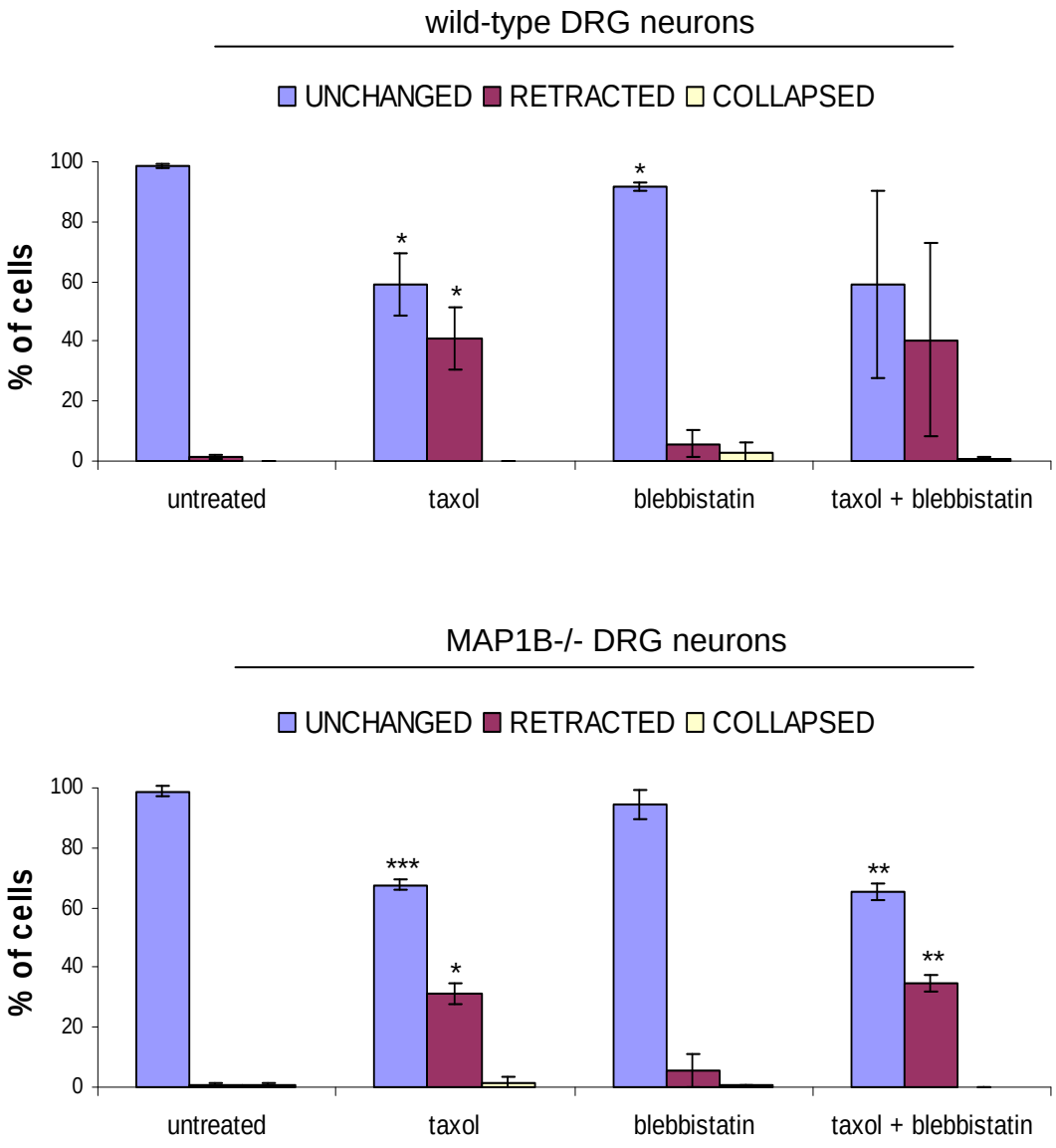

Fig. 50. Inhibition of myosin does not prevent taxol-induced neurite retraction in wild-type and MAP1B-/- DRG neurons. DRG neurons from wild-type (a) and MAP1B-/- (b) mice were grown on coverslips coated with poly-L-lysine and laminin, were left untreated, or were treated with 3nM taxol for 30min, with 100µM blebbistatin for 15min, or with 100µM blebbistatin for 15min followed by 3nM taxol for 30min, as indicated, fixed with 4% PFA, stained for tubulin

and analyzed by confocal microscopy. (a, b), for quantitative analysis, approximately 100 cells in each of 2 independent experiments were assessed for microtubule configuration, which was classified as unchanged, retracted or collapsed. Error bars represent standard deviations. Asterisks indicate that the values for cells treated with taxol, or with blebbistatin, or with blebbistatin followed by taxol were significantly different from corresponding values of untreated neurons (*, $p<0.05$,**, $p<0.01$, and **, $p<0.005$).

Inhibition of neither ROCK nor myosin did prevent retraction induced by taxol regardless of the presence of MAP1B (Fig. 49). When wild-type DRG neurons were treated with Y27632 prior to taxol application, 37% of cells showed retracted morphology in comparison to 46% when cells were treated with taxol only. This difference was statistically not significant and standard deviations were high, what is due to the two significantly different results obtained from only two independent experiments. Thus, additional experiments should be done to get a reliable results. Approximately 40% neurons retracted in response to taxol even if myosin was inhibited (41% of retracted cells in case of taxol only; Fig. 50).
About 46% and 35% of MAP1B-/- neurons displayed retraction morphology when treated with Y27632 and blebbistatin prior taxol treatment, respectively, compared to 31% when cells were treated with taxol only (Fig. 49, Fig. 50).

Taxol-induced retraction does not involve NOS activation

I also examined the potential involvement of NOSs in retraction induced by taxol. Wild-type DRG neurons were grown as described before, 300µM L-NAME was applied for 1h prior to treatment with 3nM taxol for 30min. Inhibition of NOSs with L-NAME reduced slightly the number of cells showing retraction hallmarks – about 68% of cells retracted when compared to 82% when cells were treated with taxol only, but this difference was not statistically significant (Fig. 51). Thus, it seems NOSs are not involved in axon retraction induced by taxol.

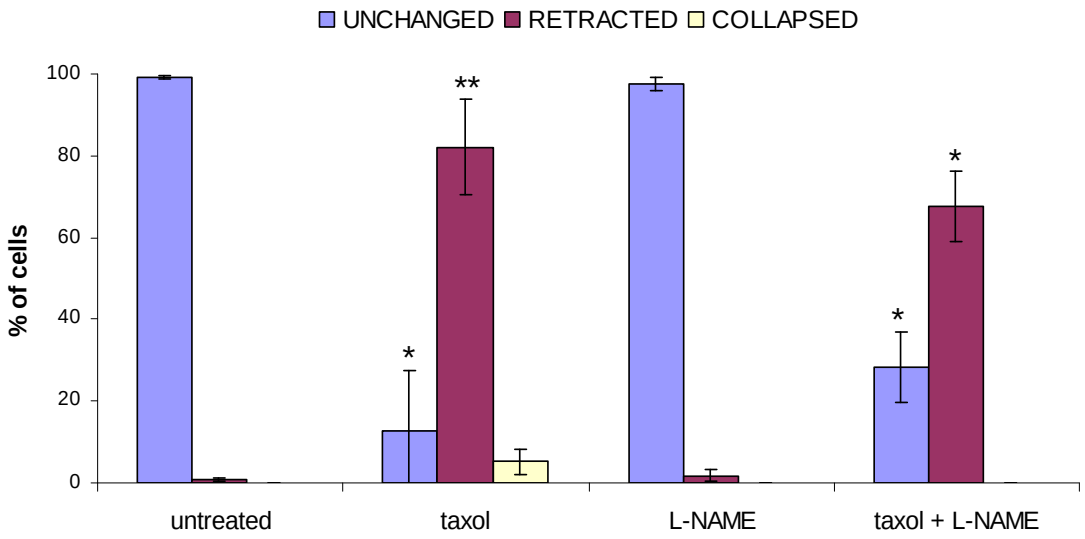

Fig. 51. Inhibition of NOS did not prevent taxol-induced neurite retraction in wild-type DRG neurons. DRG neurons from wild-type mice were grown on coverslips coated with poly-L-lysine and laminin, were left untreated, or were treated with 3nM taxol for 30min, 300µM L-NAME for 1h, or with 300µM L-NAME for 1h followed by 3nM taxol for 30min, as indicated, fixed with 4% PFA, stained for tubulin and analyzed by confocal microscopy. For quantitative analysis, approximately 100 cells in each of 2 independent experiments were assessed for microtubule configuration which was classified as unchanged, retracted or collapsed. Error bars represent standard deviations. Asterisks indicate that the values for cells treated with taxol or with L-NAME followed by taxol were significantly different from corresponding values of untreated neurons (*, $p<0.05$, and **, $p<0.01$).

SNAP and LPA induce increased microtubule binding by full length MAP1B

We hypothesized that SNAP and LPA induce increased binding of MAP1B to microtubules, for example by S-nitrosylation of MAP1B by NO, resulting in enhanced microtubule stabilization and axon retraction. To examine the effect of SNAP and LPA on MAP1B microtubule binding ability I expressed myc-tagged full length MAP1B in PtK2 cells and determined its intracellular localization. As it was shown previously these cells express very low levels of endogenous MAP1B (Tögel et al., 1998) and the studies with ectopically expressed full length MAP1B should not be influenced by endogenous MAP1B (Tögel et al., 1998).

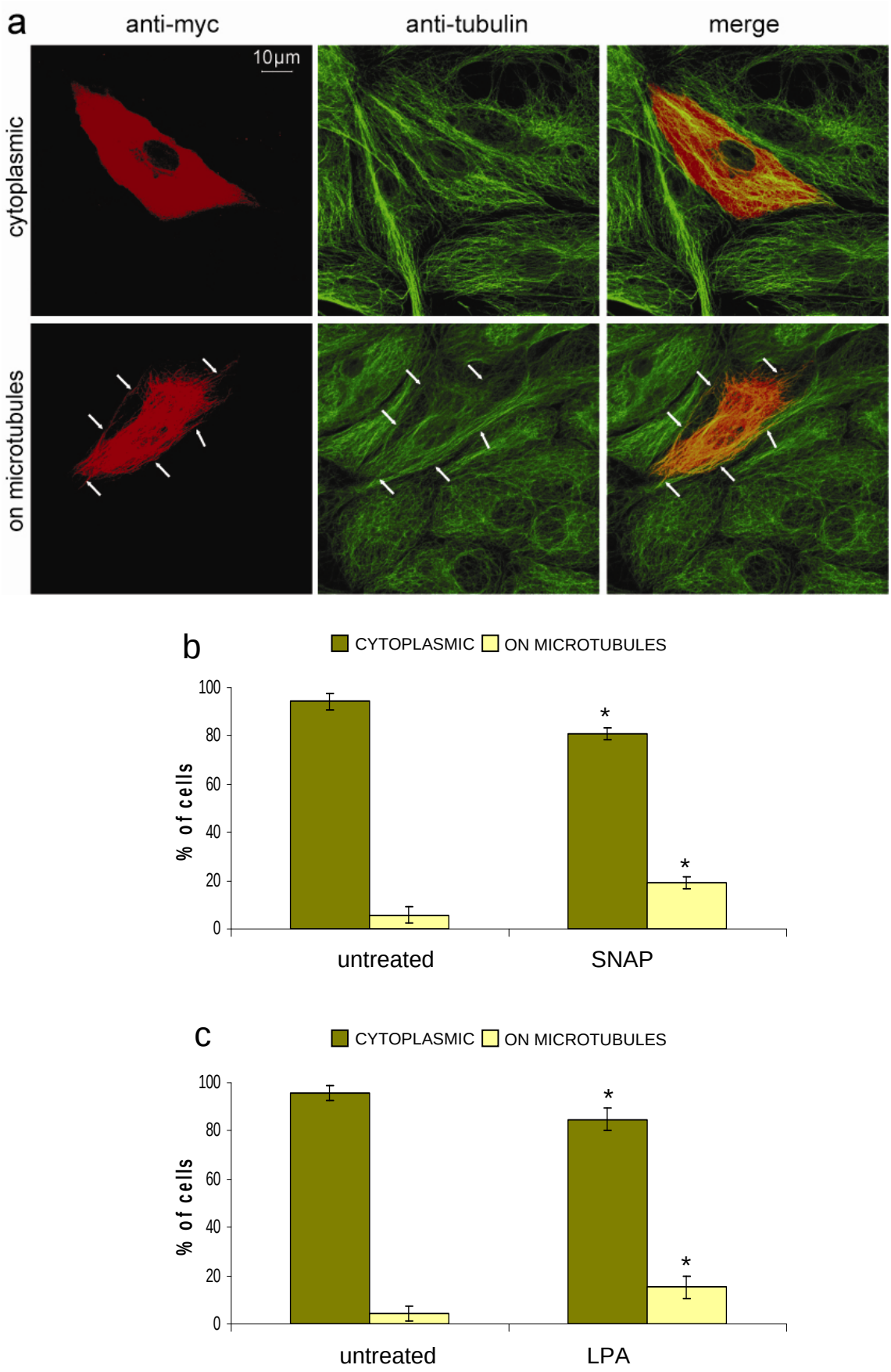

Fig. 52. Increased microtubule binding of MAP1B induced by treatment with SNAP or LPA. PtK2 cells were transiently transfected with constructs encoding myc-tagged FL MAP1B.

Before fixation, cells were left untreated or were treated with 100μM SNAP for 4h or with 100μM LPA for 2h, as indicated. Cells were scored for localization of the ectopically expressed protein in the cytoplasm, or on microtubules by double immunofluorescence microscopy using anti-tubulin antibodies and anti-myc (detection of MAP1B) antibodies. (a), representative micrographs of MAP1B localized in the cytoplasm (cytoplasmic) and associated with microtubules (on microtubules - white arrows). (b, c), for quantification, 200 cells in each of 3 independent transfections were assessed for microtubule binding of MAP1B. Error bars represent standard deviations. Asterisks indicate that the values for cells treated with SNAP or with LPA were significantly different from corresponding values of untreated neurons (*, $p<0.05$).

In most untreated cells MAP1B was found to be localized in the cytoplasm and only in 6% cells MAP1B was found to be bound to microtubules. In cells treated with the NO donor SNAP association of LC1 with microtubules increased (19% of SNAP treated cells showed MAP1B on microtubules), but no microtubule bundling was observed. LPA treatment also induced increase in microtubules binding of MAP1B (15% treated with LPA compared to 5% when cells were untreated; Fig. 52). These results support our theory that NO induced S-nitrosylation of MAP1B and LPA-treatment lead to increased microtubule interaction of full length MAP1B.

Increased microtubule dynamic in MAP1B -/- DRG neurons

For further determination if retraction of DRG neurons upon SNAP or LPA treatment involved stabilization of microtubules by MAP1B I decided to study the dynamic behaviour of the microtubule plus end-binding proteins, also called plus end-tracking proteins or +TIPs, in living cells. +TIPs bind to growing ends of microtubules. Since the growth rates of microtubules measured with +TIPs fused to green fluorescent protein (GFP) or with fluorescently labelled tubulin injected into the cells are similar, the GFP labelled +TIPs are a convenient tool to study microtubule dynamics (Stepanova et al., 2003).

For live imaging of microtubule growth dynamics I transfected adult wild-type and MAP1B-/- DRG neurons with constructs encoding end-binding protein 1 fused with GFP (EB1-GFP). After 48h, time-lapse microscopy was performed. Movements of EB1-GFP were monitored for 1min with 2s intervals (Fig. 53). EB1-GFP was found to bind to microtubule tips in all neuronal compartments (growth cones, axons), indicating that new microtubules are generated in all compartments. Most EB1-GFPs spots were moving in comet-like dashes in the same direction, from cell body to the cell periphery

(anterogradely). I observed only few dashes moving in opposite direction (retrogradely), and most of them were found within growth cone. In some cases EB1-GFP comets were pausing and/or oscillating, mainly in the growth cones. To determine dynamics of microtubule growth, four parameters were measured – the velocity, the distance, the life of EB1-GFP comets, and the stop frequency.

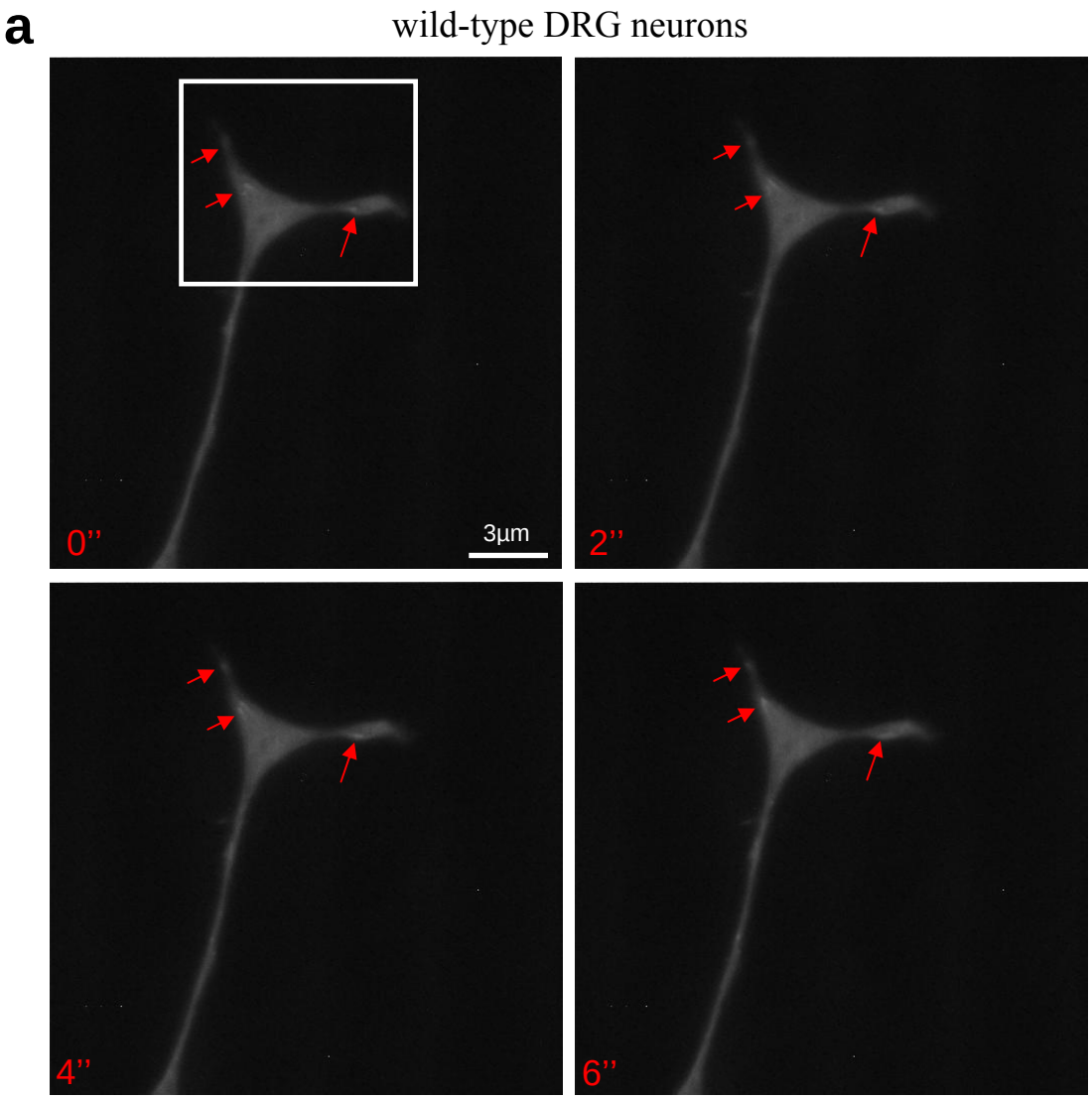

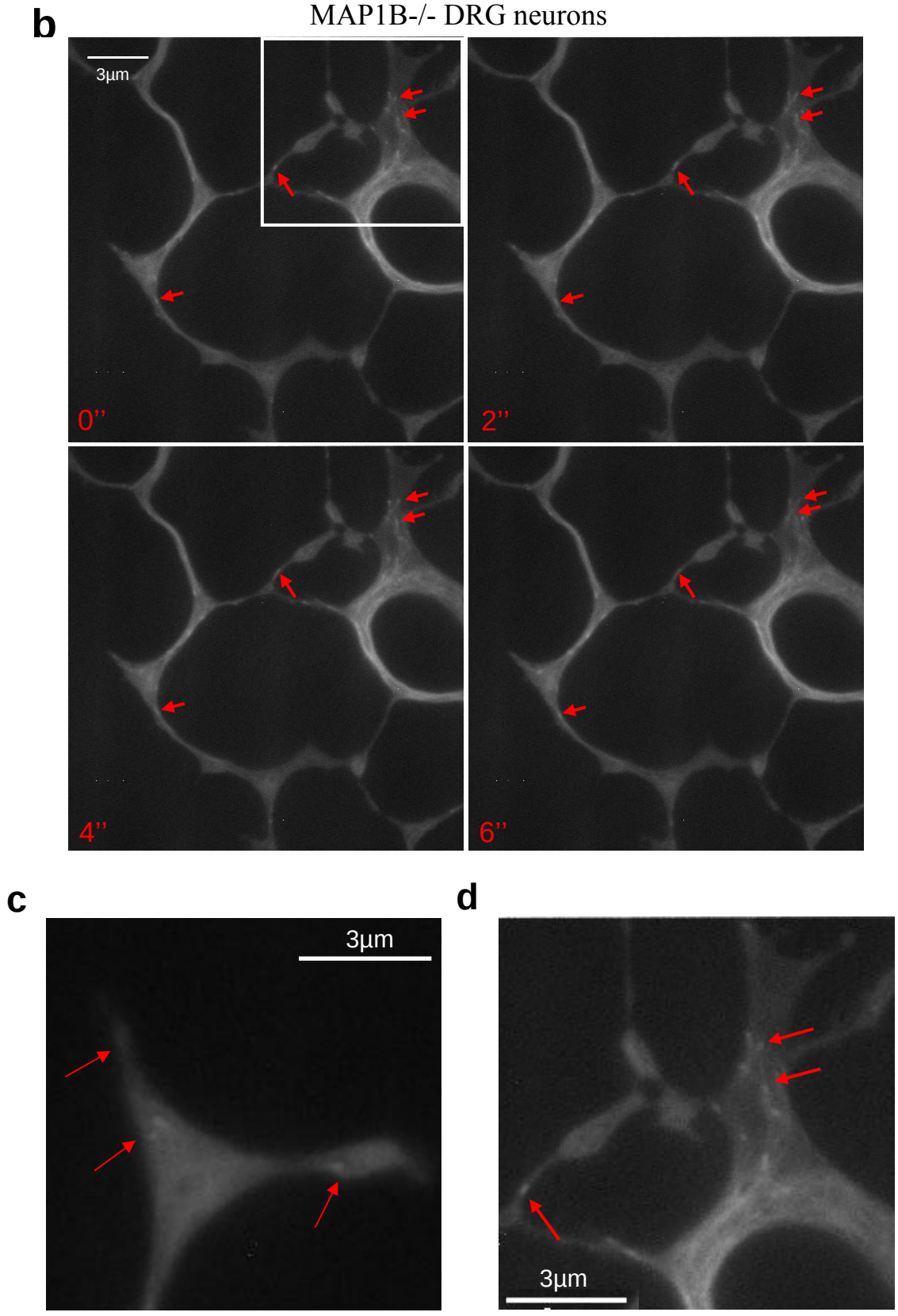

Fig. 53. EB1-GFP in wild-type and MAP1B-/- DRG neurons. DRG neurons from wild-type and MAP1B-/- mice were transfected with a construct encoding EB1-GFP, grown on coverslips coated with poly-L-lysine and laminin for 48h. Then microtubule dynamics were monitored with an inverted microscope equipped with fluorescence optics. Pictures were taken for 1min

every 2s. (a, b), representative stacks from videos (red arrows indicate EB1 comets). (c, d), higher magnification of area indicated by white boxes in pictures a, b. High expression of EB1-GFP in the neurons caused high fluorescence background. In the time-lapse movies comets were identified much easier than on the individual frames that are shown.

EB1-GFP dashes were moving faster in axons and growth cones of MAP1B-/- neurons than in wild-type neurons. The mean velocity of the dashes in axons of MAP1B-/- neurons was 0.067μm/sec, whereas in the wild-type neurons it was 0.052μm/sec. Similarly, in growth cones of MAP1B-/- DRG neurons the mean velocity of EB1-GFP comets was higher in comparison to comets from growth cones of wild-type DRG neurons (0.052μm/sec and 0.041μm/sec, respectively). In both cases differences in the velocity was statistically significant. Interestingly, the velocity of EB1-GFP dashes was significantly lower in growth cones than in axons of wild-type, as well as MAP1B-/- DRG neurons (Fig. 54).

The higher speed of comets in axons of MAP1B-/- neurons corresponded to a longer mean distance that the comets travelled. The mean lengths for the MAP1B-/- and wild-type dashes were 1.27μm and 0.97μm, respectively (the difference was statistically significant). In growth cones, EB1-GFP comets also showed the tendency to travel for longer distance in MAP1B-/- DRG neurons (1μm compared to 0.84 μm in growth cone of wild-type DRG neurons), but this difference was not significant (Fig. 55). Similarly to the mean velocity, the mean value of distance of EB1-GFP dashes was lower in the growth cones than in axons, in both wild-type and MAP1B-/- DRG neurons.

The time of comet life was longer in case of EB1-GFP comets moving in axons of MAP1B -/- DRG neurons (32.43sec compared to 28.83sec in wild-type DRG neurons). The difference was only 3.6sec, but it was statistically significant. Within the growth cones there was no significant difference between the time of comet life in wild-type and MAP1B-/- DRG neurons (30.27sec and 26.72 sec, respectively; Fig. 56).

I also measured how often EB1-GFP comets paused during polymerization of microtubules in respect to presence or absence of MAP1B. No difference in the stop frequency of comets between wild-type and MAP1B-/- DRG neurons was observed. In axons, the stop frequency was 0.092stops/sec in case of wild-type DRG neurons and 0.1stops/sec in case of MAPB-/- DRG neurons, whereas in growth cones it was 0.083stops/sec and 0.087stops/sec, respectively (Fig. 57). These results show that in the absence of MAP1B EB1-GFP comets move faster, for longer distances and their life time is longer, which according to literature indicates higher microtubule dynamics. The

differences are more robust in case of EB1-GFP dashes moving within axons than with those moving within growth cones.

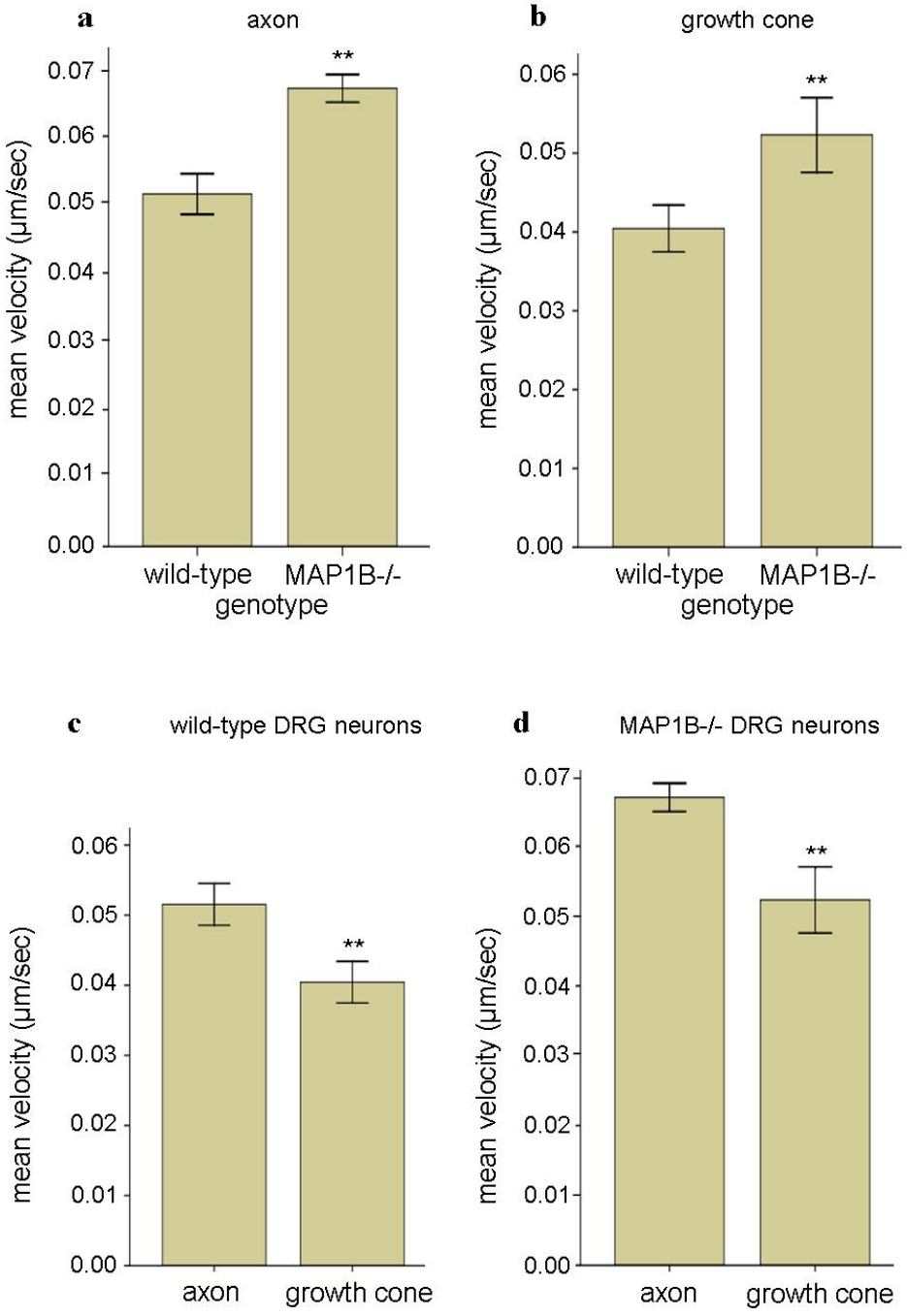

Fig. 54. Increased velocity of EB1-GFP comets in MAP1B-/- DRG neurons. DRG neurons from wild-type and MAP1B-/- mice were transfected with a construct encoding EB1-GFP, grown on coverslips coated with poly-L-lysine and laminin for 48h, and microtubule dynamics were monitored with an inverted microscope equipped with fluorescence optics. Pictures were taken for 1min every 2s. The velocity of EB1-GFP dashes within growth cones and axons was calculated with MetaMorph software. Observed comets for quantification, in axons, 120 (wild-type) and 338 (MAP1B-/-); in growth cones, 22 (wild-type) and 50 (MAP1B-/-) from 6 independent experiments. Error bars represent standard deviations. Asterisks indicate that the

values for MAP1B-/- cells were significantly different from corresponding values of wild-type neurons (**, p<0.001).

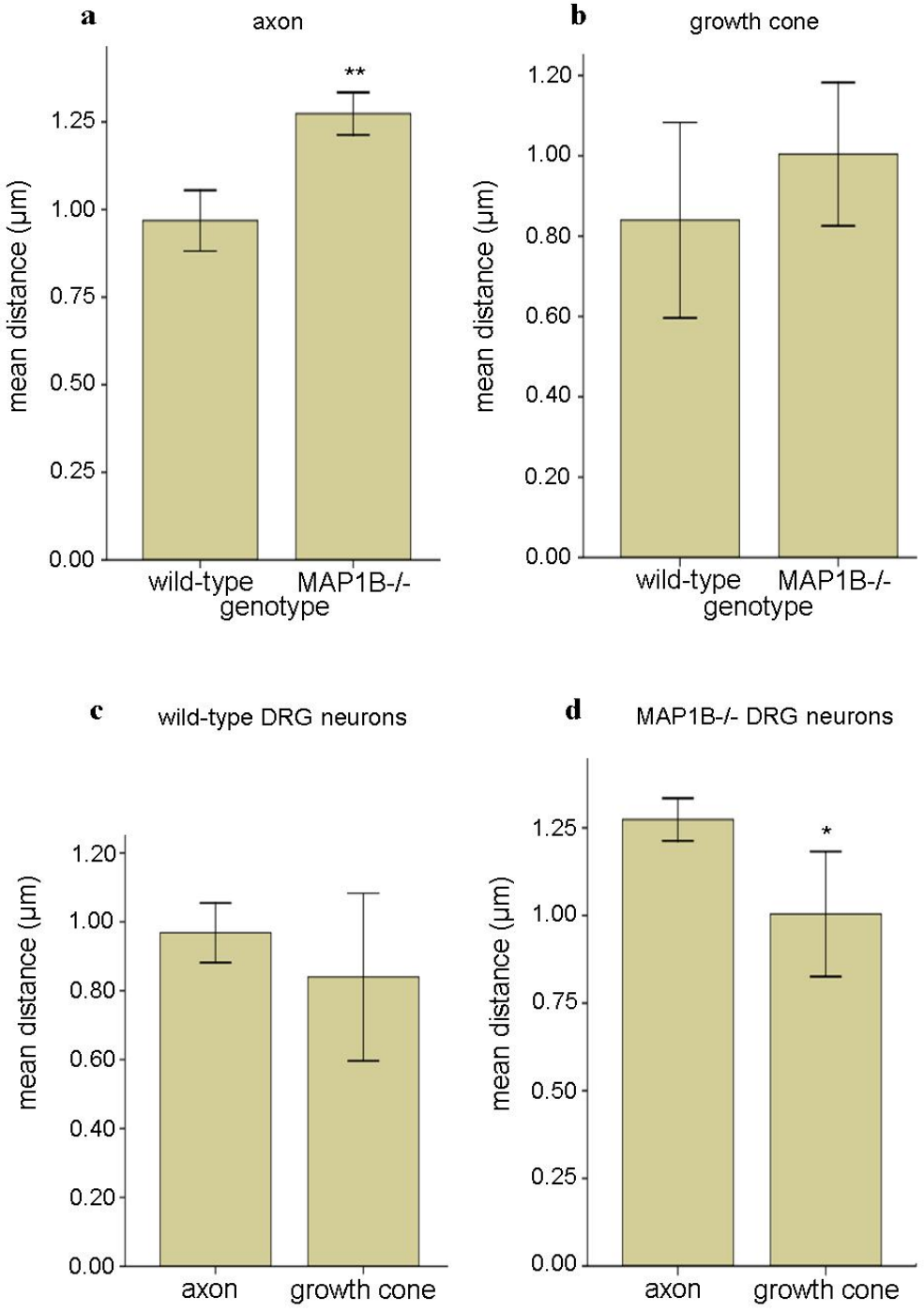

Fig. 55. Increased distance of EB1-GFP comets in MAP1B-/- DRG neurons. DRG neurons from wild-type and MAP1B-/- mice were transfected with a construct encoding EB1-GFP, grown on coverslips coated with poly-L-lysine and laminin for 48h, and microtubule dynamics were monitored with an inverted microscope equipped with fluorescence optics. Pictures were taken for 1min every 2s. The distance of EB1-GFP dashes within growth cones and axons was calculated with MetaMorph software. Observed comets for quantification, in axons, 120 (wild-type) and 338 (MAP1B-/-); in growth cones, 22 (wild-type) and 50 (MAP1B-/-) from 6 independent experiments. Error bars represent standard deviations. Asterisks indicate that the

values for MAP1B-/- cells were significantly different from corresponding values of wild-type neurons (*, $p<0.005$, and **, $p<0.001$).

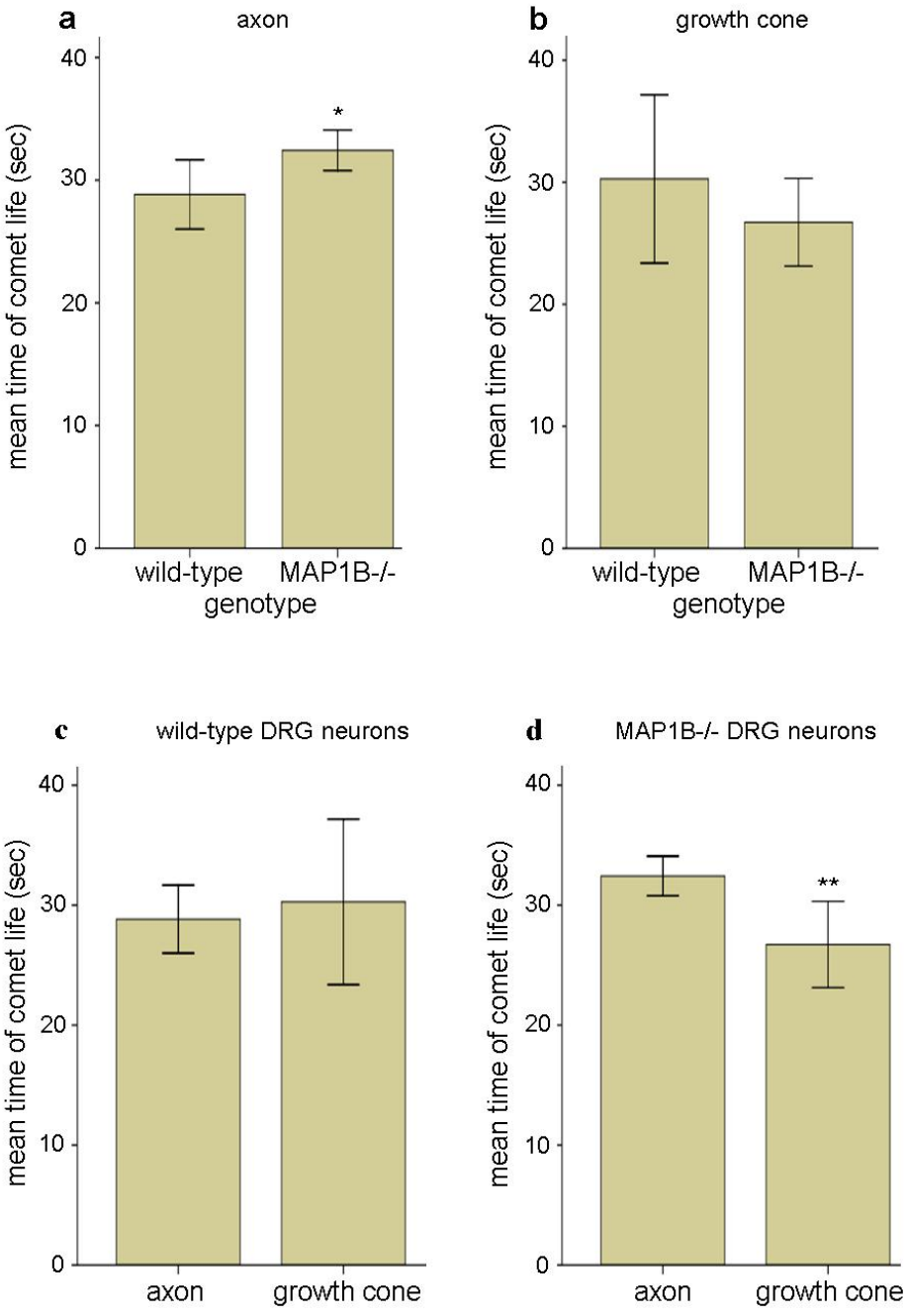

Fig. 56. Increased time of EB1-GFP comet life in MAP1B-/- DRG neurons. DRG neurons from wild-type and MAP1B-/- mice were transfected with a construct encoding EB1-GFP, grown on coverslips coated with poly-L-lysine and laminin for 48h, and microtubule dynamics were monitored with an inverted microscope equipped with fluorescence optics. Pictures were taken for 1min every 2s. The time of EB1-GFP dashes life within growth cones and axons was calculated with MetaMorph software. Observed comets for quantification, in axons, 120 (wild-type) and 338 (MAP1B-/-); in growth cones, 22 (wild-type) and 50 (MAP1B-/-) from 6 independent experiments. Error bars represent standard deviations. Asterisks indicate that the

values for MAP1B-/- cells were significantly different from corresponding values of wild-type neurons (*, $p<0.05$, and **, $p<0.01$).

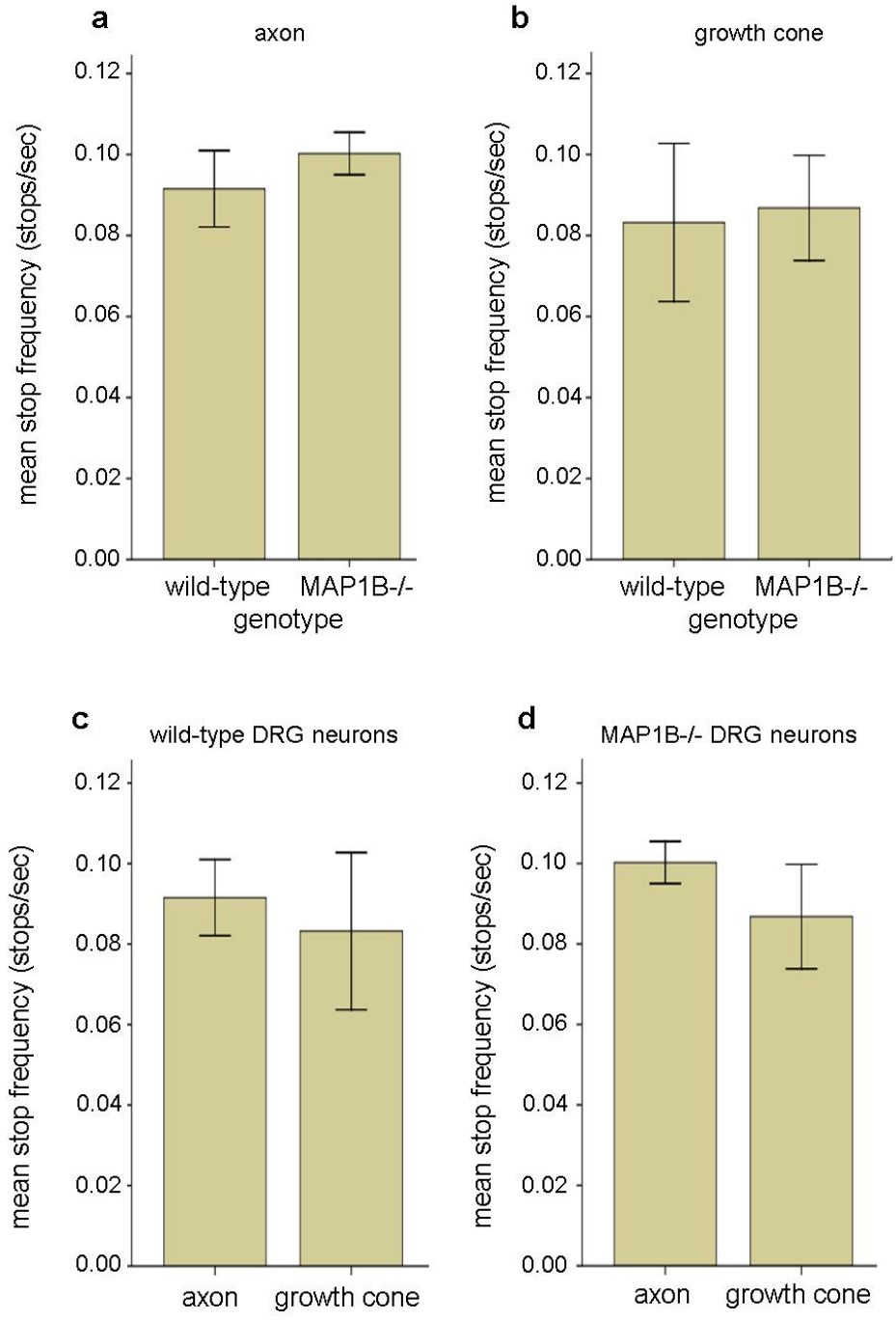

Fig. 57. The stop frequency is not altered in MAP1B-/- DRG neurons. DRG neurons from wild-type and MAP1B-/- mice were transfected with a construct encoding EB1-GFP, grown on coverslips coated with poly-L-lysine and laminin for 48h, and microtubule dynamics were monitored with an inverted microscope equipped with fluorescence optics. Pictures were taken for 1min every 2s. The stop frequency of EB1-GFP dashes within growth cones and axons was calculated with MetaMorph software. Observed comets for quantification, in axons, 120 (wild-type) and 338 (MAP1B-/-); in growth cones, 22 (wild-type) and 50 (MAP1B-/-) from 6 independent experiments. Error bars represent standard deviations.

One could expect that if MAP1B indeed stabilizes microtubules and decreases their dynamic, there should be an increase in the number of EB1-GFP dashes in MAP1B-/- neurons, since EB1-GFP binds to growing ends of microtubules and in MAP1B-/- neurons, according to our model, the number of dynamic growing microtubules should be higher. Thus, I analyzed the number of EB1-GFP comets per axon length and per growth cone area in both wild-type and MAP1B-/- DRG neurons transfected with construct encoding EB1-GFP. Indeed I found more dashes both in axons and growth cones of MAP1B-/- DRG neurons. In the axons of MAP1B-/- DRG neurons there were 0.204comets/µm, whereas in case of axons from wild-type DRG neurons there were 0.12comets/µm. In growth cones of MAP1B-/- DRG neurons there were 0.117comets/µm^2 compared to 0.025comets/µm^2 in growth cones of wild-type DRG neurons. In both cases differences were statistically significant (Fig. 58).

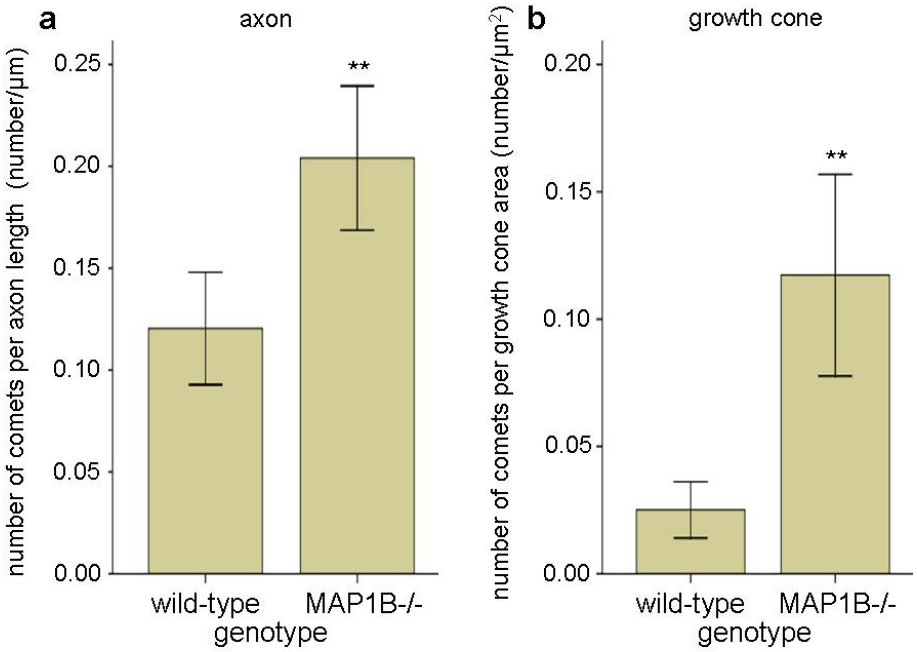

Fig. 58. Increased number of EB1-GFP comets in axons and growth cones of MAP1B -/- DRG neurons. DRG neurons from wild-type and MAP1B-/- mice were transfected with a construct encoding EB1-GFP, grown on coverslips coated with poly-L-lysine and laminin for 48h, and microtubule dynamics were monitored with an inverted microscope equipped with fluorescence optics. Pictures were taken for 1min every 2s. The number of EB1-GFP comets per axon length (number of comets/µm) and the number of EB1-GFP comets per growth cone area (number of comets/µm^2) were calculated with MetaMorph and ImageJ softwares. Observed comets for quantification, in axons, 192 (wild-type) and 248 (MAP1B-/-); in growth cones, 18 (wild-type) and 44 (MAP1B-/-) from 6 independent experiments were analysed. Error bars represent standard deviations. Asterisks indicate that the values for MAP1B-/- cells were significantly different from corresponding values of wild-type neurons (**, $p<0.001$).

To analyze if LPA has an influence on dynamic of microtubules I transfected adult wild-type and MAP1B-/- DRG neurons with constructs encoding EB1-GFP. After 48h, time-lapse microscopy was performed. Movements of EB1-GFP were monitored for 1min with 2s intervals. Then cells were treated with 10µM LPA and recording was continued for 30-50min. To determine dynamics of microtubule growth, again four parameters were measured – the velocity, the distance, the life of EB1-GFP comets and the stop frequency.

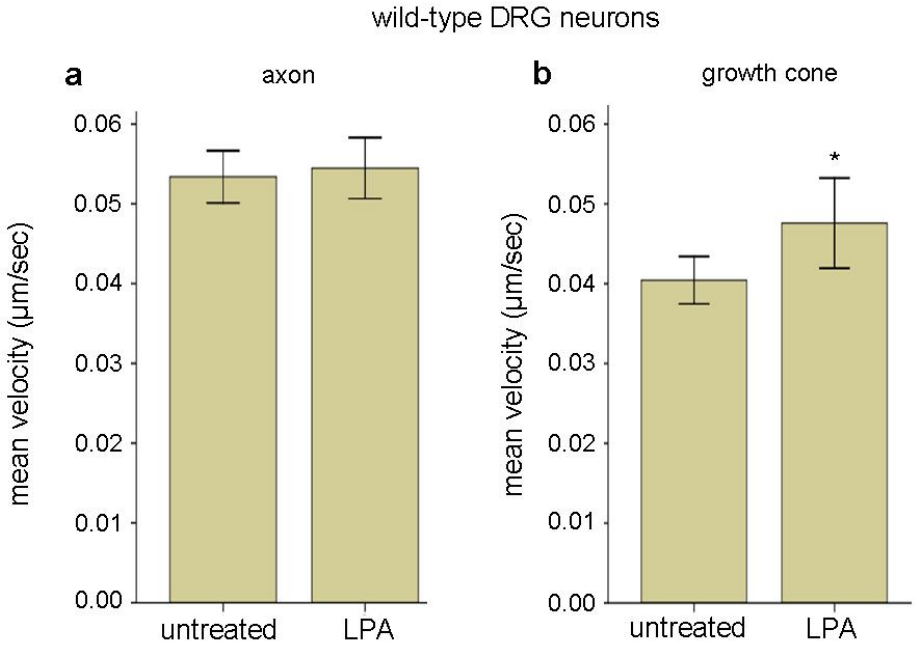

Fig. 59. LPA increases the velocity of EB1-GFP comets in growth cones of wild-type DRG neurons. DRG neurons from wild-type mice were transfected with a construct encoding EB1-GFP, grown on coverslips coated with poly-L-lysine and laminin for 48h, and microtubule dynamics were monitored with an inverted microscope equipped with fluorescence optics. Cells were treated with 10µM LPA and recording was continued for 30-50min. Pictures were taken for 1min every 2s. The velocity of EB1-GFP dashes within axons (a) and growth cones (b) was calculated with MetaMorph software. Observed comets for quantification, 95 (a) and 28 (b) from 4 independent experiments. In case of the untreated group the values came from videos taken before addition of LPA and previous experiments to obtain the same number of samples as in the LPA treated group. Error bars represent standard deviations. Asterisks indicate that the values for neurons treated with LPA were significantly different from corresponding values of untreated neurons (**, $p<0.05$).

In the growth cones of wild-type DRG neurons the velocity of EB1-GF dashes was higher after addition of LPA (0.048µm/sec compared to 0.041µm/sec in the growth cones from untreated cells). In the axons no differences were observed between the mean velocity of comets in untreated cells and in cells treated with LPA (0.053µm/sec and 0.055µm/sec, respectively; Fig. 59). When the velocity of comets was measured in the MAP1B-/- DRG neurons, no differences were observed neither in axons nor in the

growth cones. In axons the mean velocities of dashes were 0.067µm/sec and 0.064µm/sec in case of untreated and LPA treated cells, respectively, whereas in the growth cones velocities were 0.052µm/sec in both untreated and LPA treated cells (Fig. 60).

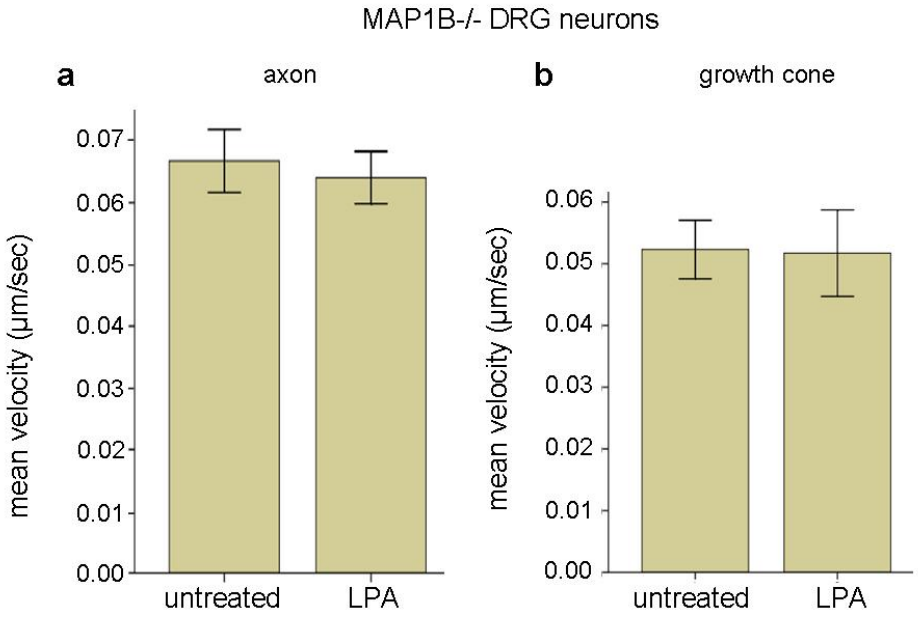

Fig. 60. LPA does not alter the velocity of EB1-GFP comets in MAP1B-/- DRG neurons. DRG neurons from MAP1B-/- mice were transfected with a construct encoding EB1-GFP, grown on coverslips coated with poly-L-lysine and laminin for 48h, and microtubule dynamics were monitored with an inverted microscope equipped with fluorescence optics. Cells were treated with 10µM LPA and recording was continued for 30-50min. Pictures were taken for 1min every 2s. The velocity of EB1-GFP dashes within axons (a) and growth cones (b) was calculated with MetaMorph software. Observed comets for quantification, 77 (a) and 25 (b) from 4 independent experiments. In case of the untreated group the values came from videos taken before addition of LPA and previous experiments to obtain the same number of samples as in the LPA treated group. Error bars represent standard deviations.

The mean distance of EB1-GFP comets was decreased in axons of wild-type DRG neurons treated with LPA when compared to untreated cells (0.79µm and 1µm, respectively). In the growth cones this value was also reduced, from 0.84µm when cells were untreated to 0.069µm when cells were treated with LPA, but difference was not statistically significant (Fig. 61). In case of MAP1B-/- DRG neurons no differences were observed concerning the distance of dashes moving in axons (1.14µm both in untreated cells and in cells treated with LPA). On the other hand, a decrease in the mean distance was found in the growth cones (0.67µm when cells were treated with LPA compared to 1.00µm in untreated cells; Fig. 62).

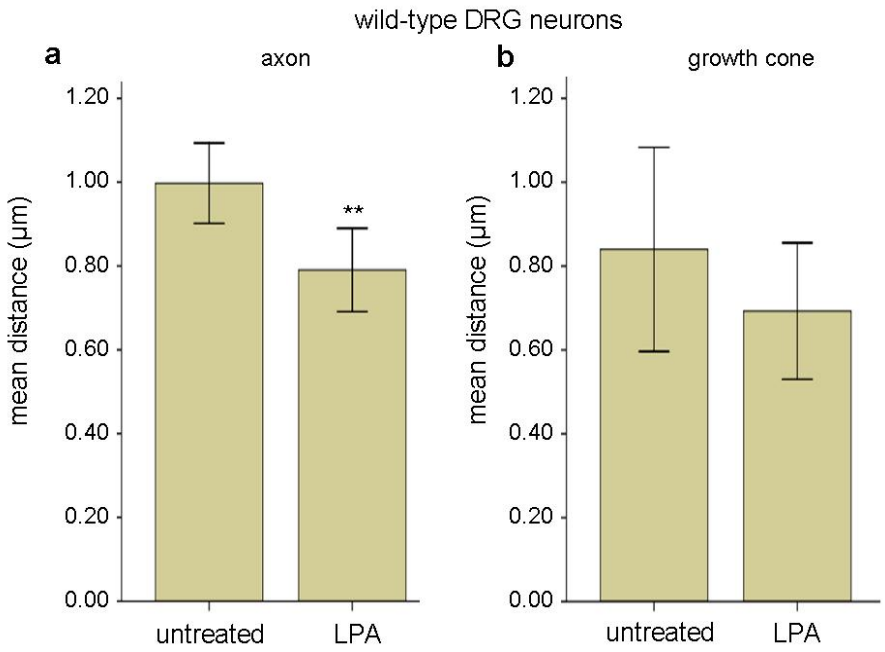

Fig. 61. EB1-GFP comets moves for shorter distance in axons of LPA-treated wild-type DRG neurons. DRG neurons from wild-type mice were transfected with a construct encoding EB1-GFP, grown on coverslips coated with poly-L-lysine and laminin for 48h, and microtubule dynamics were monitored with an inverted microscope equipped with fluorescence optics. Cells were treated with 10µM LPA and recording was continued for 30-50min. Pictures were taken for 1min every 2s. The distance of EB1-GFP dashes within axons (a) and growth cones (b) was calculated with MetaMorph software. Observed comets for quantification, 95 (a) and 28 (b) from 4 independent experiments. In case of the untreated group the values came from videos taken before addition of LPA and previous experiments to obtain the same number of samples as in the LPA treated group. Error bars represent standard deviations. Asterisks indicate that the values for neurons treated with LPA were significantly different from corresponding values of untreated neurons (*, $p<0.005$).

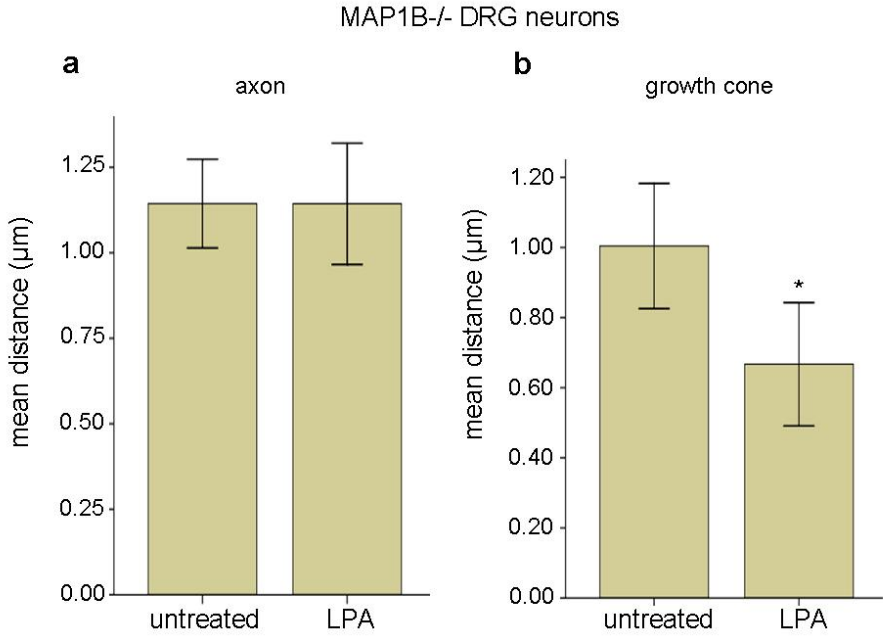

Fig. 62. EB1-GFP comets moves for shorter distance in the growth cones of LPA-treated MAP1B-/- DRG neurons. DRG neurons from MAP1B-/- mice were transfected with a

construct encoding EB1-GFP, grown on coverslips coated with poly-L-lysine and laminin for 48h, and microtubule dynamics were monitored with an inverted microscope equipped with fluorescence optics. Cells were treated with 10μM LPA and recording was continued for 30-50min. Pictures were taken for 1min every 2s. The distance of EB1-GFP dashes within axons (a) and growth cones (b) was calculated with MetaMorph software. Observed comets for quantification, 77 (a) and 25 (b) from 4 independent experiments. In case of the untreated group the values came from videos taken before addition of LPA and previous experiments to obtain the same number of samples as in the LPA treated group. Error bars represent standard deviations. Asterisks indicate that the values for neurons treated with LPA were significantly different from corresponding values of untreated neurons (*, $p<0.01$).

LPA reduced the time of EB1-GFP comet life both in axons and growth cones from wild-type DRG neurons. In axons, the time of comet life was reduced upon treatment with LPA from 28.76sec (untreated neurons) to 21,79sec (LPA treated neurons), whereas in the growth cones it was reduced from 30.27sec (untreated neurons) to 23.50sec (LPA treated neurons), but in the growth cone the difference was not statistically significant (Fig. 63). In MAP1B-/- DRG neurons no difference was observed in the axons, as well in the growth cones, upon treatment with LPA. The mean time of EB1-GFP comet life in the axons was 30.38sec after treatment with LPA, whereas without treatment the mean time was 30.11sec. In the growth cones time of comet life was 26.72sec in case of untreated cells, while after addition of LPA it was reduced to 21.20sec, but the difference was not statistically significant (Fig. 64).

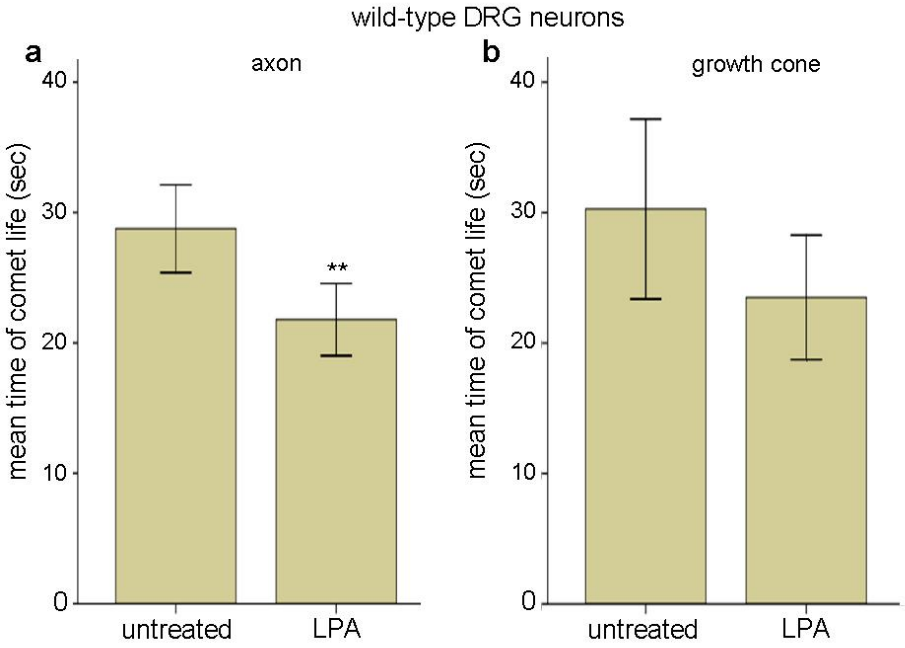

Fig. 63. LPA decreases the time of EB1-GFP comet life in axons of wild-type DRG neurons. DRG neurons from wild-type mice were transfected with a construct encoding EB1-GFP, grown on coverslips coated with poly-L-lysine and laminin for 48h, and microtubule dynamics were monitored with an inverted microscope equipped with fluorescence optics. Cells

were treated with 10µM LPA and recording was continued for 30-50min. Pictures were taken for 1min every 2s. The time of EB1-GFP dashes life within axons (a) and growth cones (b) was calculated with MetaMorph software. Observed comets for quantification, 95 (a) and 28 (b) from 4 independent experiments. In case of the untreated group the values came from videos taken before addition of LPA and previous experiments to obtain the same number of samples as in the LPA treated group. Error bars represent standard deviations. Asterisks indicate that the values for neurons treated with LPA were significantly different from corresponding values of untreated neurons (*, $p<0.005$).

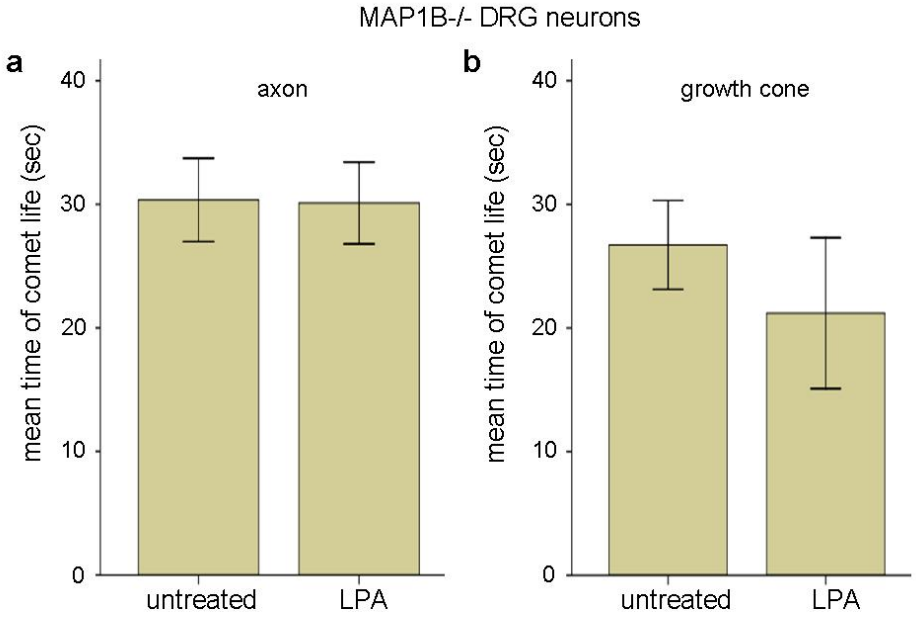

Fig. 64. LPA does not alter the time of EB1-GFP comet life in MAP1B-/- DRG neurons. DRG neurons from MAP1B-/- mice were transfected with a construct encoding EB1-GFP, grown on coverslips coated with poly-L-lysine and laminin for 48h, and microtubule dynamics were monitored with an inverted microscope equipped with fluorescence optics. Cells were treated with 10µM LPA and recording was continued for 30-50min. Pictures were taken for 1min every 2s. The time of EB1-GFP dashes life within axons (a) and growth cones (b) was calculated with MetaMorph software. Observed comets for quantification, 77 (a) and 25 (b) from 4 independent experiments. In case of the untreated group the values came from videos taken before addition of LPA and previous experiments to obtain the same number of samples as in the LPA treated group. Error bars represent standard deviations.

LPA did not alter the stop frequency of dashes, neither in axons nor in growth cones of wild-type DRG neurons. In axons, the mean stop frequency of EB1-GFP comets in case of untreated cells was 0,084stops/sec, whereas in cells treated with LPA it was 0,087stops/sec. In the growth cones, the mean stop frequency of dashes was 0.077stops/sec after treatment with LPA, compared to 0.083stops/sec when cells were left untreated (Fig. 65). Similarly, the stop frequency of EB1-GFP comets was not changed in axons and growth cones of MAP1B-/- DRG neurons. In axons it was 0.095stops/sec after application of LPA compared to 0.088stops/sec when cells were untreated. In the growth cones of neurons treated with LPA the mean stop frequency

was 0.087stops/sec whereas in the growth cones of untreated neurons it was 0.075stops/sec (Fig. 66).

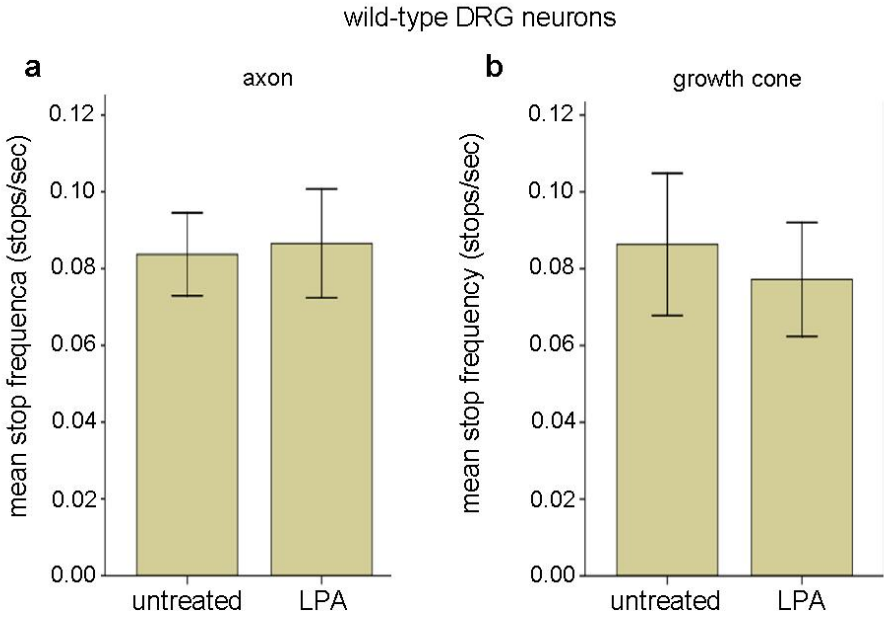

Fig. 65. LPA does not alter the stop frequency of EB1-GFP comets in wild-type DRG neurons. DRG neurons from wild-type mice were transfected with a construct encoding EB1-GFP, grown on coverslips coated with poly-L-lysine and laminin for 48h, and microtubule dynamics were monitored with an inverted microscope equipped with fluorescence optics. Cells were treated with 10µM LPA and recording was continued for 30-50min. Pictures were taken for 1min every 2s. The stop frequency of EB1-GFP dashes within axons (a) and growth cones (b) was calculated with MetaMorph software. Observed comets for quantification, 95 (a) and 28 (b) from 4 independent experiments. In case of the untreated group the values came from videos taken before addition of LPA and previous experiments to obtain the same number of samples as in the LPA treated group. Error bars represent standard deviations.

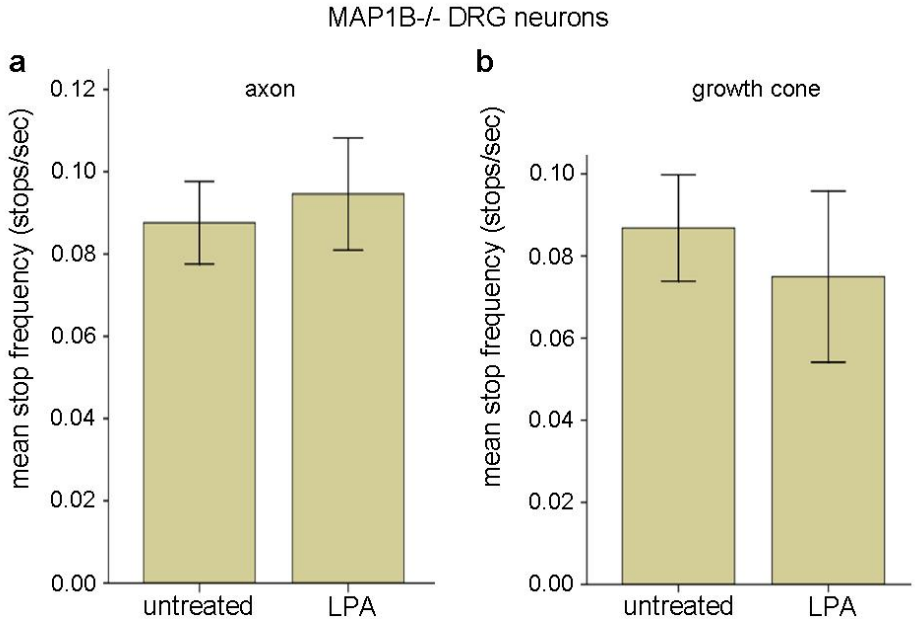

Fig. 66. LPA does not alter the stop frequency of EB1-GFP comets in MAP1B-/- DRG neurons. DRG neurons from MAP1B-/- mice were transfected with a construct encoding EB1-

GFP, grown on coverslips coated with poly-L-lysine and laminin for 48h, and microtubule dynamics were monitored with an inverted microscope equipped with fluorescence optics. Cells were treated with 10µM LPA and recording was continued for 30-50min. Pictures were taken for 1min every 2s. The stop frequency of EB1-GFP dashes within axons (a) and growth cones (b) was calculated with MetaMorph software. Observed comets for quantification, 77 (a) and 25 (b) from 4 independent experiments. In case of the untreated group the values came from videos taken before addition of LPA and previous experiments to obtain the same number of samples as in the LPA treated group. Error bars represent standard deviations.

Since I observed an increased number of comets in axons and growth cones of MAP1B-/- DRG neurons in comparison to wild-type neurons, I decided to examine if LPA has an influence on the number of EB1-GFP dashes. I hypothesized that LPA might increase microtubule binding of MAP1B, resulting in reduction of their dynamics. Therefore I expected that upon LPA treatment the number of comets is decreased. I observed that in axons of wild-type DRG neurons the number of comets was decreased upon treatment with LPA, 0.059comets/µm compared to 0.12comets/µm when cells were untreated. In the growth cones I also observed a reduction in the number of comets after application of LPA, but the difference was not statistically significant (0.020comets/µm^2 and 0.025comets/µm^2, when cells were treated with LPA and were untreated, respectively; Fig. 67).

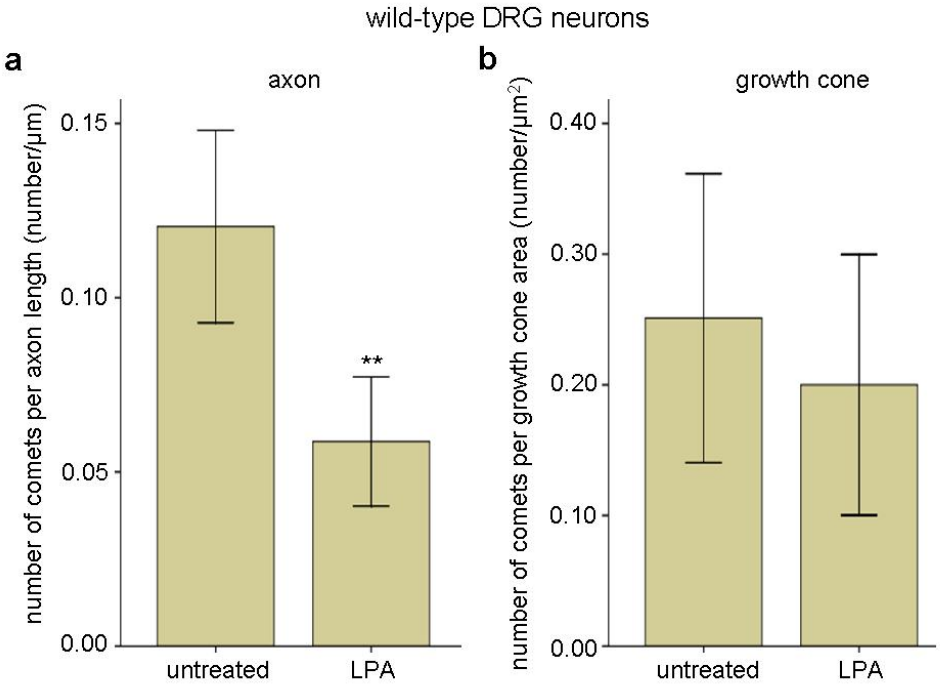

Fig. 67. LPA decreases the number of EB1-GFP comets in axons of wild-type DRG neurons. DRG neurons from wild-type mice were transfected with a construct encoding EB1-GFP, grown on coverslips coated with poly-L-lysine and laminin for 48h, and microtubule dynamics were monitored with an inverted microscope equipped with fluorescence optics. Cells

were treated with 10µM LPA and ecording was continued for 30-50min. Pictures were taken for 1min every 2s. The number of EB1-GFP comets per axon length (number of comets/µm) and the number of EB1-GFP comets per growth cone area (number of comets/µm^2) were calculated with MetaMorph and ImageJ softwares. Observed comets for quantification, in axons (a), 192 (untreated) and 187 (LPA); in growth cones (b), 18 (untreated) and 23 (LPA) from 4 (LPA) and 6 (untreated) independent experiments. Error bars represent standard deviations. The values for axons from cells treated with LPA were significantly different from corresponding values of axons from untreated neurons (**, p<0.001).

In axons of MAP1B-/- DRG neurons the number of comets was also reduced when cells were treated with LPA (0.12comets/µm in comparison to 0.204comets/µm in case of untreated cells). Similarly to wild-type neurons, in growth cones the number of EB1-GFP dashes was reduced, but the difference was not statistically significant (0.057comet/µm^2 and 0.117comet/µm^2 for cells treated with LPA and for untreated cells, respectively; Fig. 68).

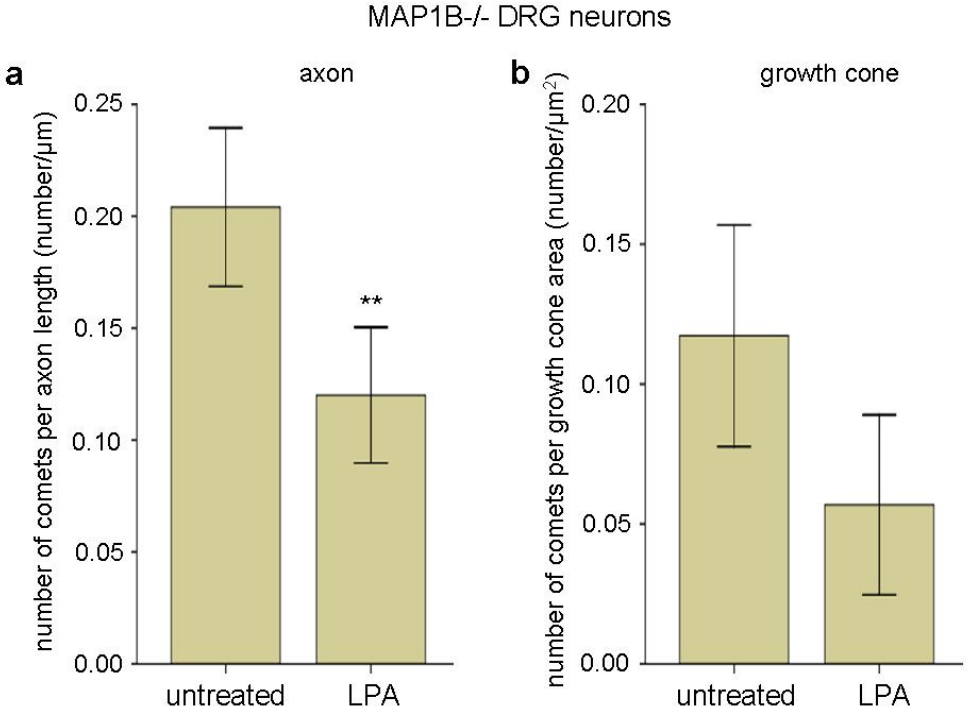

Fig. 68. LPA decreases the number of EB1-GFP comets in axons MAP1B-/- DRG neurons. DRG neurons from MAP1B-/- mice were transfected with a construct encoding EB1-GFP, grown on coverslips coated with poly-L-lysine and laminin for 48h, and microtubule dynamics were monitored with an inverted microscope equipped with fluorescence optics. Cells were treated with 10µM LPA and ecording was continued for 30-50min. Pictures were taken for 1min every 2s. The number of EB1-GFP comets per axon length (number of comets/µm) and the number of EB1-GFP comets per growth cone area (number of comets/µm^2) were calculated with MetaMorph and ImageJ softwares. Observed comets for quantification, in axons (a), 248 (untreated) and 168 (LPA); in growth cones, 44 (untreated) and 24 (LPA) from 4 (LPA) and 6 (untreated) independent experiments. The values for axons from cells treated with LPA were significantly different from corresponding values of axons from untreated neurons (**, p<0.001).

In addition, I observed increased an number of axons and growth cones without any EB1-GFP comets after treatment with LPA in both wild-type and MAP1B-/- DRG neurons. In case of growth cones after treatment with LPA many more dashes were moving retrogradely, when compared to dashes in the growth cones from untreated neurons. More EB1-GFP comets were pausing and/or oscillating, when compared to untreated cells.

DISCUSSION

Calcimycin-induced axon retraction was shown to be dependent on the activation of nNOS. It involves S-nitrosylation of LC1 on cys2457 as a critical step and S-nitrosylation increased microtubule binding of full length MAP1B in PtK2 cells (Stroissnigg et al., 2007). However, the exact mechanism leading to axon retraction remains unknown. When I inhibited nNOS prior to application of calcimycin, retraction of wild-type DRG neurons was abolished almost completely, which is consistent with previous results (Stroissnigg et al., 2007). On the other hand, calcimycin-induced increase in Ca^{2+} levels can activate other calcium effectors, which can induce or inhibit axon growth. For example, it was shown in cultured embryonic *Xenopus* spinal neurons that at the normal resting level of $[Ca^{2+}]_i$ small local Ca^{2+}signals activated calcineurin and high local Ca^{2+} signals activated CaMKII resulting in repulsion and attraction, respectively (Wen et al., 2004). In addition, repulsive turning in *Xenopus* spinal neurons induced by large changes in calcium level required activation of calpains and inhibition of calpain attenuated this repulsive effect (Robles et al., 2003). On the other hand, calpain was found to cleave proteolytically nNOS (Hajimohammadreza et al., 1995). Therefore, inhibition of calpain might enhance retraction of axons in response to calcimycin. I decided to determine the potential role of calcium transducers other than nNOS in axon retraction induced by calcimycin. Wild-type DRG neurons were treated with inhibitors specific for CaMKII, calcineurin, calpain, or PKC, followed by application of calcimycin. Inhibition of any of these Ca^{2+} effectors did not prevent retraction, suggesting that none of them is involved in axon retraction induced by calcimycin in adult mouse DRG neurons. One could expect that inhibition of CaMKII can increase the level of cells showing retraction hallmarks, since it was shown that CaMKII can phosphorylate nNOS at Ser847, resulting in decrease of nNOS activity, potentially by blocking the binding of Ca^{2+}/CaM (Komeima et al., 2000; Song et al., 2008). However, no such exacerbation of calcimycin-induced axon retraction was observed in the presence of an CaMKII inhibitor. On the other hand, it is known that NO can inhibit CaMKII via S-nitrosylation of CaMKII on Cys6 (Song et al., 2008). It is possible, that CaMKII is already inhibited by basal levels of NO and can not phosphorylate nNOS, thus has no influence on axon retraction induced by calcimycin. Increased Ca^{2+} levels can activate various pathways depending on the global Ca^{2+} level,

local Ca^{2+} signals, cell types, culture systems and age of neurons. For example, exposure of cultured young hippocampal neurons to glutamate, which induces increase in Ca^{2+} levels, leads to activation of calpain above basal levels and cell death, while it has no influence on calpain in aged neurons (Hajieva et al., 2009). It seems that calcimycin-induced retraction of adult wild-type DRG neurons is triggered by activation of nNOS, and does not involve CaMKII, calcineurin, calpain and PKC, but we can not exclude contribution of other calcium effectors, which were not examined here.

Axon elongation and retraction depend on the balance between the extension force, which is based on microtubules and dynein, and the retraction force, which is based on F-actin and myosin (Ahmad et al., 2000; Baas and Ahmad, 2001). Reduction of the extension force, for example by inhibition of dynein, or enhancement of acto-myosin contractility can lead to axon retraction. It was proposed that an increased Ca^{2+} levels activates nNOS, which leads to S-nitrosylation of LC1 on cys2457, resulting in a conformational change that enhances microtubule binding activity. Interaction between MAP1B and microtubule might inhibit dynein, leading to axon retraction (Stroissnigg et al., 2007). On the other hand, several guidance cues induce growth cone collapse and axon retraction that involve activation of the Rho/ROCK pathway and increase of acto-myosin contractility. For example, inhibition of RhoA by C3 transferase from *C.botulinum* abolished LPA-induced neurite retraction in mouse neuroblastoma NIE-115 cells (Jalink et al., 1994), and inhibition of its downstream effector ROCK with Y27632 reduced growth cone collapse induced by ephrin-A5 in retinal ganglia neurons (Wahl et al., 2000). To investigate the potential role of acto-myosin contractility in axon retraction induced by NO, wild-type DRG neurons were treated with Y27632, followed by treatment with calcimycin or SNAP. Inhibition of ROCK completely prevented retraction induced by both SNAP and calcimycin. Likewise, it was shown that increased levels of NO induced retraction of neurites in neuroblastoma N2a cells (Stroissnigg et al., 2007). Pretreatment with Y27632 reduced the level of cells retracting in response to SNAP treatment. Moreover, inhibition of myosin with blebbistatin abolished retraction of neurites induced by both calcimycin and SNAP in wild-type DRG neurons and in neuroblastoma N2a cells. These results demonstrated that ROCK and myosin are necessary for neurite retraction induced by NO, but did not elucidate if acto-myosin forces are enhanced in response to NO. Myosin II activity is stimulated by diphosphorylation of MRLC at Ser19 and Thr18 (Somlyo and Somlyo, 2003).

Monophosphorylation of MRLC at Ser19 increases its ATPase activity and the stability of myosin II filaments. Additional phosphorylation at Thr18 further enhances activity of myosin II and stabilizes its filaments. It was observed that LPA-increased intracellular tension involves the Rho/ROCK pathway and increases the phosphorylation of MRLC at both Ser19 and Thr18 (Mizutani et al., 2006). Thus, I decided to examine levels of mono- and diphosphorylation of MRLC in response to SNAP and LPA in N2a neuroblastoma cells. I observed a tendency towards an increase of mono- and diphosporylation of MRLC upon application of SNAP and LPA, but only treatment with 100μM SNAP for 1h induced a statistically significant increase in monophosphorylation of MRLC (Ser19). Although the increase in the level of mono- and diphosphorylation induced by LPA was not significant, the tendency is consistent with previous studies showing that LPA induced phosphorylation of MRLC at both Ser19 and Thr18 in hepatic myofibroblasts, resulting in enhanced contractile forces and migration velocity (Tangkijvanich et al., 2003). In addition, it was observed that LPA-enhanced intracellular tension in NIH-3T3 fibroblasts involved activation of ROCK, which directly diphosphorylated MRLC (Mizutani et al., 2006). Moreover, Y27632 was found to reduce levels of mono- and diphosphorylation of MRLC in Madin Darby canine kidney (MDCK) II epithelial cells. Thus, it was surprising that Y27632 did not decrease the level of monophosphorylation of MRLC in my experiments. It is important to mention that in previous experiments mainly diphosphorylation was affected (Watanabe et al., 2007). Likewise, Y27632 decreases levels of diphosphorylated MRLC in cortices from sea urchin eggs, but does not significantly alter levels of monophosphorylated MRLC (Uehara et al., 2008). Thus, additional experiments examing MRLC diphosphorylation in N2a cells treated with Y27632 are needed to clarify thus issue. As it stands, the main outcome from studies performed by me is that LPA and SNAP increased Ser19 monophosphorylation of MRLC in N2a cells.

Growth cone guidance can be influenced by cyclic nucleotides, such as cAMP and cGMP (Song et al., 1998; Song and Poo, 1999). It was shown that cAMP can enhance regeneration of injured adult axons, possibly by increasing their ability to grow and by reducing the repulsive response of the growth cone to inhibitory factors from the surrounding milieu (Song et al., 1998; Lu et al., 2004). It was also found that the ratio of cAMP/cGMP determined the response of the axon to the netrin-1. A high ratio of cAMP/cGMP stimulated L-type Ca^{2+} channels, resulting in increased $[Ca^{2+}]_i$ levels and

an attractive response of growth cones to netrin-1. A low ratio of cAMP/cGMP reduced $[Ca^{2+}]_i$ levels and led to the repulsive response to netrin-1, which was converted to an attractive response by increasing cAMP levels (Nishiyama, 2003). Moreover, enhanced levels of cAMP inhibited calcineurin-mediated retraction of neurites induced by high local Ca^{2+} signals in cultured embryonic *Xenopus* spinal neurons (Wen et al., 2004). Similarly, repulsion of growth cones in cultured *Xenopus* spinal neurons induced by MAG was converted to attraction, when cAMP levels were pharmacologically increased (Song et al., 1998). Finally, Sema3A-induced growth cone collapse was abolished by activation of cAMP pathway in chicken DRG (Dontchev and Letourneau, 2002). Thus, I decided to examine if stimulation of cAMP can influence axon retraction induced by NO. Bath application of either dibutryl-cAMP or forskolin, which stimulates production of cAMP, partially abolished calcimycin- and SNAP-induced retraction. In case of SNAP, effects of cAMP stimulation were more pronounced. This could be due to the fact that SNAP works as NO donor, bypassing the necessity of nNOS activation, whereas calcimycin-induced axon retraction is more complex. The exact mechanism by which cAMP prevents axon retraction and growth cone collapse is not known. It was shown that cAMP can modulate actin dynamics via activation of PKA, which phosphorylates RhoA at Ser188, leading to a decrease in guanine nucleotide exchange (Schoenwaelder and Burridge, 1999). It is proposed that the phosphorylation of RhoA increases its binding to GDIs, resulting in stabilization of RhoA in an inactive state, followed by its detachment from the membrane and translocation to the cytosol (Busca et al., 1998; Dong et al., 1998; Schoenwaelder and Burridge, 1999; Khodair et al., 2005). Moreover, phosphorylation of RhoA reduces its interaction with its effectors, such as ROCK (Dong et al., 1998; Schoenwaelder and Burridge, 1999). In addition, PKA can directly phosphorylate MLCK, which inhibits MLCK activity, leading to a decrease phosphorylation of MRLC. As a result, ATPase and motor activity of myosin II are inhibited and acto-myosin contractility is decreased (Lamb et al., 1988). Thus, the mechanism by which cAMP reduces SNAP- and calcimycin-induced axon retraction could be similarly through inhibition of ROCK and myosin, which I demonstrated to be necessary for retraction. Likewise, elevated cAMP overcome myelin-induced growth inhibition by activation of the transcription factor cAMP response element binding protein (CREB), leading to upregulated expression of Arginase I and increased synthesis of polyamines, such as putrescine (Cai et al., 2002; Filbin, 2003; Gao et al., 2004). It was shown that that putrescine is converted to spermidine to overcome

inhibition by myelin and spermidine can promote regeneration of optic nerve (Deng et al., 2009). The exact mechanism how polyamines promote axon growth on myelin or regeneration after injury is still unknown. They can influence the cytoskeleton, probably by affecting the polymerization and organization of microtubules (Kaminska et al., 1992; Banan et al., 1998). Thus, polyamines by influencing cytoskeleton might prevent its reorganization induced by SNAP or calcimycin. In addition, polyamines were found to block ion channels (Williams, 1997; Deng et al., 2009) and to modify postranslationally proteins (Huang et al., 2007). Finally, PKA was also shown to phosphorylate MAPs, for example MAP2 and MAP1B (Khodair et al., 2005). PKA phosphorylates MAP2 on specific serine residues in the microtubule binding domain and in the proline-rich region, promoting neuritogenesis (Sanchez Martin et al., 2000). On the other hand, it was shown that LPA induced an increase in phosphorylation of tau, which was prevented by application of di-butryl-cAMP before treatment with LPA (Sayas et al., 1999). Thus, PKA might potentially influence also properties of MAP1B, for example its microtubule binding activity (Fig. 71).

It seems that upon SNAP, calcimycin and LPA treatment microtubules retreat backward rather than depolymerise to accommodate the shortening of the axon, resulting in a bundled configuration. On the other hand, I did not measure the level of microtubules after treatment with SNAP, calcimycin or LPA, therefore I can not exclude that depolymerization takes place during retraction. To examine this, wild-type DRG neurons were exposed for 30min to 100nM taxol, which stabilizes microtubules against disassembly, and then they were treated with SNAP or LPA (in the presence of taxol). Surprisingly, I observed that the number of cells showing retraction hallmarks in response to SNAP or LPA was even higher in the presence of taxol than in case of cells treated with SNAP or LPA only. These results are consistent with previous reports showing that pretreatment with taxol did not prevent LPA-induced axon retraction in mouse embryonic cortical neurons (Fukushima and Morita, 2006) nor NOC7-induced axon retraction in embryonic chick DRG neurons (NOC7 is a nitric oxide donor; He et al., 2002). Even more surprising, both wild-type and MAP1B-/- DRG neurons retracted in response to treatment with taxol only, showing all characteristic hallmarks - retraction bulb, sinusoidal bundles of microtubules, and trailing remnant. It is known that high concentrations of taxol (>1μM) induce significant increase of microtubules assembly and completely inhibit their dynamics (Derry et al., 1995). The concentration

of taxol that I used was much lower and in other studies was shown not to alter morphology of axons (Derry et al., 1995; He et al., 2002). The low concentration of taxol (≤100nM) was found to suppress selectively the rate of shortening at the plus ends of microtubules what was correlated with an increase in the level of microtubule polymers, but it did not inhibit completely the dynamic of microtubules (Derry et al., 1995). I decided to use an even lower concentration of taxol (3nM), and obtained the same results as in case of 100nM taxol. Both wild-type and MAP1B-/- DRG neurons retracted in response to treatment with taxol only. In addition, I investigated the influence of taxol on LPA- and calcimycin-induced retraction in N2a cells. Similarly, taxol did not prevent neurite retraction and also induced retraction on its own. These results are contradictory to those obtained by Ertürk and colleagues (Ertürk et al., 2007). They observed that application of taxol to the site of injury after performing unilateral lesion in the dorsal column of the spinal cord prevents the formation of retraction bulbs and axonal degeneration. Moreover, taxol-induced stabilization of microtubules enhanced growth of cerebellar granule neurons on myelin overcoming its inhibitory properties (Ertürk et al., 2007). However, treatment of zebrafish forebrain neurons with 20nM taxol resulted in formation of many microtubule loops within neurites, similar to sinusoidal bundles which I observed in adult mouse DRG neurons after application of 3nM or 100nM taxol (Hendricks and Jesuthasan, 2009). In addition, forebrain neurons from zebrafish *phr* mutants (PHR is a neuronal ubiqutin ligase) showed increased microtubule looping caused by extensive polimerization, resulting in the growth cone arrest and a morphology similar to morphology of DRG neurons treated with taxol, SNAP, calcimycin or LPA. Application of nocodazole, which a microtubule depolymerising agent, to *phr* mutant neurons reduced the number of cells showing the retraction phenotype (Hendricks and Jesuthasan, 2009). The discrepancy between all theses results could be due to different types of researches (*in vivo* and *in vitro*), different conditions of culture (culture medium, temperature), different cell types, and different species. It is known that the initiation and maintenance of axon growth requires a basal level of dynamic microtubules (Letourneau and Ressler, 1984). During extension the growth cones usually pause at the intermediate targets and become larger. At this point they contain a lot of microtubules and microtubule loops (Hendricks and Jesuthasan, 2009). Taxol potentially can inhibit growth of neurites by inducing uncontrolled assembly and increased stability of microtubules, leading to arrest of the growth cone in the paused state (Letourneau and Ressler, 1984; Hendricks and

Jesuthasan, 2009). This mechanism could be also involved in SNAP-, calcimycin- and LPA-induced retraction of wild-type DRG neurons. It was shown that each of these reagents induced MAP1B-dependent axon retraction with the same hallmarks as taxol-induced retraction. I propose that LPA, SNAP and calcimycin modified MAP1B, leading to conformational changes of MAP1B characterized by increased microtubule binding activity that results in their overstabilization. Overstabilized microtubules might produce a large tension, but the growth cone can not advance, leading to microtubules retreat, growth cone collapse and axon retraction. In case of SNAP- and calcimycin-induced axon retraction microtubule binding properties of MAP1B are increased probably by a conformational change induced by S-nitrosylation on cys2457, which was shown to be critical step for NO-induced axon retraction (Stroissnigg et al., 2007). The exact mechanism by which LPA increases microtubule binding of MAP1B is still unknown, but it might involve phosphorylation of MAP1B, as it was shown that LPA activates GSK3, mainly GSK3β, by inducing its phosphorylation at a tyrosine residue in addition to serine phosphorylation (Sayas et al., 1999; Sayas et al., 2006). A transient increase in activity of GSK3β upon treatment with LPA was accompanied by enhanced phosphorylation of tau (Sayas et al., 1999; Sayas et al., 2006). Inhibition of GSK3β with specific inhibitors (LiCl, SB-216763 and SB-415286) prevented the increase in tau phosphorylation and neurite retraction in B103-LPA_1 and cerebellar granule neurons (Sayas et al., 2002a; Sayas et al., 2006). GSK3β is known to phosphorylate also MAP1B and phosphorylation of MAP1B regulates its microtubule binding activity. Indeed, it was shown that LPA increased phosphorylation of MAP1B in SH-SY5Y cells reaching a maximum level at 1h after treatment with LPA (Sayas et al., 2002b). Moreover, it was observed that LPA stabilized microtubules in 3T3 fibroblasts, although not in SH-SY5Y cells (Sayas et al., 2002b), as judged by an increased level of detyrosinated microtubules (Cook et al., 1998). Thus, it is conceivable that LPA stimulates phosphorylation of MAP1B by GSK3β, leading to increased binding to microtubules and their stabilization, resulting in axon retraction. In contrast, it was observed that LPA addition to neuroblastoma SH-SY5Y cells decreased the level of detyrosinated tubulin, while increasing the level of tyrosinated-tubulin (Sayas et al., 2002b). In addition, high levels of MAP1B-P were shown to be associated with the loss of detyrosinated microtubules in COS cells transfected with both MAP1B and GSK3β, suggesting that MAP1B phosphorylated by GSK3β regulates microtubule stability in axons (Goold et al., 1999). We have to take into consideration that different cell types

were used in all these studies and the response of cells to the same guidance cue can differ from type to type. Moreover, there are many contradictory results concerning MAP1B phosphorylation and its influence on MAP1B functions, probably resulting from the existence of more than 30 phosphorylation sites on MAP1B. Potentially in all these studies effects of phosphorylation at different sites were analysed. Thus, it should be further examined how exactly LPA increases microtubule binding of MAP1B. MAP1B deficiency impairs axon retraction in response to SNAP, calcimycin or LPA, since no stabilization takes place. Taxol stabilizes microtubules on its own without MAP1B involvement, triggering retraction in both wild-type and MAP1B-/- DRG neurons. One should take into account that taxol-induced stabilization of microtubules can involve different mechanism than stabilization stimulated by LPA or SNAP. At the very least, taxol-induced axon retraction is not MAP1B-dependent and could not be prevented by inhibition of ROCK and myosin (my results).

To test the hypothesis that SNAP and LPA increase the interaction of MAP1B with microtubules, I transfected non-neuronal PtK2 cells with constructs encoding full length MAP1B and determined its intracellular localization. MAP1B was found predominately in the cytoplasm of untreated PtK2 cells, whereas treatment with SNAP or LPA increased the level of microtubule-bound MAP1B (19% and 15% of cells expressed full length MAP1B, in case of SNAP and LPA treatment, respectively, compared to 6% when cells were left untreated). Results from experiments with SNAP confirmed previous results, which also showed increase in microtubule binding of full length MAP1B upon SNAP treatment in PtK2 cells (Stroissnigg et al., 2007).

To assess influence of MAP1B on microtubule dynamics, DRG neurons from wild-type and MAP1B-/- DRG neurons were transfected with constructs encoding EB1-GFP. As I mentioned, microtubule plus end-binding proteins are incorporated into the growing end of microtubules and after a microtubule stops to polymerize they dissociate. I observed that EB1-GFP dashes were more dynamic in MAP1B-/- DRG neurons when compared to wild-type DRG neurons. The mean velocity of the EB3-GFP dashes in axons from MAP1B-/- neurons was 0.068μm/sec, whereas in the wild-type neurons it was 0.056μm/sec. Similarly, in growth cones of MAP1B-/- DRG neurons the mean velocity of EB1-GFP comets was higher compared to comets from growth cones of wild-type DRG neurons, 0.052μm/sec and 0.041μm/sec, respectively. The velocity of EB1-GFP dashes in wild-type DRG neurons was slower than the velocity of EB3-GFP dashes in

wild-type hippocampal neurons observed by Stepanova et al. (Stepanova et al., 2003), but were comparable to the velocity of EB3-GFP dashes in neuroblastoma-spinal cord 34 (NSC34) cells (Riano et al., 2009). In addition, I observed differences in the mean velocity of the EB1-GFP comets in the growth cone and axon, whereas Stepanova et al. did not find that (Stepanova et al., 2003). This discrepancy can be due to different cell types and age of cells, different culture conditions and different +TIPs used in both experiments.

The higher speed of comets in axons of MAP1B-/- neurons corresponds to a longer mean distance that they travelled (the mean distance for EB1-GFP dashes in axons of MAP1B-/- and wild-type DRG neuons were 1.57µm and 1.16µm, respectively) and longer time of comet life (32.43sec in MAP1B-/- DRG neurons and 28.83sec in wild-type DRG neurons). I also observed a tendency towards longer distance of dashes in the growth cones of MAP1B-/- neurons. I did not find a difference in the time of comet life between comets in wild-type and MAP1B-/- DRG neurons. Lack of MAP1B did not affect stop frequency of dashes both in the growth cones and in the axons either. In addition, I found a significantly higher number of EB1-GFP comets in the growth cones and axons of MAP1B-/- DRG neurons. For example, in the axons of MAP1B-/- DRG neurons I observed 0.204comets/µm, whereas in the axons of wild-type DRG neurons only 0.120comets/µm.

Differences in the dynamics of EB1-GFP dashes in wild-type and MAP1B-/- neurons could be due to a functional interaction between MAP1B and microtubule-severing proteins, such as spastin and P60-katanin. Spastin is expressed mainly in nervous system, whereas P60-katanin can be detected in several cell types (Yu et al., 2008). Both are involved in severing long stable microtubules into short dynamic ones, which plays an important role during neurite elongation and branching. Spastin is mostly localized in regions characterized by intensive reorganization of the cytoskeleton and correlates with the presence of dynamic tyrosinated microtubules, particularly in the growth cones and branching points (Yu et al., 2008). P60-katanin is more abundant in the neuron than spastin, but it is uniformly distributed along the axons and only at low levels in actively growing areas, such as branching points (Yu et al., 2008). Overexpression of spastin in adult mouse hippocampal neurons affected preferentially acetylated and detyrosinated microtubules, since cells overxpressing spastin showed significant decrease in the level of acetylated tubulin (Riano et al., 2009). Moreover, overexpression of spastin in adult rat hippocampal neurons resulted in an increased

number of short microtubules and great loss of microtubule mass in both the cell body and the axon, whereas overexpression of P60-katanin led to diminution of microtubule mass only in the cell body (Yu et al., 2008). In addition, a striking increase in axonal branching was observed in neurons overexpressing spastin, whereas in cells overexpressing P60-katanin the number of branches was not significantly different when compared to control cells (Yu et al., 2008). Newly formed branches in cells overexpressing spastin were not transient, they did not retract, but they extended further (Yu et al., 2008; Riano et al., 2009). Finally, depletion of spastin led to decrease in the length of the longest process in hippocampal neurons and a reduction in dynamic EB3-GFP dashes in NSC34 cells (Riano et al., 2009). MAP1B-/- DRG neurons, similarly to cells overexpressing spastin, are characterized by an increased branching and a decreased level of acetylated "stable" microtubules (Bouquet et al., 2004; Riano et al., 2009). Likewise, EB1-GFP dashes in MAP1B-/- DRG neurons showed increased dynamics when compared to wild-type DRG neurons, which is what one could expect from spastin overexpressing cells, since silencing of spastin reduced velocity of EB3-GFP comets (Riano et al., 2009). In addition, it was observed that binding of MAP4 or tau to microtubules reduced their accessibility to P60-katanin, but it did not protect them from severing by spastin (Qiang et al., 2006; Yu et al., 2008). Potentially MAP1B binding to microtubules could protect them against severing by spastin, similarly to protection of microtubules by tau against severing by P60-katanin.

Taking together my results and current knowledge published in the literature (Yu et al., 2008), I propose a model for spastin-triggered increase in microtubule dynamics and branching in MAP1B-/- neurons. In wild-type DRG neurons MAP1B binds to microtubules and makes them more resistant to severing by spastin, thus promotes formation of long stable microtubules and long axons. Spastin would preferentially sever microtubules, which are associated with smaller amounts of protective MAP1B or are free from MAP1B. Microtubules protected by MAP1B could be more easily stabilized and posttranslationally modified to be even more resistant to severing by spastin (Fig. 69). In MAP1B-/- neurons microtubules are not protected by MAP1B and they are more accessible for spastin. Since it was shown that tau binding to microtubules did not protect them from cutting by spastin, it can not compensate lack of MAP1B (Yu et al., 2008). Unprotected microtubules are severed by spastin, resulting in an increased number of short microtubules, a decreased number of acetylated tubulin and increased number of branches characteristic for MAP1B-/- DRG neurons (Bouquet

et al., 2004). A greater number of free microtubule plus ends recruits more EB1-GFP comets, as the +TIP proteins were shown to be recruited by tyrosine microtubules preferentially (Peris et al., 2006). Indeed, I observed an enhanced number of EB1-GFP dashes in the growth cones and axons of MAP1B-/- DRG neurons. In addition, it was shown that low concentrations of taxol inhibit branching of neurites of adult chicken DRG and sympathetic neurons without affecting the rate of extension (Letourneau et al., 1986). MAPs, such as MAP1B, could act like taxol to control organization of the cytoskeleton and branching. The observation that EB1-GFP comets are more dynamic in MAP1B-/- DRG neurons, supports the hypothesis that MAP1B stabilizes microtubules and the absence of MAP1B enhances microtubule dynamics. Taken in consideration similar effects of an overexpression of spastin and the absence of MAP1B in neurons, I propose spastin as the main severing protein playing a role in microtubule cutting and increased branching in MAP1B-/- DRG neurons, but I can not exclude p role of P60-katanin. It is possible that tau can partially compensate absence of MAP1B, but microtubules are also more accessible for P60-katanin, in addition to spastin. On the other hand, as I mentioned no significant increase in axonal branching was observed after overexpression of P60-katanin, suggesting that spastin not P60-katanin plays a crucial role in the regulation of branching (Yu et al., 2005; Qiang et al., 2006; Yu et al., 2008).

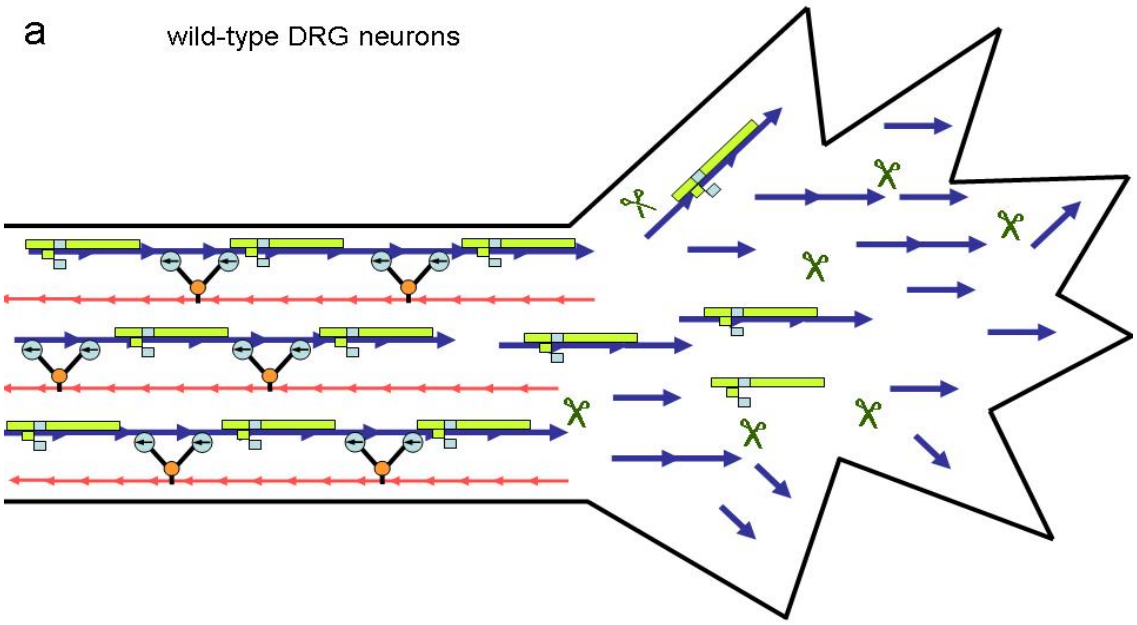

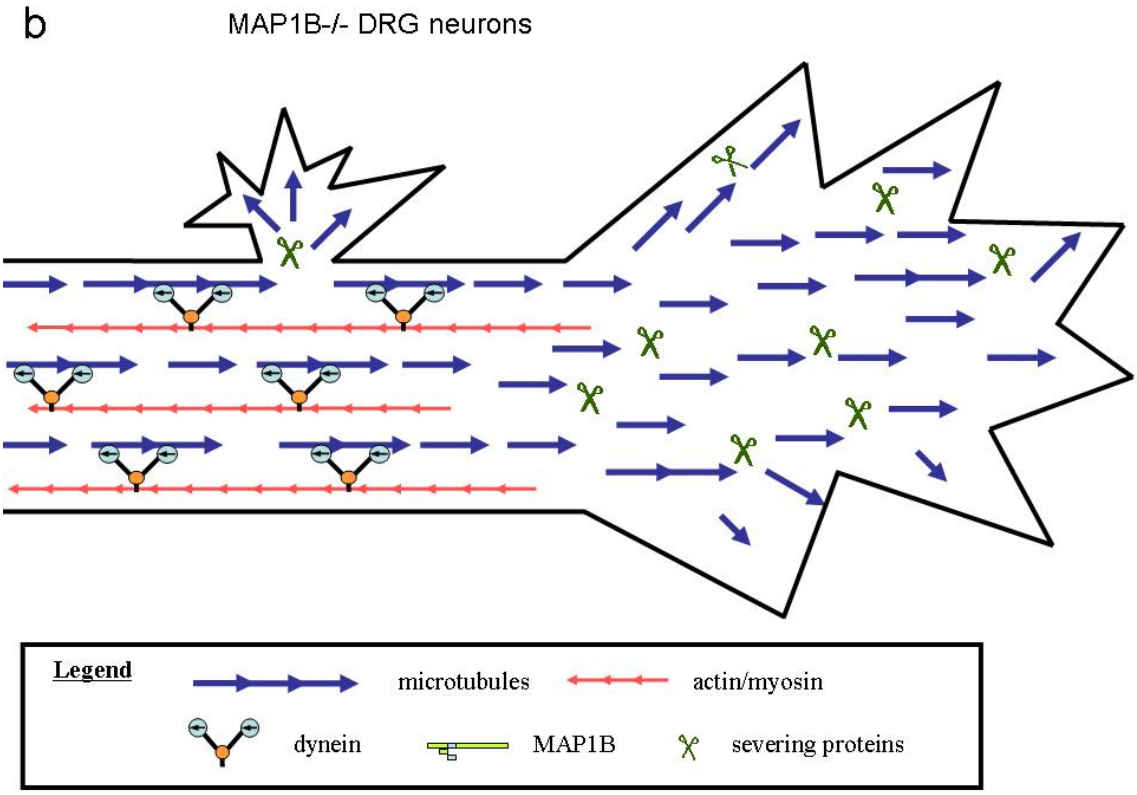

Fig. 69. Model for regulation of microtubule severing in wild-type (a) and MAP1B-/- (b) DRG neurons. Axonal elongation, branching and turning of the growth cones requires reorganization of microtubules. The axon shaft contains mainly very long stable microtubules, whereas branching points and growth cones are rich in short dynamic microtubules. The long stable microtubules within axon shaft have to be cut into short motile pieces able to move into new branches and mobile growth cone (Yu et al., 2008). Severing of microtubules is regulated by microtubule-severing proteins (green scissors), such as spastin and P60-katanin. (a) In wild-type DRG neurons cutting of microtubules by severing proteins, most likely by spastin, might be regulated by binding of MAP1B to microtubules, which makes them more resistant to severing. Despite the fact that there is enhanced concentration of spastin in the growth cones and branching points, MAP1B bound to microtubules could protect them from severing, thus preventing uncontrolled branching. (b) In MAP1B-/- DRG neurons due to the lack of MAP1B, the function of which might not be compensated for by other MAPs, such as tau, microtubules are not protected. They are more accessible for spastin, resulting in enhanced severing and an increased number of branches (adapted from Yu et al., 2008).

Treatment of wild-type DRG neurons with LPA reduced distance and the time of EB1-GFP comet life within axons. LPA also reduced the number of comets per axon length. As I mentioned +TIPs bind preferentially to free microtubule plus ends (Stepanova et al., 2003). According to model that I proposed LPA increases MAP1B binding to microtubules resulting in their overstabilization and a reduced number of free microtubule plus ends. Since the number of free microtubule plus ends is decreased less EB1-GFP comets are observed. It is consistent with previous studies showing that upon low concentration of taxol EB1- and EB3-positive comets disappeared and binding of

+TIPs to the ends of growing microtubules was abolished (Stepanova et al., 2003; Peris et al., 2006). Stabilization of microtubules by LPA is not as strong as in case of taxol treatment, thus not complete disappearance, but only reduction in the number of comets was found. In case of MAP1B-/- DRG neurons a decrease in the number of comets per axon length was also observed. This suggests that the reduction in axonal comet number is not crucial for axon retraction, since MAP1B-/- DRG neurons do not retract. Alternatively, the reduction in the number of actively polymerizing microtubules might indeed have an influence, but only when it reaches a critical value. In case of axons from wild-type DRG neurons LPA reduced the number of comets to 0.059comets/µm (compared to 0.120comets/µm in untreated cells), whereas in case of MAP1B-/- DRG neurons number of comets was reduced to 0.12comets/µm (compared to 0.204comets/µm in untreated cells). The number of EB1-GFP dashes in axons from MAP1B-/- neurons after LPA treatment is still 2-fold higher than the number in wild-type axons and is equal to the number of EB1-GFP dashes in axons from untreated wild-type DRG neurons.

Analysis of EB1-GFP comets in growth cones revealed that LPA increased velocity in wild-type DRG neurons and decreased distance in MAP1B-/- DRG neurons. My finding that during retraction the velocity of EB1-GFP dashes is enhanced is consistent with previous observations that the velocity of EB3-GFP dashes in spontaneously retracting neurons was higher than in extending neuritis (Stepanova et al., 2003). No significant changes in number of comets per growth cone area was found. On the other hand, after treatment with LPA I observed increased number of EB1-GFP comets oscillating, pausing or moving backward in the growth cones, when compared to the growth cones from untreated neurons.

I expect that NO-induced axon retraction involves a similar mechanism as retraction induced by LPA. For example, both LPA- and SNAP-induced retractions are MAP1B-dependent and both LPA and SNAP enhanced microtubule binding of full length MAP1B in PtK2 cells. However, time-lapse microscopy to analyse microtubule plus ends activity could not be performed for studies of S-nitrosylation, since this modification is highly light sensitive.

I propose that under normal conditions MAP1B binds to the microtubules at the certain optimal level and stabilized them enhancing axon extension, but upon treatment with LPA, SNAP or calcimycin microtubule binding by MAP1B is increased above this optimal level, overstabilizing them and preventing cutting by severing proteins.

Microtubules lose their dynamicity completely, they can not extent further, but also can not undergo catastrophe, thus they fold back and form sinusoidal bundles (Fig. 70).

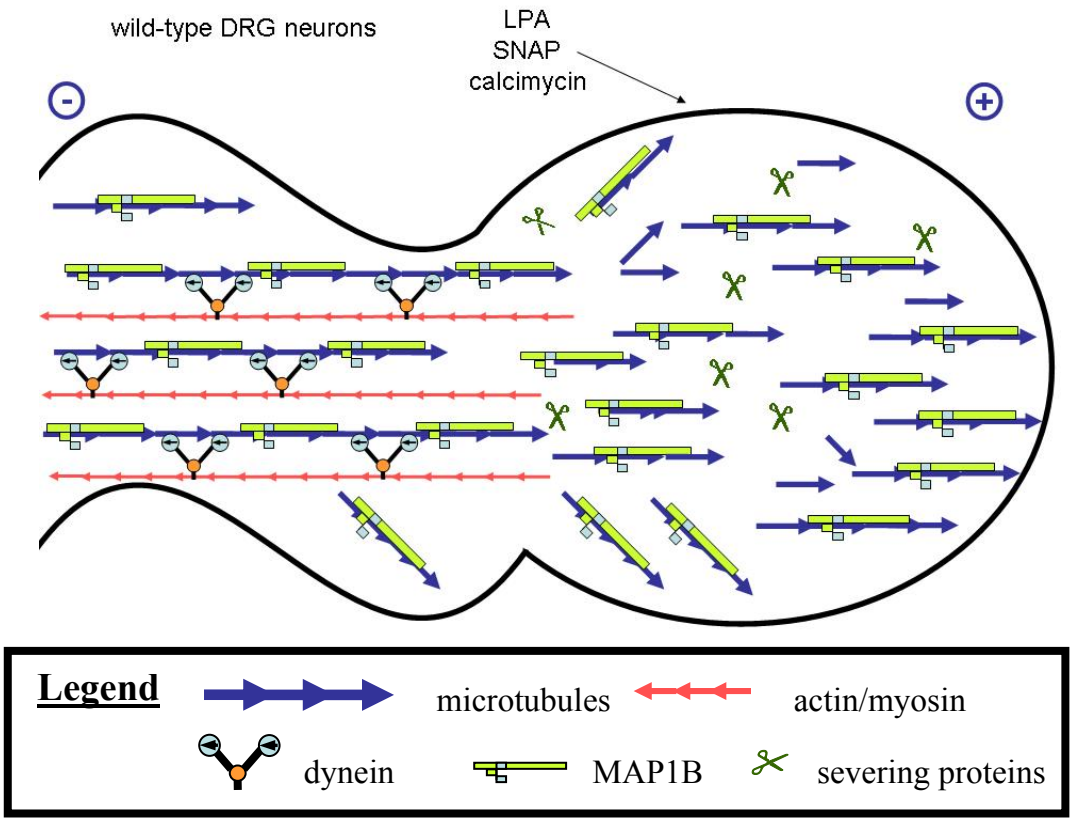

Fig. 70. Model for role of MAP1B in SNAP-, calcimycin- and LPA-induced axon retraction. According to our model in wild-type DRG neurons severing of microtubules is regulated by binding of MAP1B to them. Binding of MAP1B protects microtubules from uncontrolled cutting by spastin. We propose that SNAP, calcimycin and LPA induce modifications of MAP1B, for example by S-nitrosylation (SNAP, calcimycin), which results in a conformational change of MAP1B characterized by enhanced microtubule binding activity. Association of MAP1B with microtubules above threshold level stabilizes them and further protects from cutting by severing proteins. Thus, the number of short highly mobile microtubules is reduced and reaches a critical point. Overstabilized microtubules can not undergo reorganization, resulting in the growth cone arrest and growth cone collapse. As a consequence of the shortening of the axon it adopts a coiled and bundled configuration. In addition, binding of MAP1B to microtubules can affect dynein forces or increase acto-myosin contractility. It is also potential that the Rho/ROCKpathway is stimulated parallel inducing rearrangements of actin filaments. Another possibility is that acto-myosin forces are the primary target and MAP1B plays a role as a signal transducer linking an induced acto-myosin contraction to microtubules. Upon stimulation by actin-myosin forces MAP1B binding to microtubules increases, resulting in their overstabilization and axon retraction. In MAP1B-/- DRG neurons SNAP, calcimycin and LPA do not affect stabilization of microtubules or at least do not induce overstabilzation due to the lack of MAP1B, the functions of which can not be overtaken by other MAPs. Thus retraction is not observed (adapted from Yu et al., 2008).

It is still an open question whether the increased activity of the Rho/ROCK pathway and acto-myosin contractility, which were shown to be involved in LPA-, calcimycin- and SNAP-induced axon retraction, are the cause or consequence of MAP1B binding to

microtubules. It was shown that in MAP1B-/- DRG neurons LPA-induced retraction and backward retreat of microtubules was impaired, whereas growth cone collapse, involving actin rearrangements, was not affected and was prevented by inhibition of myosin with blebbistatin (Bouquet et al., 2007). In addition, inhibition of ROCK with Y27632 or inhibition of myosin with blebbistatin abolished LPA-induced microtubule rearrangement and neurite retraction in mouse embryonic cortical neurons (Fukushima and Morita, 2006). It is proposed that LPA interacts with G_{13} stimulating the Rho/ROCK pathway resulting in actin polymerization. In addition, LPA-induced Rho/ROCK pathway activates GSK3, leading to phosphorylation of MAPs and disorganization of microtubules (Fukushima, 2004). These studies suggest that actin is the primary target of LPA-signalling and MAP1B plays a role as a signal transducer linking LPA-induced acto-myosin contraction to microtubules, resulting in their overstabilization and formation of sinusoidal bundles and axon retraction (Fig. 71). On the other hand, I can not exclude that MAP1B-dependent overstabilization of microtubules and activation of the Rho/ROCK pathway are triggered paraller and none of them works upstream the other. Thus, observed retraction might be a result of combined acto-myosin contraction and microtubule overstabilization. Similar mechanism might be involved in calcimycin- and SNAP-induced retraction. NO might activate direct the Rho/ROCK pathway by S-nitrosylation of Rho or ROCK, or indirect by S-nitrosylation of other effectors that influence the Rho/ROCK pathway. Alternatively NO can trigger postranslational modification of the Rho/ROCK pathway effectors other than S-nitrosylation. It was found that NO induced S-gluthationylation of Rho-GDIβ, which as I mentioned stabilized Rho in an inactive GDP-bound form (Townsend et al., 2006), but the effects of this modification on Rho-GDIβ function is not clear. One possibility is that S-gluthationylation of Rho-GDIβ results in its inhibiton and activation of Rho. Most likely NO-stimulated acto-myosin contractility is not triggered via cGMP pathway, since it was shown that PKG phosphorylates RhoA at Ser188 resulting in its inhibition (Sauzeau et al., 2000; Rolli-Derkinderen et al., 2005). For example it was observed that NO-induced vasodilation of rat aorta involves cGMP-dependent inhibition of Rho (Chitaley and Webb, 2002). Thus, the mechanism by which NO stimulates acto-myosin contraction should be further investigated.

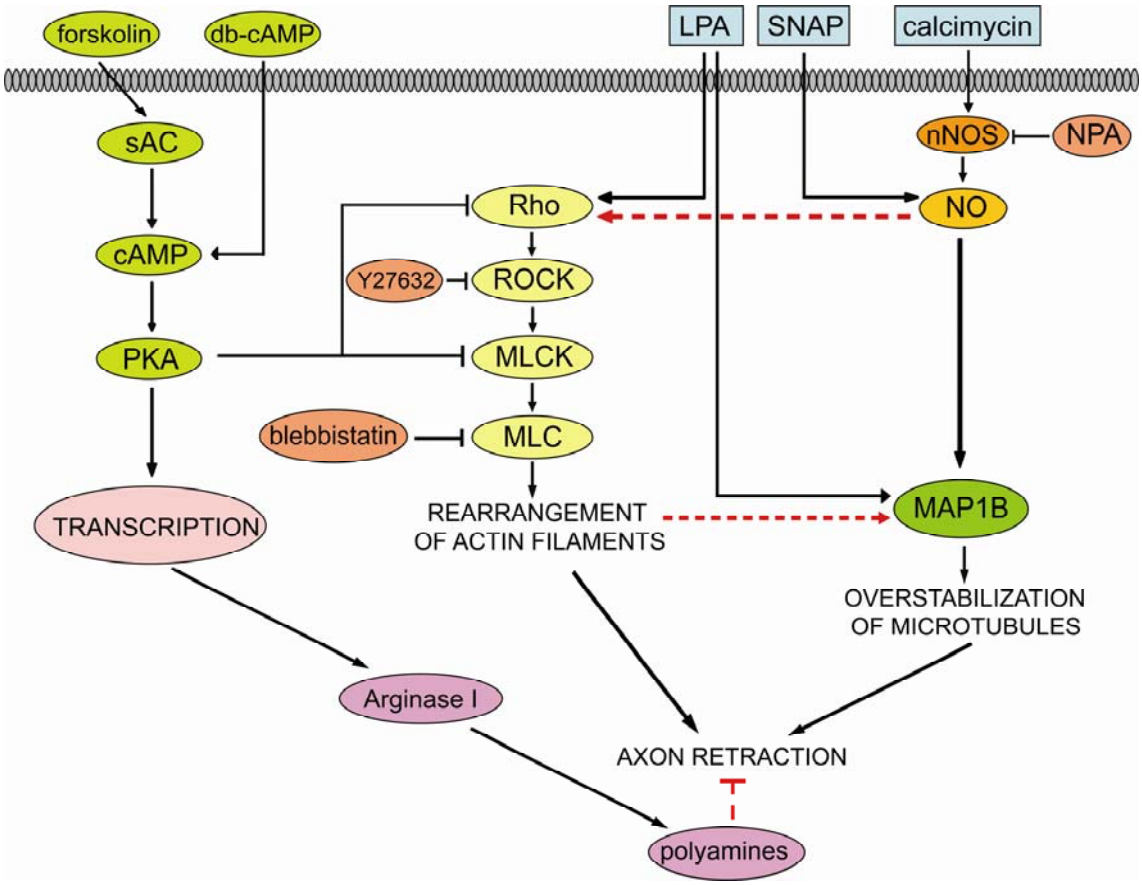

Fig. 71. Model for MAP1B-mediated axon retraction. SNAP, calcimycin and LPA induce MAP1B-dependent axon retraction. I and others (Stroissnigg et al., 2007) provide evidence that each of them increases microtubule binding activity of MAP1B. Calcimycin increases the level of Ca^{2+}, leading to activation of nNOS and enhanced production of NO. NO S-nitrosylates MAP1B increasing its affinity to microtubules and their overstabilization. Inhibition of nNOS with NPA prevents retraction induced by calcimycin. Parallel, RhoA is stimulated, activating further ROCK and MLCK. MLCK phosphorylates MRLC at Ser19 and Thr18, activates myosin and induces rearrangements of actin filaments. Another possibility is that acto-myosin forces are the primary target and MAP1B plays a role as a signal transducer linking an induced acto-myosin contraction to microtubules without direct activation by SNAP, calcimycin and LPA (red interrupted arrow). Upon stimulation by actin-myosin forces MAP1B binding to microtubules increases, resulting in their overstabilization and axon retraction. SNAP-, calcimycin- and LPA-induced retraction can be prevented by inhibition of ROCK and myosin by Y27632 and blebbistatin, respectively. The mechanism by which SNAP and calcimycin stimulate the Rho/ROCK pathway is still unknown (red interrupted arrow). NO might activate direct the Rho/ROCK pathway by S-nitrosylation of Rho or ROCK, or indirect by S-nitrosylation of other effectors that can influence the Rho/ROCK pathway. In addition, stimulation of cAMP, by application of di-butryl-cAMP (db-cAMP) or forskolin, which induces production of cAMP by soluble adenyl cyclase (sAC), partially prevents retraction induced by SNAP and calcimycin. cAMP activates PKA, which phosphorylates ROCK and MLCK, resulting in their inhibition and prevention of axon retraction. Moreover, cAMP might abolish retraction by upregulated expression of Arginase I and increased synthesis of polyamines, as it was shown to be the case in the overcoming the inhibitory properties of myelin. Polyamines were shown to affect microtubule polymerization and organization (Banan et al., 1998), and thus they might prevent reorganization of cytoskeleton induced by SNAP, calcimycin, or LPA (adapted from Filbin, 2003).

PART III - ROLE OF MAP1B AND CDK5 IN LAMININ SIGNALLING PATHWAY

RESULTS

Laminin induces different morphology of wild-type and MAP1B-/- DRG neurons

The extracellular milieu, in which axons have to grow, composes of many adhesive substrates, which promote elonagation and branching, for example laminin, collagen, tenascin, fibronectin and vitronectin. Information from the surrounding environment has to be translated into intracellular signals that act on the cytoskeleton directly or indirectly by modulation of cytoskeleton-associated proteins, resulting in extension of axons. Both microtubules and microfilaments are involved in directed growth cone migration. Microfilaments play a main role in formation of filopodia and lamellipodia, whereas microtubules are involved in elongation of the axon. Stability and assembly of microtubules are regulated by MAPs. There is considerable evidence indicating a role of MAP1B and tau in formation of axons. MAP1B and tau activity is controlled by phosphorylation (DiTella et al., 1996; Edelmann et al., 1996; Takei et al., 1997).

It was shown that laminin induced activation of cdk5 and increased mode I phosphorylation of MAP1B (DiTella et al., 1996). Activation of cdk5 was regulated by expression and distribution of p35, which is a brain-specific activator of cdk5 (Paglini et al., 1998).

It was also observed that DRG neurons from wild-type and MAP1B-/- mice show a different morphology when grown on laminin coated surfaces. Wild-type DRG neurons extended usually long, straight axons with only a few branches that covered a large area, whereas MAP1B-/- DRG neurons had wavy axons with many branches and covered a smaller surface (Bouquet et al., 2004). The number of branching points per main neurite was two-fold higher in case of MAP1B-/- neurons than in wild-type neurons (Bouquet et al., 2004). I found that the neurons showed these different morphologies only when they were grown on coverslips coated with both poly-L-lysine and laminin. When MAP1B-/- and wild-type DRG neurons were grown on coverslips coated with poly-L-lysine only, they were indistinguishable from one another. Neurons extended long axons, which were coiled rather than straight (Fig. 72). In addition, neuritic extension appeared between 24 and 48h when DRG neurons were grown on

poly-L-lysine, whereas DRG neurons cultured on coverslips coated with poly-L-lysine and laminin showed advanced processes within 20-24h after plating. It seems that laminin signals through a pathway that involves MAP1B and lack of MAP1B triggers branching in DRG neurons. Thus, I investigated the role of MAP1B during laminin-promoted axonal growth using DRG neurons from wild-type and MAP1B-/-neurons.

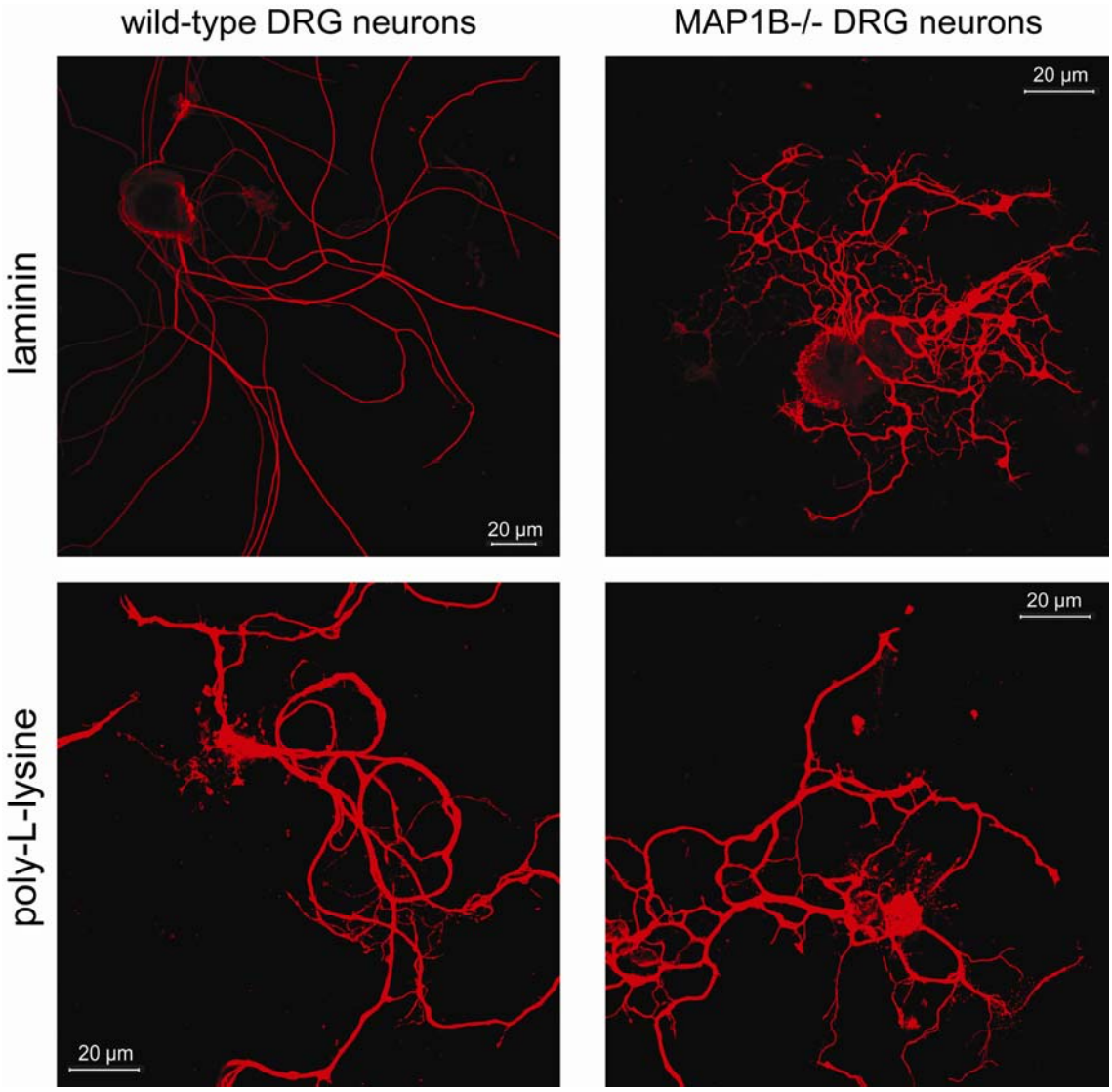

Fig. 72. Laminin induces different morphology of regenerating wild-type and MAP1B-/- DRG neurons. DRG neurons from wild-type and MAP1B-/- mice were grown on coverslips coated with poly-L-lysine and laminin or on coverslips coated with poly-L-lysine only, fixed with 4% PFA, stained for tubulin, and analyzed by confocal microscopy.

Axon retraction induced by roscovitine is MAP1B-dependent

Since it was shown that inhibition of cdk5 with antisense oligonucleotides reduces elongation of axons and decreases phosphorylation of MAP1B (DiTella et al., 1996), we inhibited cdk5 with roscovitine to see whether it has an influence on growth of axons from wild-type and MAP1B-/- DRG neurons grown on laminin. Roscovitine is an olomoucine-related purine flavopiridol, and is an selective inhibitor for the kinase activity of cdk1, cdk2, cdk5, and cdk7, but is a poor inhibitor for cdk4 and cdk6. Roscovitine competes with ATP at the ATP binding site of the kinase leading to inhibition of the kinase activity. Adult DRG neurons from wild-type and MAP1B-/- mice were grown on poly-L-lysine and laminin coated coverslips. After 20-24h cells were treated with 50µM roscovitine for 1h, with 3µl of DMSO for 1h (a solvent control), or were left untreated, fixed and stained for tubulin and MAP1B HC as a control. Application of solvent (DMSO) did not influence the morphology of the neurons, the level of retracted neurons was comparable to the level in case of untreated cells (not shown). Approximately 48% of wild-type neurons showed retraction hallmarks (sinusoidal bundles along axonal shaft, retraction bulb and trailing remnant) compared to 1% when cells were treated with DMSO only (Fig. 73). In contrast, only 21% of MAP1B-/- DRG neurons retracted in response to roscovitine treatment (when cells were treated with DMSO about 3% neurons showed hallmarks of retraction). Additionally, I compared the behaviour of wild-type and MAP1B-/- DRG neurons after inhibition of cdk5 using time-lapse microscopy. Cells were cultured for 20-24h and then were monitored for 45min prior to application of roscovitine. After the first 15min of observation, half of the medium in the dish was exchanged with fresh medium to exclude any influence of medium change per se on axonal behaviour (-30'), then observation was continued for another 30min. Without any stimulation, axons from both types of neurons elongated at the same rate, and exchange of medium did not affect axon growth. Addition of 50µM roscovitine to wild-type DRG neurons (time point 0' on graphs) induced growth cone collapse within 3-5min followed by retraction with formation of sinusoidal bends, reminiscent of the sinusoidal microtubule bundles revealed by immunofluorescences (Fig. 74). After addition of roscovitine to MAP1B-/- DRG neurons I did not observe growth cone collapse and neurites continued elongation at the same rate as before treatment (Fig. 74).

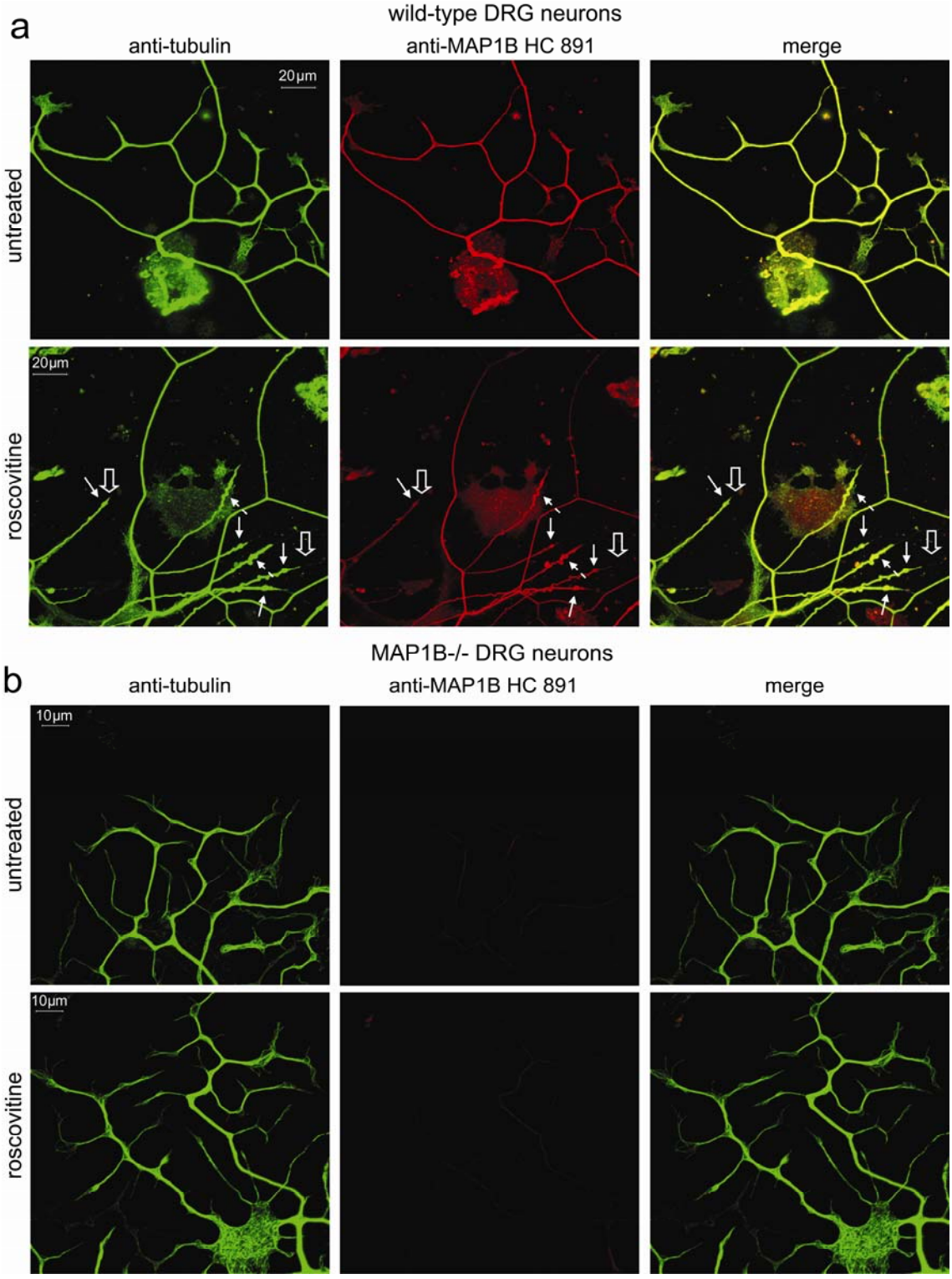
a
wild-type DRG neurons
anti-tubulin
anti-MAP1B HC 891
merge
untreated
roscovitine
20µm
20µm
b
MAP1B-/- DRG neurons
anti-tubulin
anti-MAP1B HC 891
merge
untreated
roscovitine
10µm
10µm

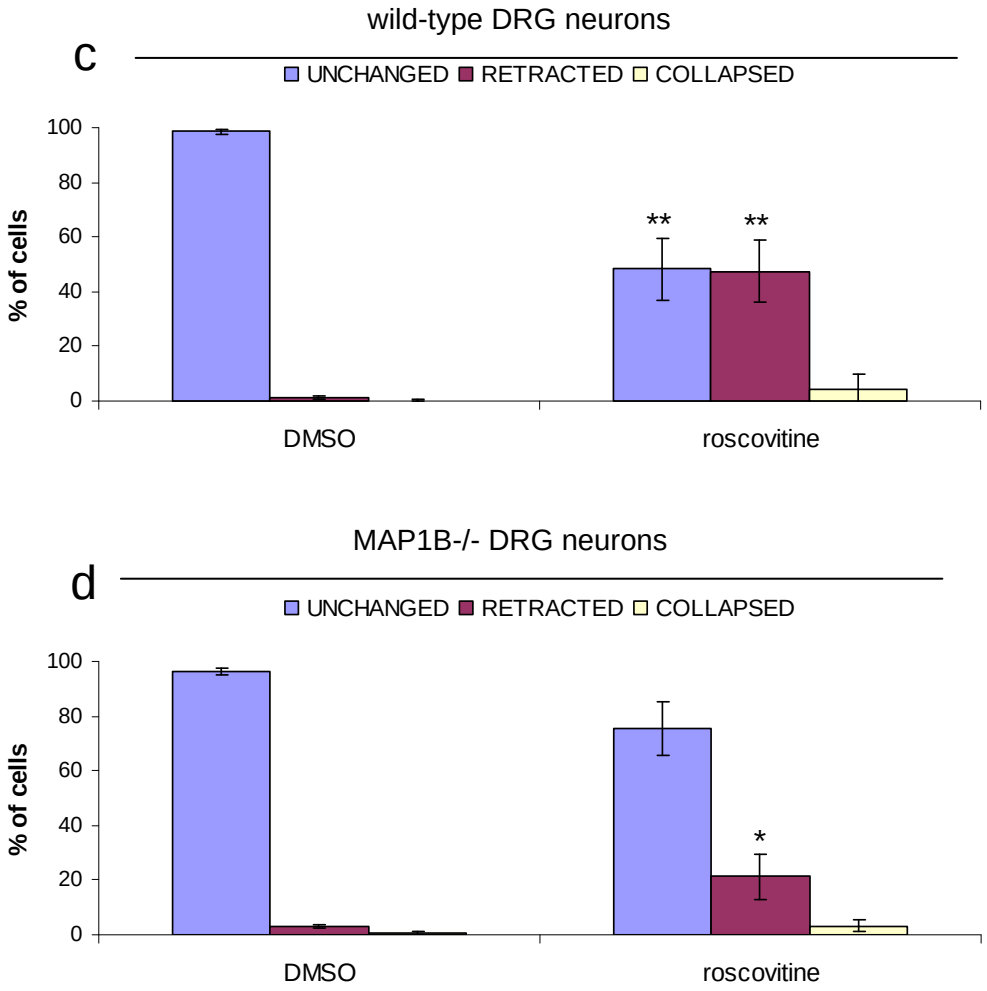

Fig. 73. Roscovitine-induced axon retraction is impaired in MAP1B-/- DRG neurons. DRG neurons from wild-type and MAP1B-/- mice were grown on coverslips coated with poly-L-lysine and laminin, were treated with 50µM roscovitine for 1h or with 3µl of DMSO for 1h, fixed with 4% PFA, stained for tubulin and MAP1B HC. (a, b) Representative micrographs of axons from wild-type (a) and MAP1B-/- (b) DRG neurons. Wild-type DRG neurons retracted in response to roscovitine treatment with all characteristic hallmarks (sinusoidal microtubules (interrupted arrow), retraction bulb (filled arrows), trailing remnant (open arrow)). (c, d), for quantitative analysis, approximately 100 cells in each of 5 independent (c) or 3 (d) experiments were assessed for microtubule configuration which was classified as unchanged, retracted or collapsed. Error bars represent standard deviations. Asterisks indicate that the values for cells treated with roscovitine were significantly different from corresponding values of neurons treated with DMSO (*, $p<0.05$, and **, $p<0.001$).

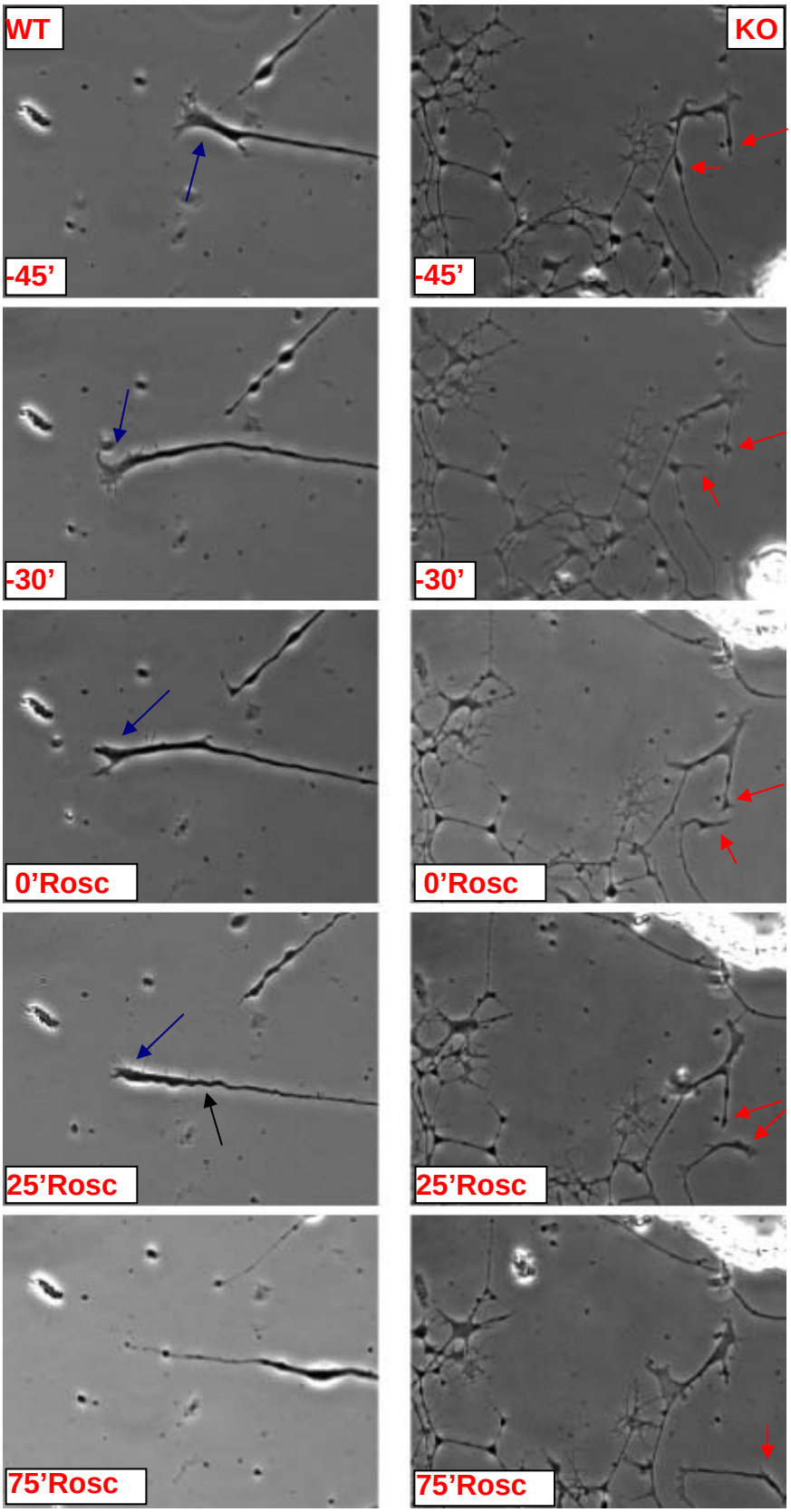

Fig. 74. Response of wild-type and MAP1B-/- neurons to roscovitine treatment. Adult wild-type (WT) and MAP1B-/- (KO) DRG neurons were grown for 24h on coverslips coated with poly-L-lysine and laminin. Images were recorded with 5min intervals and selected images taken at the indicated times are shown. After 15min of observation the medium was changed to determine if changing the medium does have an influence on growing axons (-30'), and

observation was continued for 30min. No retraction or retraction and reextension of axon was observed after the medium exchange. Stack taken 30min after changing the medium is shown, as indicated, the pictures from time between these two times points are not shown. After 30min 50µM roscovitine was added and recording was continued for 2h 30min with 5min intervals between images. Application of roscovitine induced growth cone collapse (blue arrows) within 3-5min followed by axon retraction with sinusoidal bundles (black arrow) in wild-type neurons. Axons retracted completely after 60-75min and no reextension was observed. Axons of MAP1B-/- neurons did not retract and continued growth (protrusion of filopodia by axons is indicated by red arrows).

Axon retraction induced by roscovitine involves ROCK and myosin

As axon retraction induced by inhibition of cdk5 by roscovitine is MAP1B-dependent as are retractions induced by SNAP, calcimycin, or LPA and shows the same retraction hallmarks, it was interesting to see whether it involved ROCK and myosin too. To investigate involvement of ROCK, DRG neurons from wild-type and MAP1B-/- mice were grown on poly-L-lysine and laminin coated coverslips for 20-24h and then were treated with 3µl of DMSO for 1h, with 10µM Y27632 for 1h, with 50µM roscovitine for 1h, or with 10µM Y27632 for 1h followed by treatment with 50µM roscovitine for 1h. Inhibition of ROCK reduced the amount of retracted neurons from wild-type mice; 12% in comparison to 48% when cells were treated with roscovitine only (Fig. 75). In addition, pretreatment with Y27632 also decreased the number of neurons showing retracted hallmarks in case of MAP1B-/- DRG neurons (11% when compared to 21% when cells were treated with roscovitine only; Fig. 75).

To investigate involvement of myosin in axon retraction induced by inhibition of cdk5, DRG neurons from wild-type and MAP1B-/- mice were cultured as described before and treated with 100µM blebbistatin for 15min prior to treatment with 50µM roscovitine for 1h. Inhibition of myosin abolished roscovitine-induced retraction, only 10% of wild-type neurons showed the retraction phenotype in comparison to 40% when cells were treated with roscovitine only (Fig. 76). In case of MAP1B-/- DRG neurons there were no differences in the number of retracted neurons between untreated cells and cells treated with DMSO, roscovitine, blebbistatin, or blebbistatin and roscovitine. In all cases no more than 10-15% of neurons showed retraction hallmarks. This is slightly higher than what I saw in previous experiments with MAP1B-/- DRG neurons (for example, Fig. 75) and might be due to slightly diverse culture conditions (pH,

temperature) in theses experiments. In any case, roscovitine and blebbistatin were without effect.

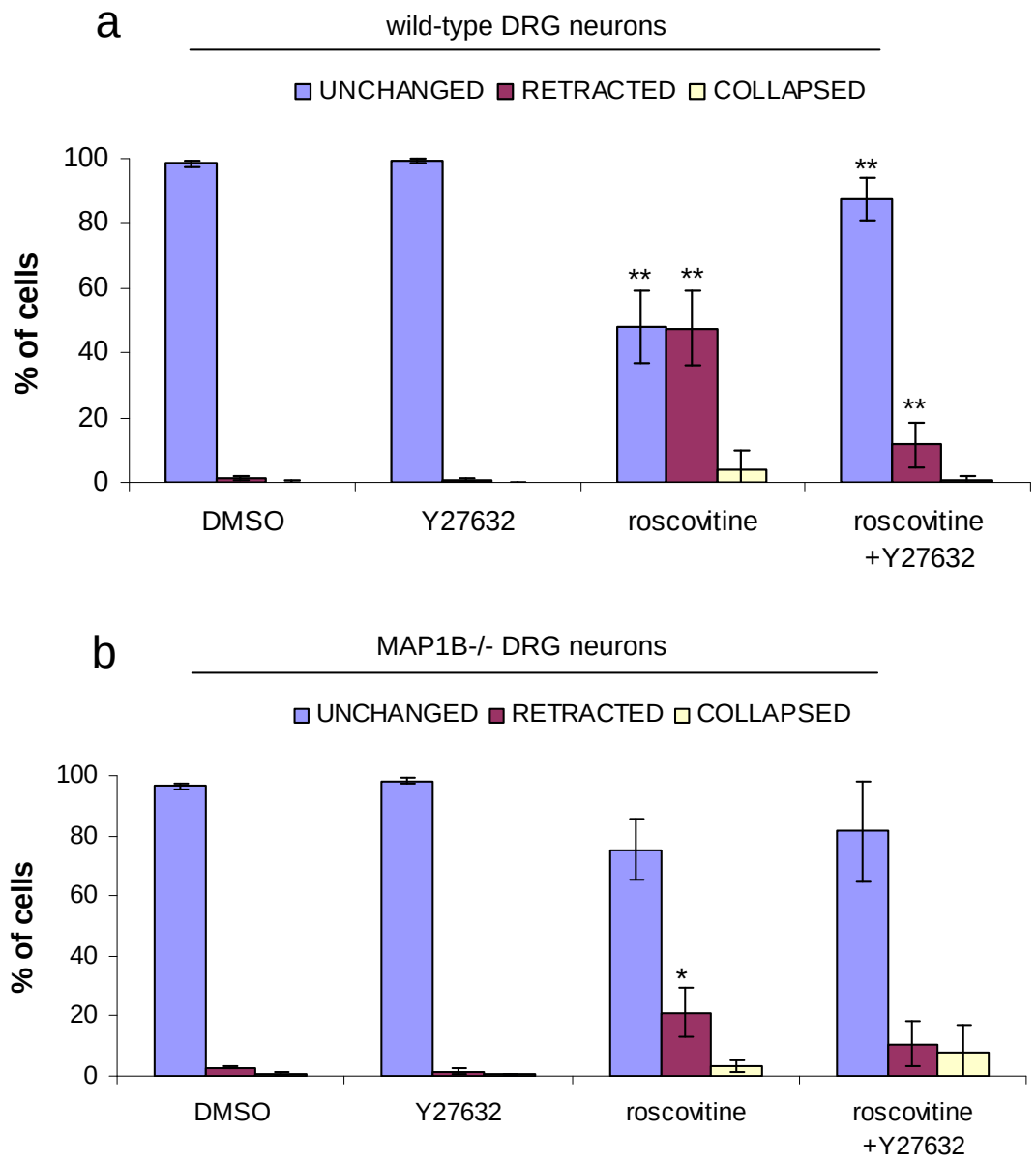

Fig. 75. Axon retraction induced by roscovitine is MAP1B- and ROCK-dependent. DRG neurons from wild-type (a) and MAP1B-/- (b) mice were grown on coverslips coated with poly-L-lysine and laminin, were treated with 3µl DMSO for 1h, with 50µM roscovitine for 1h, with 10µM Y27632 for 1h, or with 10µM Y27632 for 1h followed by 50µM roscovitine for 1h, as indicated, fixed with 4% PFA, stained for tubulin and analyzed by confocal microscopy. For quantitative analysis, approximately 100 cells in each of 5 independent (a) or 3 (b) experiments were assessed for microtubule configuration which was classified as unchanged, retracted or collapsed. Error bars represent standard deviations. Asterisks indicate that the values for cells treated with roscovitine were significantly different from corresponding values of cells treated with DMSO (solvent for roscovitine) and values for cells treated with roscovitine and Y27632 were significantly different from corresponding values of cells treated with roscovitine only (*, $p<0.05$, and **, $p<0.001$).

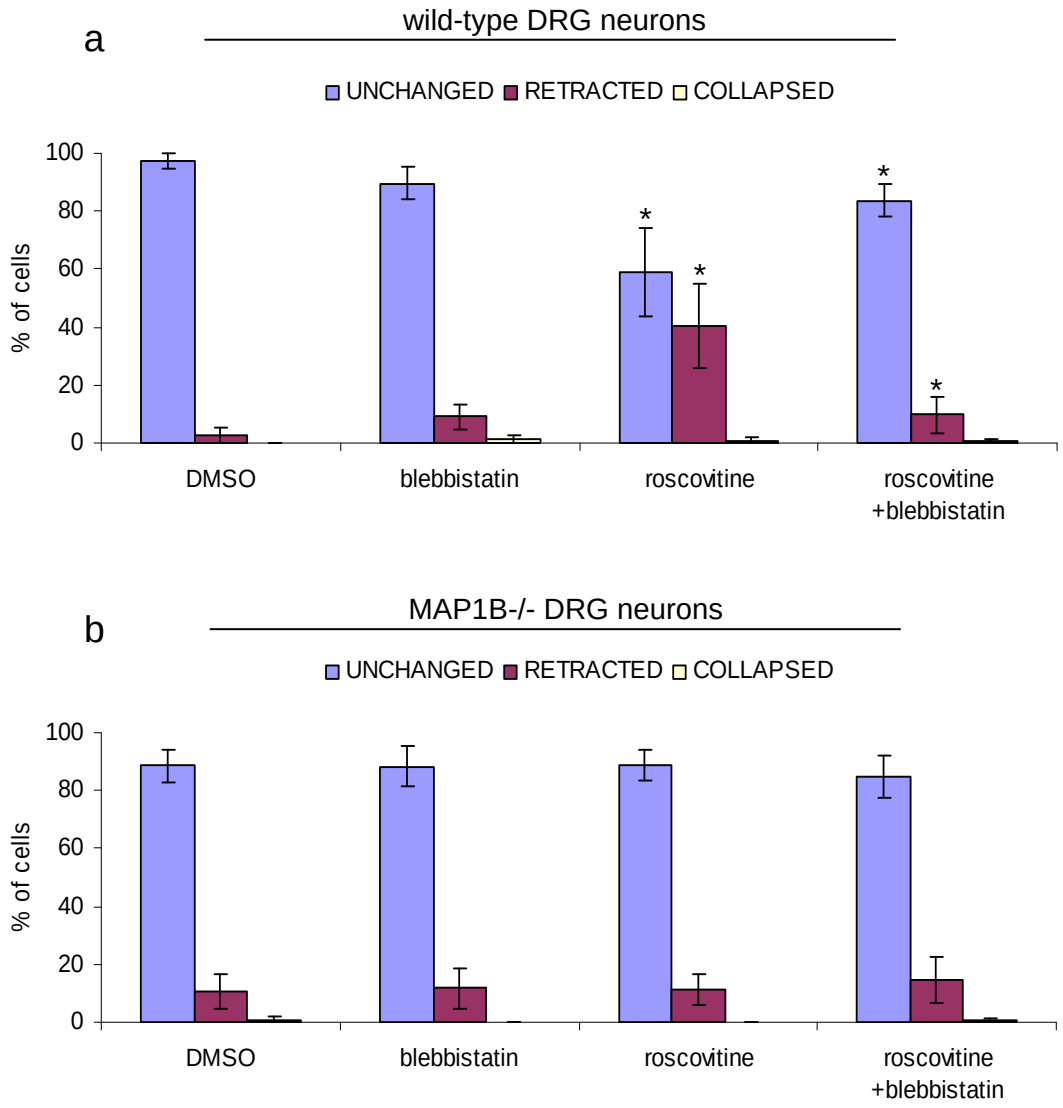

Fig. 76. Axon retraction induced by roscovitine involves myosin. DRG neurons from wild-type (a) and MAP1B-/- (b) mice were grown on coverslips coated with poly-L-lysine and laminin, were treated with 3µl DMSO for 1h, with 50µM roscovitine for 1h, with 100µM blebbistatin for 15min, or with 100µM blebbistatin for 15min followed by 50µM roscovitine for 1h, as indicated, fixed with 4% PFA, stained for tubulin and analyzed by confocal microscopy. For quantitative analysis, approximately 100 cells in each of 3 independent (a) or 4 (b) experiments were assessed for microtubule configuration which was classified as unchanged, retracted or collapsed. Error bars represent standard deviations. Asterisks indicate that the values for cells treated with roscovitine were significantly different from corresponding values of cells treated with DMSO (solvent for roscovitine) (*, $p<0.05$).

These results demonstrated that ROCK and myosin are necessary for axon retraction induced by roscovitine. To examine if acto-myosin forces are enhanced in response to roscovitine I decided to study the level of monophosphorylation of MRLC in response to roscovitine treatment in N2a neuroblastoma cells. As I mentioned in second part of my thesis myosin II activity is stimulated by phosphorylation of MRLC at Ser19 and

Thr18 (Somlyo and Somlyo, 2003). I observed an increased level of monophosphorylated MRLC after treatment with roscovitine, 186% of values from untreated cells (Fig. 77), suggesting activation of myosin by roscovitine.

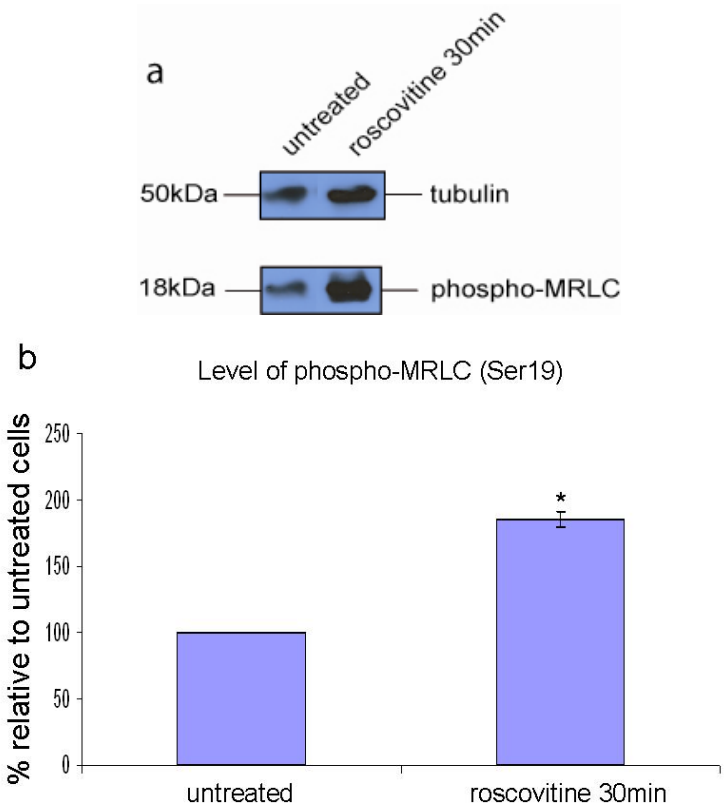

Fig. 77. Roscovitine-induced axon retraction involves activation of myosin. (a) N2a cells were grown on 6cm plates, and either were left untreated, or treated with 50µM roscovitine for 30min, as indicated. Cell lysates were fractioned by SDS-PAGE and analyzed by immunoblotting using anti-Ser19 antibody (phospho-MRLC). (b), bands were quantified using the Quanti Scan 3 software. For quantitative analysis, blots from 2 independent experiments were scored. In each treatment the values show levels of phosphorylation at Ser19 normalized to tubulin that was used as a loading control. Error bars represent standard deviations. Asterisks indicate that the level of phospho-MRLC from lysates of cells treated with roscovitine for 30min was significantly different from corresponding value of untreated cells (*, $p<0.05$).

Axon retraction induced by roscovitine does not involve nNOS activation

We were also interested if axon retraction induced by roscovitine involves activation of nNOS, NO and S-nitrosylation. Thus, DRG neurons from wild-type and MAP1B mice were cultured as described before, treated with 300µM NPA for 1h to inhibit nNOS and then treated with 50µM roscovitine for 1h. Inhibition of nNOS did not affect retraction induced by roscovitine in wild-type DRG neurons, 58% of neurons showed retracted

morphology when compared to 64% when cells were treated with roscovitine only (Fig. 78). Likewise, application of NPA prior to treatment with roscovitine did not influence the response of MAP1B-/- DRG (22% of neurons showed retraction hallmarks when treated with NPA followed by roscovitine compare to 21% when cells were treated with roscovitine only).

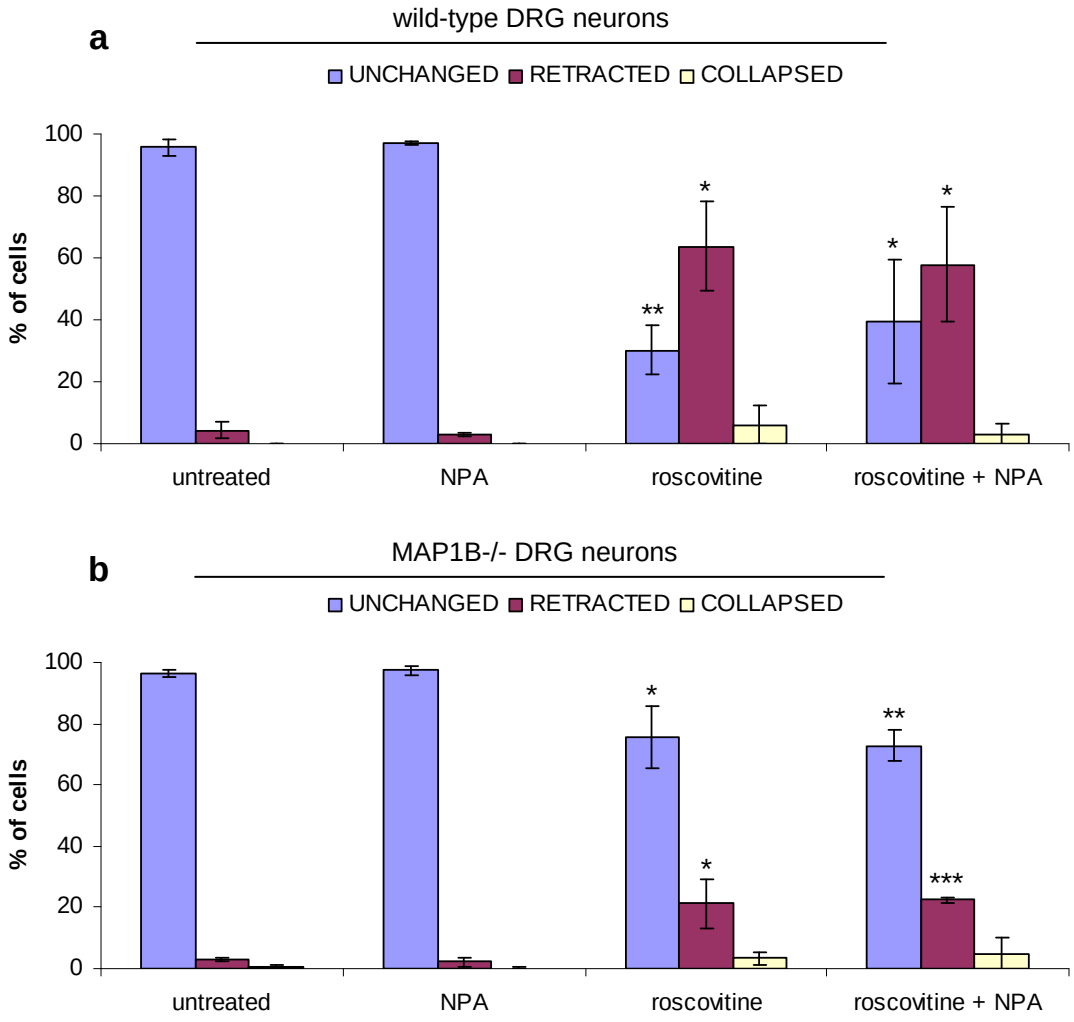

Fig. 78. Axon retraction induced by roscovitine does not involve nNOS. DRG neurons from wild-type (a) and MAP1B-/- (b) mice were grown on coverslips coated with poly-L-lysine and laminin, were left untreated, or were treated with 50µM roscovitine for 1h, with 300µM NPA for 1h, or with 300µM NPA followed by 50µM roscovitine for 1h, as indicated, fixed with 4% PFA, stained for tubulin and analyzed by confocal microscopy. For quantitative analysis, approximately 100 cells in each of 3 independent experiments were assessed for microtubule configuration which was classified as unchanged, retracted or collapsed. Error bars represent standard deviations. Asterisks indicate that the values for cells treated with roscovitine or with NPA followed by treatment with roscovitine were significantly different from corresponding values of untreated neurons (*, $p<0.05$ the same; **, $p<0.005$ and ***, $p<0.001$).

Axon retraction induced by roscovitine involves GSK3β

It was observed that inhibition of cdk5 with olomoucine increased activity of GSK3β in the axoplasm extruded from squid giant axons (Morfini et al., 2004). As mentioned above, GSK3β phosphorylates MAP1B in mode I. It is possible that inhibition of cdk5 leads to increased phosphorylation of MAP1B by GSK3β, resulting in increased binding of MAP1B to microtubules and axon retraction. To examine the potential involvement of GSK3β, wild-type DRG neurons were cultured as described before and GSK3β was inhibited with 20mM LiCl, which was applied for 14-16h before treatment with roscovitine. Inhibition of GSK3β reduced the number of neurons showing retraction hallmarks in response roscovitine, 24% compared to 57% when cells were treated with roscovitine only, and this difference was statistically significant (Fig. 79). In addition, neurons treated with LiCl grow shorter axons with more branches than untreated cells (not shown).

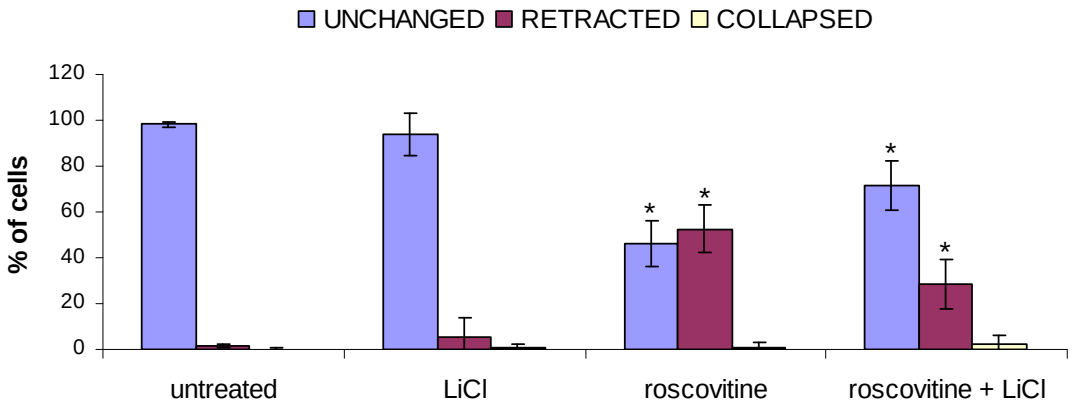

Fig. 79. Inhibition of GSKβ partially abolishes axon retraction induced by roscovitine. Wild-type DRG neurons were grown on coverslips coated with poly-L-lysine and laminin, were left untreated, or were treated with 50μM roscovitine for 1h, with 20mM LiCl over night (14-16h), or with 20mM LiCl over night (14-16h) followed by 50μM roscovitine for 1h, as indicated, fixed with 4% PFA, stained for tubulin and analyzed by confocal microscopy. For quantitative analysis, approximately 100 cells in each of 3 independent experiments were assessed for microtubule configuration which was classified as unchanged, retracted or collapsed. Error bars represent standard deviations. Asterisks indicate that the values for cells treated with roscovitine were significantly different from corresponding values of untreated neurons and the values from cell treated with LiCl followed by roscovitine were significantly different from corresponding values of cells treated with roscovitine only (*, $p<0.05$).

Axon retraction induced by roscovitine does not involve depolymerization of microtubules

It seems that roscovitine, similar to SNAP, calcimycin, and LPA, induces backward retreat of microtubules resulting in their coiled and bundled configuration, rather than their depolymerization. To examine whether depolymerization does not take place like in case of SNAP-, calcimycin- and LPA-induced neurite retraction, wild-type and MAP1B-/- DRG neurons were grown on poly-L-lysine and laminin coated coverslips for 20-24h, treated with 3nM taxol for 30min, with 50µM roscovitine for 1h, or with 3nM taxol for 30min followed by treatment with 50µM roscovitine for 1h, or were left untreated.

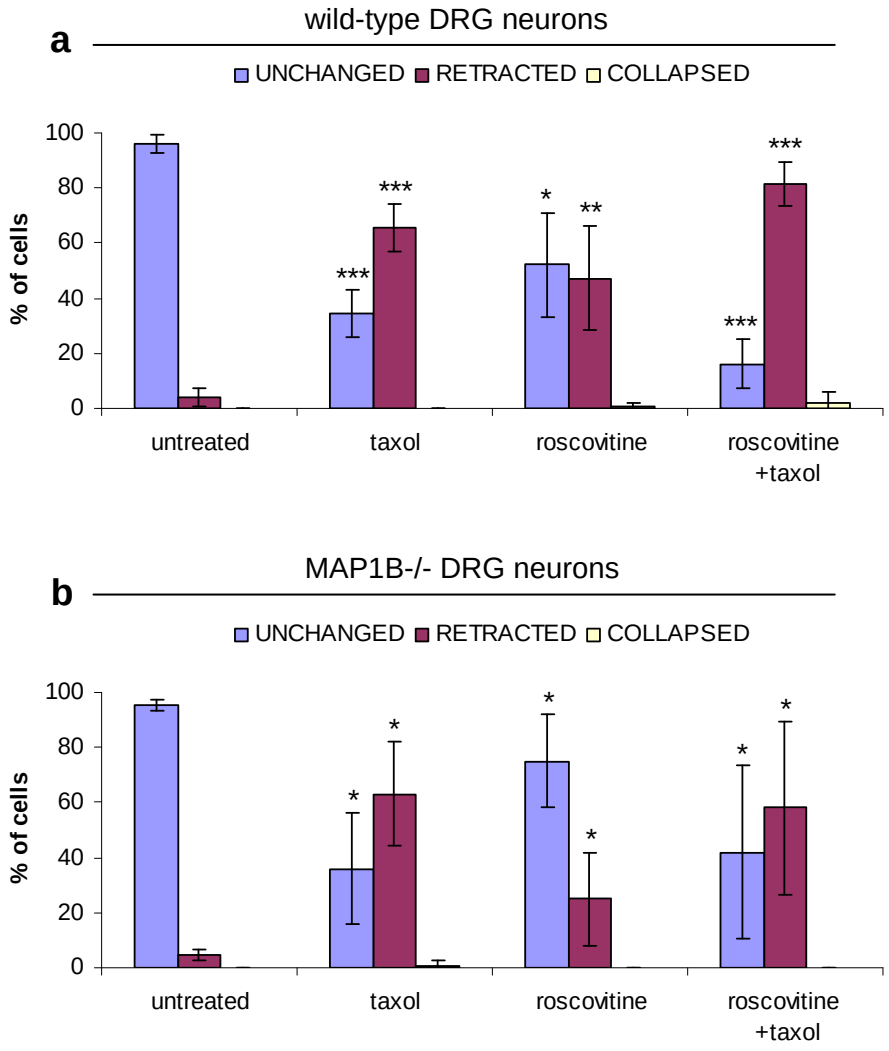

Fig. 80. Axon retraction induced by roscovitine does not involve depolymerization of microtubules. DRG neurons from wild-type (a) and MAP1B-/- (b) mice were grown on coverslips coated with poly-L-lysine and laminin, were left untreated, or were treated with

50µM roscovitine for 1h, with 3nM taxol for 30min, or with 3nM taxol for 30min followed by 50µM roscovitine for 1h, as indicated, fixed with 4% PFA, stained for tubulin and analyzed by confocal microscopy. For quantitative analysis, approximately 100 cells in each of 4 independent experiments were assessed for microtubule configuration which was classified as unchanged, retracted or collapsed. Error bars represent standard deviations. Asterisks indicate that the values for cells treated with roscovitine, with taxol and with taxol followed by treatment with roscovitine were significantly different from corresponding values of untreated neurons (*, $p<0.05$; **, $p<0.01$ and ***, $p<0.001$).

As in case of LPA, calcimycin and SNAP, taxol pretreatment did not prevent axon retraction induced by roscovitine in wild-type DRG neurons, but rather increased it, 82% of neurons showing retraction hallmarks when compared to 47% when cells were treated with roscovitine only (Fig. 80). Approximately 58% and 63% of MAP1B-/- DRG neurons retracted when treated with taxol or with taxol and roscovitine, respectively (Fig. 80).

Roscovitine and LPA induce retraction only in the presence of laminin

Since DRG neurons grown on laminin showed a different morphology than DRG neurons grown on poly-L-lysine, it was interesting to investigate if roscovitine has an influence on the morphology of neurons grown on poly-L-lysine only. Wild-type DRG neurons were cultured on coverslips coated with poly-L-lysine and laminin or on poly-L-lysine only, treated with 50µM roscovitine for 1h or were left untreated. When cells were grown on poly-L-lysine only, 9% of cells showed retraction hallmarks in response to roscovitine treatment, compared to 5% when neurons were untreated (Fig. 81). This is in contrast to 35% of retracted neurons in response to application of roscovitine when cells were grown on poly-L-lysine and laminin coated coverslips.

SNAP, calcimycin and LPA induced retractions in wild-type DRG neurons cultured on coverslips covered by poly-L-lysine and laminin. As response of DRG neruons to treatment with roscovitine was impaired when cells were grown on poly-L-lysine only, I decided to examine if LPA induces retraction when neurons are grown on poly-L-lysine. Wild-type DRG neurons were cultured on coverslips coated with poly-L-lysine and laminin or poly-L-lysine only, treated with 10µM LPA or were left untreated. I found that levels of cells showing retraction hallmarks were almost the same in case of untreated neurons and neurons treated with LPA when cells were grown in the absence of laminin. In case of DRG neurons cultured on coverslips coated with poly-L-lysine only approximately 13% of cells retracted in response to LPA treatment, whereas in

case of cells cultured on coverslips coated with poly-L-ysine and laminin about 30% showed retraction hallarks (Fig. 82). These results suggest that laminin signalling, in addition to MAP1B, plays an important role in mediating axon retraction.

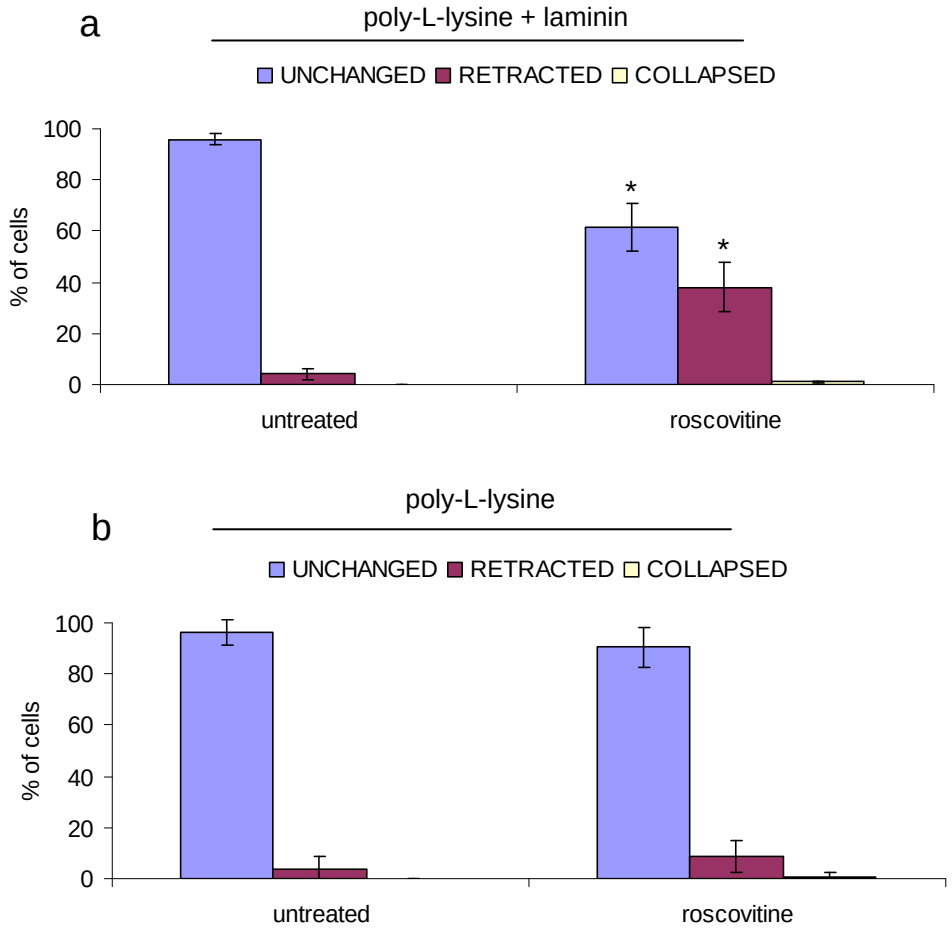

Fig. 81. Axon retraction induced by roscovitine is laminin-dependent. DRG neurons from wild-type mice were grown on coverslips coated with poly-L-lysine and laminin (a) or with poly-L-lysine only (b) for 24h or 48h, respecively, were left untreated, or were treated with 50µM roscovitine for 1h, as indicated, fixed with 4% PFA, stained for tubulin and analyzed by confocal microscopy. For quantitative analysis approximately 50 cells in each of 3 independent experiments were assessed for microtubule configuration which was classified as unchanged, retracted or collapsed. Error bars represent standard deviations. Asterisks indicate that the values for cells treated with roscovitine were significantly different from corresponding values of untreated neurons (*, $p<0.05$).

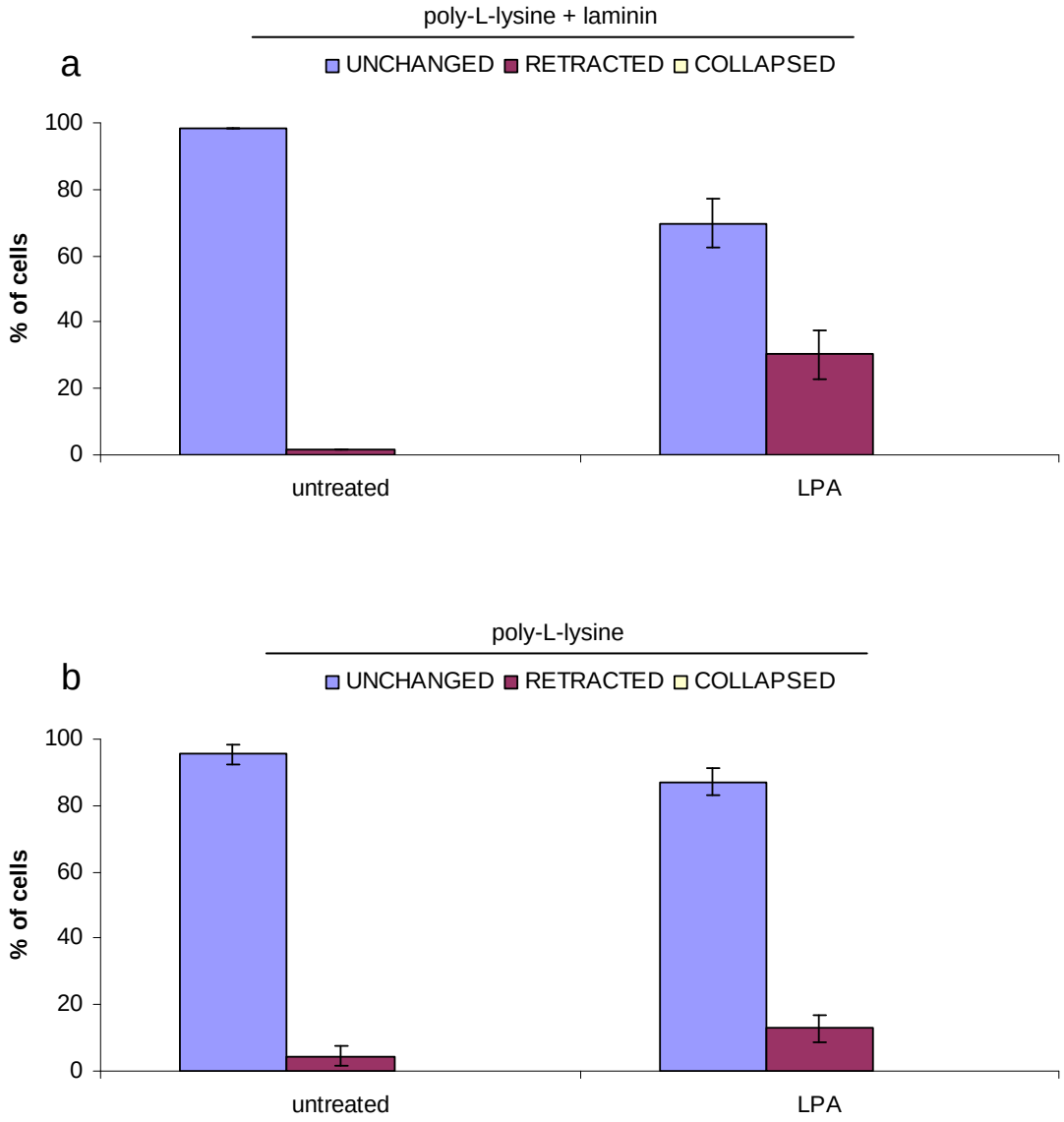

Fig. 82. Axon retraction induced by LPA is laminin-dependent. DRG neurons from wild-type mice were grown on coverslips coated with poly-L-lysine and laminin (a) or with poly-L-lysine only (b) for 24h or 48h, respecively, were left untreated, or were treated with 10µM LPA for 30min, as indicated, fixed with 4% PFA, stained for tubulin and analyzed by confocal microscopy. For quantitative analysis approximately 50 cells in each of 2 independent experiments were assessed for microtubule configuration which was classified as unchanged, retracted or collapsed. Error bars represent standard deviations.

Roscovitine induces increased microtubule binding by full length MAP1B

In previous experiments I observed that SNAP and LPA increased binding of MAP1B to microtubules in non-neuronal cells. A construct encoding full length MAP1B was

overexpressed in PtK2 cells and MAP1B was predominantly found in the cytoplasm of untreated cells, while treatment with SNAP and LPA increased binding of MAP1B to microtubules. I also examined the effect of roscovitine on MAP1B microtubule binding properties by expressing myc-tagged full length MAP1B in PtK2 cells. As in previous experiments, in most of untreated cells MAP1B was found localized in the cytoplasm and only in 4% of cells MAP1B was bound to microtubules. In cells treated with roscovitine, microtubular association of MAP1B increased to 26%, but no induction of microtubule reconfiguration was observed (Fig. 83). These results suggest that a potential mechanism by which roscovitine induces axon retraction is similar or even the same as the mechanism by which SNAP or LPA induce axon retraction. This mechanism involves an increase of MAP1B binding to microtubules, leading to their stabilization and retraction of neurites.

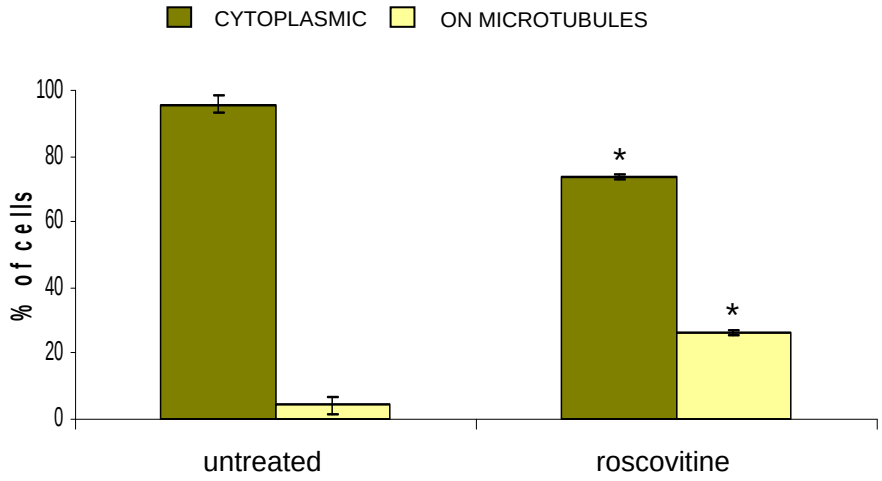

Fig. 83. Increased microtubule binding by MAP1B induced by treatment with roscovitine. PtK2 cells were transiently transfected with constructs encoding myc-tagged FL MAP1B. Before fixation, cells were left untreated, or were treated with 50μM roscovitine for 2h, as indicated. Cells were scored for localization of the ectopically expressed protein in the cytoplasm, or on microtubules by double immunofluorescence microscopy using anti-myc and anti-tubulin antibodies. For quantification, 200 cells from 4 independent transfections were assessed for microtubule binding of MAP1B. Error bars represent standard deviations. Asterisks indicate that the values for cells treated with roscovitine were significantly different from corresponding values of untreated neurons (**, $p<0.001$).

Expression of cdk5 and p35 is not altered in MAP1B-/- mice

As it was mentioned above, laminin stimulates cdk5 activity and axonal elongation by regulating the expression and subcellular localization of p35. Thus, we decided to

examine whether different response of wild-type and MAP1B-/- DRG neurons to laminin signalling is due to altered expression of p35. I stained wild-type and MAP1B-/- DRG neurons for p35 to determine its localization, but I could not see any differences. p35 staining was continuous within cell bodies and along axons, with a significant levels in the periphery of the growth cones, in both types of neurons (not shown).

We also tested expression of p35 and cdk5 in tissues from wild-type and MAP1B mice. Protein lysates from brains and DRGs from wild-type and MAP1B-/- mice were fractioned on polyacrylamide gels and analyzed by immunoblot for expression of p35 and cdk5. I did not observed any consistent differences between tissues from both types of mice in 2 separate experiments (not shown).

DISCUSSION

Laminin is an extracellular matrix protein, which modulates the extension and morphology of neurites (Kohno et al., 2005). *In vitro*, of neurite growth is stimulated both by surface-bound laminin and by soluble laminin added to the medium (Kohno et al., 2005). For example, it was shown that addition of soluble laminin into the medium stimulated branching and elongation of small-diameter collaterals in adult mouse DRG neurons (Kohno et al., 2005). How exactly the presence of laminin is translated into intracellular events is unknown. It is postulated that laminin promotes axonal growth by its interaction with integrin receptors followed by activation of the p35/cdk5 pathway and recruitment of MAP1B, which regulates microtubule dynamics (Rossino et al., 1991; Choi et al., 1994; Pigino et al., 1997; Paglini et al., 1998; Li et al., 2000). During laminin-induced axonal elongation in cerebellar macroneurons cdk5 was redistributed from the cell body to the periphery of the growth cone and expression of its activator p35 was upregulated (Pigino et al., 1997; Paglini et al., 1998). It was shown in SH-SY5Y neuroblastoma cells that laminin stimulated upregulation of p35 and activation of cdk5 by interaction with the intergrin receptors $\alpha_1\beta_1$ (Rossino, 1991; Choi, 1994; Li, 2000). Inhibition of α_1- and β_1- integrins with specific antibodies abolished laminin-induced upregulation of p35 and cdk5 activity (Li et al., 2000), and inhibition of p35 with antisense oligonucleotides prevented laminin-induced axonal elongation (Paglini, 1998). In embryonic chick retina neurons cdk5 and its activator p35 are expressed in the distal parts the growth cone, where they colocalize with mode I phosphorylated MAP1B (Hahn et al., 2005). Moreover, laminin-induced increase in axonal length and formation of minor neurites in adult rat cerebellar macroneurons was found to correlate with enhanced association of MAP1B with microtubules, whereas in neurons grown on poly-L-lysine only small amounts of MAP1B were integrated with microtubules (DiTella et al., 1996; Pigino et al., 1997). Inhibition of cdk5 suppressed elongation of neurites and reduced mode I phosphorylation of MAP1B and resulted in decreased binding of MAP1B to microtubules (Pigino et al., 1997). Application of MAP1B antisense oligonucleotides reduced extension of neurites in neurons cultured on laminin, whereas it did not influence axonal growth of cells cultured on poly-L-lysine (DiTella et al., 1996). In addition, inhibition of tau with antisense oligonucleotides had no influence on cells grown on laminin, while it abolished axon formation in neurons grown on poly-L-

lysine, suggesting role of MAP1B in laminin signalling and a role of tau in poly-L-lysine signalling (DiTella et al., 1996).

It was also observed that DRG neurons from wild-type and MAP1B-/- mice show a different morphology when grown on laminin. Wild-type DRG neurons extended usually long, straight axons with only a few branches that covered a large surface, whereas MAP1B-/- DRG neurons had curled axons with many more collaterals and covered a smaller area (Bouquet et al., 2004). The number of branch points per parent neurite was two-fold higher in MAP1B-/- DRG neurons when compared to wild-type DRG neurons (Bouquet et al., 2004). Thus, I decided to examine whether wild-type and MAP1B-/- DRG neurons show different morphology when they are cultured on another substrate. I observed that when they were grown on coverslips coated with poly-L-lysine only they did not show any difference in growth pattern. Most neurons extended long processes, which were coiled rather than straight. Moreover, DRG neurons grown on coverslips coated with poly-L-lysine and laminin showed advanced processes within 20-24h after plating, whereas in neurons grown on poly-L-lysine axon extension was observed later, between 24 and 48h. It seems that laminin promotes axonal elongation through a pathway that involves MAP1B and lack of MAP1B alters laminin signalling resulting in increased branching in DRG neurons. In addition, it seems that axonal formation is not altered in MAP1B-/- DRG neurons grown on laminin, but rather branching and directionality of the growth cone (Bouquet et al., 2004). This is consistent with previous results showing that inhibition of MAP1B with antisense oligonuclotides did not abolish formation of axons in cerebellar macroneurons grown on laminin, but altered their growth (DiTella et al., 1996). Likewise, relocalization of cdk5 stimulated by laminin was observed after axons were already formed, suggesting that laminin and cdk5 stimulate elongation of neurites rather than their formation (Paglini et al., 1998). Moreover, when embryonic chick RGC neurons were cultured from the beginning with roscovitine, an inhibitor of cdk5, axons were initially formed, but they retracted after 4h (Hahn et al., 2005).

Since it was shown that inhibition of cdk5 abolished axonal extension induced by laminin and decreases mode I phosphorylation of MAP1B (DiTella et al., 1996), I decided to examine if inhibition of cdk5 with roscovitine has an influence on growth of wild-type and MAP1B-/- DRG neurons. In case of wild-type DRG neurons about 48% of neurons retracted in response to roscovitine treatment, showing characteristic hallmarks – retraction bulb, sinusoidal bundles and trailing remnant. In MAP1B-/- DRG

neurons the response seemed to be impaired, since only 21% of neurons showed retraction morphology. These results were confirmed by time-lapse microscopy, as in wild-type DRG neurons roscovitine induced growth collapse within 3-5min, which was followed by axon retraction, while the majority of MAP1B-/- neurons did not respond and continued extend at the normal rate. Retraction was not reversible and once the growth cone collapsed it did not reextend within the time that images were taken (90min). Similarly, retraction was observed in embryonic chick RGC neurons after inhibition of cdk5 with roscovitine or with an anti-cdk5 antibody (Hahn et al., 2005). In addition, Hahn and colleagues observed that after inhibition of cdk5 mode I phosphorylated MAP1B was not detected anymore in neurons, supporting a role of MAP1B in laminin signalling through the p35/cdk5 pathway (Hahn et al., 2005) .

Neurons retracting in response to roscovitine showed hallmarks similar to those retracting in response to SNAP, calcimycin and LPA. Therefore, it was interesting to see if the mechanism underlying roscovitine-induced retraction is the similar. First, I decided to examine if ROCK and myosin are necessary for axon retraction induced by roscovitine. Indeed, inhibition of ROCK with Y27632, as well as inhibition of myosin with blebbistatin, abolished retraction of neurons. In addition, I observed that in N2a neuroblastoma cells upon treatment with roscovitine the level of monophosphorylation of MRLC increased, which corresponds to an increase in the activity of myosin and suggests that acto-myosin forces are enhanced during roscovitine-stimulated axon retraction. To our knowledge these are the first studies showing involvement of the Rho/ROCK pathway and acto-myosin contractility in neurite retraction induced by roscovitine. Growth cone collapse and axon retraction induced by several guidance cues involve activation of the Rho/ROCK pathway and increase of acto-myosin forces. For example, I showed in the first and second parts of my thesis that LPA-, SNAP- and calcimycin-induced axon retraction involved acto-myosin contractility. In addition, it was shown that ROCK was necessary for growth cone collapse induced by ephrin-A5 in retinal ganglia neurons (Wahl et al., 2000) and by Sema3A in embryonic chick DRG explants (Dontchev and Letourneau, 2002). These results show that different cues can induce growth cone collapse and axon retraction through analogous mechanisms.

Since it appears that NO- and roscovitine-induced retractions involve similar mechanisms, I decided to examine the potential involvement of nNOS. DRG neurons were treated with NPA, a specific nNOS inhibitor, followed by roscovitine. As in case of LPA treatment, inhibition of nNOS did not abolish retraction induced by roscovitine.

Thus, it seems that retraction induced by inhibition of cdk5 with roscovitine does not involve activation of nNOS or NO.

Inhibition of cdk5 with olomoucine increased activity of GSK3β in the axoplasm extruded from squid giant axons (Morfini et al., 2004). In addition, in p35-/- mice increased phosphorylation of tau and enhanced activity of GSK3β was observed (Hallows et al., 2003). Phosphorylation of GSK3β on Ser9 leads to its inactivation and it was shown that PP1 dephosphorylated GSK3β *in vitro* (Morfini et al., 2004). Since it was observed that cdk5 inhibited protein phosphatase 1 (PP1) and inhibition of cdk5 led to dephosphorylation of GSK3β, it is proposed that inhibition of PP1 by cdk5 maintains GSK3β in an inactive state (Morfini et al., 2004). It is important to mention that decreased levels of mode I phosphorylated MAP1B observed after inhibition of cdk5 were measured by antibodies specific for mode I phosphorylated MAP1B, but only for sites specific for cdk5 (mAB150; DiTella et al., 1996; Gordon-Weeks and Fisher, 2000) and not for other kinases, such as GSK3β. GSK3β is supposed to phosphorylate proteins at sites primed by cdk5 phosphorylation, but it can phosphorylate MAP1B also at non-primed sites (Gonzalez-Billault, 2005; Scales et al., 2009). As GSK3β is known to phosphorylate MAP1B one possibility is that inhibition of cdk5 leads to increased phosphorylation of MAP1B by GSK3β, resulting in axon retraction. To analyze a potential involvement of GSK3β in axon retraction induced by roscovitine, wild-type DRG neurons were pretreated with LiCl, the GSK3β inhibitor, followed by roscovitine. Inhibition of GSK3β reduced the number of retracting neurons, 24% compared to 57% when cells were treated with roscovitine only. I have to point here that LiCl had an effect on neurons on its own, since neurons treated with LiCl only and with LiCl and roscovitine grow shorter axons with more branches and larger growth cones than untreated cells. This is consistent with previous results showing that inhibition of GSK3β with LiCl and SB-216763 reduced the length of axons and enhanced growth cone area in embryonic chick DRG explants and in early postnatal mouse DRG neurons (Goold et al., 1999; Owen and Gordon-Weeks, 2003). I did not see a severe phenotype as Goold and colleagues, but most likely it is due to a shorter time of treatment with LiCl.

As I showed in a previous part of my thesis, axon retraction of adult mouse DRG neurons induced by LPA, SNAP, or calcimycin was accomplished by backfolding of microtubules rather than microtubules destabilization. My experiments showed that in case of all three reagents axon retraction was not prevented by taxol and seemed to be

induced by enhanced binding of MAP1B to microtubules, resulting in their overstabilization. Similarly, stabilization of microtubules by taxol did not prevent roscovitine-induced axon retraction. Moreover, roscovitine increased binding of MAP1B to microtubules in PtK2 cells, like SNAP and LPA. All these results suggest that a potential mechanism by which roscovitine induces axon retraction is similar or even the same as the mechanism by which SNAP or LPA induce axon retraction.

It was found that wild-type and MAP1B-/- DRG neurons show different morphology when they are grown on laminin, but not on poly-L-lysine (my results; Bouquet et al., 2004). Suppression of MAP1B with antisense oligonuleotides reduced growth of axons stimulated by laminin, but had no influence on extension of axons from neurons grown on poly-L-lysine (DiTella et al., 1996). Thus, I decided to investigate if roscovitine has an influence on axon growth when neurons are cultured on poly-L-lysine. I found that neurons did not retract in response to roscovitine when they were grown on poly-L-lysine, suggesting a specific role of the p35/cdk5 pathway and MAP1B in laminin signalling. Moreover, I observed that also LPA did not induce axon retraction when neurons were grown on poly-L-lysine. Thus, it seems that in addition to MAP1B also laminin/integrin signalling plays a crucial role in mediating axon retraction. It would be interesting to examine if laminin/integrin signalling is involved in growth cone collapse and axon retraction induced by cues other than roscovitine and LPA.

One could expect that the morphology of MAP1B-/- DRG neurons grown on laminin and their impaired response to inhibition of cdk5 by roscovitine can be due to altered expression of p35 or cdk5 in these neurons rather than due to lack of MAP1B. Therefore, I decided to examine expression of both p35 and cdk5 in DRG neurons. DRG neurons from wild-type and MAP1B-/- mice were immunostained with p35 antibody, but I did not see any difference. p35 staining was continuous within cell bodies and along axons in both types of neurons, with a higher levels in the periphery of the growth cones. To further confirm that expression of p35 is not altered in MAP1B-/- DRG neurons I measured expression of p35 in DRG and brain extracts by western blot, but I did not observe any consistent differences. In addition, I did not find differences in the level of cdk5 in DRGs and brains from wild-type and MAP1B-/- mice. These results suggest that the impaired response of MAP1B-/- DRG neurons to laminin signalling is not due to altered expression of p35 and cdk5.

To summarize, all these results suggest that laminin, perhaps by interaction with integrin $\alpha_1\beta_1$, induces relocation of cdk5 from the cell body to the distal regions of the

growth cone and upregulates expression of p35 (Rossino et al., 1991; Choi et al., 1994; DiTella et al., 1996; Pigino et al., 1997; Paglini et al., 1998; Li et al., 2000). As a consequence p35 activates cdk5, which phophorylates MAP1B and induces a conformation characterized by increased microtubules binding properties. MAP1B binds to microtubules and stabilizes them, promoting axon growth (Fig. 84). It was observed that microtubules in COS cells transfected with constructs encoding full length MAP1B and in PtK2 cells transfected with constructs encoding LC1 were stabilized against nocodazole, a microtubule depolymerising agent, and the levels of acetylated tubulin in theses cells was enhanced (Takemura et al., 1992; Tögel et al., 1998), supporting a role of MAP1B in microtubule stabilization. Moreover, MAP1B phosphorylated by cdk5 was shown to bind mirotubules more efficiently than unphosphorylated MAP1B (Mack et al., 2000).

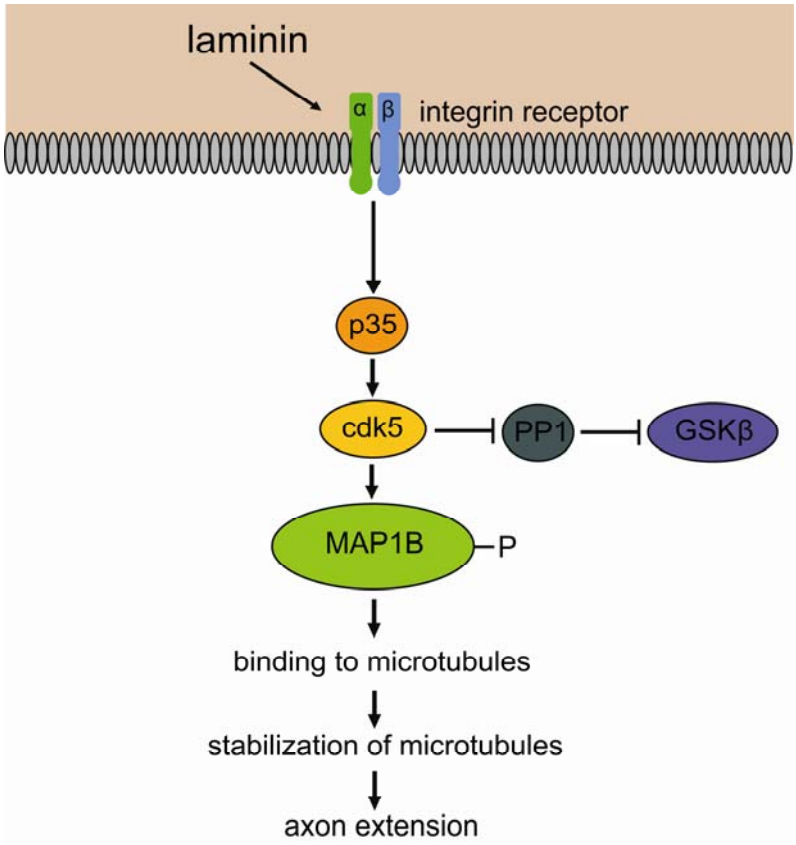

Fig. 84. Model for p35/cdk5 and MAP1B-mediated laminin signaling. Laminin interacts with the integrin receptor $\alpha_1\beta_1$ stimulating upregulation of p35, which activates cdk5. Activated cdk5 phosphorylates many proteins, for example MAP1B. In addition, it inhibits PP1 keeping GSK3β in an inactive state. Upon phosphorylation MAP1B binds more efficiently to microtubules, leading to their stabilization and promotion of axon growth.

In MAP1B-/- DRG microtubules are not protected, thus they are more accessible to microtubule severing proteins, such as spastin or P60-katanin, which cut long microtubules into more dynamic short microtubules, resulting in an increased number of collateral neurites, what I described in more detail in the second part of my thesis, titled "Mechanism of NO-induced axon retraction", in section concerning microtubule dynamics in wild-type and MAP1B-/- DRG neurons. It seems that laminin signalling plays an important role in regulation of morphology of wild-type and MAP1B-/- DRG neurons, since increased branching of MAP1B-/- DRG neurons was observed only when neurons were cultured on laminin.

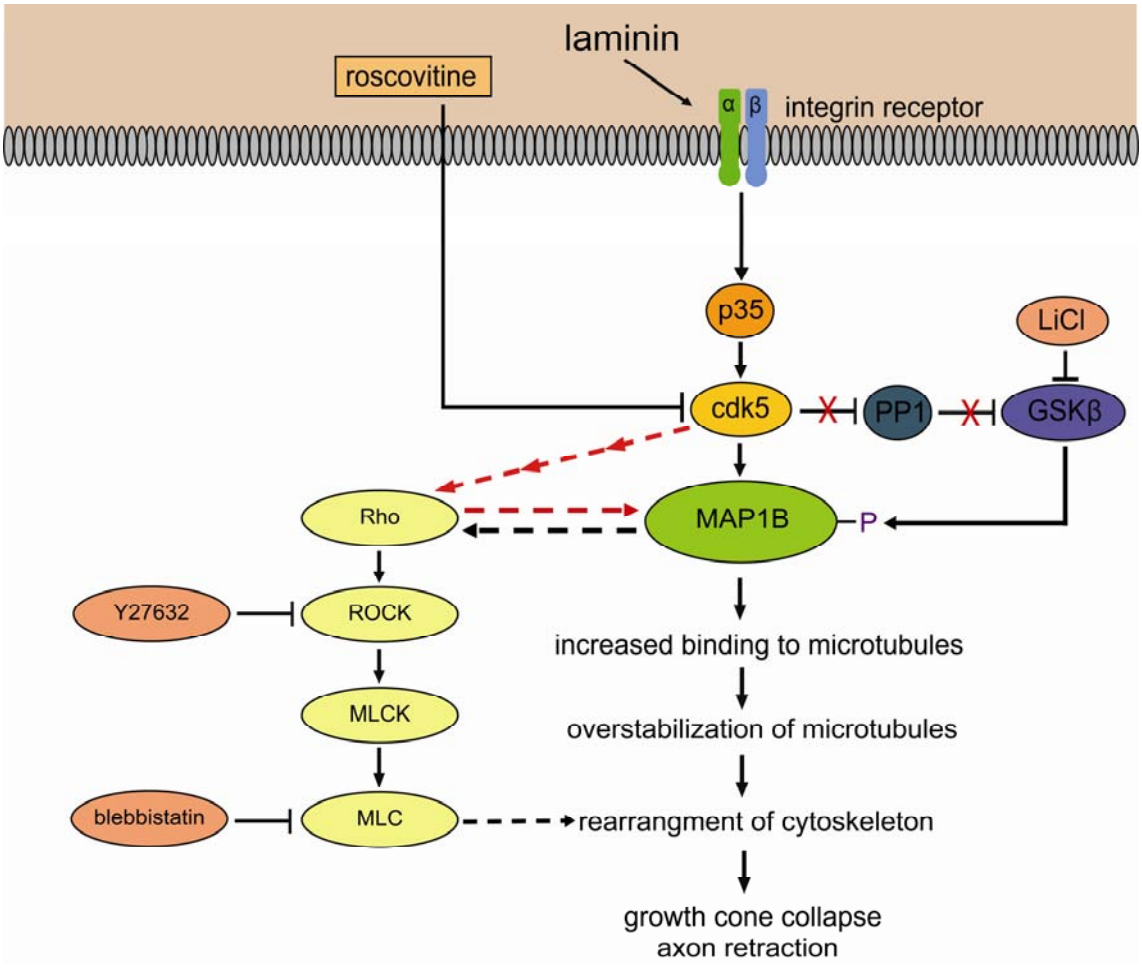

Fig. 85. Model for role of MAP1B in axon retraction induced by roscovitine. Interaction between laminin and the integrin receptor $\alpha_1\beta_1$ stimulates upregulation of p35 and activation of cdk5. Activated cdk5 phosphorylates MAP1B, leading to its increased binding to microtubules, their stabilization and promotion of axon growth. In addition, cdk5 inhibits PP1 maintaining GSK3β in an inactive state. Inhibition of cdk5 with roscovitine releases PP1 from inhibition by cdk5. PP1 dephosphorylates GSK3β, which in turn phosphorylates MAP1B. This, further enhances MAP1B microtubule binding activity, resulting in overstabilization of microtubules, growth cone collapse and axon retraction. Axon retraction can be partially prevented by inhibition of GSK3β with LiCl. In addition, roscovitine-induced axon retraction involves also the Rho/ROCK pathway and acto-myosin contractility. Axon retraction can be almost

completely abolished by inhibition of ROCK with Y27632 or myosin with blebbistatin . It is not known whether activation of the Rho/ROCK pathway is cause or a consequence of MAP1B-mediated axon retraction.

Inhibition of cdk5 by roscovitine results in decreased phosphorylation of MAP1B by cdk5, but increases phosphorylation by other kinases, for example by GSK3β. Increased phosphorylation of MAP1B results in its upregulated binding to microtubules, their overstabilization and axon retraction (Fig. 85). I propose that MAP1B binding to microtubules at the certain optimal level leads to their stabilization promoting axon growth (what seems to be triggered by laminin), but when this binding is enhanced above a critical value, microtubules are overstabilized resulting in growth cone collapse and axon retraction, what one could observe after treatment of neurons with LPA, SNAP, calcimycin or roscovitine. When MAP1B does not bind or binds microtubules with affinity lower than the optimal, axon growth is also affected, resulting for example in uncontrolled branching and misguidance of the growth cones (morphology of MAP1B-/- DRG neurons). Similarly, regulation of growth cone motility and turning by Ca^{2+} is proposed to depend on the optimal range of Ca^{2+} signals (Gomez and Zheng, 2006). It was observed that a small range local elevation in Ca^{2+} levels induced growth cone repulsion, whereas a medium range local increase in Ca^{2+} levels triggered attractive response of the growth cone (Wen et al., 2004; Henley et al., 2004b). On the other hand, a high range local increase in Ca^{2+} levels also stimulated growth cone repulsion (Robles et al., 2003). Likewise, Letourneau and colleagues observed that when Ca^{2+} levels were decreased below 200nM or enhanced above 300nM the motility and the extension of neurites in chicken DRG neurons were inhibited. The neurite growth was observed only when Ca^{2+} levels were between 200nM and 300nM (Lankford and Letourneau, 1991). These results suggest that only optimal elevations of Ca^{2+} promotes growth and/or attraction, while signals below or above the medium range inhibit neurites extension and/or induce growth cone collapse (Kater and Mills, 1991; Gomez and Zheng, 2006).

In addition, roscovitine-induced axon retraction involves acto-myosin contractility, but whether it is a cause or a consequence of increased binding of MAP1B to microtubules it is not clear (Fig. 85). Finally, laminin/integrin signalling seems to play an important role in triggering axon retraction in addition to promoting axonal growth, since it was found that DRG neurons do not retract in response to LPA or roscovitine, when they are grown on poly-L-lysine only.

Finally, MAP1B can play a role in laminin-integrin signalling *in vivo* during development of nervous system. It is proposed that laminin can regulate neurite extension *in vivo*, since it was found to be expressed at stages crucial for terminal differentiation (DiTella et al., 1996). MAP1B also seems to play a role during development of nervous system as its expression is developmentally regulated, with the highest expression in both growing and regenerating neurons (Calvert et al., 1987; Avila et al., 1994; Gordon-Weeks and Fischer, 2000). The most striking defect in MAP1B-/- mice is the lack of corpus callosum (Meixner et al., 2000). As laminin is expressed by midline glial cells and MAP1B was shown to play a role in laminin signalling *in vitro*, potentially MAP1B could play a role in laminin signalling *in vivo* too. Its absence would render axons unable to cross the midline (Meixner et al., 2000). In addition, in p35-/- mice corpus callosum is missing and they show severe defects in cortical lamination (Chae et al., 1997). Thus, results from *in vitro* studies and phenotypes of MAP1B-/- mice and p35-/- mice, suggest that indeed the p35/cdk5 pathway and MAP1B are the components of a signalling pathway capable of responding to laminin signalling during development of the nervous system. Lack of one of them affects laminin signalling and leads to severe developmental brain defects.

MATERIALS AND METHODS

DNA METHODS

DNA preparation, restriction digest and ligation

JetStar 2.0 Midi columns (Genomed, Bad Oeynhausen, Germany) were used for plasmid DNA purification from bacteria. The alkaline method was used for small-quantity plasmid DNA preparation (Sambrook et al., 2001). All other basic cloning techniques like DNA restriction digest, ligation of DNA fragments, precipitation of DNA was performed as described (Sambrook et al., 2001). DNA fragment gel extraction was performed according the manufacturer's protocol (QIAquick gel extraction kit, QIAGEN or NucleoSpin Extract II, MACHEREY-NAGEL, Germany). The concentration of double stranded DNA was measured spectrophotometrically at 260nm.

Agarose gel

1g of agarose powder was dissolved in 100ml of electrophoresis TAE buffer, heated in the microwave oven and cooled down to ~60°C. After adding ethidium bromide (0.5µg/ml final concentration) it was poured into a casting tray.

10x TAE buffer (for 1 l)

Tris base	48.4g/l
Glacial acetic acid	10.9g/l
EDTA	2.92g/l
H_2O	up to 1l

Transformation of E. coli

Preparation of competent cells

Rubidium chloride competent cells

DH5α and BL21 bacteria were inoculated and grown overnight. 5ml of this fresh overnight culture were inoculated into 500ml LB medium and shacked at 37°C until an OD600 of 0.5 was obtained. The bacterial cells were incubated on ice for 15 minutes, pelleted for 5min at 5000rpm (GSA rotor, 4°C) and resuspended in 200ml TfbI buffer. The bacterial resuspension was placed again on ice for 15 min and centrifuged afterwards for 5 minutes at 5000rpm (GSA rotor, 4°C). The pelleted cells were resuspended in 20ml TfbII buffer, put on ice for 15 minutes and aliquoted. The aliquots of competent cells were stored at -80°C.

$CaCl_2$ competent cells

DH5α and BL21 bacteria were inoculated and grown overnight. 2.5ml of this fresh overnight culture were inoculated into 500ml LB medium and shacked at 37°C until an OD600 of 0.5 was obtained. The bacterial cells were incubated on ice for 15 minutes, pelleted for 5min at 5000rpm (GSA rotor, 4°C) and resuspended in 250ml 100mM $CaCl_2$. The bacterial resuspension was placed again on ice for 30-45 min and centrifuged afterwards for 5 minutes at 5000rpm (GSA rotor, 4°C). The pelleted cells were resuspended in 5ml 100mM $CaCl_2$ and aliquoted with 10% glycerol. The aliquots of competent cells were stored at -80°C.

Transormation of cells

Rb competent *E.coli* (DH5α or BL21) were thawed on ice for 5min, mixed with 1µg plasmid DNA or ligation mixture at ratio 5:1 (E.coli:DNA) and incubated on ice for 30min. After heat shock (45sec at 42°C) cells were cooled down on ice, 1ml of fresh LB

medium (Sambrook at al., 1989) was added and cells were incubated for 1h at 37°C with gentle shaking. Then they were centrifuge for 4min at 2000rpm, 900µl of medium was discarded and bacteria were resuspended in the rest volume of medium. Afterwards bacteria were plated on appropriate solid medium with antibiotics (ampicillin or kanamycin).

LB (Luria Bertani Medium) medium (for 1l), pH 7.5

Bacto-Trypton	10g/l
Bacto-Yeast extract	5g/l
NaCl	10g/l

TfbI buffer (pH 5.8)

30mM potassium acetate
100mM rubidium chloride
10mM calcium chloride
50mM manganese chloride
15% v/v glycerol

TfbII buffer (pH 6.5)

10mM MOPS
75mM calcium chloride
10mM rubidium chloride
15% v/v glycerol

Cloning

pMT22emptymCherry – pMT22mCherry was cut with restriction enzymes, so LC1A was cut out from pMT22mCherry and vector was religated;

pMT22emptyGFP – pMT22GFP was cut with restriction enzymes, so LC1A was cut out from pMT22mCherry and vector was religated;

pMT22mCherry – mCherry was recloned from mCherry-C1 plasmid into pMT22Tet plasmid; both plasmids (mCherry-C1 and pMT22tet) were opened with NheI and ApaI restriction enzymes. The construct encodes MAP1B LC (LC1) and mCherry protein.

pMT5mCherry - mCherry was recloned from mCherry-C1 plasmid into pMT5Tet plasmid; both plasmids (mCherry-C1 and pMT5tet) were opened with NheI and ApaI restriction enzymes. The construct encodes full length MAP1B and mCherry protein.

pMT22C246SmCherry - mCherry was recloned from mCherry-C1 plasmid into pMT22C246STet plasmid; both plasmids (mCherry-C1 and pMT22C246STet) were opened with NheI and ApaI restriction enzymes. The construct encodes full length MAP1B and mCherry protein.

pMT22C143SmCherry - mCherry was recloned from mCherry-C1 plasmid into pMT22C143STet plasmid; both plasmids (mCherry-C1 and pMT22C143STet) were opened with NheI and ApaI restriction enzymes. The construct encodes full length MAP1B and mCherry protein.

pEF1aHis-Tag – EF1a was recloned from plasmid pEGFPEfull into pMA1a plasmid; Both plasmids (pEGFPEfull and pMA1a) were opened with XhoI and EcoRI restriction enzymes. The construct encodes EF1a and COOH-terminally located 6xHIS tag.

pEF1aStag - EF1a was recloned from pEGFPEfull plasmid into pET32a(+) plasmid; Both plasmids (pEGFPEfull and pET32a(+)) were opened with XhoI and EcoRI restriction enzymes. The construct encodes EF1a, Trx-tag, His-tag, S-protein.

PROTEIN METHODS

Preparation of cell extracts

Cells grown on 6 dishes in DMEM medium supplemented with 10% FCS, L-glutamate and antibiotics. Then they were washed with PBS and 200µl of 2x sample buffer

(100mM Tris-HCl pH 6.8, 4% SDS, 20% (v/v) glycerol, 12mM EDTA, 0.2% bromphenol blue, 0.3% DTT and Complete Mini protease inhibitors tablets (Roche Diagnostics)) was added, and cells were scraped with plastic cell scrapers off the substrate and transferred to eppendorf tubes. Samples were sonicated 2 times 30sec. at 80% of intensity, heated at 95°C for 5 min., and stored at -20°C.

Preparation of brain and DRG homogenates

Whole brains or DRGs were homogenized in 2x sample buffer (100mM Tris-HCl pH 6.8, 4% SDS, 20% (v/v) glycerol, 12mM EDTA, 0.2% bromphenol blue, 0.3% DTT and Complete Mini protease inhibitors tablets (Roche Diagnostics)) in a Dounce homogenizer. Then the samples were centrifuged at 14 000rpm for 10min. Supernatants were sonicated 2 times 30 sec. at 80% of intensity, heated at 95°C for 5 min., and stored at -20°C.

Deteremination of protein concentration (Bradford Method)

100mg of Coomassie Brilliant Blue G-250 was dissolved in 50 ml 95% ethanol, 100 ml of 5% phosphoric acid was added and adjusted to 1l with ddH_2O. The solution was filtrated through Whatman No.1 filter paper and stored at 4°C. 1ml of Coomassie solution was added to 100 µl of (diluted) protein sample. The solution was mixed, incubated for 5-10 min.at RT and absorbance was measured at 595nm. BSA solutions were used as a standard.

Immunoblot analysis

Proteins were separated on 12% SDS polyacrylamide gels according to protein size as described (Sambrook et al., 1989) and then were transferred to a nitrocellulose membrane (0.2µM, Schleicher Schuell, Dassel, Germany) in transfer buffer (48mM Tris, 40mM glycine 20% methanol) using BioRad Semi-Dry Electrophoretic Transfer Cell (Biorad, München, Germany) for 30-40min at 15V, 500mA. After the transfer

proteins on membrane were stained with Ponceau S solution or amidoblack solution and blots were blocked in 2% BSA or 5% milk in PBS/0.25% Tween20 for 1h at RT or over night at 4˚C. After washing 3 times 5 min with PBS/0.25% Tween20 blots were incubated with primary antibodies diluted in 1% BSA in PBS/0.25% Tween20 for 1h at RT or over night at 4°C. The immune complexes were detected with appropriate secondary antibodies conjugated with horseradish peroxidase (HRP) or with alkaline phosphatase (AP) (Promega, Mannheim, Germany).

Solutions:

Ponceau solution
0.2% Ponceau-S
3% Trichloroacetic acid

Amidoblack solution
0.1% Amidoblack
45% Ethanol
10% Acetic Acid

Phosphate buffered saline (PBS), pH 7.4
137mM NaCl
2.6mM KCl
8mM Na_2HPO_4
1.5mM KH_2PO_4

AP-buffer
100mM Tris/HCl (pH 9.5)
100mM NaCl
5mM $MgCl_2$

NBT-solution
0.5g Nitro blue tretrazolium (NBT)
10ml 70% DMF, stored at -20°C

BCIP-solution

0.5g Bromchoroindolyl phosphate (BCIP)

10ml 100% DMF, stored at -20°C

STE buffer

10mM Tris pH 8,0

150mM NaCl

1mM EDTA

5xMg^{++}buffer

125mM Hepes pH 7,5

750mM NaCl

5% NP.-40

50mM $MgCl_2$

5mM EDTA

2xMg^{++}buffer

50mM NaF

2mM NaO_4Va

20µg/ml Aprotinine

20µg/ml benzamidine

200µM PMSF

20% Glycerol

1xMg^{++}buffer

50mM NaF

2mM NaO_4Va

20µg/ml Aprotinine

20µg/ml benzamidine

200µM PMSF

20% Glycerol

MAMMALIAN CELL CULTURE METHODS

Maintenance of the cell lines

Frozen cells were thawed in 37°C water-bath, transferred into a 15ml Falcon tube, which contained 9ml DMEM (Dulbecco`s Modified Eagle Medium) supplemented with 10% FCS (Fetal Calf Serum), 2mM L-glutamate and 50u/ml Penicillin/Streptomycin. Cells were pelleted by centrifugation at 1000rpm for 5 min. at RT (Heraeus Megafuge) and resulted pellets were resuspended in adequate volume of growth medium. PtK2, NIH3T3, COS7 and N2a cells were cultured in T75 culture flask or 10cm Petri Dish in growth medium that consisted of DMEM, 10% FCS, 2mM L-glutamate and 50u/ml Penicillin/Streptomycin, in case of PtK2 cells additionally Fungizone and non-essential amnioacids were added to medium. Cells were incubated at 37°C in humidified atmosphere containing 8.5% CO_2. When confluence of cells was about 80% they were washed with PBS and treated with the 2ml of trypsin solution (0.05% trypsin, 0.2% EDTA) for 5min. at 37°C. Growth medium was added to stop trypsinization and detached cells were transferred to Falcon tube and pelleted by centrifugation at 1000rpm for 3 min. at RT. Pellets were resuspended in fresh growth medium and transferred into new culture flasks T75 or 10cm Petri Dish.

For freezing, cells were washed with PBS, trypsinized, centrifuged and resuspended in growth medium containing 10% DMSO, aliquoted into cryotubes (Nunc) and frozen on dry ice. Then they were stored at -80°C for 2-3months or after 24h stored at -80°C transferred into a liquid nitrogen tank.

Designation	**Cell type**	**Organism**
N2a (Neuro-2a)	neuroblast	*Mus musculus*
PtK2 (NBL-5)	epithelial	*Potorous tridactylis*
NIH3T3	fibroblast	*Mus musculus*
COS7	fibroblast	*Cercopithecus ethiops*

Table 1. List of cell lines.

Cultivation of dissociated adult DRG neurons

Isolation and cultivation of mouse DRG neurons was performed following the protocol described by Tonge (Tonge et al., 1996). Mice were anesthetized with IsoFlo (Abbott, Rungis, France) and killed by decapitation. DRG neurons were harvested in F-12 medium, cut into smaller pieces and dissociated by collagenase (4 000U/ml, Sigma, St. Louis, MO) in DMEM/F12 medium with 4% Horse Serum for 90min. at 37°C followed by trypsin/EDTA (Invitrogen) and DNAseI (50µg/ml; Sigma) treatment for 9min. at 37°C. Trypsinization was stopped by adding heat-inactivated Horse Serum and DRG neurons were finally triturated several times with narrowed Pasteur pipettes. After harvesting cells with centrifugation at 800rpm for 5min, cells were resuspended in fresh F-12 medium and centrifuged again, which was repeated 2 times. Finally cells were resuspended in growth medium (DMEM/F-12 medium supplemented with N3 (Romijn et al., 1981) , 5% Horse Serum, 40% glucose, penicillin-streptomycin (Bottenstein and Sato, 1979), plated of density 100cells/cm^2 on 13mm glass coverslips pre-coated with poly-L-lysine and laminin and incubated at 37°C, 5% CO_2 incubator. After 20-24h neurons were treated as indicated, fixed with solution containing 8% PFA (paraformaldehyde) and 22% sucrose for 45min at RT. After blocking with 5% BSA in PBS and 0.3% Triton X-100 for 1h at RT or over night at 4°C, cells were incubated with primary and secondary antibodies as described above.

Chemical	Concentration	company/cat.nr	volume for 10 ml (ml)
HBSS –Ca, -Mg		invitrogen	6
BSA in HBSS-/-	10 mg/ml (150µM)	Sigma, A4261	1
Transferine in Hanks	100 mg/ml (1.1mM)	Sigma, T1147	1
Na-Selenite in HBSS-/-	0.01 mg/ml (58µM)	Sigma, S9133	1
Petrescine in HBSS-/-	80 mg/ml (500µM)	Sigma, P5780	0.4
Progesterone in EtOH	0.125 mg/ml (400Mm)	Sigma, P6149	0.1
Corticosterone in EtOH	2 mg/ml (5.8mM)	Sigma, C2505	0.02
Triiodothyronine in 0,01N NaOH	0.2 mg/ml (300µM)	Sigma, T6397	0.1
Insuline in 20mM HCl	25 mg/ml (4.4M)	Sigma, I6634	0.

Table 2. N3 components.

Coating of coverslips for N2a cells and DRG neurons

13mm glass coverslips were washed with ethanol and methanol, autoclaved and then coated with 10µg/µl poly-L-lysine in H_2O for 1h or over night at 37°C. Afterwards they were washed with PBS and cells were plated on them, or after washing with PBS they were coated with 10µg/µl laminin for at least 3h at 37°C, then washed three times with PBS and cells were plated on them.

Transfection of mammalian cells using Fugene6

Cells were transfected with the Fugene6 (Roche Diagnostics), which is a lipid based transfection reagent, that efficiently transfect a wide variety of eukaryotic cells with high efficiency and minimal cytotoxicity. Cells were seeded onto 13mm glass coverslips in 24-well plates 24h before transfection. All constructs were expressed in Tet responsive expression vector and DNA mixture was prepared in ratio 1:6 vector:Tet transactivator.

Name of plazmid	**construct**	**Tag**	**Expression system**	**source**
pMT5 Tet ***(FL)***	Full length MAP1B (FL)	C-myc	Tet-off	M. Tögel
pMT22tet ***(LC1)***	Light chain of MAP1B (LC1)	C-myc	Tet-off	M. Tögel
pMT22C2457Stet ***(LC1 C2354S)***	Mutated light of MAP1B (LC1)	C-myc	Tet-off	A. Trancikova
pMT22C2354Stet ***(LC1 C2354S)***	Mutated light of MAP1B (LC1)	C-myc	Tet-off	A. Trancikova
pMT5mCherry	Full length (FL)	C-mCherry	Tet-off	E.Krupa
pMT22mCherry ***(LC1)***	Light chain (LC1)	C-mCherry	Tet-off	E.Krupa
pMT22C2457SmCherry ***(LC1 C2354S)***	Mutated light of MAP1B (LC1)	C-mCherry	Tet-off	E.Krupa
pMT22C2354SmCherry ***(LC1 C2354S)***	Mutated light of MAP1B (LC1)	C-mCherry	Tet-off	E.Krupa
EB3-GFP	EB3	EGFP	CMV	
EB1-GFP	EB1	EGFP	CMV	

Table 3. Construct used for transfection of mammalian cell lines

0.5µg of DNA mixture and 1.5µl of Fugene6 was required for one 13mm coverslip in 24-well plate. Fugene6 was added directly to 25µl of serum free medium (DMEM) in polypropylene tubes and DNA was diluted in this mixture. The solution was gently mixed and incubated for 30 min. at RT. Then 75µl of OptiMEM was added and mixture was added drop-wise directly on the cells (100µl/well containing 900µl medium). After gentle mixing, the plates were incubated at 37°C for 48-72h.

Transfection of DRG neurons with Amaxa

DRG neurons were isolated as described above, but in all steps RPMI medium was used instead of F12 medium. After trituration cells were harvestd by centrifugation at 800rpm for 5min, resuspended in 1,8ml of RPMI medium and solution was divided into two aliquots – 300µl which was a control and 1500µl which was taken for transfection. Both aliquots were centrifuged at 1000rpm for 3min. Cells from control part were resuspended in 300µl of growth medium and plated on poly-L-lysine and laminin coated dishes. The second part of cells were resuspended in 20µl of Nucleofactor solution and 0,6-1,0µg of DNA was added. The mixture was transferred into CSN cuvette, transfection was done in Amaxa machine with SCN Basic Neuro Program 6, then 400µl of prewarmed growth medium was apllied into cuvette, which was then put into incubator to let cells to recover. After 10min cells were plated onto dishes coated with poly-L-lysine and laminin and images were taken after 48h.

Treatment DRG neurons, N2a cells and Ptk2

Treatment of DRG neurons, N2a cells and transfected PtK2 cells with LPA

DRG neurons, N2a cells and transfected Ptk2 cells were grown on coverslips, treated with 10µM LPA for 30min (DRG neurons, N2a cells) or for 2h (PtK2 cells), fixed, stained and analyzed by microscopy.

Inhibition of cdk5 in DRG neurons, N2a cells and transfected Ptk2 cells

To inhibit cdk5 DRG neurons, N2a cells and transfected Ptk2 cells were grown on coverslips, treated with 50µM roscovitine (Sigma, Table 6) for 1h (DRG neurons, N2a cells) or 2h (PtK2 cells) at 37˚C. DRG neurons were treated with 20mM LiCl (Sigma, Table 6) for 3h at 37˚C to inhibit GSK3β. Afterwards N2a and PtK2 cells were fixed, stained with antibodies and analyzed by microscopy.

Inhibition of cdk5/GSK3β in DRG neurons

DRG neurons were treated with 20mM LiCl (Sigma, Table 6) for 14-16h at 37˚C to inhibit GSK3β, fixed with PFA, stained with antibodies and analyzed by microscopy.

Treatment of DRG neurons, N2a cells and transfected PtK2 cells with LPA

DRG neurons, N2a cells and transfected Ptk2 cells grown on coverslips were treated with 10µM LPA (Cayman, Table 6) for 30min (N2a cells, DRG neurons) or for 2h (PtK2 cells) at 37˚C. Afterwards cells were fixed with PFA, stained with antibodies as described and analyzed by microscopy.

Inhibition of ROCK (Rho-associated kinase) and myosin in DRG neurons and N2a cells

DRG neurons and N2a cells were treated with 10µM Y27632 (Sigma, Alexis, Table 6) for over night or 1h before to inhibit ROCK or with 100µM blebbistatin (Sigma, Table 6) for 15min to inhibit myosin, left untreated or followed by treatment with or followed by 50µM roscovitine for 1h, 10µM LPA for 30min, 10µM calcimycin for 15min, or 100µM SNAP for 1h (Table 6). Afterwards cells were fixed, stained and analyzed by microscopy.

Inhibition of CaMKII, calcineurin, calpain, PKC in DRG neurons

DRG neurons were pretreated with 10µM myrAIP (Alexis, Table 6) for 30min, 5µM Cyclosporin A (CSA, Calbiochem, Table 6) for 20min, 200µM ALLN (Calbiochem, Table 6) for 1h or 50µM GÖ6976 for (Sigma, Table 6) 1,5h to inhibit respectively CaMKII, calcineurin, calpain or PKC, and then treated with 10µM calcimycin for 15min (Sigma, Table 6). Afterwards cells were fixed with PFA, stained and analyzed by microscopy.

S-nitrosylation of MAP1B in DRG neurons and transfected PtK2 cells

DRG neurons and transfected Ptk2 cells were grown on 13mm coverslips, treated with 100µM S-Nitroso-N-acetylpenicillamin (SNAP, Calbiochem, Table 6) for 1h (DRG neurons) or 4h (Ptk2 cells) at 37°C in the dark. After PFA (DRG neurons) or methanol (Ptk2 cells) fixation cells were stained as described above and analyzed by microscopy.

Inhibition and activation of nNOS in DRG neurons

DRG neurons were grown on coverslips coated with poly-L-lysine and laminin, nNOS or all NOSs were inhibited by adding inhibitor N-ω-propyl-L-arginine NPA, (Tocris biosciences, Table 6) at a final concentration of 300µM or 1mM for 1h or L-NAME (Cayman, Table 6) at a final concentration 300µM for 1h, respectively. Afterwards cells were left untreated or were treated with 50µM roscovitine for 1h, 10µM LPA for 30min, 10µM calcimycin for 15min or 3nM taxol for 30min (Table 6). To activate nNOS cells were treated with the calcium ionophore calcimycin A23187 (Sigma, Table 6) at a final concentration of 10µM and incubated for 15min. at 37°C. Neurons were fixed with PFA, stained and analyzed by microscopy.

Stabilization of microtubules with taxol in DRG neurons and N2a cells

Wild-type and MAP1B -/- neurons were treated with 3nM or 100nM taxol (Sigma, Table 6) for 30min only, or followed by treatment with reagents as indicated. Afterwards cells were fixed, stained and analyzed by microscopy.

Stimulation of cAMP in DRG neurons

Stimulation of cAMP was induced by addition of 1µM dibutryl-cAMP (Sigma, Table 6) or 20µM forskolin (Calbiochem, Table 6), triggers production of cAMP by sAC, for 3h. Afterwards cells were treated with 100µM SNAP for 1h or 10µM calcimycin for 15min (Sigma, Table 6), fixed, stained and analyzed by microscopy.

Treatment with DMSO –a solvent control

DRG neurons were cultured as described, treated with 3µl or 6µl of DMSO for indicated time, fixed, stained and analyzed by microscopy.

MICROSCOPY STUDIES OF CELLS

Immunofluorescence microscopy of the cells

PtK2 or NIH3T3 cells were grown on glass coverslips and N2a neuroblastoma cells were grown on laminin-2 (Sigma) precoated 13mm coverslips. When they reached the desired density they were transfected and/or treated with drugs and/or inhibitors, then cells were washed once with PBS and fixed with pre-cooled (-20°C) methanol for 2-5min at RT on pre-cooled (-20˚C)metal block. Afterwards cells were washed 3 times with PBS. For blocking of unspecific binding sites, they were incubated with 5% BSA in PBS for 1h at RT or over night at 4˚C. Following 3 times 5min. washing with PBS cells were incubated with first antibodies diluted in 1% BSA in PBS for 1h at RT. Then cells were washed again 3 times 5 min with PBS and incubated with secondary

antibodies diluted again in 1% BSA in PBS for 1h at RT in the dark. Finally cells were washed 3 times 5 min with PBS and once with water. Coverslips with the samples were put on 6µl of Mowiol 4-88 placed onto a microscope slide. Samples were stored at 4°C.
DRG neurons were plated of density 100cells/cm^2 on laminin-2 (Sigma) pre-coated 13mm glass coverslips and incubated at 37°C, 5% CO_2 incubator for 24h. After treatment mouse DRG neurons were fixed with solution containing 8% PFA (paraformaldehyde) and 22% sucrose for 45min. at RT. After extensive washing 3 times 5 min with PBS, unspecific binding sites were blocked and cells were permeabilized with blocking solution containing 5% BSA in PBS and 0.3% Triton X-100 for 1h at RT or over night at 4°C. Then cells were washed 3 times 5 min. with PBS and incubated with primary antibodies, diluted in 5% BSA in PBS for 3h at RT, washed again 3 times 5min. with PBS and incubated with secondary antibodies for 2h at RT in the dark. Finally samples were washed 3 times with PBS and once with water and mounted on glass slides with Mowiol 4-88. Slides were stored at 4°C.

Time-lapse video microscopy studies of DRG neurons

For analysis of drug effect on axon growth, DRG neurons were isolated as described, plated of density 100cells/cm^2 on laminin (Sigma) pre-coated 13mm glass coverslips fixed with 35mm Petri Dish, and incubated at 37°C, 5% CO_2 incubator. After 20-24h, 20 mM HEPES, pH 7.4, was added to growth medium, and cultures were placed at 37 C on the stage of an inverted microscope equipped with phase contrast and a Plan Apo 100×/0.7 numerical aperture lens. Acquisition and illumination devices were driven by MetaMorph software (Universal Imaging, West Chester, PA) or Axiophot (Zeiss). Images of wild-type and MAP1B -/- neurons transfected with EB1-EGFP were taken for 15min or 20min with 1min or 5min intervals. In case of roscovitine treatment, after 15min of observation the medium was changed to determine if changing the medium does have an influence on growing axons, and observation was continued for 30min. Afterwards, 10µM LPA or 50µM roscovitine was added and recording was continued for 30 min (LPA) or 2h 30min with 1min (LPA) and 5min (roscovitine) intervals between images.
For analysis of microtubule dynamic, DRG neurons were isolated as described, transfected with construct encoding EB1-GFP, plated of density 100cells/cm^2 on

laminin (Sigma) pre-coated 13mm glass coverslips fixed with 35mm Petri Dish, and incubated at 37°C, 5% CO_2 incubator. After 48h, 20 mM HEPES, pH 7.4, was added to growth medium, and cultures were placed at 37 C on the stage of an inverted microscope () equipped with phase contrast and fluorescence optics, and a Plan Apo 100×/0.7 numerical aperture lens. Acquisition and illumination devices were driven by MetaMorph software (Universal Imaging, West Chester, PA). For analysis of microtubule dynamics, images of wild-type and MAP1B -/- neurons transfected with EB1-EGFP were taken for 1min with 2sec intervals. For analysis of the drug effects images were taken for at least 5min (1min from each video) before adding drug. After addition of 10μM LPA or 100μM SNAP (at the time-point indicated in results), image recording was continued for 30min or 90min (1min for each video) with 2sec intervals.

PREPARATION OF AGGRECAN-LAMININ SPOT GRADIENT COVERSLIPS

Preparation was done according to protocol published by (Tom 2004). Coverslips were coated with 10μg/ml or 100μg/ml Poly-L-lysine or Poly-D-lysine for 1h or over night at 37ºC. Then coverslips were spotted with 2 μl of a solution of aggrecan (0.7mg/ml) and laminin (5μg/ml or 10μg/ml) in calcium- and magnesium-free PBS. After the spots were allowed to air dry, the coverslips were completely covered with laminin (10μg/ml) in PBS or left uncovered and kept at 37°C until cell plating (~5 hr). . DRG neurons were plated on coverslips, 6h or 12h after plating 25μM Y27632, 100μM blebbistatin, 300μM NPA or 300μM L-NAME were applied or cells were left untreated. For immunofluorescence microscopy cells fixed with PFA after 24h or 48h and stained as listed above.

PREPARATION OF MYELIN SPOTTED COVERSLIPS

Isolation of myelin from mouse brain

Isolation of the CNS myelin was done according to protocol from Norton and Poduslo 1973 with some modification (Norton and Poduslo, 1973; Sheads et al., 1977). Brains from adult wild-type mice were homogenized in 25ml of 0.3M sucrose diluted in PBS

(5% (w/v), then homogenates were softly laid on 25ml of 0.085M sucrose in PBS and centrifuged at 25000 x g for 90min. The crude myelin formed an interface, which was harvested and c submitted to a hypoosmotic shock in 50ml H_20 and centrifuged at 25000 x g for 25min. Then the myelin fraction was again resuspended in H_20 and centrifuged at 10000 x g for 15min. Pellet was resuspended in 0.3M sucrose and layered on 0.85 sucrose, centrifuged at 25000 x g for 90min. Interface again was dissolved in H_20 and centrifuged at 25000 x g for 25min. The pellet was resuspended in 10mM Hepes buffer. The protein concentration was determined by Bradford Method and the myelin was stored at -20ºC.

Preparation of coverslips

Coverslips were coated with 100µg/ml Poly-L-lysine for 1h or over night at 37ºC. Then coverslips were spotted with a myelin (1.5-6µg/spot) in calcium- and magnesium-free PBS. And the spots were allowed to air dry at RT. DRG neurons were plated on coverslips, 6h or 12h after plating 25µM Y27632, 100µM blebbistatin, 300µM NPA or 300µM L-NAME were applied or cells were left untreated. For immunofluorescence microscopy cells fixed with PFA after 24h or 48h and stained as listed above.

ANTIBODIES

All primary and secondary antibodies used for immunofluorescence were diluted in 1%BSA in PBS. Antibodies used for the western blot analysis were diluted in 1%BSA in PBS/0.25% Tween20 and in case of blot overlay assay in 1%BSA in PBS/0.25% Tween20 with 150mM NaCl. All antibodies are listed below (Table 4; Table 5.).

Antygen	name/clone	spieces	IF	WB	company/source
α-tubulin	B512	Mouse	1:1000	1:5000	Sigma
α-tubulin	YL1/2	Rat	1:300	1:1000	Abcam/Acris
α-/β-actin	AC74/15	Mouse	1:400	1:1000	Sigma
MAP1B HC	HC891	Rabbit	1:200	1:800	A.Meixner
MAP1B HC	AA6	Mouse	1:100	1:500	Sigma
MAP1B LC	LC1A	Rabbit	1:200	1:1000	M.Tögel

myc (IF)	myc1/2	Rabbit	1:300	-	M.Tögel
phosphorylated myosin light chain 2 (Ser19)	Ser19	Mouse	1:50	1:1000	Cell signalling
diphosphorylated myosin light chain 2 (Ser19/Thr18)	Thr18/Ser19	Rabbit	-	1:1000	Cell signalling
cdk5	C-8	Rabbit	1:50	1:200	Santa Cruz
p35	N-20	Rabbit	1:50	1:100	Santa Cruz
Laminin		Rabbit	1:100	-	Sigma
CSPG	CS-56	Mouse	1:200	-	Sigma
MAP1B type-1 phosphorylated population	mab1E11	Mouse	ready to use solution	-	Elizabeth Pollerberg
MAG	513	Mouse	1:400	1:1000	Chemicon
MBP		Rat	1:1000	1:2000	Chemicon
acetylated tubulin	6-11B-1	mouse	1:300	1:2000	Sigma

Table 4. List of primary antibodies

Antygen	**spieces**	**IF**	**WB**	**company/source**
HRP-anti rabbit IgG	goat	-	1:10000	Jackson lab./Vector
HRP-anti mouse IgG	goat	-	1:10000	Jackson lab.
AP-anti rabbit IgG	goat		1:7500	Jackson lab.
AP-anti mouse IgG	goat	-	1:3000	Jackson lab.
Alexa 488-anti-mouse IgG	goat	1:1000	-	Mol. Probes
Alexa 488-anti-rabbit IgG	goat	1:1000	-	Mol. Probes
FITC-anti-rat IgG	goat	1:1000	-	Jackson lab
Texas red-anti-mouse IgG	goat	1:1000	-	Jackson lab.
Texas red-anti-rabbit IgG	donkey	1:1000	-	Jackson lab.
Texas red-anti-rat IgG	goat	1:1000	-	Jackson lab.
Rhodamine Red-anti-mouse IgG	donkey	1:1000	-	Jackson lab.
Cy5-anti-mouse IgG	donkey	1:1000	-	Jackson lab.
Cy5-anti-rabbit IgG	donkey	1:1000	-	Jackson lab.
Cy5-anti-rat IgG	donkey	1:1000	-	Jackson lab.
Texas Red–X-phalloidine		1:50	-	Invitrogen

Table 5. List of secondary antibodies

INHIBITIORS

Inhibitor/Activator	Function	Final concentration	Incubation time	Company
SNAP	Nitrosylating agent	100µM	1h or 4h	Calbiochem
calcimycin A23187	Activation of nNOS	10µM	15min.	Sigma
NPA	Inhibition of nNOS	1mM or 300µM	1h or over night	Tocris biosciences
L-NAME	Inhibition of NOSs	300µM	1h or over night	Cayman
Y27632	Inhibition of ROCK	10µM	1h or over night	Sigma/Alexis
myrAIP	Inhibition of CaMKII	10µM	30min	Alexis
Cylosporine A (CSA)	Inhibition of calcineurin	5µM	20min	Calbiochem
ALLN	Inhibition of calpain	200µM	1h	Calbiochem
GÖ6976	Inhibition of PKC	50µM	1,5h	Sigma
roscovitine	Inhibiton of cdk5α	50µM	1h or 2h	Sigma
LiCl	Inhibition of GSK3β	20mM	over night (14-16h)	Sigma
blebbistatin	Inhibition of myosin	100µM	15min	Sigma
LPA	Retraction of axons	10µM	30min or 2h	Cayman
aggrecan	Inhibition of axon growth	100µM	4h, 8h or over night	Sigma
taxol	Stabilization of microtubules	3nM or 100nM	30min	Sigma
dibutryl-cAMP	Stimulation of cAMP pathway	1µM	1h	Sigma
forskolin	Induction of cAMP production and stimulation of cAMP pathway	20µM	3h	Calbiochem

Table 6. List of inhibitors and activators.

REFERENCES

Abeliovich A, Chen C, Goda Y, Silva AJ, Stevens CF, Tonegawa S (1993) Modified hippocampal long-term potentiation in PKC gamma-mutant mice. Cell 75:1253-1262.

Abu-Soud HM, Stuehr DJ (1993) Nitric oxide synthases reveal a role for calmodulin in controlling electron transfer. Proc Natl Acad Sci U S A 90:10769-10772.

Ahmad FJ, Hughey J, Wittmann T, Hyman A, Greaser M, Baas PW (2000) Motor proteins regulate force interactions between microtubules and microfilaments in the axon. Nat Cell Biol 2:276-280.

Alberts B, J. A. LJ, M. R, K. R, P. W (2008) Molecular Biology of the cell, 5th edition edn.

Aletta JM, Lewis SA, Cowan NJ, Greene LA (1988) Nerve growth factor regulates both the phosphorylation and steady-state levels of microtubule-associated protein 1.2 (MAP1.2). J Cell Biol 106:1573-1581.

Allingham JS, Smith R, Rayment I (2005) The structural basis of blebbistatin inhibition and specificity for myosin II. Nat Struct Mol Biol 12:378-379.

Amano M, Mukai H, Ono Y, Chihara K, Matsui T, Hamajima Y, Okawa K, Iwamatsu A, Kaibuchi K (1996) Identification of a putative target for Rho as the serine-threonine kinase protein kinase N. Science 271:648-650.

Antar LN, Dictenberg JB, Plociniak M, Afroz R, Bassell GJ (2005) Localization of FMRP-associated mRNA granules and requirement of microtubules for activity-dependent trafficking in hippocampal neurons. Genes Brain Behav 4:350-359.

Antoni FA, Palkovits M, Simpson J, Smith SM, Leitch AL, Rosie R, Fink G, Paterson JM (1998) Ca2+/calcineurin-inhibited adenylyl cyclase, highly abundant in forebrain regions, is important for learning and memory. J Neurosci 18:9650-9661.

Argiro V, Bunge MB, Johnson MI (1984) Correlation between growth form and movement and their dependence on neuronal age. J Neurosci 4:3051-3062.

Aslan M, Ryan TM, Townes TM, Coward L, Kirk MC, Barnes S, Alexander CB, Rosenfeld SS, Freeman BA (2003) Nitric oxide-dependent generation of reactive species in sickle cell disease. Actin tyrosine induces defective cytoskeletal polymerization. J Biol Chem 278:4194-4204.

Avila J, Ulloa L, Diez-Guerra J, Diaz-Nido J (1994) Role of phosphorylated MAPlB in neuritogenesis. Cell Biol Int 18:309-314.

Baas PW, Ahmad FJ (2001) Force generation by cytoskeletal motor proteins as a regulator of axonal elongation and retraction. Trends Cell Biol 11:244-249.

Baas PW, Deitch JS, Black MM, Banker GA (1988) Polarity orientation of microtubules in hippocampal neurons: uniformity in the axon and nonuniformity in the dendrite. Proc Natl Acad Sci U S A 85:8335-8339.

Baker KA, Moore SW, Jarjour AA, Kennedy TE (2006) When a diffusible axon guidance cue stops diffusing: roles for netrins in adhesion and morphogenesis. Curr Opin Neurobiol 16:529-534.

Banan A, McCormack SA, Johnson LR (1998) Polyamines are required for microtubule formation during gastric mucosal healing. Am J Physiol 274:G879-885.

Bandtlow CE, Schmidt MF, Hassinger TD, Schwab ME, Kater SB (1993) Role of intracellular calcium in NI-35-evoked collapse of neuronal growth cones. Science 259:80-83.

Barallobre MJ, Pascual M, Del Rio JA, Soriano E (2005) The Netrin family of guidance factors: emphasis on Netrin-1 signalling. Brain Res Brain Res Rev 49:22-47.

Barritt AW, Davies M, Marchand F, Hartley R, Grist J, Yip P, McMahon SB, Bradbury EJ (2006) Chondroitinase ABC promotes sprouting of intact and injured spinal systems after spinal cord injury. J Neurosci 26:10856-10867.

Bates CA, Trinh N, Meyer RL (1993) Distribution of microtubule-associated proteins (MAPs) in adult and embryonic mouse retinal explants: presence of the embryonic map, MAP5/1B, in regenerating adult retinal axons. Dev Biol 155:533-544.

Battaini F, Pascale A (2005) Protein kinase C signal transduction regulation in physiological and pathological aging. Ann N Y Acad Sci 1057:177-192.

Behar O, Golden, J. A., Mashimo, H., Schoen, F. J., Fishman, M. C. (1996) Semaphorin III is needed for normal patterning and growth of nerves, bones and heart. Nature 383:525-528.

Belanger D, Farah CA, Nguyen MD, Lauzon M, Cornibert S, Leclerc N (2002) The projection domain of MAP2b regulates microtubule protrusion and process formation in Sf9 cells. J Cell Sci 115:1523-1539.

Bicker G (2005) STOP and GO with NO: nitric oxide as a regulator of cell motility in simple brains. Bioessays 27:495-505.

Billuart P, Winter CG, Maresh A, Zhao X, Luo L (2001) Regulating axon branch stability: the role of p190 RhoGAP in repressing a retraction signaling pathway. Cell 107:195-207.

Bito H, Furuyashiki T, Ishihara H, Shibasaki Y, Ohashi K, Mizuno K, Maekawa M, Ishizaki T, Narumiya S (2000) A critical role for a Rho-associated kinase, p160ROCK, in determining axon outgrowth in mammalian CNS neurons. Neuron 26:431-441.

Black MM, Slaughter T, Fischer I (1994) Microtubule-associated protein 1b (MAP1b) is concentrated in the distal region of growing axons. J Neurosci 14:857-870.

Bloom GS, Schoenfeld TA, Vallee RB (1984) Widespread distribution of the major polypeptide component of MAP 1 (microtubule-associated protein 1) in the nervous system. J Cell Biol 98:320-330.

Book AA, Fischer I, Yu XJ, Iannuzzelli P, Murphy EH (1996) Altered expression of microtubule-associated proteins in cat trochlear motoneurons after peripheral and central lesions of the trochlear nerve. Exp Neurol 138:214-226.

Borisoff JF, Chan CC, Hiebert GW, Oschipok L, Robertson GS, Zamboni R, Steeves JD, Tetzlaff W (2003) Suppression of Rho-kinase activity promotes axonal growth on inhibitory CNS substrates. Mol Cell Neurosci 22:405-416.

Bouquet C, Ravaille-Veron M, Propst F, Nothias F (2007) MAP1B coordinates microtubule and actin filament remodeling in adult mouse Schwann cell tips and DRG neuron growth cones. Mol Cell Neurosci 36:235-247.

Bouquet C, Soares S, von Boxberg Y, Ravaille-Veron M, Propst F, Nothias F (2004) Microtubule-associated protein 1B controls directionality of growth cone migration and axonal branching in regeneration of adult dorsal root ganglia neurons. J Neurosci 24:7204-7213.

Boyne LJ, Martin K, Hockfield S, Fischer I (1995) Expression and distribution of phosphorylated MAP1B in growing axons of cultured hippocampal neurons. J Neurosci Res 40:439-450.

Bradbury EJ, Moon LD, Popat RJ, King VR, Bennett GS, Patel PN, Fawcett JW, McMahon SB (2002) Chondroitinase ABC promotes functional recovery after spinal cord injury. Nature 416:636-640.

Bradford D, Cole SJ, Cooper HM (2009) Netrin-1: diversity in development. Int J Biochem Cell Biol 41:487-493.

Bradke F, Dotti CG (1999) The role of local actin instability in axon formation. Science 283:1931-1934.

Bray D, Chapman K (1985) Analysis of microspike movements on the neuronal growth cone. J Neurosci 5:3204-3213.

Bredt DS, Snyder SH (1994) Transient nitric oxide synthase neurons in embryonic cerebral cortical plate, sensory ganglia, and olfactory epithelium. Neuron 13:301-313.

Brody BA, Ley CA, Parysek LM (1989) Selective distribution of the 57 kDa neural intermediate filament protein in the rat CNS. J Neurosci 9:2391-2401.

Brookes PS, Salinas EP, Darley-Usmar K, Eiserich JP, Freeman BA, Darley-Usmar VM, Anderson PG (2000) Concentration-dependent effects of nitric oxide on mitochondrial permeability transition and cytochrome c release. J Biol Chem 275:20474-20479.

Brose K, Tessier-Lavigne M (2000) Slit proteins: key regulators of axon guidance, axonal branching, and cell migration. Curr Opin Neurobiol 10:95-102.

Brose K, Bland KS, Wang KH, Arnott D, Henzel W, Goodman CS, Tessier-Lavigne M, Kidd T (1999) Slit proteins bind Robo receptors and have an evolutionarily conserved role in repulsive axon guidance. Cell 96:795-806.

Brown GC (1999) Nitric oxide and mitochondrial respiration. Biochim Biophys Acta 1411:351-369.

Brugg B, Reddy D, Matus A (1993) Attenuation of microtubule-associated protein 1B expression by antisense oligodeoxynucleotides inhibits initiation of neurite outgrowth. Neuroscience 52:489-496.

Brune B, Lapetina EG (1991) Phosphorylation of nitric oxide synthase by protein kinase A. Biochem Biophys Res Commun 181:921-926.

Bueno OF, van Rooij E, Molkentin JD, Doevendans PA, De Windt LJ (2002) Calcineurin and hypertrophic heart disease: novel insights and remaining questions. Cardiovasc Res 53:806-821.

Busca R, Bertolotto C, Abbe P, Englaro W, Ishizaki T, Narumiya S, Boquet P, Ortonne JP, Ballotti R (1998) Inhibition of Rho is required for cAMP-induced melanoma cell differentiation. Mol Biol Cell 9:1367-1378.

Bush MS, Tonge DA, Woolf C, Gordon-Weeks PR (1996) Expression of a developmentally regulated, phosphorylated isoform of microtubule-associated protein 1B in regenerating axons of the sciatic nerve. Neuroscience 73:553-563.

Cai D, Deng K, Mellado W, Lee J, Ratan RR, Filbin MT (2002) Arginase I and polyamines act downstream from cyclic AMP in overcoming inhibition of axonal growth MAG and myelin in vitro. Neuron 35:711-719.

Calvert RA, Woodhams PL, Anderton BH (1987) Localization of an epitope of a microtubule-associated protein 1x in outgrowing axons of the developing rat central nervous system. Neuroscience 23:131-141.

Cassina AM, Hodara R, Souza JM, Thomson L, Castro L, Ischiropoulos H, Freeman BA, Radi R (2000) Cytochrome c nitration by peroxynitrite. J Biol Chem 275:21409-21415.

Chae T, Kwon YT, Bronson R, Dikkes P, Li E, Tsai LH (1997) Mice lacking p35, a neuronal specific activator of Cdk5, display cortical lamination defects, seizures, and adult lethality. Neuron 18:29-42.

Chedotal A, Del Rio JA, Ruiz M, He Z, Borrell V, de Castro F, Ezan F, Goodman CS, Tessier-Lavigne M, Sotelo C, Soriano E (1998) Semaphorins III and IV repel hippocampal axons via two distinct receptors. Development 125:4313-4323.

Chen H, Chedotal A, He Z, Goodman CS, Tessier-Lavigne M (1997) Neuropilin-2, a novel member of the neuropilin family, is a high affinity receptor for the semaphorins Sema E and Sema IV but not Sema III. Neuron 19:547-559.

Cheng A, Wang S, Cai J, Rao MS, Mattson MP (2003) Nitric oxide acts in a positive feedback loop with BDNF to regulate neural progenitor cell proliferation and differentiation in the mammalian brain. Dev Biol 258:319-333.

Chitaley K, Webb RC (2002) Nitric oxide induces dilation of rat aorta via inhibition of rho-kinase signaling. Hypertension 39:438-442.

Choi ES, Rettig WJ, Wayner EA, Srour ML, Clegg DO (1994) Functional identification of integrin laminin receptors that mediate process outgrowth by human SY5Y neuroblastoma cells. J Neurosci Res 37:475-488.

Choi ES, Rettig, W. J., Wayner, E. A., Srour, M. L., Clegg, D. O. (1994) Functional identification of integrin laminin receptors that mediate process outgrowth by human SY5Y neuroblastoma cells. J Neurosci Res 37:475-488.

Choo QL, Bray D (1978) Two forms of neuronal actin. J Neurochem 31:217-224.

Coghlan VM, Perrino BA, Howard M, Langeberg LK, Hicks JB, Gallatin WM, Scott JD (1995) Association of protein kinase A and protein phosphatase 2B with a common anchoring protein. Science 267:108-111.

Collins JH, Korn ED (1980) Actin activation of Ca2+-sensitive Mg2+-ATPase activity of Acanthamoeba myosin II is enhanced by dephosphorylation of its heavy chains. J Biol Chem 255:8011-8014.

Collins MO, Yu L, Coba MP, Husi H, Campuzano I, Blackstock WP, Choudhary JS, Grant SG (2005) Proteomic analysis of in vivo phosphorylated synaptic proteins. J Biol Chem 280:5972-5982.

Connor JA (1986) Digital imaging of free calcium changes and of spatial gradients in growing processes in single, mammalian central nervous system cells. Proc Natl Acad Sci U S A 83:6179-6183.

Contos JJ, Ishii I, Chun J (2000) Lysophosphatidic acid receptors. Mol Pharmacol 58:1188-1196.

Cook TA, Nagasaki T, Gundersen GG (1998) Rho guanosine triphosphatase mediates the selective stabilization of microtubules induced by lysophosphatidic acid. J Cell Biol 141:175-185.

Cooper CE (2002) Nitric oxide and cytochrome oxidase: substrate, inhibitor or effector? Trends Biochem Sci 27:33-39.

Cork RJ, Perrone ML, Bridges D, Wandell J, Scheiner CA, Mize RR (1998) A web-accessible digital atlas of the distribution of nitric oxide synthase in the mouse brain. Prog Brain Res 118:37-50.

Cote GP, Collins JH, Korn ED (1981) Identification of three phosphorylation sites on each heavy chain of Acanthamoeba myosin II. J Biol Chem 256:12811-12816.

Cowan CA, Yokoyama N, Bianchi LM, Henkemeyer M, Fritzsch B (2000) EphB2 guides axons at the midline and is necessary for normal vestibular function. Neuron 26:417-430.

Cramer KS, Angelucci A, Hahm JO, Bogdanov MB, Sur M (1996) A role for nitric oxide in the development of the ferret retinogeniculate projection. J Neurosci 16:7995-8004.

Das AK, Hajra AK (1989) Quantification, characterization and fatty acid composition of lysophosphatidic acid in different rat tissues. Lipids 24:329-333.

Davies SJ, Goucher DR, Doller C, Silver J (1999) Robust regeneration of adult sensory axons in degenerating white matter of the adult rat spinal cord. J Neurosci 19:5810-5822.

Dawson VL, Dawson TM (1996) Nitric oxide actions in neurochemistry. Neurochem Int 29:97-110.

Dawson VL, Dawson TM, London ED, Bredt DS, Snyder SH (1991) Nitric oxide mediates glutamate neurotoxicity in primary cortical cultures. Proc Natl Acad Sci U S A 88:6368-6371.

de Castro F (2003) Chemotropic molecules: guides for axonal pathfinding and cell migration during CNS development. News Physiol Sci 18:130-136.

de Lanerolle P, Nishikawa M (1988) Regulation of embryonic smooth muscle myosin by protein kinase C. J Biol Chem 263:9071-9074.

De Lozanne A, Spudich JA (1987) Disruption of the Dictyostelium myosin heavy chain gene by homologous recombination. Science 236:1086-1091.

Del Rio JA, Gonzalez-Billault C, Urena JM, Jimenez EM, Barallobre MJ, Pascual M, Pujadas L, Simo S, La Torre A, Wandosell F, Avila J, Soriano E (2004) MAP1B is required for Netrin 1 signaling in neuronal migration and axonal guidance. Curr Biol 14:840-850.

Dempsey EC, Newton AC, Mochly-Rosen D, Fields AP, Reyland ME, Insel PA, Messing RO (2000) Protein kinase C isozymes and the regulation of diverse cell responses. Am J Physiol Lung Cell Mol Physiol 279:L429-438.

Deng K, He H, Qiu J, Lorber B, Bryson JB, Filbin MT (2009) Increased synthesis of spermidine as a result of upregulation of arginase I promotes axonal regeneration in culture and in vivo. J Neurosci 29:9545-9552.

Dent EW, Gertler FB (2003) Cytoskeletal dynamics and transport in growth cone motility and axon guidance. Neuron 40:209-227.

Dergham P, Ellezam B, Essagian C, Avedissian H, Lubell WD, McKerracher L (2002) Rho signaling pathway targeted to promote spinal cord repair. J Neurosci 22:6570-6577.

Derkach V, Barria A, Soderling TR (1999) Ca2+/calmodulin-kinase II enhances channel conductance of alpha-amino-3-hydroxy-5-methyl-4-isoxazolepropionate type glutamate receptors. Proc Natl Acad Sci U S A 96:3269-3274.

DerMardirossian C, Bokoch GM (2005) GDIs: central regulatory molecules in Rho GTPase activation. Trends Cell Biol 15:356-363.

Derry WB, Wilson L, Jordan MA (1995) Substoichiometric binding of taxol suppresses microtubule dynamics. Biochemistry 34:2203-2211.

Diaz-Nido J, Serrano L, Mendez E, Avila J (1988) A casein kinase II-related activity is involved in phosphorylation of microtubule-associated protein MAP-1B during neuroblastoma cell differentiation. J Cell Biol 106:2057-2065.

Dickson BJ (2002) Molecular mechanisms of axon guidance. Science 298:1959-1964.

Dinerman JL, Dawson TM, Schell MJ, Snowman A, Snyder SH (1994) Endothelial nitric oxide synthase localized to hippocampal pyramidal cells: implications for synaptic plasticity. Proc Natl Acad Sci U S A 91:4214-4218.

Ding J, Liu JJ, Kowal AS, Nardine T, Bhattacharya P, Lee A, Yang Y (2002) Microtubule-associated protein 1B: a neuronal binding partner for gigaxonin. J Cell Biol 158:427-433.

DiTella MC, Feiguin F, Carri N, Kosik KS, Caceres A (1996) MAP-1B/TAU functional redundancy during laminin-enhanced axonal growth. J Cell Sci 109 (Pt 2):467-477.

Dong JM, Leung T, Manser E, Lim L (1998) cAMP-induced morphological changes are counteracted by the activated RhoA small GTPase and the Rho kinase ROKalpha. J Biol Chem 273:22554-22562.

Dontchev VD, Letourneau PC (2002) Nerve growth factor and semaphorin 3A signaling pathways interact in regulating sensory neuronal growth cone motility. J Neurosci 22:6659-6669.

Dubreuil CI, Winton MJ, McKerracher L (2003) Rho activation patterns after spinal cord injury and the role of activated Rho in apoptosis in the central nervous system. J Cell Biol 162:233-243.

Ebadi M, Sharma SK (2003) Peroxynitrite and mitochondrial dysfunction in the pathogenesis of Parkinson's disease. Antioxid Redox Signal 5:319-335.

Edelmann W, Zervas M, Costello P, Roback L, Fischer I, Hammarback JA, Cowan N, Davies P, Wainer B, Kucherlapati R (1996) Neuronal abnormalities in microtubule-associated protein 1B mutant mice. Proc Natl Acad Sci U S A 93:1270-1275.

Edson K, Weisshaar B, Matus A (1993) Actin depolymerisation induces process formation on MAP2-transfected non-neuronal cells. Development 117:689-700.

Egea J, Klein R (2007) Bidirectional Eph-ephrin signaling during axon guidance. Trends Cell Biol 17:230-238.

Eliasson MJ, Huang Z, Ferrante RJ, Sasamata M, Molliver ME, Snyder SH, Moskowitz MA (1999) Neuronal nitric oxide synthase activation and peroxynitrite formation in ischemic stroke linked to neural damage. J Neurosci 19:5910-5918.

Elmes SJ, Millns PJ, Smart D, Kendall DA, Chapman V (2004) Evidence for biological effects of exogenous LPA on rat primary afferent and spinal cord neurons. Brain Res 1022:205-213.

Endo T, Naka M, Hidaka H (1982) Ca2+-phospholipid dependent phosphorylation of smooth muscle myosin. Biochem Biophys Res Commun 105:942-948.

Ernst AF, Gallo G, Letourneau PC, McLoon SC (2000) Stabilization of growing retinal axons by the combined signaling of nitric oxide and brain-derived neurotrophic factor. J Neurosci 20:1458-1469.

Ertürk A, Hellal F, Enes J, Bradke F (2007) Disorganized microtubules underlie the formation of retraction bulbs and the failure of axonal regeneration. J Neurosci 27:9169-9180.

Escurat M, Djabali K, Gumpel M, Gros F, Portier MM (1990) Differential expression of two neuronal intermediate-filament proteins, peripherin and the low-molecular-mass neurofilament protein (NF-L), during the development of the rat. J Neurosci 10:764-784.

Farah CA, Leclerc N (2008) HMWMAP2: new perspectives on a pathway to dendritic identity. Cell Motil Cytoskeleton 65:515-527.

Fawcett JW, Mathews G, Housden E, Goedert M, Matus A (1994) Regenerating sciatic nerve axons contain the adult rather than the embryonic pattern of microtubule associated proteins. Neuroscience 61:789-804.

Feldman S, Weidenfeld J (2004) Involvement of endogeneous glutamate in the stimulatory effect of norepinephrine and serotonin on the hypothalamo-pituitary-adrenocortical axis. Neuroendocrinology 79:43-53.

Filbin MT (2003) Myelin-associated inhibitors of axonal regeneration in the adult mammalian CNS. Nat Rev Neurosci 4:703-713.

Fink CC, Bayer KU, Myers JW, Ferrell JE, Jr., Schulman H, Meyer T (2003) Selective regulation of neurite extension and synapse formation by the beta but not the alpha isoform of CaMKII. Neuron 39:283-297.

Fischer I, Romano-Clarke G (1990) Changes in microtubule-associated protein MAP1B phosphorylation during rat brain development. J Neurochem 55:328-333.

Fischer I, Romano-Clarke G, Grynspan F (1991) Calpain-mediated proteolysis of microtubule associated proteins MAP1B and MAP2 in developing brain. Neurochem Res 16:891-898.

Fliegner KH, Kaplan MP, Wood TL, Pintar JE, Liem RK (1994) Expression of the gene for the neuronal intermediate filament protein alpha-internexin coincides with the onset of neuronal differentiation in the developing rat nervous system. J Comp Neurol 342:161-173.

Fournier AE, Takizawa BT, Strittmatter SM (2003) Rho kinase inhibition enhances axonal regeneration in the injured CNS. J Neurosci 23:1416-1423.

French PJ, Bijman J, Edixhoven M, Vaandrager AB, Scholte BJ, Lohmann SM, Nairn AC, de Jonge HR (1995) Isotype-specific activation of cystic fibrosis transmembrane conductance regulator-chloride channels by cGMP-dependent protein kinase II. J Biol Chem 270:26626-26631.

Fukunaga K, Muller D, Miyamoto E (1995) Increased phosphorylation of Ca2+/calmodulin-dependent protein kinase II and its endogenous substrates in the induction of long-term potentiation. J Biol Chem 270:6119-6124.

Fukushima N (2004) LPA in neural cell development. J Cell Biochem 92:993-1003.

Fukushima N, Morita Y (2006) Actomyosin-dependent microtubule rearrangement in lysophosphatidic acid-induced neurite remodeling of young cortical neurons. Brain Res 1094:65-75.

Fukushima N, Weiner JA, Chun J (2000) Lysophosphatidic acid (LPA) is a novel extracellular regulator of cortical neuroblast morphology. Dev Biol 228:6-18.

Fukushima N, Ye X, Chun J (2002b) Neurobiology of lysophosphatidic acid signaling. Neuroscientist 8:540-550.

Fukushima N, Weiner JA, Kaushal D, Contos JJ, Rehen SK, Kingsbury MA, Kim KY, Chun J (2002a) Lysophosphatidic acid influences the morphology and motility of young, postmitotic cortical neurons. Mol Cell Neurosci 20:271-282.

Gallo G (2006) RhoA-kinase coordinates F-actin organization and myosin II activity during semaphorin-3A-induced axon retraction. J Cell Sci 119:3413-3423.

Gao Y, Deng K, Hou J, Bryson JB, Barco A, Nikulina E, Spencer T, Mellado W, Kandel ER, Filbin MT (2004) Activated CREB is sufficient to overcome inhibitors in myelin and promote spinal axon regeneration in vivo. Neuron 44:609-621.

Garcia ML, Strehler EE (1999) Plasma membrane calcium ATPases as critical regulators of calcium homeostasis during neuronal cell function. Front Biosci 4:D869-882.

Garthwaite J, Charles SL, Chess-Williams R (1988) Endothelium-derived relaxing factor release on activation of NMDA receptors suggests role as intercellular messenger in the brain. Nature 336:385-388.

Giese KP, Fedorov NB, Filipkowski RK, Silva AJ (1998) Autophosphorylation at Thr286 of the alpha calcium-calmodulin kinase II in LTP and learning. Science 279:870-873.

Giger RJ, Wolfer DP, De Wit GM, Verhaagen J (1996) Anatomy of rat semaphorin III/collapsin-1 mRNA expression and relationship to developing nerve tracts during neuroembryogenesis. J Comp Neurol 375:378-392.

Giovannoni G, Heales SJ, Silver NC, O'Riordan J, Miller RF, Land JM, Clark JB, Thompson EJ (1997) Raised serum nitrate and nitrite levels in patients with multiple sclerosis. J Neurol Sci 145:77-81.

Giovannoni G, Silver NC, O'Riordan J, Miller RF, Heales SJ, Land JM, Elliot M, Feldmann M, Miller DH, Thompson EJ (1999) Increased urinary nitric oxide metabolites in patients with multiple sclerosis correlates with early and relapsing disease. Mult Scler 5:335-341.

Go YM, Patel RP, Maland MC, Park H, Beckman JS, Darley-Usmar VM, Jo H (1999) Evidence for peroxynitrite as a signaling molecule in flow-dependent activation of c-Jun NH(2)-terminal kinase. Am J Physiol 277:H1647-1653.

Goldberg DJ, Burmeister DW (1986) Stages in axon formation: observations of growth of Aplysia axons in culture using video-enhanced contrast-differential interference contrast microscopy. J Cell Biol 103:1921-1931.

Goldman RD, Grin B, Mendez MG, Kuczmarski ER (2008) Intermediate filaments: versatile building blocks of cell structure. Curr Opin Cell Biol 20:28-34.

Goll DE, Thompson VF, Li H, Wei W, Cong J (2003) The calpain system. Physiol Rev 83:731-801.

Gomez TM, Zheng JQ (2006) The molecular basis for calcium-dependent axon pathfinding. Nat Rev Neurosci 7:115-125.

Gong CX, Wegiel J, Lidsky T, Zuck L, Avila J, Wisniewski HM, Grundke-Iqbal I, Iqbal K (2000) Regulation of phosphorylation of neuronal microtubule-associated proteins MAP1b and MAP2 by protein phosphatase-2A and -2B in rat brain. Brain Res 853:299-309.

Gonzalez-Billault C, Del Rio JA, Urena JM, Jimenez-Mateos EM, Barallobre MJ, Pascual M, Pujadas L, Simo S, Torre AL, Gavin R, Wandosell F, Soriano E, Avila J (2005) A role of MAP1B in Reelin-dependent neuronal migration. Cereb Cortex 15:1134-1145.

Gonzalez-Billault C, Del Rio, J. A., Urena, J. M., Jimenez-Mateos, E. M., Barallobre, M. J., Pascual, M., Pujadas, L., Simo, S., Torre, A. L.,Gavin, R., Wandosell, F., Soriano, E., Avila, J. (2005) A role of MAP1B in Reelin-dependent neuronal migration. Cereb Cortex 15:1134-1145.

Goold RG, Gordon-Weeks PR (2001) Microtubule-associated protein 1B phosphorylation by glycogen synthase kinase 3beta is induced during PC12 cell differentiation. J Cell Sci 114:4273-4284.

Goold RG, Owen R, Gordon-Weeks PR (1999) Glycogen synthase kinase 3beta phosphorylation of microtubule-associated protein 1B regulates the stability of microtubules in growth cones. J Cell Sci 112 (Pt 19):3373-3384.

Gordh T, Sharma HS, Alm P, Westman J (1998) Spinal nerve lesion induces upregulation of neuronal nitric oxide synthase in the spinal cord. An immunohistochemical investigation in the rat. Amino Acids 14:105-112.

Gordon-Weeks PR, Fischer I (2000) MAP1B expression and microtubule stability in growing and regenerating axons. Microsc Res Tech 48:63-74.

Gordon-Weeks PR, Johnstone M, Bush M (1995) Phosphorylation of microtubule-associated protein IB and axonal growth. Biochem Soc Trans 23:37-40.

Gordon-Weeks PR, Mansfield SG, Alberto C, Johnstone M, Moya F (1993) A phosphorylation epitope on MAP 1B that is transiently expressed in growing axons in the developing rat nervous system. Eur J Neurosci 5:1302-1311.

Griffith LC (2004) Calcium/calmodulin-dependent protein kinase II: an unforgettable kinase. J Neurosci 24:8391-8393.

Gu Z, Kaul M, Yan B, Kridel SJ, Cui J, Strongin A, Smith JW, Liddington RC, Lipton SA (2002) S-nitrosylation of matrix metalloproteinases: signaling pathway to neuronal cell death. Science 297:1186-1190.

Guijarro P, Simo S, Pascual M, Abasolo I, Del Rio JA, Soriano E (2006) Netrin1 exerts a chemorepulsive effect on migrating cerebellar interneurons in a Dcc-independent way. Mol Cell Neurosci 33:389-400.

Guix FX, Uribesalgo I, Coma M, Munoz FJ (2005) The physiology and pathophysiology of nitric oxide in the brain. Prog Neurobiol 76:126-152.

Hahn CM, Kleinholz H, Koester MP, Grieser S, Thelen K, Pollerberg GE (2005) Role of cyclin-dependent kinase 5 and its activator P35 in local axon and growth cone stabilization. Neuroscience 134:449-465.

Hajieva P, Kuhlmann C, Luhmann HJ, Behl C (2009) Impaired calcium homeostasis in aged hippocampal neurons. Neurosci Lett 451:119-123.

Hajimohammadreza I, Probert AW, Coughenour LL, Borosky SA, Marcoux FW, Boxer PA, Wang KK (1995) A specific inhibitor of calcium/calmodulin-dependent protein kinase-II provides neuroprotection against NMDA- and hypoxia/hypoglycemia-induced cell death. J Neurosci 15:4093-4101.

Hall A (1994) Small GTP-binding proteins and the regulation of the actin cytoskeleton. Annu Rev Cell Biol 10:31-54.

Hall KT, Boumsell L, Schultze JL, Boussiotis VA, Dorfman DM, Cardoso AA, Bensussan A, Nadler LM, Freeman GJ (1996) Human CD100, a novel leukocyte semaphorin that promotes B-cell aggregation and differentiation. Proc Natl Acad Sci U S A 93:11780-11785.

Hallows JL, Chen K, DePinho RA, Vincent I (2003) Decreased cyclin-dependent kinase 5 (cdk5) activity is accompanied by redistribution of cdk5 and cytoskeletal proteins and increased cytoskeletal protein phosphorylation in p35 null mice. J Neurosci 23:10633-10644.

Halpain S, Dehmelt L (2006) The MAP1 family of microtubule-associated proteins. Genome Biol 7:224.

Hanger DP, Anderton BH, Noble W (2009) Tau phosphorylation: the therapeutic challenge for neurodegenerative disease. Trends Mol Med.

Hao G, Derakhshan B, Shi L, Campagne F, Gross SS (2006) SNOSID, a proteomic method for identification of cysteine S-nitrosylation sites in complex protein mixtures. Proc Natl Acad Sci U S A 103:1012-1017.

Hao W, Myhre AP, Palmer JP (1999) Nitric oxide mediates IL-1beta stimulation of heat shock protein but not IL-1beta inhibition of glutamic acid decarboxylase. Autoimmunity 29:93-101.

Haque N, Gong CX, Sengupta A, Iqbal K, Grundke-Iqbal I (2004) Regulation of microtubule-associated proteins, protein kinases and protein phosphatases during differentiation of SY5Y cells. Brain Res Mol Brain Res 129:163-170.

Harada A, Teng J, Takei Y, Oguchi K, Hirokawa N (2002) MAP2 is required for dendrite elongation, PKA anchoring in dendrites, and proper PKA signal transduction. J Cell Biol 158:541-549.

Hasegawa Y, Fujitani M, Hata K, Tohyama M, Yamagishi S, Yamashita T (2004) Promotion of axon regeneration by myelin-associated glycoprotein and Nogo through divergent signals downstream of Gi/G. J Neurosci 24:6826-6832.

Hayashi S, Ueyama T, Kajimoto T, Yagi K, Kohmura E, Saito N (2005) Involvement of gamma protein kinase C in estrogen-induced neuroprotection against focal brain ischemia through G protein-coupled estrogen receptor. J Neurochem 93:883-891.

He Y, Yu W, Baas PW (2002) Microtubule reconfiguration during axonal retraction induced by nitric oxide. J Neurosci 22:5982-5991.

He Y, Yu, W., Baas, P. W. (2002) Microtubule reconfiguration during axonal retraction induced by nitric oxide. J Neurosci 22:5982-5991.

Hendricks M, Jesuthasan S (2009) PHR regulates growth cone pausing at intermediate targets through microtubule disassembly. J Neurosci 29:6593-6598.

Henkemeyer M, Orioli D, Henderson JT, Saxton TM, Roder J, Pawson T, Klein R (1996) Nuk controls pathfinding of commissural axons in the mammalian central nervous system. Cell 86:35-46.

Henley J, Poo MM (2004a) Guiding neuronal growth cones using Ca2+ signals. Trends Cell Biol 14:320-330.

Henley JR, Huang KH, Wang D, Poo, M. M (2004b) Calcium mediates bidirectional growth cone turning induced by myelin-associated glycoprotein. Neuron 44:909-916.

Hensley K, Maidt ML, Yu Z, Sang H, Markesbery WR, Floyd RA (1998) Electrochemical analysis of protein nitrotyrosine and dityrosine in the Alzheimer brain indicates region-specific accumulation. J Neurosci 18:8126-8132.

Hess DT, Patterson SI, Smith DS, Skene JH (1993) Neuronal growth cone collapse and inhibition of protein fatty acylation by nitric oxide. In: Nature, pp 562-565.

Hess DT, Matsumoto A, Kim SO, Marshall HE, Stamler JS (2005) Protein S-nitrosylation: purview and parameters. Nat Rev Mol Cell Biol 6:150-166.

Hink U, Oelze M, Kolb P, Bachschmid M, Zou MH, Daiber A, Mollnau H, August M, Baldus S, Tsilimingas N, Walter U, Ullrich V, Munzel T (2003) Role for peroxynitrite in the inhibition of prostacyclin synthase in nitrate tolerance. J Am Coll Cardiol 42:1826-1834.

Hirose M, Ishizaki T, Watanabe N, Uehata M, Kranenburg O, Moolenaar WH, Matsumura F, Maekawa M, Bito H, Narumiya S (1998) Molecular dissection of the Rho-associated protein kinase (p160ROCK)-regulated neurite remodeling in neuroblastoma N1E-115 cells. J Cell Biol 141:1625-1636.

Ho CL, Chin SS, Carnevale K, Liem RK (1995) Translation initiation and assembly of peripherin in cultured cells. Eur J Cell Biol 68:103-112.

Holtsberg FW, Steiner MR, Bruce-Keller AJ, Keller JN, Mattson MP, Moyers JC, Steiner SM (1998) Lysophosphatidic acid and apoptosis of nerve growth factor-differentiated PC12 cells. J Neurosci Res 53:685-696.

Hong K, Nishiyama M, Henley J, Tessier-Lavigne M, Poo M (2000) Calcium signalling in the guidance of nerve growth by netrin-1. Nature 403:93-98.

Hoshi M, Nishida E, Inagaki M, Gotoh Y, Sakai H (1990) Activation of a serine/threonine kinase that phosphorylates microtubule-associated protein 1B in vitro by growth factors and phorbol esters in quiescent rat fibroblastic cells. Eur J Biochem 193:513-519.

Huang PL (1999) Neuronal and endothelial nitric oxide synthase gene knockout mice. Braz J Med Biol Res 32:1353-1359.

Huang Y, Higginson DS, Hester L, Park MH, Snyder SH (2007) Neuronal growth and survival mediated by eIF5A, a polyamine-modified translation initiation factor. Proc Natl Acad Sci U S A 104:4194-4199.

Hubbard MJ, Klee CB (1989) Functional domain structure of calcineurin A: mapping by limited proteolysis. Biochemistry 28:1868-1874.

Hudmon A, Schulman H (2002a) Neuronal CA2+/calmodulin-dependent protein kinase II: the role of structure and autoregulation in cellular function. Annu Rev Biochem 71:473-510.

Hudmon A, Schulman H (2002b) Structure-function of the multifunctional Ca2+/calmodulin-dependent protein kinase II. Biochem J 364:593-611.

Hyman BT, Marzloff K, Wenniger JJ, Dawson TM, Bredt DS, Snyder SH (1992) Relative sparing of nitric oxide synthase-containing neurons in the hippocampal formation in Alzheimer's disease. Ann Neurol 32:818-820.

Iadecola C, Zhang F, Xu S, Casey R, Ross ME (1995) Inducible nitric oxide synthase gene expression in brain following cerebral ischemia. J Cereb Blood Flow Metab 15:378-384.

Iadecola C, Zhang F, Casey R, Nagayama M, Ross ME (1997) Delayed reduction of ischemic brain injury and neurological deficits in mice lacking the inducible nitric oxide synthase gene. J Neurosci 17:9157-9164.

Ignarro LJ (1991) Signal transduction mechanisms involving nitric oxide. Biochem Pharmacol 41:485-490.

Ikebe M, Hartshorne DJ, Elzinga M (1986) Identification, phosphorylation, and dephosphorylation of a second site for myosin light chain kinase on the 20,000-dalton light chain of smooth muscle myosin. J Biol Chem 261:36-39.

Irikura K, Huang PL, Ma J, Lee WS, Dalkara T, Fishman MC, Dawson TM, Snyder SH, Moskowitz MA (1995) Cerebrovascular alterations in mice lacking neuronal nitric oxide synthase gene expression. Proc Natl Acad Sci U S A 92:6823-6827.

Ischiropoulos H, Zhu L, Chen J, Tsai M, Martin JC, Smith CD, Beckman JS (1992) Peroxynitrite-mediated tyrosine nitration catalyzed by superoxide dismutase. Arch Biochem Biophys 298:431-437.

Ishii I, Contos JJ, Fukushima N, Chun J (2000) Functional comparisons of the lysophosphatidic acid receptors, LP(A1)/VZG-1/EDG-2, LP(A2)/EDG-4, and LP(A3)/EDG-7 in neuronal cell lines using a retrovirus expression system. Mol Pharmacol 58:895-902.

Ishizaki I, Contos JJ, Fukushima N, C, hun J (2000) Functional comparisons of the lysophosphatidic acid receptors, LP(A1)/VZG-1/EDG-2, LP(A2)/EDG-4, and LP(A3)/EDG-7 in neuronal cell lines using a retrovirus expression system. Mol Pharmacol 58:895-902.

Ishizaki Y, Tashiro T, Kurokawa M (1983) A calcium-activated protease which preferentially degrades the 160-kDa component of the neurofilament triplet. Eur J Biochem 131:41-45.

Jalink K, Eichholtz T, Postma FR, van Corven EJ, Moolenaar WH (1993) Lysophosphatidic acid induces neuronal shape changes via a novel, receptor-mediated signaling pathway: similarity to thrombin action. Cell Growth Differ 4:247-255.

Jalink K, van Corven EJ, Hengeveld T, Morii N, Narumiya S, Moolenaar WH (1994) Inhibition of lysophosphatidate- and thrombin-induced neurite retraction and neuronal cell rounding by ADP ribosylation of the small GTP-binding protein Rho. J Cell Biol 126:801-810.

Jen JC, Chan WM, Bosley TM, Wan J, Carr JR, Rub U, Shattuck D, Salamon G, Kudo LC, Ou J, Lin DD, Salih MA, Kansu T, Al Dhalaan H, Al Zayed Z, MacDonald DB, Stigsby B, Plaitakis A, Dretakis EK, Gottlob I, Pieh C, Traboulsi EI, Wang Q, Wang L, Andrews C, Yamada K, Demer JL, Karim S, Alger JR, Geschwind DH, Deller T, Sicotte NL, Nelson SF, Baloh RW, Engle EC (2004) Mutations in a human ROBO gene disrupt hindbrain axon pathway crossing and morphogenesis. Science 304:1509-1513.

Jimenez-Mateos EM, Wandosell F, Reiner O, Avila J, Gonzalez-Billault C (2005) Binding of microtubule-associated protein 1B to LIS1 affects the interaction between dynein and LIS1. Biochem J 389:333-341.

Jimenez-Mateos EM, Gonzalez-Billault C, Dawson HN, Vitek MP, Avila J (2006) Role of MAP1B in axonal retrograde transport of mitochondria. Biochem J 397:53-59.

Jin Z, Strittmatter SM (1997) Rac1 mediates collapsin-1-induced growth cone collapse. J Neurosci 17:6256-6263.

Johnson GV, Jope RS, Binder LI (1989) Proteolysis of tau by calpain. Biochem Biophys Res Commun 163:1505-1511.

Johnson GV, Litersky JM, Whitaker JN (1991) Proteolysis of microtubule-associated protein 2 and tubulin by cathepsin D. J Neurochem 57:1577-1583.

Julien JP, Mushynski WE (1998) Neurofilaments in health and disease. Prog Nucleic Acid Res Mol Biol 61:1-23.

Kaehler ST, Singewald N, Sinner C, Philippu A (1999) Nitric oxide modulates the release of serotonin in the rat hypothalamus. Brain Res 835:346-349.

Kalman D, Gomperts SN, Hardy S, Kitamura M, Bishop JM (1999) Ras family GTPases control growth of astrocyte processes. Mol Biol Cell 10:1665-1683.

Kaminska B, Kaczmarek L, Grzelakowska-Sztabert B (1992) Inhibitors of polyamine biosynthesis affect the expression of genes encoding cytoskeletal proteins. FEBS Lett 304:198-200.

Kampfl A, Posmantur RM, Zhao X, Schmutzhard E, Clifton GL, Hayes RL (1997) Mechanisms of calpain proteolysis following traumatic brain injury: implications for pathology and therapy: implications for pathology and therapy: a review and update. J Neurotrauma 14:121-134.

Kashishian A, Howard M, Loh C, Gallatin WM, Hoekstra MF, Lai Y (1998) AKAP79 inhibits calcineurin through a site distinct from the immunophilin-binding region. J Biol Chem 273:27412-27419.

Kater SB, Mills LR (1991) Regulation of growth cone behavior by calcium. J Neurosci 11:891-899.

Katoh H, Aoki J, Ichikawa A, Negishi M (1998) p160 RhoA-binding kinase ROKalpha induces neurite retraction. J Biol Chem 273:2489-2492.

Kawauchi T, Chihama K, Nabeshima Y, Hoshino M (2003) The in vivo roles of STEF/Tiam1, Rac1 and JNK in cortical neuronal migration. Embo J 22:4190-4201.

Kawauchi T, Chihama K, Nishimura YV, Nabeshima Y, Hoshino M (2005) MAP1B phosphorylation is differentially regulated by Cdk5/p35, Cdk5/p25, and JNK. Biochem Biophys Res Commun 331:50-55.

Keino-Masu K, Masu M, Hinck L, Leonardo ED, Chan SS, Culotti JG, Tessier-Lavigne M (1996) Deleted in Colorectal Cancer (DCC) encodes a netrin receptor. Cell 87:175-185.

Khodair MA, Zarbin MA, Townes-Anderson E (2005) Cyclic AMP prevents retraction of axon terminals in photoreceptors prepared for transplantation: an in vitro study. Invest Ophthalmol Vis Sci 46:967-973.

Kidd T, Brose K, Mitchell KJ, Fetter RD, Tessier-Lavigne M, Goodman CS, Tear G (1998) Roundabout controls axon crossing of the CNS midline and defines a novel subfamily of evolutionarily conserved guidance receptors. Cell 92:205-215.

Kim MJ, Jo DG, Hong GS, Kim BJ, Lai M, Cho DH, Kim KW, Bandyopadhyay A, Hong YM, Kim DH, Cho C, Liu JO, Snyder SH, Jung YK (2002) Calpain-dependent cleavage of cain/cabin1 activates calcineurin to mediate calcium-triggered cell death. Proc Natl Acad Sci U S A 99:9870-9875.

Kim YM, Talanian RV, Billiar TR (1997) Nitric oxide inhibits apoptosis by preventing increases in caspase-3-like activity via two distinct mechanisms. J Biol Chem 272:31138-31148.

Kingsbury TJ, Cunningham KW (2000) A conserved family of calcineurin regulators. Genes Dev 14:1595-1604.

Kitsukawa T, Shimono A, Kawakami A, Kondoh H, Fujisawa H (1995) Overexpression of a membrane protein, neuropilin, in chimeric mice causes anomalies in the cardiovascular system, nervous system and limbs. Development 121:4309-4318.

Kitto KF, Haley JE, Wilcox GL (1992) Involvement of nitric oxide in spinally mediated hyperalgesia in the mouse. Neurosci Lett 148:1-5.

Klee CB, Draetta GF, Hubbard MJ (1988) Calcineurin. Adv Enzymol Relat Areas Mol Biol 61:149-200.

Klein R (2009) Bidirectional modulation of synaptic functions by Eph/ephrin signaling. Nat Neurosci 12:15-20.

Kohno K, Kawakami T, Hiruma H (2005) Effects of soluble laminin on organelle transport and neurite growth in cultured mouse dorsal root ganglion neurons: difference between primary neurites and branches. J Cell Physiol 205:253-261.

Kolb JP (2000) Mechanisms involved in the pro- and anti-apoptotic role of NO in human leukemia. Leukemia 14:1685-1694.

Kolo LL, Westfall TC, Macarthur H (2004) Nitric oxide decreases the biological activity of norepinephrine resulting in altered vascular tone in the rat mesenteric arterial bed. Am J Physiol Heart Circ Physiol 286:H296-303.

Kolodkin AL, Matthes DJ, Goodman CS (1993) The semaphorin genes encode a family of transmembrane and secreted growth cone guidance molecules. Cell 75:1389-1399.

Kolodkin AL, Levengood, D. V., Rowe, E. G., Tai, Y. T., Giger, R. J., Ginty, D. D. (1997) Neuropilin is a semaphorin III receptor. Cell 90:753-762.

Kolodziej SJ, Hudmon A, Waxham MN, Stoops JK (2000) Three-dimensional reconstructions of calcium/calmodulin-dependent (CaM) kinase IIalpha and truncated CaM kinase IIalpha reveal a unique organization for its structural core and functional domains. J Biol Chem 275:14354-14359.

Komeima K, Hayashi Y, Naito Y, Watanabe Y (2000) Inhibition of neuronal nitric-oxide synthase by calcium/ calmodulin-dependent protein kinase IIalpha through Ser847 phosphorylation in NG108-15 neuronal cells. J Biol Chem 275:28139-28143.

Koonce MP, Tikhonenko I (2000) Functional elements within the dynein microtubule-binding domain. Mol Biol Cell 11:523-529.

Kozma R, Sarner S, Ahmed S, Lim L (1997) Rho family GTPases and neuronal growth cone remodelling: relationship between increased complexity induced by Cdc42Hs, Rac1, and acetylcholine and collapse induced by RhoA and lysophosphatidic acid. Mol Cell Biol 17:1201-1211.

Kubes P, Suzuki M, Granger DN (1991) Nitric oxide: an endogenous modulator of leukocyte adhesion. Proc Natl Acad Sci U S A 88:4651-4655.

Kullander K, Mather NK, Diella F, Dottori M, B, oyd AW, K, lein R (2001) Kinase-dependent and kinase-independent functions of EphA4 receptors in major axon tract formation in vivo. Neuron 29:73-84.

Kumanogoh A, Kikutani H (2004) Biological functions and signaling of a transmembrane semaphorin, CD100/Sema4D. Cell Mol Life Sci 61:292-300.

Kumanogoh A, Marukawa S, Suzuki K, Takegahara N, Watanabe C, Ch'ng E, Ishida I, Fujimura H, Sakoda S, Yoshida K, Kikutani H (2002) Class IV semaphorin

Sema4A enhances T-cell activation and interacts with Tim-2. Nature 419:629-633.

Kumanogoh A, Watanabe C, Lee I, Wang X, Shi W, Araki H, Hirata H, Iwahori K, Uchida J, Yasui T, Matsumoto M, Yoshida K, Yakura H, Pan C, Parnes JR, Kikutani H (2000) Identification of CD72 as a lymphocyte receptor for the class IV semaphorin CD100: a novel mechanism for regulating B cell signaling. Immunity 13:621-631.

Kutschera W, Zauner W, Wiche G, Propst F (1998) The mouse and rat MAP1B genes: genomic organization and alternative transcription. Genomics 49:430-436.

Lai MM, Burnett PE, Wolosker H, Blackshaw S, Snyder SH (1998) Cain, a novel physiologic protein inhibitor of calcineurin. J Biol Chem 273:18325-18331.

Lallier TE (2004) Semaphorin profiling of periodontal fibroblasts and osteoblasts. J Dent Res 83:677-682.

Lamb NJ, Fernandez A, Conti MA, Adelstein R, Glass DB, Welch WJ, Feramisco JR (1988) Regulation of actin microfilament integrity in living nonmuscle cells by the cAMP-dependent protein kinase and the myosin light chain kinase. J Cell Biol 106:1955-1971.

Lamoureux P, Altun-Gultekin ZF, Lin C, Wagner JA, Heidemann SR (1997) Rac is required for growth cone function but not neurite assembly. J Cell Sci 110 (Pt 5):635-641.

Langkopf A, Hammarback JA, Muller R, Vallee RB, Garner CC (1992) Microtubule-associated proteins 1A and LC2. Two proteins encoded in one messenger RNA. J Biol Chem 267:16561-16566.

Lankford KL, Letourneau PC (1991) Roles of actin filaments and three second-messenger systems in short-term regulation of chick dorsal root ganglion neurite outgrowth. Cell Motil Cytoskeleton 20:7-29.

Lau KL, Kong SK, Ko WH, Kwan HY, Huang Y, Yao X (2003) cGMP stimulates endoplasmic reticulum Ca(2+)-ATPase in vascular endothelial cells. Life Sci 73:2019-2028.

Lautermilch NJ, Spitzer NC (2000) Regulation of calcineurin by growth cone calcium waves controls neurite extension. J Neurosci 20:315-325.

LeClerc N, Kosik KS, Cowan N, Pienkowski TP, Baas PW (1993) Process formation in Sf9 cells induced by the expression of a microtubule-associated protein 2C-like construct. Proc Natl Acad Sci U S A 90:6223-6227.

Lee MK, Xu Z, Wong PC, Cleveland DW (1993) Neurofilaments are obligate heteropolymers in vivo. J Cell Biol 122:1337-1350.

Lee T, Winter C, Marticke SS, Lee A, Luo L (2000) Essential roles of Drosophila RhoA in the regulation of neuroblast proliferation and dendritic but not axonal morphogenesis. Neuron 25:307-316.

Lehmann M, Fournier A, Selles-Navarro I, Dergham P, Sebok A, Leclerc N, Tigyi G, McKerracher L (1999) Inactivation of Rho signaling pathway promotes CNS axon regeneration. J Neurosci 19:7537-7547.

Lei SZ, Pan ZH, Aggarwal SK, Chen HS, Hartman J, Sucher NJ, Lipton SA (1992a) Effect of nitric oxide production on the redox modulatory site of the NMDA receptor-channel complex. Neuron 8:1087-1099.

Leitges M, Kovac J, Plomann M, Linden DJ (2004) A unique PDZ ligand in PKCalpha confers induction of cerebellar long-term synaptic depression. Neuron 44:585-594.

Letourneau PC, Ressler AH (1984) Inhibition of neurite initiation and growth by taxol. J Cell Biol 98:1355-1362.

Letourneau PC, Shattuck TA, Ressler AH (1986) Branching of sensory and sympathetic neurites in vitro is inhibited by treatment with taxol. J Neurosci 6:1912-1917.

Li BS, Zhang L, Gu J, Amin ND, Pant HC (2000) Integrin alpha(1) beta(1)-mediated activation of cyclin-dependent kinase 5 activity is involved in neurite outgrowth and human neurofilament protein H Lys-Ser-Pro tail domain phosphorylation. J Neurosci 20:6055-6062.

Li BS, Zhang, L., Gu, J., Amin, N. D., Pant, H. C. (2000) Integrin alpha(1) beta(1)-mediated activation of cyclin-dependent kinase 5 activity is involved in neurite outgrowth and human neurofilament protein H Lys-Ser-Pro tail domain phosphorylation. J Neurosci 20:6055-6062.

Li R, Gundersen GG (2008) Beyond polymer polarity: how the cytoskeleton builds a polarized cell. Nat Rev Mol Cell Biol 9:860-873.

Li Z, Banik NL (1995) The localization of mcalpain in myelin: immunocytochemical evidence in different areas of rat brain and nerves. Brain Res 697:112-121.

Lin CH, Espreafico EM, Mooseker MS, Forscher P (1996) Myosin drives retrograde F-actin flow in neuronal growth cones. Neuron 16:769-782.

Lin X, Sikkink RA, Rusnak F, Barber DL (1999) Inhibition of calcineurin phosphatase activity by a calcineurin B homologous protein. J Biol Chem 274:36125-36131.

Lipton SA (1999) Neuronal protection and destruction by NO. Cell Death Differ 6:943-951.

Liu F, Grundke-Iqbal I, Iqbal K, Oda Y, Tomizawa K, Gong CX (2005) Truncation and activation of calcineurin A by calpain I in Alzheimer disease brain. J Biol Chem 280:37755-37762.

Liu J, Farmer JD, Jr., Lane WS, Friedman J, Weissman I, Schreiber SL (1991) Calcineurin is a common target of cyclophilin-cyclosporin A and FKBP-FK506 complexes. Cell 66:807-815.

Liu J, Farmer, J. D., Jr., Lane, W. S., Friedman, J., Weissman, I., Schreiber, S. L. (1991) Calcineurin is a common target of cyclophilin-cyclosporin A and FKBP-FK506 complexes. Cell 66:807-815.

Liu JS, Zhao ML, Brosnan CF, L, ee SC (2001) Expression of inducible nitric oxide synthase and nitrotyrosine in multiple sclerosis lesions. Am J Pathol 158:2057-2066.

Löschinger J, Bandtlow CE, Jung J, Klostermann S, Schwab ME, Bonhoeffer F, Kater SB (1997) Retinal axon growth cone responses to different environmental cues are mediated by different second-messenger systems. J Neurobiol 33:825-834.

lSchaefer AW, Kabir N, Forscher P (2002) Filopodia and actin arcs guide the assembly and transport of two populations of microtubules with unique dynamic parameters in neuronal growth cones. J Cell Biol 158:139-152.

Lu P, Yang H, Jones LL, Filbin MT, Tuszynski MH (2004) Combinatorial therapy with neurotrophins and cAMP promotes axonal regeneration beyond sites of spinal cord injury. J Neurosci 24:6402-6409.

Lu WY, Xiong ZG, Lei S, Orser BA, Dudek E, Browning MD, MacDonald JF (1999) G-protein-coupled receptors act via protein kinase C and Src to regulate NMDA receptors. Nat Neurosci 2:331-338.

Lucas FR, Goold RG, Gordon-Weeks PR, Salinas PC (1998) Inhibition of GSK-3beta leading to the loss of phosphorylated MAP-1B is an early event in axonal remodelling induced by WNT-7a or lithium. J Cell Sci 111 (Pt 10):1351-1361.

Luduena RF (1998) Multiple forms of tubulin: different gene products and covalent modifications. Int Rev Cytol 178:207-275.

Luo L (2000) Rho GTPases in neuronal morphogenesis. Nat Rev Neurosci 1:173-180.

Luo L, Liao YJ, Jan LY, Jan YN (1994) Distinct morphogenetic functions of similar small GTPases: Drosophila Drac1 is involved in axonal outgrowth and myoblast fusion. Genes Dev 8:1787-1802.

Luo Y, Raible D, Raper JA (1993) Collapsin: a protein in brain that induces the collapse and paralysis of neuronal growth cones. Cell 75:217-227.

Ma D, Connors T, Nothias F, Fischer I (2000) Regulation of the expression and phosphorylation of microtubule-associated protein 1B during regeneration of adult dorsal root ganglion neurons. Neuroscience 99:157-170.

Ma D, Chow S, Obrocka M, Connors T, Fischer I (1999) Induction of microtubule-associated protein 1B expression in Schwann cells during nerve regeneration. Brain Res 823:141-153.

Mack TG, Koester MP, Pollerberg GE (2000) The microtubule-associated protein MAP1B is involved in local stabilization of turning growth cones. Mol Cell Neurosci 15:51-65.

Madura T, Yamashita T, Kubo T, Fujitani M, Hosokawa K, Tohyama M (2004) Activation of Rho in the injured axons following spinal cord injury. EMBO Rep 5:412-417.

Maiese K, Boccone L (1995) Neuroprotection by peptide growth factors against anoxia and nitric oxide toxicity requires modulation of protein kinase C. J Cereb Blood Flow Metab 15:440-449.

Malenka RC, Kauer JA, Perkel DJ, Mauk MD, Kelly PT, Nicoll RA, Waxham MN (1989) An essential role for postsynaptic calmodulin and protein kinase activity in long-term potentiation. Nature 340:554-557.

Malinow R, Schulman H, Tsien RW (1989) Inhibition of postsynaptic PKC or CaMKII blocks induction but not expression of LTP. Science 245:862-866.

Mann F, Ray S, Harris W, Holt C (2002) Topographic mapping in dorsoventral axis of the Xenopus retinotectal system depends on signaling through ephrin-B ligands. Neuron 35:461-473.

Mannick JB, Hausladen A, Liu L, Hess DT, Zeng M, Miao QX, Kane LS, Gow AJ, Stamler JS (1999) Fas-induced caspase denitrosylation. Science 284:651-654.

Martinez-Ruiz A, Lamas S (2004) S-nitrosylation: a potential new paradigm in signal transduction. Cardiovasc Res 62:43-52.

Mattson MP, Kater SB (1987) Calcium regulation of neurite elongation and growth cone motility. J Neurosci 7:4034-4043.

Mayer B, John M, Heinzel B, Werner ER, Wachter H, Schultz G, Bohme E (1991) Brain nitric oxide synthase is a biopterin- and flavin-containing multi-functional oxido-reductase. FEBS Lett 288:187-191.

McCobb DP, Haydon PG, Kater SB (1988) Dopamine and serotonin inhibition of neurite elongation of different identified neurons. J Neurosci Res 19:19-26.

Meffert MK, Haley JE, Schuman EM, Schulman H, Madison DV (1994) Inhibition of hippocampal heme oxygenase, nitric oxide synthase, and long-term potentiation by metalloporphyrins. Neuron 13:1225-1233.

Meixner A, Haverkamp S, Wassle H, Fuhrer S, Thalhammer J, Kropf N, Bittner RE, Lassmann H, Wiche G, Propst F (2000) MAP1B is required for axon guidance and Is involved in the development of the central and peripheral nervous system. J Cell Biol 151:1169-1178.

Meyer T, Hanson PI, Stryer L, Schulman H (1992) Calmodulin trapping by calcium-calmodulin-dependent protein kinase. Science 256:1199-1202.

Miranda S, Opazo C, Larrondo LF, Munoz FJ, Ruiz F, Leighton F, nestrosa NC (2000) The role of oxidative stress in the toxicity induced by amyloid beta-peptide in Alzheimer's disease. Prog Neurobiol 62:633-648.

Mizutani T, Haga H, Koyama Y, Takahashi M, Kawabata K (2006) Diphosphorylation of the myosin regulatory light chain enhances the tension acting on stress fibers in fibroblasts. J Cell Physiol 209:726-731.

Mochly-Rosen D (1995) Localization of protein kinases by anchoring proteins: a theme in signal transduction. Science 268:247-251.

Mochly-Rosen D, Gordon AS (1998) Anchoring proteins for protein kinase C: a means for isozyme selectivity. Faseb J 12:35-42.

Monnier PP, Sierra A, Schwab JM, Henke-Fahle S, Mueller BK (2003) The Rho/ROCK pathway mediates neurite growth-inhibitory activity associated with the chondroitin sulfate proteoglycans of the CNS glial scar. Mol Cell Neurosci 22:319-330.

Monti JM, Jantos H (2004) Effects of L-arginine and SIN-1 on sleep and waking in the rat during both phases of the light-dark cycle. Life Sci 75:2027-2034.

Moolenaar WH, Kranenburg O, Postma FR, Zondag GC (1997) Lysophosphatidic acid: G-protein signalling and cellular responses. Curr Opin Cell Biol 9:168-173.

Moon SY, Zheng Y (2003) Rho GTPase-activating proteins in cell regulation. Trends Cell Biol 13:13-22.

Moreau-Fauvarque C, Kumanogoh A, Camand E, Jaillard C, Barbin G, Boquet I, Love C, Jones EY, Kikutani H, Lubetzki C, Dusart I, Chedotal A (2003) The transmembrane semaphorin Sema4D/CD100, an inhibitor of axonal growth, is expressed on oligodendrocytes and upregulated after CNS lesion. J Neurosci 23:9229-9239.

Morfini G, Szebenyi G, Brown H, Pant HC, Pigino G, DeBoer S, Beffert U, Brady ST (2004) A novel CDK5-dependent pathway for regulating GSK3 activity and kinesin-driven motility in neurons. Embo J 23:2235-2245.

Morioka M, Nagahiro S, Fukunaga K, Miyamoto E, Ushio Y (1997) Calcineurin in the adult rat hippocampus: different distribution in CA1 and CA3 subfields. Neuroscience 78:673-684.

Murase S, Horwitz AF (2002) Deleted in colorectal carcinoma and differentially expressed integrins mediate the directional migration of neural precursors in the rostral migratory stream. J Neurosci 22:3568-3579.

Nagase S, Takemura K, Ueda A, Hirayama A, Aoyagi K, Kondoh M, Koyama A (1997) A novel nonenzymatic pathway for the generation of nitric oxide by the reaction of hydrogen peroxide and D- or L-arginine. Biochem Biophys Res Commun 233:150-153.

Nakamura F, Tanaka M, Takahashi T, Kalb RG, Strittmatter SM (1998) Neuropilin-1 extracellular domains mediate semaphorin D/III-induced growth cone collapse. Neuron 21:1093-1100.

Nakane M, Mitchell J, Forstermann U, Murad F (1991) Phosphorylation by calcium calmodulin-dependent protein kinase II and protein kinase C modulates the activity of nitric oxide synthase. Biochem Biophys Res Commun 180:1396-1402.

Newton AC (2003) Regulation of the ABC kinases by phosphorylation: protein kinase C as a paradigm. Biochem J 370:361-371.

Nguyen Ba-Charvet KT, Brose K, Marillat V, Kidd T, Goodman CS, Tessier-Lavigne M, Sotelo C, Chedotal A (1999) Slit2-Mediated chemorepulsion and collapse of developing forebrain axons. Neuron 22:463-473.

Niederost B, Oertle T, Fritsche J, McKinney RA, Bandtlow CE (2002) Nogo-A and myelin-associated glycoprotein mediate neurite growth inhibition by antagonistic regulation of RhoA and Rac1. J Neurosci 22:10368-10376.

Nishiyama M, Hoshino A, Tsai L, Henley JR, Goshima Y, Tessier-Lavigne M, Poo MM, Hong K (2003) Cyclic AMP/GMP-dependent modulation of Ca2+ channels sets the polarity of nerve growth-cone turning. Nature 423:990-995.

Nishiyama M, Hoshino A., Tsai L., Henley J. R., Goshima Y., Tessier-Lavigne M., Poo M. M., Hong K. (2003) Cyclic AMP/GMP-dependent modulation of Ca2+ channels sets the polarity of nerve growth-cone turning. Nature 423:990-995.

Nobes CD, Hall A (1995) Rho, rac, and cdc42 GTPases regulate the assembly of multimolecular focal complexes associated with actin stress fibers, lamellipodia, and filopodia. Cell 81:53-62.

Noiges R, Eichinger R, Kutschera W, Fischer I, Nemeth Z, Wiche G, Propst F (2002) Microtubule-associated protein 1A (MAP1A) and MAP1B: light chains determine distinct functional properties. J Neurosci 22:2106-2114.

Noren NK, Pasquale EB (2004) Eph receptor-ephrin bidirectional signals that target Ras and Rho proteins. Cell Signal 16:655-666.

Norton WT, Poduslo SE (1973) Myelination in rat brain: method of myelin isolation. J Neurochem 21:749-757.

Nothias F, Fischer I, Murray M, Mirman S, Vincent JD (1996) Expression of a phosphorylated isoform of MAP1B is maintained in adult central nervous system areas that retain capacity for structural plasticity. J Comp Neurol 368:317-334.

Okabe S, Hirokawa N (1990) Turnover of fluorescently labelled tubulin and actin in the axon. Nature 343:479-482.

Ono K, Trautwein W (1991) Potentiation by cyclic GMP of beta-adrenergic effect on Ca2+ current in guinea-pig ventricular cells. J Physiol 443:387-404.

Opal P, Garcia JJ, Propst F, Matilla A, Orr HT, Zoghbi HY (2003) Mapmodulin/leucine-rich acidic nuclear protein binds the light chain of microtubule-associated protein 1B and modulates neuritogenesis. J Biol Chem 278:34691-34699.

Orban-Nemeth Z, Simader H, Badurek S, Trancikova A, Propst F (2005) Microtubule-associated protein 1S, a short and ubiquitously expressed member of the microtubule-associated protein 1 family. J Biol Chem 280:2257-2265.

Owen R, Gordon-Weeks PR (2003) Inhibition of glycogen synthase kinase 3beta in sensory neurons in culture alters filopodia dynamics and microtubule distribution in growth cones. Mol Cell Neurosci 23:626-637.

Pachter JS, Liem RK (1985) alpha-Internexin, a 66-kD intermediate filament-binding protein from mammalian central nervous tissues. J Cell Biol 101:1316-1322.

Paglini G, Pigino G, Kunda P, Morfini G, Maccioni R, Quiroga S, Ferreira A, Caceres A (1998) Evidence for the participation of the neuron-specific CDK5 activator P35 during laminin-enhanced axonal growth. J Neurosci 18:9858-9869.

Paglini G, Pigino, G., Kunda, P., Morfini, G., Maccioni, R., Quiroga, S., Ferreira, A., Caceres, A. (1998) Evidence for the participation of the neuron-specific CDK5 activator P35 during laminin-enhanced axonal growth. J Neurosci 18:9858-9869.

Paige JS, Xu G, Stancevic B, Jaffrey SR (2008) Nitrosothiol reactivity profiling identifies S-nitrosylated proteins with unexpected stability. Chem Biol 15:1307-1316.

Parekh DB, Ziegler W, Parker PJ (2000) Multiple pathways control protein kinase C phosphorylation. Embo J 19:496-503.

Parysek LM, McReynolds MA, Goldman RD, Ley CA (1991) Some neural intermediate filaments contain both peripherin and the neurofilament proteins. J Neurosci Res 30:80-91.

Pawloski JR, Swaminathan RV, Stamler JS (1998) Cell-free and erythrocytic S-nitrosohemoglobin inhibits human platelet aggregation. Circulation 97:263-267.

Pearson RB, Jakes R, John M, Kendrick-Jones J, Kemp BE (1984) Phosphorylation site sequence of smooth muscle myosin light chain (Mr = 20 000). FEBS Lett 168:108-112.

Pedrotti B, Islam K (1996b) Dephosphorylated but not phosphorylated microtubule associated protein MAP1B binds to microfilaments. FEBS Lett 388:131-133.

Pedrotti B, Colombo R, Islam K (1994) Microtubule associated protein MAP1A is an actin-binding and crosslinking protein. Cell Motil Cytoskeleton 29:110-116.

Pedrotti B, Ulloa L, Avila J, Islam K (1996a) Characterization of microtubule-associated protein MAP1B: phosphorylation state, light chains, and binding to microtubules. Biochemistry 35:3016-3023.

Peris L, Thery M, Faure J, Saoudi Y, Lafanechere L, Chilton JK, Gordon-Weeks P, Galjart N, Bornens M, Wordeman L, Wehland J, Andrieux A, Job D (2006) Tubulin tyrosination is a major factor affecting the recruitment of CAP-Gly proteins at microtubule plus ends. J Cell Biol 174:839-849.

Perrin BJ, Huttenlocher A (2002) Calpain. Int J Biochem Cell Biol 34:722-725.

Perrot V, Vazquez-Prado J, Gutkind JS (2002) Plexin B regulates Rho through the guanine nucleotide exchange factors leukemia-associated Rho GEF (LARG) and PDZ-RhoGEF. J Biol Chem 277:43115-43120.

Pigino G, Paglini G, Ulloa L, Avila J, Caceres A (1997) Analysis of the expression, distribution and function of cyclin dependent kinase 5 (cdk5) in developing cerebellar macroneurons. J Cell Sci 110 (Pt 2):257-270.

Plump AS, Erskine L, Sabatier C, Brose K, Epstein CJ, Goodman CS, Mason CA, Tessier-Lavigne M (2002) Slit1 and Slit2 cooperate to prevent premature midline crossing of retinal axons in the mouse visual system. Neuron 33:219-232.

Potter DA, Tirnauer JS, Janssen R, Croall DE, Hughes CN, Fiacco KA, Mier JW, Maki M, Herman IM (1998) Calpain regulates actin remodeling during cell spreading. J Cell Biol 141:647-662.

Prast H, Tran MH, Fischer H, Philippu A (1998) Nitric oxide-induced release of acetylcholine in the nucleus accumbens: role of cyclic GMP, glutamate, and GABA. J Neurochem 71:266-273.

Qiang L, Yu W, Andreadis A, Luo M, Baas PW (2006) Tau protects microtubules in the axon from severing by katanin. J Neurosci 26:3120-3129.

Ramamurthy B, Yengo CM, Straight AF, Mitchison TJ, Sweeney HL (2004) Kinetic mechanism of blebbistatin inhibition of nonmuscle myosin IIb. Biochemistry 43:14832-14839.

Rameau GA, Chiu LY, Ziff EB (2004) Bidirectional regulation of neuronal nitric-oxide synthase phosphorylation at serine 847 by the N-methyl-D-aspartate receptor. J Biol Chem 279:14307-14314.

Ramon-Cueto A, Avila J (1997) Differential expression of microtubule-associated protein 1B phosphorylated isoforms in the adult rat nervous system. Neuroscience 77:485-501.

Ramon-Cueto A, Avila J (1999) Two modes of microtubule-associated protein 1B phosphorylation are differentially regulated during peripheral nerve regeneration. Brain Res 815:213-226.

Ramón y Cajal S (1890) Á quelle époque apparaissent les expansions des cellules nerveuses de la moëlle épiniére du poulet? Anatomomischner Anzeiger 21-22:609-639.

Redowicz MJ (1999) Rho-associated kinase: involvement in the cytoskeleton regulation. Arch Biochem Biophys 364:122-124.

Ren XD, Kiosses WB, Schwartz MA (1999) Regulation of the small GTP-binding protein Rho by cell adhesion and the cytoskeleton. Embo J 18:578-585.

Reverter D, Sorimachi H, Bode W (2001) The structure of calcium-free human m-calpain: implications for calcium activation and function. Trends Cardiovasc Med 11:222-229.

Riano E, Martignoni M, Mancuso G, Cartelli D, Crippa F, Toldo I, Siciliano G, Di Bella D, Taroni F, Bassi MT, Cappelletti G, Rugarli EI (2009) Pleiotropic effects of spastin on neurite growth depending on expression levels. J Neurochem 108:1277-1288.

Ridley AJ, Paterson HF, Johnston CL, Diekmann D, Hall A (1992) The small GTP-binding protein rac regulates growth factor-induced membrane ruffling. Cell 70:401-410.

Robles E, Huttenlocher A, Gomez TM (2003) Filopodial calcium transients regulate growth cone motility and guidance through local activation of calpain. Neuron 38:597-609.

Roehm PC, Xu N, Woodson EA, Green SH, Hansen MR (2008) Membrane depolarization inhibits spiral ganglion neurite growth via activation of multiple types of voltage sensitive calcium channels and calpain. Mol Cell Neurosci 37:376-387.

Rolli-Derkinderen M, Sauzeau V, Boyer L, Lemichez E, Baron C, Henrion D, Loirand G, Pacaud P (2005) Phosphorylation of serine 188 protects RhoA from ubiquitin/proteasome-mediated degradation in vascular smooth muscle cells. Circ Res 96:1152-1160.

Romijn HJ, Habets AM, Mud MT, Wolters PS (1981) Nerve outgrowth, synaptogenesis and bioelectric activity in fetal rat cerebral cortex tissue cultured in serum-free, chemically defined medium. Brain Res 254:583-589.

Rossino P, Defilippi P, Silengo L, Tarone G (1991) Up-regulation of the integrin alpha 1/beta 1 in human neuroblastoma cells differentiated by retinoic acid: correlation with increased neurite outgrowth response to laminin. Cell Regul 2:1021-1033.

Rossino P, Defilippi, P., Silengo, L., Tarone, G. (1991) Up-regulation of the integrin alpha 1/beta 1 in human neuroblastoma cells differentiated by retinoic acid: correlation with increased neurite outgrowth response to laminin. Cell Regul 2:1021-1033.

Round J, Stein E (2007) Netrin signaling leading to directed growth cone steering. Curr Opin Neurobiol 17:15-21.

Saito S (1997) Effects of lysophosphatidic acid on primary cultured chick neurons. Neurosci Lett 229:73-76.

Salvemini D, Misko TP, Masferrer JL, Seibert K, Currie MG, Needleman P (1993) Nitric oxide activates cyclooxygenase enzymes. Proc Natl Acad Sci U S A 90:7240-7244.

Sambrook J, MacCallum P, Russell D (2001) Molecular Cloning: A Laboratory Manual, Third Edition edn: Cold Spring Harbor Laboratory Press.

Sanchez Martin C, Ledesma D, Dotti CG, Avila J (2000) Microtubule-associated protein-2 located in growth regions of rat hippocampal neurons is highly phosphorylated at its proline-rich region. Neuroscience 101:885-893.

Sauzeau V, Le Jeune H, Cario-Toumaniantz C, Smolenski A, Lohmann SM, Bertoglio J, Chardin P, Pacaud P, Loirand G (2000) Cyclic GMP-dependent protein kinase signaling pathway inhibits RhoA-induced Ca2+ sensitization of contraction in vascular smooth muscle. J Biol Chem 275:21722-21729.

Sayas CL, Avila J, Wandosell F (2002a) Glycogen synthase kinase-3 is activated in neuronal cells by Galpha12 and Galpha13 by Rho-independent and Rho-dependent mechanisms. J Neurosci 22:6863-6875.

Sayas CL, Avila J, Wandosell F (2002b) Regulation of neuronal cytoskeleton by lysophosphatidic acid: role of GSK-3. Biochim Biophys Acta 1582:144-153.

Sayas CL, Moreno-Flores MT, Avila J, Wandosell F (1999) The neurite retraction induced by lysophosphatidic acid increases Alzheimer's disease-like Tau phosphorylation. J Biol Chem 274:37046-37052.

Sayas CL, Ariaens A, Ponsioen B, Moolenaar WH (2006) GSK-3 is activated by the tyrosine kinase Pyk2 during LPA1-mediated neurite retraction. Mol Biol Cell 17:1834-1844.

Scales TM, Lin S, Kraus M, Goold RG, Gordon-Weeks PR (2009) Nonprimed and DYRK1A-primed GSK3{beta}-phosphorylation sites on MAP1B regulate microtubule dynamics in growing axons. J Cell Sci 122:2424-2435.

Schiaffino S, Serrano A (2002) Calcineurin signaling and neural control of skeletal muscle fiber type and size. Trends Pharmacol Sci 23:569-575.

Schnell L, Schwab ME (1990) Axonal regeneration in the rat spinal cord produced by an antibody against myelin-associated neurite growth inhibitors. Nature 343:269-272.

Schoenfeld TA, McKerracher L, Obar R, Vallee RB (1989) MAP 1A and MAP 1B are structurally related microtubule associated proteins with distinct developmental patterns in the CNS. J Neurosci 9:1712-1730.

Schoenfeld TA, Obar, R. A. (1994) Diverse distribution and function of fibrous microtubule-associated proteins in the nervous system. Int Rev Cytol 151:67-137.

Schoenwaelder SM, Burridge K (1999) Bidirectional signaling between the cytoskeleton and integrins. Curr Opin Cell Biol 11:274-286.

Schuman EM, Madison DV (1994) Nitric oxide and synaptic function. Annu Rev Neurosci 17:153-183.

Schwab ME, Caroni P (1988) Oligodendrocytes and CNS myelin are nonpermissive substrates for neurite growth and fibroblast spreading in vitro. J Neurosci 8:2381-2393.

Seasholtz TM, Radeff-Huang J, Sagi SA, Matteo R, Weems JM, Cohen AS, Feramisco JR, Brown JH (2004) Rho-mediated cytoskeletal rearrangement in response to LPA is functionally antagonized by Rac1 and PIP2. J Neurochem 91:501-512.

Sekido Y, Bader S, Latif F, Chen JY, Duh FM, Wei MH, Albanesi JP, Lee CC, Lerman MI, Minna JD (1996) Human semaphorins A(V) and IV reside in the 3p21.3 small cell lung cancer deletion region and demonstrate distinct expression patterns. Proc Natl Acad Sci U S A 93:4120-4125.

Selkoe DJ (2001) Alzheimer's disease: genes, proteins, and therapy. Physiol Rev 81:741-766.

Sheads LD, Eby MJ, Sampugna J (1977) Myelin subfractions isolated from mouse brain. Studies of normal mice during development, quaking mutants, and three brain regions. J Neurobiol 8:67-89.

Shi SH, Hayashi Y, Petralia RS, Zaman SH, Wenthold RJ, Svoboda K, Malinow R (1999) Rapid spine delivery and redistribution of AMPA receptors after synaptic NMDA receptor activation. Science 284:1811-1816.

Shimohama S, Suenaga T, Araki W, Yamaoaka Y, Shimizu K, Kimura J (1991) Presence of calpain II immunoreactivity in senile plaques in Alzheimer's disease. Brain Res 558:105-108.

Shiraha H, Glading A, Chou J, Jia ZW, A. (2002) Activation of m-calpain (calpain II) by epidermal growth factor is limited by protein kinase A phosphorylation of m-calpain. Mol Cell Biol 22:2716-2727.

Silva AJ, Paylor R, Wehner JM, Tonegawa S (1992) Impaired spatial learning in alpha-calcium-calmodulin kinase II mutant mice. Science 257:206-211.

Silver RA, Lamb AG, Bolsover SR (1989) Elevated cytosolic calcium in the growth cone inhibits neurite elongation in neuroblastoma cells: correlation of behavioral states with cytosolic calcium concentration. J Neurosci 9:4007-4020.

Singel DJ, Stamler JS (2005) Chemical physiology of blood flow regulation by red blood cells: the role of nitric oxide and S-nitrosohemoglobin. Annu Rev Physiol 67:99-145.

Sivasankaran R, Pei J, Wang KC, Zhang YP, Shields CB, Xu XM, He Z (2004) PKC mediates inhibitory effects of myelin and chondroitin sulfate proteoglycans on axonal regeneration. Nat Neurosci 7:261-268.

Snow DM, Atkinson PB, Hassinger TD, Letourneau PC, Kater SB (1994) Chondroitin sulfate proteoglycan elevates cytoplasmic calcium in DRG neurons. Dev Biol 166:87-100.

Soares S, Fischer I, Ravaille-Veron M, Vincent JD, Nothias F (1998) Induction of MAP1B phosphorylation in target-deprived afferent fibers after kainic acid lesion in the adult rat. J Comp Neurol 396:193-210.

Soares S, Barnat M, Salim C, von Boxberg Y, Ravaille-Veron M, Nothias F (2007) Extensive structural remodeling of the injured spinal cord revealed by phosphorylated MAP1B in sprouting axons and degenerating neurons. Eur J Neurosci 26:1446-1461.

Soares S, von Boxberg Y, Lombard MC, Ravaille-Veron M, Fischer I, Eyer J, Nothias F (2002) Phosphorylated MAP1B is induced in central sprouting of primary afferents in response to peripheral injury but not in response to rhizotomy. Eur J Neurosci 16:593-606.

Somlyo AP, Somlyo AV (2003) Ca2+ sensitivity of smooth muscle and nonmuscle myosin II: modulated by G proteins, kinases, and myosin phosphatase. Physiol Rev 83:1325-1358.

Son H, Hawkins RD, Martin K, Kiebler M, Huang PL, Fishman MC, Kandel ER (1996) Long-term potentiation is reduced in mice that are doubly mutant in endothelial and neuronal nitric oxide synthase. Cell 87:1015-1023.

Song H, Ming G, He Z, Lehmann M, McKerracher L, Tessier-Lavigne M, Poo M (1998) Conversion of neuronal growth cone responses from repulsion to attraction by cyclic nucleotides. Science 281:1515-1518.

Song HJ, Poo MM (1999) Signal transduction underlying growth cone guidance by diffusible factors. Curr Opin Neurobiol 9:355-363.

Song T, Hatano N, Kambe T, Miyamoto Y, Ihara H, Yamamoto H, Sugimoto K, Kume K, Yamaguchi F, Tokuda M, Watanabe Y (2008) Nitric oxide-mediated

modulation of calcium/calmodulin-dependent protein kinase II. Biochem J 412:223-231.

Song T, Hatano, N., Kambe, T., Miyamoto, Y., Ihara, H., Yamamoto, H., Sugimoto, K., Kume, K., Yamaguchi, F., Tokuda, M., Watanabe, Y. (2008) Nitric oxide-mediated modulation of calcium/calmodulin-dependent protein kinase II. Biochem J 412:223-231.

Stamler JS, Toone EJ, Lipton SA, Sucher NJ (1997a) (S)NO signals: translocation, regulation, and a consensus motif. Neuron 18:691-696.

Stamler JS, Jia L, Eu JP, McMahon TJ, Demchenko IT, Bonaventura J, Gernert K, Piantadosi CA (1997b) Blood flow regulation by S-nitrosohemoglobin in the physiological oxygen gradient. Science 276:2034-2037.

Steiner JP, Dawson TM, Fotuhi M, Glatt CE, Snowman AM, Cohen N, Snyder SH (1992) High brain densities of the immunophilin FKBP colocalized with calcineurin. Nature 358:584-587.

Stemmer P, Klee CB (1991) Serine/threonine phosphatases in the nervous system. Curr Opin Neurobiol 1:53-64.

Stepanova T, Slemmer J, Hoogenraad CC, Lansbergen G, Dortland B, De Zeeuw CI, Grosveld F, van Cappellen G, Akhmanova A, Galjart N (2003) Visualization of microtubule growth in cultured neurons via the use of EB3-GFP (end-binding protein 3-green fluorescent protein). J Neurosci 23:2655-2664.

Steup A, Ninnemann O, Savaskan NE, Nitsch R, Puschel AW, Skutella T (1999) Semaphorin D acts as a repulsive factor for entorhinal and hippocampal neurons. Eur J Neurosci 11:729-734.

Stroissnigg H, Trancikova A, Descovich L, Fuhrmann J, Kutschera W, Kostan J, Meixner A, Nothias F, Propst F (2007) S-nitrosylation of microtubule-associated protein 1B mediates nitric-oxide-induced axon retraction. Nat Cell Biol 9:1035-1045.

Sugiura T, Nakane S, Kishimoto S, Waku K, Yoshioka Y, Tokumura A, Hanahan DJ (1999) Occurrence of lysophosphatidic acid and its alkyl ether-linked analog in rat brain and comparison of their biological activities toward cultured neural cells. Biochim Biophys Acta 1440:194-204.

Takegahara N, Kumanogoh A, Kikutani H (2005) Semaphorins: a new class of immunoregulatory molecules. Philos Trans R Soc Lond B Biol Sci 360:1673-1680.

Takei K, Shin RM, Inoue T, Kato K, Mikoshiba K (1998) Regulation of nerve growth mediated by inositol 1,4,5-trisphosphate receptors in growth cones. Science 282:1705-1708.

Takei Y, Kondo S, Harada A, Inomata S, Noda T, Hirokawa N (1997) Delayed development of nervous system in mice homozygous for disrupted microtubule-associated protein 1B (MAP1B) gene. J Cell Biol 137:1615-1626.

Takemura R, Okabe S, Umeyama T, Kanai Y, Cowan NJ, Hirokawa N (1992) Increased microtubule stability and alpha tubulin acetylation in cells transfected with microtubule-associated proteins MAP1B, MAP2 or tau. J Cell Sci 103 (Pt 4):953-964.

Tan JL, Ravid S, Spudich JA (1992) Control of nonmuscle myosins by phosphorylation. Annu Rev Biochem 61:721-759.

Tan JL, Ravid S., Spudich J. A. (1992) Control of nonmuscle myosins by phosphorylation. Annu Rev Biochem 61:721-759.

Tanaka E, Sabry J (1995) Making the connection: cytoskeletal rearrangements during growth cone guidance. Cell 83:171-176.

Tang F, Kalil K (2005) Netrin-1 induces axon branching in developing cortical neurons by frequency-dependent calcium signaling pathways. J Neurosci 25:6702-6715.

Tangkijvanich P, Melton AC, Santiskulvong C, Yee HF, Jr. (2003) Rho and p38 MAP kinase signaling pathways mediate LPA-stimulated hepatic myofibroblast migration. J Biomed Sci 10:352-358.

Taniguchi M, Yuasa S, Fujisawa H, Naruse I, Saga S, Mishina M, Yagi T (1997) Disruption of semaphorin III/D gene causes severe abnormality in peripheral nerve projection. Neuron 19:519-530.

Tapon N, Hall A (1997) Rho, Rac and Cdc42 GTPases regulate the organization of the actin cytoskeleton. Curr Opin Cell Biol 9:86-92.

Thippeswamy T, McKay JS, Morris R (2001) Bax and caspases are inhibited by endogenous nitric oxide in dorsal root ganglion neurons in vitro. Eur J Neurosci 14:1229-1236.

Thippeswamy T, McKay JS, Quinn J, Morris R (2005) Either nitric oxide or nerve growth factor is required for dorsal root ganglion neurons to survive during embryonic and neonatal development. Brain Res Dev Brain Res 154:153-164.

Thorns V, Hansen L, Masliah E (1998) nNOS expressing neurons in the entorhinal cortex and hippocampus are affected in patients with Alzheimer's disease. Exp Neurol 150:14-20.

Tigyi G, Miledi R (1992) Lysophosphatidates bound to serum albumin activate membrane currents in Xenopus oocytes and neurite retraction in PC12 pheochromocytoma cells. J Biol Chem 267:21360-21367.

Tigyi G, Fischer DJ, Sebok A, Yang C, Dyer DL, Miledi R (1996a) Lysophosphatidic acid-induced neurite retraction in PC12 cells: control by phosphoinositide-Ca2+ signaling and Rho. J Neurochem 66:537-548.

Tilney LG, Bonder EM, DeRosier DJ (1981) Actin filaments elongate from their membrane-associated ends. J Cell Biol 90:485-494.

To KC, Church J, O'Connor TP (2007) Combined activation of calpain and calcineurin during ligand-induced growth cone collapse. Mol Cell Neurosci 36:425-434.

To KC, Church J, O'Connor TP (2008) Growth cone collapse stimulated by both calpain- and Rho-mediated pathways. Neuroscience 153:645-653.

Tögel M, Wiche G, Propst F (1998) Novel features of the light chain of microtubule-associated protein MAP1B: microtubule stabilization, self interaction, actin filament binding, and regulation by the heavy chain. J Cell Biol 143:695-707.

Tom VJ, Steinmetz MP, Miller JH, Doller CM, Silver J (2004) Studies on the development and behavior of the dystrophic growth cone, the hallmark of regeneration failure, in an in vitro model of the glial scar and after spinal cord injury. J Neurosci 24:6531-6539.

Tonge DA, Golding JP, Gordon-Weeks PR (1996) Expression of a developmentally regulated, phosphorylated isoform of microtubule-associated protein 1B in sprouting and regenerating axons in vitro. Neuroscience 73:541-551.

Townsend DM, Findlay VJ, Fazilev F, Ogle M, Fraser J, Saavedra JE, Ji X, Keefer LK, Tew KD (2006) A glutathione S-transferase pi-activated prodrug causes kinase activation concurrent with S-glutathionylation of proteins. Mol Pharmacol 69:501-508.

Trabace L, Kendrick KM (2000) Nitric oxide can differentially modulate striatal neurotransmitter concentrations via soluble guanylate cyclase and peroxynitrite formation. J Neurochem 75:1664-1674.

Tran MH, Yamada K, Nakajima A, Mizuno M, He J, Kamei H, Nabeshima T (2003) Tyrosine nitration of a synaptic protein synaptophysin contributes to amyloid beta-peptide-induced cholinergic dysfunction. Mol Psychiatry 8:407-412.

Trančíková A (2007) Regulation of MAP1B microtubule binding. PhD thesis.

Tsuji T, Shimohama S, Kimura J, Shimizu K (1998) m-Calpain (calcium-activated neutral proteinase) in Alzheimer's disease brains. Neurosci Lett 248:109-112.

Tumlin JA (1997) Expression and function of calcineurin in the mammalian nephron: physiological roles, receptor signaling, and ion transport. Am J Kidney Dis 30:884-895.

Uehara R, Hosoya H, Mabuchi I (2008) In vivo phosphorylation of regulatory light chain of myosin II in sea urchin eggs and its role in controlling myosin localization and function during cytokinesis. Cell Motil Cytoskeleton 65:100-115.

Uehata M, Ishizaki T, Satoh H, Ono T, Kawahara T, Morishita T, Tamakawa H, Yamagami K, Inui J, Maekawa M, Narumiya S (1997) Calcium sensitization of smooth muscle mediated by a Rho-associated protein kinase in hypertension. Nature 389:990-994.

Ulloa L, Avila J, Diaz-Nido J (1993a) Heterogeneity in the phosphorylation of microtubule-associated protein MAP1B during rat brain development. J Neurochem 61:961-972.

Ulloa L, Diaz-Nido J, Avila J (1993b) Depletion of casein kinase II by antisense oligonucleotide prevents neuritogenesis in neuroblastoma cells. Embo J 12:1633-1640.

Ulloa L, Diez-Guerra FJ, Avila J, Diaz-Nido J (1994a) Localization of differentially phosphorylated isoforms of microtubule-associated protein 1B in cultured rat hippocampal neurons. Neuroscience 61:211-223.

Ulloa L, Montejo de Garcini E, Gomez-Ramos P, Moran MA, Avila J (1994b) Microtubule-associated protein MAP1B showing a fetal phosphorylation pattern is present in sites of neurofibrillary degeneration in brains of Alzheimer's disease patients. Brain Res Mol Brain Res 26:113-122.

Ulloa L, Dombradi V, Diaz-Nido J, Szucs K, Gergely P, Friedrich P, Avila J (1993c) Dephosphorylation of distinct sites on microtubule-associated protein MAP1B by protein phosphatases 1, 2A and 2B. FEBS Lett 330:85-89.

van Leeuwen FN, van Delft S, Kain HE, van der Kammen RA, Collard JG (1999) Rac regulates phosphorylation of the myosin-II heavy chain, actinomyosin disassembly and cell spreading. Nat Cell Biol 1:242-248.

Vecino E, Avila J (2001) Distribution of the phosphorylated form of microtubule associated protein 1B in the fish visual system during optic nerve regeneration. Brain Res Bull 56:131-137.

Vouyiouklis DA, Brophy PJ (1993) Microtubule-associated protein MAP1B expression precedes the morphological differentiation of oligodendrocytes. J Neurosci Res 35:257-267.

Wahl S, Barth H, Ciossek T, Aktories K, Mueller BK (2000) Ephrin-A5 induces collapse of growth cones by activating Rho and Rho kinase. J Cell Biol 149:263-270.

Wang KH, Brose K, Arnott D, Kidd T, Goodman CS, Henzel W, Tessier-Lavigne M (1999) Biochemical purification of a mammalian slit protein as a positive regulator of sensory axon elongation and branching. Cell 96:771-784.

Wang KK, Roufogalis BD, Villalobo A (1989) Characterization of the fragmented forms of calcineurin produced by calpain I. Biochem Cell Biol 67:703-711.

Watanabe T, Hosoya H, Yonemura S (2007) Regulation of myosin II dynamics by phosphorylation and dephosphorylation of its light chain in epithelial cells. Mol Biol Cell 18:605-616.

Webber A, Raz Y (2006) Axon guidance cues in auditory development. Anat Rec A Discov Mol Cell Evol Biol 288:390-396.

Wen Z, Zheng JQ (2006) Directional guidance of nerve growth cones. Curr Opin Neurobiol 16:52-58.

Wen Z, Guirland C, Ming GL, Zheng JQ (2004) A CaMKII/calcineurin switch controls the direction of Ca(2+)-dependent growth cone guidance. Neuron 43:835-846.

Wessels D, Soll DR, Knecht D, Loomis WF, De Lozanne A, Spudich J (1988) Cell motility and chemotaxis in Dictyostelium amebae lacking myosin heavy chain. Dev Biol 128:164-177.

Weston C, Yee B, Hod E, Prives J (2000) Agrin-induced acetylcholine receptor clustering is mediated by the small guanosine triphosphatases Rac and Cdc42. J Cell Biol 150:205-212.

Wilkinson DG (2001) Multiple roles of EPH receptors and ephrins in neural development. Nat Rev Neurosci 2:155-164.

Williams K (1997) Interactions of polyamines with ion channels. Biochem J 325 (Pt 2):289-297.

Wong ST, Henley JR, Kanning KC, Huang KH, Bothwell M, Poo MM (2002) A p75(NTR) and Nogo receptor complex mediates repulsive signaling by myelin-associated glycoprotein. Nat Neurosci 5:1302-1308.

Wu HH, Williams CV, McLoon SC (1994) Involvement of nitric oxide in the elimination of a transient retinotectal projection in development. Science 265:1593-1596.

Wu HY, Tomizawa K, Matsui H (2007) Calpain-calcineurin signaling in the pathogenesis of calcium-dependent disorder. Acta Med Okayama 61:123-137.

Wu HY, Tomizawa K, Oda Y, Wei FY, Lu YF, Matsushita M, Li ST, Moriwaki A, Matsui H (2004) Critical role of calpain-mediated cleavage of calcineurin in excitotoxic neurodegeneration. J Biol Chem 279:4929-4940.

Xia C, Bao Z, Yue C, Sanborn BM, Liu M (2001) Phosphorylation and regulation of G-protein-activated phospholipase C-beta 3 by cGMP-dependent protein kinases. J Biol Chem 276:19770-19777.

Xie Q, Nathan C (1994) The high-output nitric oxide pathway: role and regulation. J Leukoc Biol 56:576-582.

Xu J, Wang F, Van Keymeulen A, Herzmark P, Straight A, Kelly K, Takuwa Y, Sugimoto N, Mitchison T, Bourne HR (2003) Divergent signals and cytoskeletal assemblies regulate self-organizing polarity in neutrophils. Cell 114:201-214.

Yamamoto T, Shimoyama N, Mizuguchi T (1993) Nitric oxide synthase inhibitor blocks spinal sensitization induced by formalin injection into the rat paw. Anesth Analg 77:886-890.

Yamashima T (2000) Implication of cysteine proteases calpain, cathepsin and caspase in ischemic neuronal death of primates. Prog Neurobiol 62:273-295.

Yamashita T, Ando Y, Obayashi K, Uchino M, Ando M (1997) Changes in nitrite and nitrate (NO2-/NO3-) levels in cerebrospinal fluid of patients with multiple sclerosis. J Neurol Sci 153:32-34.

Yee KT, Simon HH, Tessier-Lavigne M, O'Leary DM (1999) Extension of long leading processes and neuronal migration in the mammalian brain directed by the chemoattractant netrin-1. Neuron 24:607-622.

Yiu G, He Z (2006) Glial inhibition of CNS axon regeneration. Nat Rev Neurosci 7:617-627.

Yoon S, Choi J, Huh JW, Hwang O, Kim D (2006) Calpain activation in okadaic-acid-induced neurodegeneration. Neuroreport 17:689-692.

Yoshikawa S (2000) Reaction mechanism of bovine heart cytochrome oxidase. Keio J Med 49:99-105.

Yu W, Solowska JM, Qiang L, Karabay A, Baird D, Baas PW (2005) Regulation of microtubule severing by katanin subunits during neuronal development. J Neurosci 25:5573-5583.

Yu W, Qiang L, Solowska JM, Karabay A, Korulu S, Baas PW (2008) The microtubule-severing proteins spastin and katanin participate differently in the formation of axonal branches. Mol Biol Cell 19:1485-1498.

Zauner W, Kratz J, Staunton J, Feick P, Wiche G (1992) Identification of two distinct microtubule binding domains on recombinant rat MAP 1B. Eur J Cell Biol 57:66-74.

Zhang J, Snyder SH (1995) Nitric oxide in the nervous system. Annu Rev Pharmacol Toxicol 35:213-233.

Zhang XF, Schaefer AW, Burnette DT, Schoonderwoert VT, Forscher P (2003) Rho-dependent contractile responses in the neuronal growth cone are independent of classical peripheral retrograde actin flow. Neuron 40:931-944.

Zheng JQ (2000) Turning of nerve growth cones induced by localized increases in intracellular calcium ions. Nature 403:89-93.

Zheng JQ, Poo MM (2007) Calcium signaling in neuronal motility. Annu Rev Cell Dev Biol 23:375-404.

Zheng JQ, Wan JJ, Poo MM (1996) Essential role of filopodia in chemotropic turning of nerve growth cone induced by a glutamate gradient. J Neurosci 16:1140-1149.

Zheng JQ, Felder M, Connor JA, Poo MM (1994) Turning of nerve growth cones induced by neurotransmitters. Nature 368:140-144.

Zhou FQ, Walzer M, Wu YH, Zhou J, Dedhar S, Snider WD (2006) Neurotrophins support regenerative axon assembly over CSPGs by an ECM-integrin-independent mechanism. J Cell Sci 119:2787-2796.

Zipkin ID, Kindt RM, Kenyon CJ (1997) Role of a new Rho family member in cell migration and axon guidance in C. elegans. Cell 90:883-894.

Zochodne DW, Misra M, Cheng C, Sun H (1997) Inhibition of nitric oxide synthase enhances peripheral nerve regeneration in mice. Neurosci Lett 228:71-74.

Zorumski CF, Izumi Y (1993) Nitric oxide and hippocampal synaptic plasticity. Biochem Pharmacol 46:777-785.

LIST OF FIGURES AND TABLES

Fig. 1. The domain structure of CaMKII. 26
Fig. 2. Schematic of calpain structure. 28
Fig. 3. Schematic of calcineurin structure. 29
Fig. 4. The morphology of the growth cone. 34
Fig. 5. Stages of axon growth. 35
Fig. 6. The cytoskeleton of the growth cone. 38
Fig. 7. Schematic of Rho GTPase activation. 42
Fig. 8. Splice variants of nNOS. 45
Fig. 9. Schematic structure of NOS. 45
Fig. 10. NO plays a role as a transcellular secondary messenger in LTP. 53
Fig. 11. Schematic representation of the MAP1 family. 56
Fig. 12. Schematic representation of MAP1B. 58
Fig. 13. Response of wild-type neurons to activation of nNOS by calcimycin. 68
Fig. 14. LPA-induced axon retraction is impaired in MAP1B-/- DRG neurons. 69
Fig. 15. Response of wild-type and MAP1B-/- neurons to LPA treatment. 70
Fig. 16. Inhibition of ROCK prevents LPA-induced axon retraction. 71
Fig. 17. Inhibition of myosin prevents axon retraction induced by LPA in wild-type DRG neurons. 72
Fig. 18. Inhibition of ROCK abolishes neurite retraction of N2a neuroblastoma cells induced by LPA. 73
Fig. 19. Inhibition of myosin abolishes LPA-induced neurite retraction of N2a neuroblastoma cells. 74
Fig. 20. Inhibition of nNOS does not prevent axon retraction induced by LPA in wild-type DRG neurons. 75
Fig. 21. Inhibition of NOSs does not abolish LPA-induced neurite retraction of N2a neuroblastoma cells. 76
Fig. 22. Inhibition of ROCK, myosin and NOS does not overcome inhibition of axon outgrowth induced by aggrecan in wild-type DRG neurons. 78
Fig. 23. Inhibition of ROCK, myosin and NOS does not overcome inhibition of axon outgrowth induced by aggrecan in MAP1B-/- DRG neurons. 79
Fig. 24. Aggrecan inhibits growth of axons. 80
Fig. 25. Myelin inhibits growth of axons. 82
Fig. 26. Calcimycin-induced axon retraction requires the activity of nNOS. 91
Fig. 27. Inhibition of CaMKII does not prevent axon retraction induced by calcimycin in wild-type DRG neurons. 93
Fig. 28. Inhibition of calcineurin does not prevent axon retraction induced by calcimycin in wild-type DRG neurons. 94
Fig. 29. Inhibition of PKC does not prevent axon retraction induced by calcimycin in wild-type DRG neurons. 95
Fig. 30. Inhibition of calpain does not prevent axon retraction induced by calcimycin in wild-type DRG neurons. 96
Fig. 31. A model for MAP1B mediated effects of nNOS activation. 98
Fig. 32. Inhibition of ROCK prevents axon retraction induced by calcimycin in wild-type DRG neurons. 99
Fig. 33. Inhibition of ROCK prevents axon retraction induced by SNAP in wild-type DRG neurons. 100
Fig. 34. Inhibition of ROCK abolishes neurite retraction of N2a neuroblastoma cells induced by SNAP. 101
Fig. 35. Inhibition of myosin prevents axon retraction induced by calcimycin in wild-type DRG neurons. 102
Fig. 36. Inhibition of myosin abolishes neurite retraction of N2a neuroblastoma cells induced by calcimycin. 103
Fig. 37. Inhibition of myosin prevents axon retraction induced by SNAP in wild-type DRG neurons. 103

Fig. 38. Inhibition of myosin abolished neurite retraction of N2a neuroblastoma cells induced by SNAP. 104
Fig. 39. NO- and LPA-induced axon retraction involves activation of myosin. 106
Fig. 40. Addition of cAMP partially abolishes retraction of axons induced by calcimycin in wild-type DRG neurons. 107
Fig. 41. Addition of forskolin partially abolishes retraction of axons induced by calcimycin in wild-type DRG neurons. 108
Fig. 42. Addition of cAMP partially abolishes retraction of axons induced by SNAP in wild-type DRG neurons. 109
Fig. 43. Addition of forskolin partially abolishes retraction of axons induced by SNAP in wild-type DRG neurons. 109
Fig. 44. Treatment with taxol does not abolish SNAP-induced neurite retraction in wild-type neurons and induces axon retraction on its own. 110
Fig. 45. Taxol induces axon retraction also in MAP1B-/- DRG neurons. 111
Fig. 46. Treatment with taxol does not abolish calcimycin-induced neurite retraction in N2a cells. 112
Fig. 47. Treatment with taxol does not prevent LPA-induced neurite retraction of wild-type neurons. 113
Fig. 48. Treatment with taxol does not abolish LPA-induced neurite retraction in N2a cells. 114
Fig. 49. Inhibition of ROCK does not prevent taxol-induced neurite retraction in wild-type and MAP1B-/- DRG neurons. 115
Fig. 50. Inhibition of myosin does not prevent taxol-induced neurite retraction in wild-type and MAP1B-/- DRG neurons. 116
Fig. 51. Inhibition of NOS did not prevent taxol-induced neurite retraction in wild-type DRG neurons. 118
Fig. 52. Increased microtubule binding of MAP1B induced by treatment with SNAP or LPA. 119
Fig. 53. EB1-GFP in wild-type and MAP1B-/- DRG neurons. 122
Fig. 54. Increased velocity of EB1-GFP comets in MAP1B-/- DRG neurons. 124
Fig. 55. Increased distance of EB1-GFP comets in MAP1B-/- DRG neurons. 125
Fig. 56. Increased time of EB1-GFP comet life in MAP1B-/- DRG neurons. 126
Fig. 57. The stop frequency is not altered in MAP1B-/- DRG neurons. 127
Fig. 58. Increased number of EB1-GFP comets in axons and growth cones of MAP1B -/- DRG neurons. 128
Fig. 59. LPA increases the velocity of EB1-GFP comets in growth cones of wild-type DRG neurons. 129
Fig. 60. LPA does not alter the velocity of EB1-GFP comets in MAP1B-/- DRG neurons. 130
Fig. 61. EB1-GFP comets moves for shorter distance in axons of LPA-treated wild-type DRG neurons. 131
Fig. 62. EB1-GFP comets moves for shorter distance in the growth cones of LPA-treated MAP1B-/- DRG neurons. 131
Fig. 63. LPA decreases the time of EB1-GFP comet life in axons of wild-type DRG neurons. 132
Fig. 64. LPA does not alter the time of EB1-GFP comet life in MAP1B-/- DRG neurons. 133
Fig. 65. LPA does not alter the stop frequency of EB1-GFP comets in wild-type DRG neurons. .. 134
Fig. 66. LPA does not alter the stop frequency of EB1-GFP comets in MAP1B-/- DRG neurons. 134
Fig. 67. LPA decreases the number of EB1-GFP comets in axons of wild-type DRG neurons. 135
Fig. 68. LPA decreases the number of EB1-GFP comets in axons MAP1B-/- DRG neurons. 136
Fig. 69. Model for regulation of microtubule severing in wild-type (a) and MAP1B-/- (b) DRG neurons. 149
Fig. 70. Model for role of MAP1B in SNAP-, calcimycin- and LPA-induced axon retraction. 151
Fig. 71. Model for MAP1B-mediated axon retraction. SNAP, calcimycin and LPA induce MAP1B-dependent axon retraction. 153
Fig. 72. Laminin induces different morphology of regenerating wild-type and MAP1B-/- DRG neurons. 156
Fig. 73. Roscovitine-induced axon retraction is impaired in MAP1B-/- DRG neurons. 159
Fig. 74. Response of wild-type and MAP1B-/- neurons to roscovitine treatment. 160
Fig. 75. Axon retraction induced by roscovitine is MAP1B- and ROCK-dependent. 162
Fig. 76. Axon retraction induced by roscovitine involves myosin. 163
Fig. 77. Roscovitine-induced axon retraction involves activation of myosin. 164
Fig. 78. Axon retraction induced by roscovitine does not involve nNOS. 165
Fig. 79. Inhibition of GSKβ partially abolishes axon retraction induced by roscovitine. 166

Fig. 80. Axon retraction induced by roscovitine does not involve depolymerization of microtubules. 167
Fig. 81. Axon retraction induced by roscovitine is laminin-dependent. 169
Fig. 82. Axon retraction induced by LPA is laminin-dependent. 170
Fig. 83. Increased microtubule binding by MAP1B induced by treatment with roscovitine. 171
Fig. 84. Model for p35/cdk5 and MAP1B-mediated laminin signaling. 178
Fig. 85. Model for role of MAP1B in axon retraction induced by roscovitine. 179

Table 1. List of cell lines..... 189
Table 2. N3 components. 190
Table 3. Construct used for transfection of mammalian cell lines 191
Table 4. List of primary antibodies 199
Table 5. List of secondary antibodies 199
Table 6. List of inhibitors and activators. 200

CURRICULUM VITAE

PERSONAL DETAILS

Name :	Ewa Krupa
Maiden name:	Kokoszka
Nationality:	Polish
Date of birth:	23.10.1981
Address:	Buchengasse 23/1/5, 1100 Wien, Austria
Emai:	ewa.krupa@univie.ac.at
Phone:	0680/2081717

EDUCATION

11.2005 – now	PhD thesis "A role of MAP1B and NO in axon guidance" under the supervision of Univ. Prof. Dr. Friedrich Propst at the Department of Biochemistry and Cell Biology, University of Vienna, Max F. Perutz Laboratories, Vienna, Austria
21.06.2005	Master Degree in Biotechnology, passed with distinction, award for The Best Diploma Thesis 2004/2005
2000 – 2005	Interfaculty of Biotechnology, Warsaw University of Life Sciences, Poland
06/2000	Matura passed with successfulness
09.1996 – 06.2000	The Major Henryk Sucharski High School in Myszków, profile: biology-chemistry, Poland
09.1988 – 06.1996	Basic School nr 5 in Myszków, Poland

WORKING EXPERIENCE

03.2009 – now	scientific employee at the Department of Biochemistry and Cell Biology, University of Vienna, Max F. Perutz Laboratories, Austria
11.2005 – 03.2009	scientific employee at the Medical University of Vienna, Austria

11.2008 – 12.2008	fellowship, Laboratory Neurobiologie des Signaux Intercellulaires, Université Pierre et Marie Curie, Centre National de la Recherche Scientifique, Paris, France (Fatiha Nothias, PhD)
02.2003 – 06.2005	diploma student at the NeuroRepair Department of M. Mossakowski Medical Research Centre, Polish Academy of Sciences in Warsaw, Poland (The involvement of protein tyrosine kinase PYK2 in the delayed neuronal death in gerbil hippocampus after transient cerebral ischemia) (Assoc. Prof. Teresa Zalewska)
08.2003	lab assistant, Analytical Laboratory in Hospital in Myszków, Poland

TEACHING EXPERIENCE

03.2007-07.2009	tutor at the University of Vienna for „Molekulare Biologie UE II, Teil A + Biochemisches Praktikum C (Proteinbiochemie) für Chemiker“
08.2006-07.2009	supervising undergraduate students in the context of their „Wahlbeispiel Molekulare Zellbiologie: Einzelunterweisung zur Anwendung moderner molekularbiologischer und zellbiologischer Techniken“

CONFERENCES

12.02.2009 – 21.02.2009	Axonal Connections: Molecular Cues for Development and Regeneration (J6), Keystone, Colorado, USA (poster)

ADDITIONAL SKILS

18-22.02.2008	Medical English I: Scientific Writing
06.2004	Level 1 Certificate in English (ESOL), FCE
Language skills	Polish: mother tongue English: fluent in written and spoken English (C2) German: basic (B1)
Computer skills	MS Office, Zeiss confocal microscopy software LSM510, Zeiss Apotome Microscopy software AxioVision, Adobe Photoshop, Adobe Illustrator, SPSS